Dissertation zur Erlangung des Doktorgrades

der Fakultät für Chemie und Pharmazie

der Ludwig-Maximilians-Universität München

Pulmonary delivery of drugs for the treatment of inflammatory and infectious diseases

Domizia Baldassi

aus

San Daniele del Friuli, Italien

2023

Erklärung

Diese Dissertation wurde im Sinne von § 7 der Promotionsordnung vom 28. November 2011 von Frau Prof. Dr. Olivia M. Merkel betreut.

Eidesstattliche Versicherung

Diese Dissertation wurde eigenständig und ohne unerlaubte Hilfe erarbeitet.

Sedegliano, 15. September 2023

Domizia Baldassi

Dissertation eingereicht am: 20.09.2023

1. Gutachterin: Prof. Dr. Olivia. M. Merkel

2. Gutachter: Prof. Dr. Francesca Ungaro

Mündliche Prüfung am: 21.11.2023

To my Family

“Per aspera ad astra”

Table of Contents

Abstract – Summary

Due to the high incidence of acute and chronic lung disorders, respiratory diseases are considered as a major health, economic and social burden worldwide. The respiratory tract is situated in direct contact with the external environment, and thus at high risk of exposure to infectious agents and toxic chemicals. The ease of access of the respiratory tract can be exploited to directly administer drugs to the lungs to address pulmonary diseases. This offers several advantages, including avoiding systemic side effects and improving patients' compliance. Therefore, the development of formulations for pulmonary delivery appears as a promising strategy. In this view, the development of nanoparticle-based formulations for inhalation can be exploited encapsulate small molecules or to deliver next generation drugs like RNA-based therapeutics. The encapsulation of chemotherapeutics or antibiotics in nanoparticles facilitates a more precise delivery of the cargo to the site of action, reducing adverse systemic side effects. In the case of RNA-based therapeutics, the formulation of the cargo with a suitable nanocarrier is essential to achieve the desired therapeutic activity. Among these, siRNAs have been the subject of extensive studies for the past 20 years as they can be designed to ideally downregulate any target sequence and thus offer new therapeutic options for diseases considered uncurable. However, susceptibility to nucleases and impossibility to penetrate the negatively charged cell membrane amongst others, makes the formulation of siRNA with a suitable delivery system fundamental to deliver the cargo to the site of action as well as to overcome the major barriers found in the lung.

Within this work, we sought to identify formulations with optimized features for lung delivery of therapeutics, focusing on the development of non-viral delivery systems for pulmonary administration of siRNA and nanoparticles for the encapsulation antimicrobial agents. The formulations were developed to target different inflammatory and infectious states of the lungs, which spanned from cystic fibrosis to asthma, from SARS-CoV-2 to methicillin-resistant *S. aureus* infections.

Overall, the aim of this work was to investigate formulation strategies that could contribute to the state-of the-art of therapeutics for direct administration to the lungs, focusing on the development of delivery systems for pulmonary administration of siRNA.

Chapter I – General Introduction

1. Diseases of the respiratory tract

The lung is considered the organ at highest risk of infection and injury from external environment due to the constant exposure to particles, chemicals and infectious organisms found in ambient air. Respiratory diseases represent indeed a health, social and economic burden worldwide, with more than 1 billion people affected by a chronic or acute disorder. Chronic respiratory diseases such as asthma, cystic fibrosis and chronic obstructive lung disease (COPD), together with lung cancer and respiratory infections, both viral and bacterial, are major causes of death, and their incidence is constantly increasing. On top of that, the recent Covid-19 pandemic dramatically increased the number of people suffering from pulmonary dysfunctions (1).

Cystic fibrosis (CF) is considered the most prevalent autosomal recessive disease of the Caucasian population, affecting about 100.000 people worldwide. It is caused by mutations of the Cystic Fibrosis Transmembrane conductance Regulator (CFTR) gene, which encodes for a transmembrane protein essential for the transport of chloride and bicarbonate ions across epithelial cells (2). Many different mutations have been identified at the CFTR level, wherein the most common one is as phenylalanine deletion in position 508 (ΔF508), which is observed in about 70% of the population, leading to reduced channel functionality, number, or both. CF is a multiorgan disease, with the lungs being the organ most affected. The mutations at the CFTR level cause an imbalanced transport of ions and fluids across lung epithelial cells, leading to impaired mucociliary clearance, chronic inflammation, recurrent bacterial infections, and respiratory failure, being the primary cause of death and morbidity (3).

Asthma and COPD are the most widespread chronic respiratory diseases, with more than 300 million people affected worldwide and more than 90% of mortality in low-and middle-income countries (4). The main asthma hallmark is a generalized inflammatory state of the upper airways, which lead to recurrent episodes of coughing, chest tightness, wheezing and dyspnea. Chronic inflammation has severe consequences on lung structure and functionality, particularly in terms of airways obstruction, remodeling, hyper-responsiveness and mucus hypersecretion. Currently, asthma can be treated only symptomatically, mainly with bronchodilators and anti-inflammatory drugs such as glucocorticoids. However, in 5-10% of the asthmatic population the symptoms remain uncontrolled, exposing patients to worse symptoms, increased incidence of concomitant comorbidities and higher risk of mortality (5). Asthma inflammatory status is triggered by inappropriate immunological responses to common-inhaled allergens that lead to

activation, infiltration and accumulation of T helper 2 (Th2) cells in the airways mucosa, followed by release of Th2 proinflammatory cytokines IL-4, IL-5 and IL-13, leading a perpetuated inflammatory state (6).

COPD is a chronic respiratory disease resulting from persistent exposure to toxic gases and particles, with exposure to tobacco smoke considered a key risk factor, as it causes a chronic inflammatory status of the airways that eventually leads to progressive obstruction and lung failure (7). Clinical manifestations can be divided into two categories, chronic bronchitis and emphysema. The former is found in the upper airways and it is characterized by chronic inflammation, airway remodeling and mucus secretion. The latter is typical of the lower airways and it consists in a progressive deterioration of airway walls and loss of alveolar cells, which leads to impaired gas exchange. The abnormal inflammatory response in response to persistent exposure to toxic agents such as tobacco smoke is mediated by an increased number of inflammatory cells, particularly neutrophils, macrophages and Th1 cells in the airways, secreting pro-inflammatory cytokines and chemokines, which mediate a continuous inflammatory condition (8).

Respiratory tract infections are the deadliest disease of infectious etiology and the fourth leading cause of mortality worldwide. Their widespread distribution, high mortality and morbidity defines them as main concern for public health worldwide. Respiratory infections can be of different severity, can be found from the upper to the lower airways and can be caused by viruses, bacteria, or both (9). Lower respiratory tract infections are the most common cause of death in children and elderly, with pneumonia, both of bacterial and viral origin, being the most common complication. In young children, the highest incidence is observed for infections caused by respiratory syncytial virus. In addition, the recent COVID-19 pandemic has revealed how fast respiratory viruses can spread and the effect they can have on health, politics and economics on a global scale (10). Among bacteria, S. *pneumonia* is the most frequent cause of infection, but an important role is played also by other bacteria such as P. *aeruginosa* and S. *aureus*, particularly considering the arising concern of antimicrobial resistance.

2. Pulmonary administration

The respiratory system is a set of organs and structures that enable gas exchange throughout the vital process of breathing. The respiratory tract is divided into two parts, the upper respiratory tract and the lower respiratory tract. The latter is composed by nasal cavities, pharynx and larynx, whilst the former consists of the trachea, bronchi, bronchioles and alveoli (11).

The respiratory tract can be further divided in three regions, that are the extratoracic, tracheobronchial and alveolar regions. The extratoracic region comprises the oral and nasal cavity, the pharyngeal and laryngeal tract to the entrance, and it is composed mainly of ciliated columnar cells and goblet cells. The tracheobronchial region is located between the trachea and the terminal bronchioles, and it is lined by a columnar, pseudostratified epithelium of goblet cells, basal cells and ciliated cells as well as cuboidal ciliated cells and club cells in the bronchioles. The alveolar region is the more distal part of the lungs and it is composed by type I pneumocytes, which are responsible for gas exchanges, and type II pneumocytes, which are accountable for several functions such as regulation of the lung surfactant system, alveolar fluid content as well as secretion of antimicrobial and surface-active components (12).

Considering the high incidence of pathologies affecting the respiratory tract, especially at the epithelial level, pulmonary administration emerges as an attractive route of administration. Local delivery to the lung has several advantages, such as a large surface area (hundreds of square meters), high perfusion (5 L/min), a thin epithelial barrier (0.1-0.2 μm) and a high blood volume in the capillaries (0.25 L). Furthermore, the lungs are characterized by low enzymatic activity and absence of serum proteins, a condition that is particularly favorable for nucleic acid therapeutics (13). In addition, local delivery to the lungs is non-invasive, improves patients' compliance and allows for a reduced dose in comparison to systemic delivery, thus decreasing side effects as well as avoiding first-pass effect. Also, it is a more economical platform that could be provided to patient populations within different settings and on a daily basis if required. Despite the several advantages offered by local delivery to the lungs, there are also a number of anatomic, physiological, metabolic and immunologic hurdles that prevent the inhaled therapeutic agent from reaching the target site (14). Major barriers to pulmonary delivery include mucociliary clearance by ciliated epithelial cells and alveolar macrophages together with the presence of lung fluids such as mucus and surfactant. This is particularly important in the diseased state, where thickness, viscosity and composition of the mucus is altered and could strongly affect the efficacy of the administered therapeutic agent. However, the most prominent barrier of the lungs is the high degree of branching with variable lengths and diameters. To overcome lung barriers to inhaled pulmonary delivery, newly developed formulations should be carefully optimized in terms of size as this will determine the site of deposition in the lungs (15). Particles with aerodynamic diameter > 6 μm will deposit in the oro-pharynx due to impaction. On the other hand, particles < 1 μm are governed by Brownian motion and are mainly exhaled, except for nanoparticles < 100 nm which can successfully reach the alveolar tract by

diffusive deposition. Therefore, the optimal aerodynamic diameter range is considered between 1 and 5 µm. By controlling these parameters, it is possible to precisely target specific regions within the lungs, e.g. by incorporating drugs or nanoparticles into microparticles with aerodynamic diameters between 1 and 5 µm, whose matrices are made of excipients such as lactose or mannitol. Once the microparticles deposit within the lung fluids, they readily dissolve and release the therapeutic cargo. Pulmonary administration is generally performed intranasally or via inhalation, in form of liquid or dry powder aerosols. For inhalation, devices commonly used are nebulizers, soft-mist inhalers, dry powder inhalers as well as metered dose inhalers (16).

Overall, local delivery to the lungs offers several advantages over systemic delivery. However, formulations must be carefully optimized to overcome major hurdles found in the lung and thus efficiently exert the therapeutic activity at the target site.

3. RNAi therapeutics and lung delivery systems

The approval of the first mRNA vaccines for the prophylaxis of COVID-19 in 2020 has unveiled the promises and advantages of RNA therapeutics for the treatment of respiratory diseases (17). Differently from other conventional approaches, they provide high selectivity, potency and possibility for personalized therapy. Besides mRNA vaccines, in the last years we have witnessed the approval of four siRNA-based therapies (18). By inducing the RNA interference (RNAi) mechanism, siRNAs can be theoretically tuned to downregulate any target sequence, whether endogenously or exogenously expressed. The RNAi mechanism was discovered by Fire and Mellow at the end of the previous century, and they were awarded the Nobel Prize in Physiology for this discovery in 2006 (19). RNAi can be experimentally triggered by introducing short hairpin RNA (shRNA), which is expressed by a plasmid, double strand RNA (dsRNA), or by directly delivering small interfering RNA (siRNA), to the cytoplasm of the cells. shRNA and dsRNA take advantage of the endogenous pathway using the enzyme complex Dicer, which cleaves them into short, double stranded dsRNA with a typical structure of 19 nucleotides complementary to the target mRNA and two nucleotide terminal 3’ overhangs. Afterwards, siRNAs are introduced in the RNA-induced silencing complex (RISC) where the sense strand is degraded and the antisense strand guides the RISC to recognize the target mRNA by binding to the complementary target sequence. Here, the target sequence is cleaved by the endonuclease Argonaute to achieve post-transcriptional silencing of the target gene expression (Figure 1).

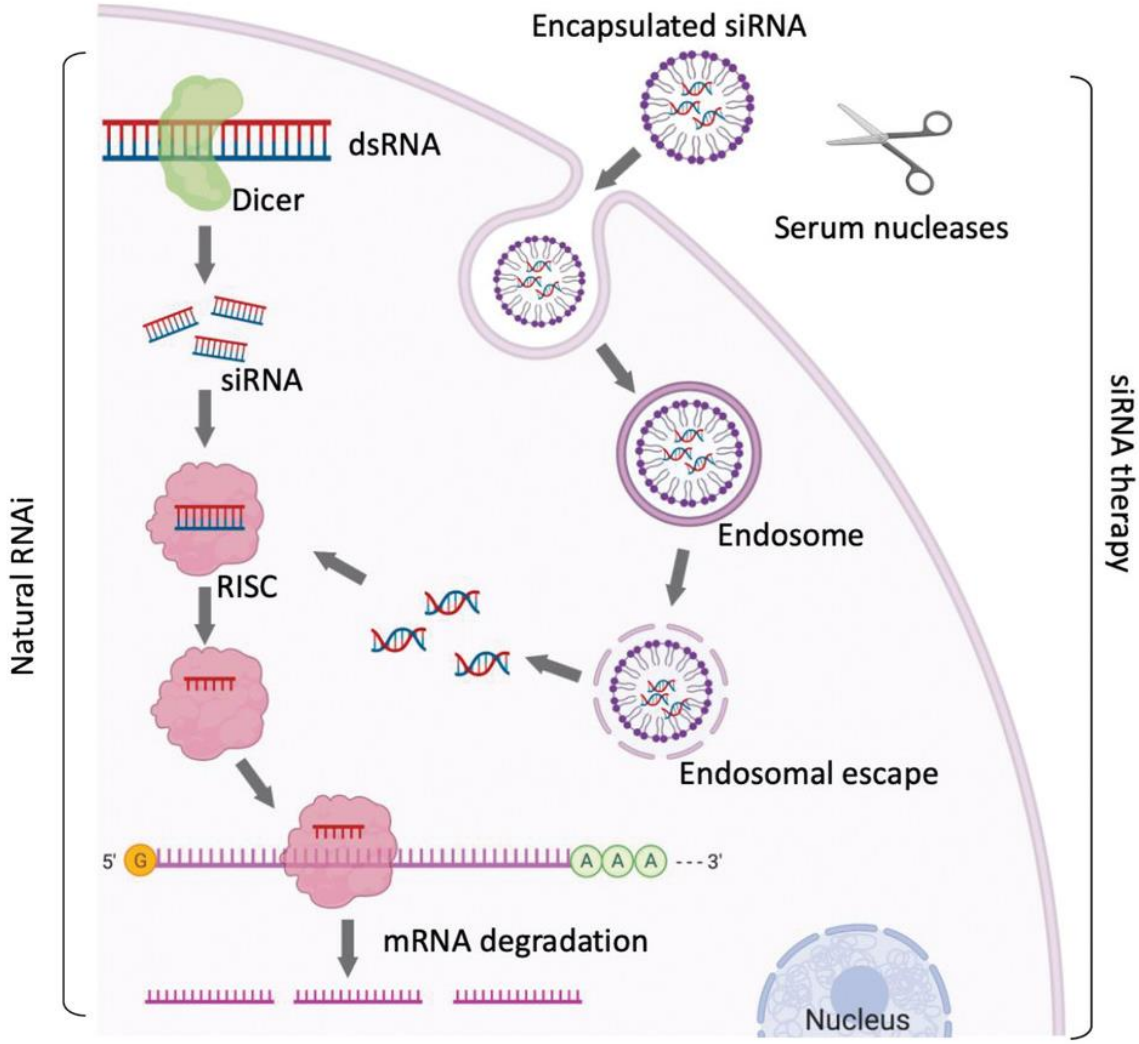

Figure 1. The mechanism of the RNA interference pathway. Dicer cleaves double-stranded RNA into short interfering RNA and it is loaded into the RISC. siRNA recognizes base-complementary mRNA and guides its cleavage. siRNA-loaded nanoparticles are taken up by cells and enter the early endosome. Following endosomal escape, siRNA is released into the cytoplasm and loaded into the RISC (20).

Considering that all mammalian cells have the RNAi machinery, siRNAs can be ideally developed to target and degrade any mRNA, thus being potentially able to treat a great number of conditions for which no therapy is currently available (20). Despite the great potential offered by siRNAs, they are negatively charged macromolecules that cannot penetrate the negatively charged cell membrane. Furthermore, when administered systemically, siRNAs are readily degraded by nucleases present in blood stream and removed by renal filtration (21). To overcome delivery challenges of nucleic acids, siRNA has been chemically modified to improve overall stability or encapsulated in nanocarriers (22). Nanocarriers are generally divided in two main families, viral and non-viral delivery systems. While the former show higher transfection efficacy, the latter hold superior safety profile as well as reproducible manufacturing, which makes them the preferred

commercial delivery vectors. Furthermore, they can be tailored to reach specific cell targets. A variety of materials has been investigated as non-viral delivery systems, from polymers to lipids, from peptides to inorganic materials. The materials used for siRNA delivery should not only be biocompatible and possibly biodegradable, but also facilitate cellular internalization and allow endosomal escape with the release of the cargo into the cytoplasm. Endosomal entrapment is indeed considered the bottleneck in the development of novel nanocarriers. The first siRNA therapy to reach the clinics, Onpattro®, was based on the encapsulation of siRNA in lipid nanoparticles (LNPs) (23). Lipid-based delivery systems such as liposomes, solid lipid nanoparticles or lipoplexes have indeed been widely studied for the delivery of nucleic acids. LNPs are composed of phospholipids, cholesterol, PEG-lipids and ionizable lipids. The latter are a class of lipids that remain neutral at physiological pH but are protonated and thus positively charged at low pH. This peculiar structure gives them high transfection efficacy and offers a way to overcome endosomal entrapment of siRNA (24).

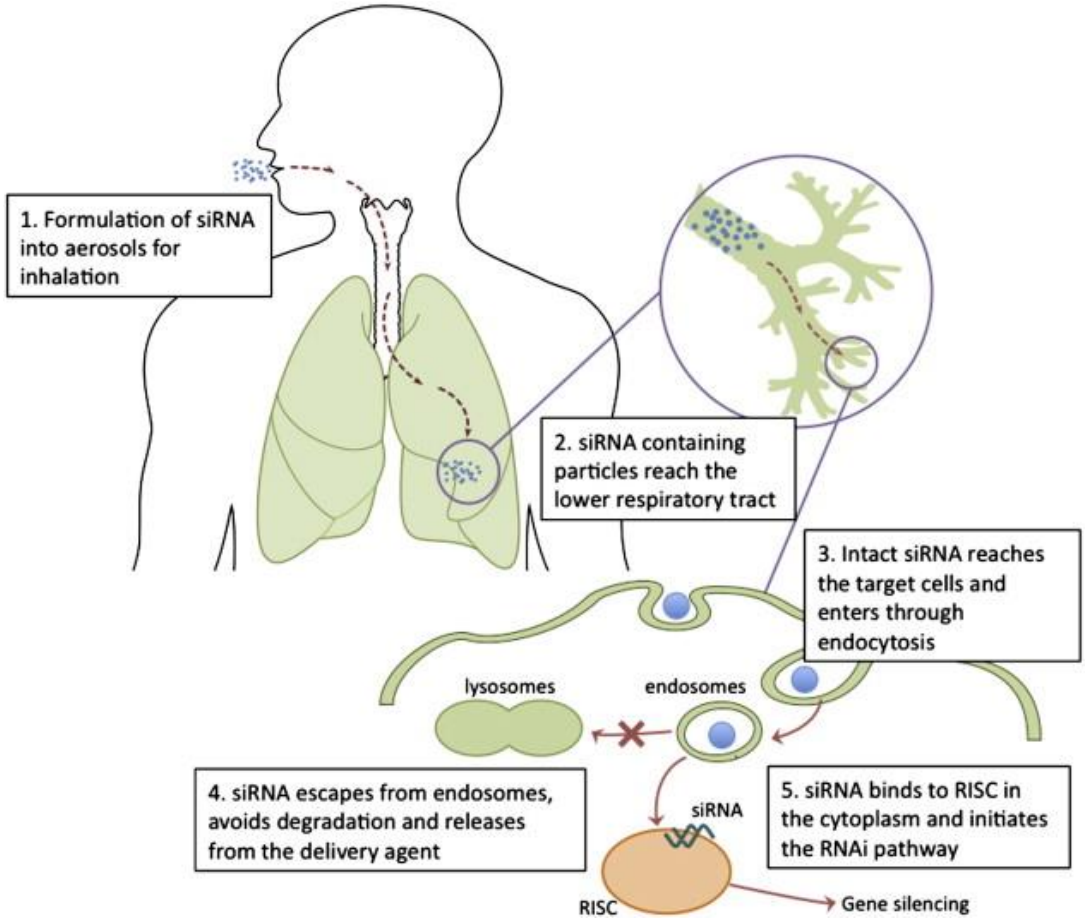

Figure 2. siRNA-loaded nanoparticles for pulmonary delivery via inhalation (25).

Polymer-based delivery systems have also been widely studied for nucleic acid delivery. They are cheaper to produce and can be easily modified to achieve specific characteristics such as biodegradability or cell-specific targeting effects (26,27). Polyplexes, solid nanoparticles and dendrimers are some of the groups of nanocarriers that can be created starting from polymers. Polyplexes are formed by the electrostatic interaction between a positively charged polymer and negatively charged siRNA. Polycations can generally condense siRNA very efficiently but are associated with limited endosomal escape and with toxicity. One of the most widely studied polycations is polyethylenimine (PEI) (28). On the other hand, solid nanoparticles, such as PLGA nanoparticles, can efficiently protect the cargo and can be easily processed to achieve a solid dosage form but tend to demonstrate low loading capacity (29). Nanocarriers for pulmonary administration of siRNA therefore need to be further optimized to overcome lung barriers (30). In this view, polymer-based delivery systems seem advantageous over lipid delivery systems as they can be easily nebulized or processed for spray drying (31). Nonetheless, we recently showed that LNPs can also be spray dried for inhalation (32) and that hybrid materials can combine the best of both worlds (33,34). Nanocarriers should also help in overcoming the mucus layer of the lungs. The presence of mucins in lung mucus, which are negatively charged glycoproteins, may affect the stability of the delivery system (35). Ultimately, pulmonary siRNA delivery requires the development of suitable vectors that can penetrate through the environment of the lungs and reach the desired target cells.

4. Nanotechnology approaches for inhalation therapies

Nanotechnology holds promises not only for the development of new generation therapies, but also for repurposing well-known active compounds. Considering the advantages of nanoformulations for pulmonary delivery, the encapsulation of small molecules into nanoparticles, such as chemotherapeutics and antibiotics, is considered a promising strategy for the development of inhalable drug formulations. Encapsulation in nanoparticles can indeed deliver the therapeutic agent directly to the site of action, thus increasing the efficacy of the treatment, lowering the penetration of the drug into the bloodstream and consequently reducing adverse systemic side effects (36).

In this view, the encapsulation of antibiotics in nanoparticles for inhalation can enhance their antimicrobial activity by providing protection from enzymatic or chemical degradation, mucoadhesive properties as well as sustained drug release, which avoids high drug concentrations and prolongs residence time in lung tissue (37). An FDA approved inhalation powder containing tobramycin is already available to treat P. *aeruginosa* lung infection in cystic fibrosis patients. This formulation is based on an

emulsion-based spray-drying process for the production of light porous particles. Furthermore, two nebulized liposomal formulations based on ciprofloxacin and amikacin have reached clinical trials or the treatment of CF and non-CF bronchiectasis (38). Nonetheless, polymer-based formulations, such as PLGA nanoparticles, appear also promising for this application as they can be easily processed for producing a dry powder for inhalation (39).

As for antibiotics, the development of formulations for inhalation is advantageous also for cancer therapies. Local delivery of highly toxic drugs reduces the total drug concentration, thus limiting adverse side effects of chemotherapy. Several anticancer drugs, such as paclitaxel, cisplatin and doxorubicin, have been successfully delivered by inhalation, and nanoparticle-based inhalation therapy has been shown to be safe and effective against lung cancer in pre-clinical and clinical studies (36,40).

5. *In vitro* models of the respiratory tract

The complex cellular composition of the respiratory tract together with its location at the air-liquid interface (ALI) limit their physiological reproducibility for research purposes. Although rodent animal models are considered the most reliable choice for drug screening, they have some major anatomical differences that hamper the replication of physiological functionality in terms of drug deposition rates and location. Indeed, mice have a different airway and alveolar architecture than humans. While humans have 20 or more generations of branching airways, mice only have 6-8 generations. Furthermore, terminal bronchioles of mice empty into alveolar ducts and alveoli, while in humans, respiratory bronchioles empty into alveolar ducts and alveoli. Most importantly, one of the main problems with animal models is that they fail to reproduce the underlying pathophysiology of the human disease (41). In addition to the limitations of animal models, the strong drive towards complying with the 3Rs principle of reducing, refining and replacing animal experiments is constantly increasing. Taken together, these factors have pushed research interest towards the development of alternative *in vitro* and *iin* cell culture models that can closely mimic the respiratory tract (42). Air-liquid interface cultures, precision-cut lung slices (PCLS), microfluidic systems, spheroids, *ex vivo* perfused and ventilated lungs are just some examples of 3D research models available nowadays for the replication of the respiratory tract *in vitro* (43).

Air-liquid interface culture is a valid tool to reproduce *in vitro* typical features of the respiratory tract. In this configuration, by exposing cells to the culture medium on one side and to the air on the other, cells form a pseudostratified epithelium with tight junctions and mucus secretion. ALI models can be constructed both from immortalized

lung epithelial cells and from primary cells, and more cell types can be combined to develop co-culture models. ALI models have been used to replicate several disease states of the lungs *in vitro*, such as cystic fibrosis, asthma, COPD, lung cancer as well as bacterial and viral infections (44). Commercially available ALI models have also been developed, as they ensure higher data reproducibility, lower batch-to-batch variabilities and long-term cultivation (45).

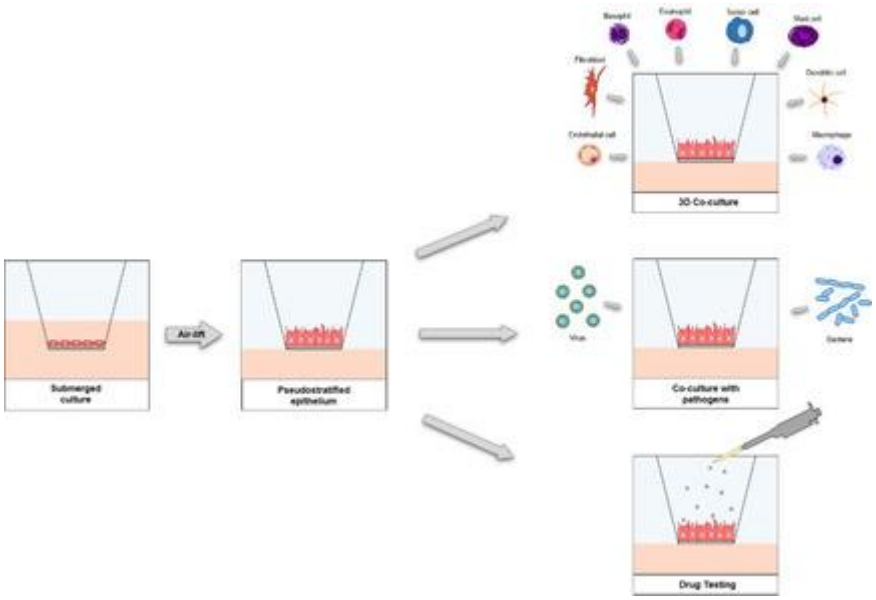

Figure 3. Air-liquid interface culture of the respiratory tract (45).

Another 3D *in vitro* model to reproduce the lung architecture and cellular environment is the lung-on-a-chip approach. This device consists of continuously perfused and controlled microchannels lined by living human cells that reproduce *in vivo* vascular perfusion, concentration gradients and fluid-flow-induced mechanical forces. Different cells types can be combined to mimic different functional units of the lung and different disease conditions, such as COPD, asthma, lung cancer, bacterial and viral infections (46).

PCLS are an *ex vivo* model that holds potential for closing the translational gap between *in vitro* and *in vivo* models of the respiratory tract. Slices are prepared from animal or human explants and can be cultured *in vitro*. They contain all cell types of the source tissue, they retain the anatomical and cellular structure of the lung, and they can replicate respiratory and immune responses in response to inflammatory stimuli, infection and novel drug compounds (47).

6. Aims of the thesis

The aim of this work is the development of formulations based on non-viral delivery systems for pulmonary administration of therapeutics, particularly siRNA. As described

above, lungs are at high risk of infection and injury due to constant exposure to particles, chemicals and infectious organisms. Respiratory diseases retain a great economic and social burden worldwide, and in many cases they still represent an unmet medical need. RNA therapeutics could indeed contribute to this cause. Therefore, different non-viral delivery strategies, based mainly on polymers, have been investigated to achieve a successful formulation of siRNA (and in one case also of an antimicrobial agent) for pulmonary administration.

Chapter 1 describes the optimization of a lung surfactant coating based on commercially available lung surfactant for siRNA/PEI polyplexes to improve siRNA delivery to the lungs.

Chapter 2 aims at describing the effect of helper lipids for pulmonary administration of siRNA loaded lipid nanoparticles (LNPs): LNPs with different helper lipids have been investigated *in vitro* to investigate how the different lipids affect safety, cellular uptake and transfection efficacy in lung epithelial cells.

Chapter 3 describes the development of an siRNA-based formulation using VIPER block copolymer as a potential antiviral therapy against SARS-CoV-2 infections.

Chapter 4 investigates the development of PLGA-based formulation for pulmonary administration of a novel benzophenone antibiotic for the treatment of S. aureus methicillin-resistant infections.

Chapter 5 reviews an siRNA-based approach for the treatment of asthma, describing the identification of the cellular target, formulation development as well as the production of a final dosage form for inhalation.

Chapter 6 focuses on the *ex vivo* testing in human precision-cut lung slices from human donors of an siRNA-based formulation for the treatment of asthma.

Chapter 7 explores the *in vitro* development of an siRNA-based formulation for the treatment of inflammation in patients affected by cystic fibrosis.

Chapter 8 gives a general overview on the advantages and challenges of air-liquid interface 3D cultures as models of the healthy and diseased respiratory tract.

Chapter II - Optimization of lung surfactant coating of siRNA polyplexes for pulmonary delivery

Domizia Baldassi[1†], Thi My Hanh Ngo[1†], Olivia M. Merkel[1]

[1]Department of Pharmacy, Pharmaceutical Technology and Biopharmaceutics, Ludwig-Maximilians University of Munich, Butenandtstraße 5, 81377, Munich, Germany

[†]These authors contributed equally to this work.

The following chapter was published in Pharmaceutical Research.

Baldassi D, Ngo TMH, Merkel OM. Optimization of Lung Surfactant Coating of siRNA Polyplexes for Pulmonary Delivery. Pharm Res. 2022 Nov 29:1–15. doi: 10.1007/s11095-022-03443-3. Epub ahead of print. PMID: 36447020; PMCID: PMC9708138.

Abstract

Purpose The aim of this study was to understand how coating with a pulmonary surfactant, namely Alveofact, affects the physicochemical parameters as well as *in vitro* behavior of polyethylenimine (PEI) polyplexes for pulmonary siRNA delivery.

Methods Alveofact-coated polyplexes were prepared at different Alveofact:PEI coating ratios and analyzed in terms of size, PDI and zeta potential as well as morphology by transmission electron microscopy. The biological behavior was evaluated in a lung epithelial cell line regarding cell viability, cellular uptake via flow cytometry and gene downregulation by qRT-PCR. Furthermore, a 3D ALI culture model was established to test the mucus diffusion and cellular uptake by confocal microscopy as well as gene silencing activity by qRT-PCR.

Results After optimizing the coating process by testing different Alveofact:PEI coating ratios, a formulation with suitable parameters for lung delivery was obtained. In lung epithelial cells, Alveofact-coated polyplexes were well tolerated and internalized. Furthermore, the coating improved the siRNA-mediated gene silencing efficiency. Alveofact-coated polyplexes were then tested on a 3D air-liquid interface (ALI) culture model that, by expressing tight junctions and secreting mucus, resembles important traits of the lung epithelium. Here, we identified the optimal Alveofact:PEI coating ratio to achieve diffusion through the mucus layer while retaining gene silencing activity. Interestingly, the latter underlined the importance of establishing appropriate *in vitro* models to achieve more consistent results that better predict the *in vivo* activity.

Conclusion The addition of a coating with pulmonary surfactant to polymeric cationic polyplexes represents a valuable formulation strategy to improve local delivery of siRNA to the lungs.

KEYWORDS siRNA delivery, polyplexes, pulmonary delivery, pulmonary surfactant, air-liquid interface

1. Introduction

The recent authorization of the first mRNA vaccines for the prophylaxis of COVID-19 has shed the light on the advantages of RNA-based therapeutics as potential treatment for a variety of diseases. Besides the mRNA vaccines, in the last four years we have witnessed the approval of four siRNA therapies (48,49). RNA interference, in fact, can theoretically be tuned to downregulate any target sequence, whether endogenously or exogenously produced (50). Although the currently approved siRNA drugs are administered intravenously and target the liver, research efforts are focused on the development of delivery systems that can target tissues beyond the liver and that are designed for local administration (51,52). Particularly pulmonary administration appears as a desirable route of delivery for siRNA. Due to its large surface area, low enzymatic activity and ease of access, the development of formulations for direct administration to the lung appears as a promising strategy (13). Furthermore, the development of an siRNA therapy for direct administration to the airways could be beneficial for treating several pathological conditions affecting the lung for which no curing treatment is available yet, such as cystic fibrosis, asthma, acute lung injury, lung cancer but also viral infections as in the case of the recent SARS-CoV-2 outbreak (34,53–56). Although two siRNA formulations reached clinical trials for intranasal administration, no formulation for direct administration to the lungs has been approved yet (57). Despite the undeniable benefits offered by pulmonary administration, some major obstacles must be overcome to reach the target site as well as an efficient downregulation. Branching of the airways, mucus secretion and mucociliary clearance represent indeed crucial barriers hampering the activity of siRNA. For this reason, suitable delivery systems that can overcome the hurdles of the lung should be developed (30). The nanocarrier, in fact, should not only protect the payload from degradation, but also diffuse through the mucus layer typical for the airways, particularly in the diseased state (58). While the upper airways are covered by a mucus layer rich in lipids and glycoproteins, particularly mucin, the lower tract is covered by a thin layer of lung surfactant. Lung surfactant is secreted by alveolar type II cells and is responsible for reducing surface tension as well as for first line defense

against external intruders (59). It is composed mainly of lipids such as phosphatidylcholine, phosphatidylglycerol and cholesterol, which account for about 90% of the total mass. The remaining 10% consists of proteins, to which the surfactant specific hydrophilic proteins SP-A and SP-B belong that play a role in the innate immune and inflammatory response, and the hydrophobic SP-B and SP-C proteins, which help exerting the biophysical function of the lung surfactant. Pulmonary surfactant represents in fact the first biological fluid encountered by the delivery system when reaching the deep lung and it forms a biomolecular corona around the nanoparticles that can alter biodistribution, cellular uptake and cytotoxicity of the nanoparticles (60). Although pulmonary surfactant can be considered an obstacle for delivering siRNA to the deep lung, previous studies suggest that it could represent an ally indeed (61). Notably, pulmonary surfactant coating of polymeric delivery systems was reported to have a beneficial effect on siRNA delivery of different systems, such as PLGA-based nanoparticles (62) or dextran nanogels (63). Additional studies also suggested that lung surfactant did not negatively influence the transfection efficiency of polymer-based delivery systems, while lipid-based delivery systems were in fact negatively affected (64). On this basis, we decided to repurpose a broadly studied cationic polymer for siRNA delivery, polyethylenimine, with the addition of Alveofact coating, a commercially available pulmonary surfactant, following the formation of PEI/siRNA polyplexes. Although cationic polymers can efficiently condense and deliver siRNA to the cells, limitations are generally observed in terms of inadequate endosomal escape as well as high toxicity linked to the cationic nature of the polymer (65,66). In contrast, coating with pulmonary surfactant was shown to improve the safety as well gene silencing profile of non-viral delivery systems for siRNA (67). Therefore, we have established a method for coating PEI polyplexes with Alveofact pulmonary surfactant at different PEI:Alveofact coating ratios. We tested the different formulations in terms of physicochemical behavior, stability and *in vitro* activity to identify the most promising one. We observed that Alveofact coating improved the gene silencing activity in comparison to uncoated polyplexes in a lung epithelial cell line. To further investigate the polyplexes in a more relevant *in vitro* setting, we developed an air-liquid interface culture of the respiratory tract that retains tight junctions as well as mucus secretion. ALI cultures represent a valid tool to reproduce some of the main features of the healthy as well as diseased respiratory tract *in vitro* and can be thus considered a more suitable instrument to test drug delivery systems for pulmonary delivery (45). After testing Alveofact-coated polyplexes at ALI, we identified a formulation able to penetrate the mucus layer as well as to efficiently downregulate the expression of an endogenously expressed housekeeping gene. The experiment underlined the importance of testing delivery

systems in appropriate *in vitro* models that better predict the *in vivo* behavior of the formulation. The resulting formulation is considered an efficient strategy to improve the delivery of siRNA to lung epithelial cells particularly in disease conditions accompanied with a deficiency of endogenous pulmonary surfactant, such as in patients suffering from acute respiratory distress syndrome (ARDS), or even in CARDS resulting from severe course of COVID-19 infection (68). In this regard, Alveofact coating not only improved the transfection efficiency, but also helped drug spreading and absorption after pulmonary administration to more distal lung regions and thus lead to better therapeutic outcomes.

2. Experimental methods

2.1 Materials

HEPES (4-(2-hydroxyethyl)–1-piperazineethanesulfonic acid), PEI 25kDa, heparin sodium salt, paraformaldehyde solution, FluorSave™ Reagent, Eagle's Minimum Essential Medium (EMEM), RPMI-1640 Medium, fetal bovine serum (FBS), Penicillin-Streptomycin solution, Dulbecco's Phosphate Buffered Saline (PBS), trypsin-EDTA solution, 200 mM L-glutamine solution, Paraformaldehyde, Tween20, agarose and Alcian Blue solution (1% in 3% acetic acid pH 2.5) were purchased from Sigma-Aldrich (Darmstadt, Germany). Lipofectamine 2000, SYBR gold dye, AF488-anti-rabbit secondary antibody, rhodamine phalloidin, 4′,6–diamidino–2-phenylindole dihydrochloride (DAPI), Alexa Fluor™ 647 NHS ester and Alexa Fluor™ 488 NHS ester were obtained from Life technologies (Carlsbad, California, USA). Transwell® polyester membrane cell culture inserts (0.4 µm pore size) were purchased from Corning (New York, USA). PneumaCult ALI differentiation medium, hydrocortisone and heparin were purchased from Stemcell Technologies (Vancouver, Canada). Alveofact was purchased from Lyomark Pharma (Oberhaching, Germany). ROTI®GelStain Red and bovine serum albumin were purchased from Carl Roth GmbH (Karlsruhe, Germany). Dicer substrate double-stranded siRNA (DsiRNA) targeting human GAPDH, non-specific DsiRNA and amine-modified siRNA were purchased from integrated DNA Technologies (Leuven, Belgium).

2.2 Preparation of Alveofact-coated polyplexes

Alveofact-coated polyplexes were formed by first preparing dilutions of PEI 10 kDa in RNase free water at a concentration of 1 mg/ml. Stocks of polymer and siRNA were further diluted in 10 mM HEPES buffer pH 7.4 to reach the desired concentration. The polymer dilution was added to the siRNA dilution and incubated for 20 min to obtain

polyplexes at a defined N/P ratio of 6. In the meantime, different dilutions of Alveofact were prepared for Alveofact:PEI ratios (w/w) of 0, 1:5, 1:2.5, 1:1, 2.5:1, 5:1, 10:1, followed by sonication in a water bath without heating for 20 min. Two stocks of Alveofact were used, 0.2 mg/ml and 2 mg/ml, to keep the volume for each formulation constant. Alveofact:PEI ratio of 0 equals to no Alveofact added. Once the polyplex incubation time was completed, polyplexes were gently mixed with post-sonicated solutions of Alveofact and incubated for 10 min. The forming particles were subsequently subjected to a second sonication step for 20 min in the water bath to establish the Alveofact outer coating.

2.3 Characterization of polyplexes

2.3.1 Size, polydispersity index and zeta (ζ) potential of Alveofact-coated polyplexes

Hydrodynamic size and polydispersity index (PDI) were measured by dynamic light scattering using a Zetasizer Nano ZS (Malvern Instruments, Malvern, UK). Polyplexes were prepared with siRNA in 10 mM HEPES pH 7.4 and 100 µl were added to a disposable microcuvette for analysis. Measurements were performed at 173° backscatter angle running 10 runs three times per sample. Results are shown as average size (± SD). For ζ-potential measurements, the samples were further diluted to 700 µl with 10 mM HEPES buffer pH 7.4 and added to a folded capillary cell for ζ-potential measurement, which were analyzed by Laser Doppler Anemometry (LDA). A total of three runs per sample was performed, with each run consisting of 30-50 scans. Results are shown as mV ± SD.

2.3.2 TEM

The morphology of uncoated and coated polyplexes was analyzed at transmission electron microscopy. Briefly, 3.5 µl of freshly prepared polyplexes were applied to pre-coated Quantifoil holey carbon supported grids and negatively stained using 2% uranyl acetate. Micrographs were digitally recorded on a Tecnai G2 Spirit TEM at 120 kV. Data was collected under low dose conditions at a nominal magnification of 90,000 X and a nominal defocus of – 0.9 µm using an TVIPS XF216 2048 x 2048 pixel CCD camera (TVIPS, Gauting, Germany).

2.3.3 SYBR gold

SYBR Gold Assay was used to assess the percentage of free siRNA in the formulations after production of Alveofact-coated polyplexes produced by different coating methods. Alveofact-coated polyplexes were prepared at N/P 6 with 100 pmol siRNA at different Alveofact:PEI ratios (w/w). Of each polyplex suspension, 100 µL of was added to a white FluoroNunc 96-well plate. Subsequently, 30 µL of a 4X SYBR Gold solution was added

to each well, and the plate was incubated for 10 min in the dark. Fluorescence was measured on a FLUOstar OMEGA plate reader (BMG Labtech, Ortenberg, Germany) using a 492 and 555 nm excitation and emission wavelength, respectively. Free siRNA was used as 100% value. Measurements were carried out in triplicate, and the results were shown as mean value ± SD (n=3).

2.3.4 Release study

Stability of polyplexes is influenced by the presence of anions in biological fluids and cell culture medium containing serum. Therefore, heparin, a polyanion that potentially competes with nucleotides, was used to investigate the release capacity of siRNA from polyplexes. Alveofact-coated polyplexes were prepared in HEPES 10 mM pH 7.4 at N/P 6 with 100 pmol at different Alveofact:PEI ratio (w/w). Heparin was dissolved in HEPES 10 mM pH 7.4 to obtain the concentration of 0.2 USP units/µL, followed by 2-fold serial dilutions. Aliquots of 100 µL of each polyplexes solution were added to a white FluoroNunc 96-well plate with subsequent addition of 10 µL of heparin at different concentrations (0.125, 0.25, 0.5, 1, 2 USP units/well). After 30 minutes of incubation, 30 µL of a 4X SYBR Gold solution was added to each well and the plate was incubated for 10 min in absence of light. Fluorescence determination and free siRNA calculation were performed similarly to SYBR Gold Assay as described above. Measurements were executed in triplicate, and results were shown as mean value ± SD (n=3).

2.3.5 Gel integrity assay

To confirm the integrity of Alveofact-coated polyplexes after sonication, a gel retardation assay was performed. A 1% Agarose gel was prepared and stained with ROTI®GelStain Red. Polyplexes were prepared with 300 pmol siRNA at three different Alveofact:PEI ratios (0, 2.5:1 and 5:1). As positive control, polyplexes were treated with 1 USP unit of heparin. 3 µL of low range ssRNA ladder (New England BioLabs, Ipswich, Massachusetts, USA) and 3 µL of siRNA were respectively diluted in 27 µL of RNA free water. 30 µL of each sample were mixed with 5 µL of loading dye (New England BioLabs, Ipswich, Massachusetts, USA), loaded into the slots of a gel, and electrophoresis was run at constant voltage of 200 V for 15 minutes in Tris-borate EDTA buffer. The gel was visualized using a ChemiDoc MP imaging system (Bio Rad, Hercules, California, USA).

2.4 Polyplexes stability in storage condition

To evaluate the stability of Alveofact-coated polyplexes, batches at different coating conditions were prepared and stored at room temperature protected from light. At specific time points (0, 24, 48, 72, 96 and 168 h), hydrodynamic size was measured by dynamic light scattering. Briefly, 100 µl were added to a disposable microcuvette and

measurements were performed at 173° backscatter angle performing 10 runs three times per sample. Results are shown as average size (± SD).

2.5 Polyplexes stability in presence of mucin

Stability of polyplexes in presence of mucin was evaluated by gel retardation assay. Briefly, a 1% Agarose gel stained with ROTI®GelStain Red was prepared as well as polyplexes loaded with 200 pmol siRNA at two Alveofact:PEI ratios (2.5:1 and 5:1). Two stock solutions of mucin were prepared at two different concentrations, 3 and 6 mg/mL, to achieve final mucin solutions of 1 mg/mL and 2 mg/mL respectively after the addition of polyplexes. 20 µL of each formulation was mixed with either 10 µL of HEPES 10 mM pH 7.4, 10 µL of mucin 3 mg/mL or 10 µL of mucin 6 mg/mL and incubated for 30 minutes. As positive controls, 2 USP units of heparin were subsequently added to samples containing 20 µL polyplexes and 10 µL of mucin 6 mg/mL. After incubation, each sample was mixed with 5 µL of loading dye, loaded into gel and electrophoresis was run at 200 V for 15 minutes in Tris-borate EDTA buffer solution. The gel was visualized using a ChemiDoc MP imaging system (Bio Rad, Hercules, California, USA).

2.6 Cell culture

The human non-small carcinoma cell line H1299 was cultured in RMPI-1640 medium supplemented with 10% FBS and 1% P/S. 16HBE14o- cells were grown in EMEM medium supplemented with 10% FBS and 1% P/S. Cells were passaged every 3 days with trypsin 0.25% and subcultured in 75 cm^2 flasks. Cells were maintained in a humidified atmosphere at 37°C and 5% CO_2.

2.7 Cellular uptake by flow cytometry

To evaluate the cellular uptake of Alveofact-coated polyplexes, amine-modified siRNA was labeled with succinimidyl ester (NHS) AlexaFluor488 fluorescent dye according to the manufacturer's protocol. The resulting AF488-siRNA was then purified via ethanol precipitation and spin column as previously described (69). H1299 cells were seeded at a density of 50.000 cells/well in 500 µl medium and incubated for 24 h at 37°C and 5% CO_2. The day after, cells were transfected with polyplexes prepared at different Alveofact:PEI coating ratios (0, 1:5, 1:2.5, 1:1, 2.5:1, 5:1) with 50 pmol AF488-siRNA. Positive controls consisted of Lipofectamine 2000 lipoplexes, whereas untreated cells and samples treated with free siRNA were used as negative controls. Cells were incubated for 24 h at 37°C and 5% CO_2. Cells were then harvested, washed in PBS and resuspended in PBS/2mM EDTA for analysis via flow cytometer (Attune NxT, Thermo Fisher Scientific, Waltham, Massachusetts, USA) for the median fluorescence intensity (MFI) of AF488-siRNA using 488 nm excitation and a 530/30 nm bandpass emission

filter. Samples were gated by morphology based on forwards/sideward scattering with a minimum of 10.000 viable cells. Results are displayed as mean values ± SD.

2.8 In vitro GAPDH gene knockdown

For gene silencing experiments, 100.000 16HBE14o- cells were seeded in a 12-well-plate in 1 ml medium and were incubated for 24 h at 37°C and 5% CO_2. The day after, cells were transfected with 100 µl of polyplexes prepared at different Alveofact:PEI coating ratios (0, 1:5, 1:2.5, 1:1, 2.5:1, 5:1) with 100 pmol of GAPDH or scrambled siRNA. Positive controls consisted of Lipofectamine 2000 lipoplexes, while negative controls consisted of untreated cells. After 24 h, cells were harvested and processed to isolate RNA using the PureLink RNA mini kit according to the manufacturer's protocol (Life technologies, Carlsbad, USA) with additional DNase digestion. Afterwards, cDNA was synthesized from total RNA using the high-capacity cDNA synthesis kit (Applied Biosystems, Waltham, Massachusetts, USA). The obtained cDNA was then diluted 1:10 in water and amplified on QuantStudio 3 Real-Time PCR (Thermo Fisher Scientific, Waltham, Massachusetts, USA) using the SYBR™ Green PCR Master Mix (Thermo Fisher Scientific, Waltham, Massachusetts, USA) with primers of human GAPDH (Qiagen, Hilden Germany) and β-actin (Qiagen, Hilden Germany). The RT-qPCR template consisted of an initial denaturation step for 10 min at 95°C, subsequently 40 cycles of 95°C for 15s, annealing and elongation at 60°C for 1 min. Cycle threshold (Ct) values were obtained and GAPDH gene expression was normalized by corresponding β-Actin expression for each sample. The qPCR results were analyzed using the $2^{-\Delta\Delta Ct}$ method and presented as a relative quantity of transcripts. Values are given as mean values ± SEM.

2.9 In vitro cell viability

To evaluate the cell viability after incubation with Alveofact-coated polyplexes, an MTT assay was performed. 16HBE14o- cells were seeded at a density of 10.000 cells/well in 100 µl medium in a 96-well-plate. The day after, cells were then transfected with Alveofact-coated polyplexes at different Alveofact:PEI coating ratios (0, 1:5, 1:2.5, 1:1, 2.5:1, 5:1) containing 20 pmol scrambled siRNA and incubated for 24 h at 37°C and 5% CO_2. Afterwards, medium was removed and replaced with 100 µl of a sterile 0.5 mg/ml 3-(4,5-dimethylthiazol-2-yl)-2,5-diphenyltetrazolium bromide (MTT) solution and incubated for 3 h at 37°C and 5% CO_2. Medium was then removed and 200 µl DMSO was added to dissolve formazan crystals. Absorbance was read at 570 nm using a microplate reader (Tecan, Männedorf, Switzerland). Results are given as mean values of triplicates ± SD.

2.10 Polyplexes behavior in 16HBE14o- cells grown at ALI

2.10.1 16HBE14o- characterization under ALI conditions

16HBE14o- cells were seeded at the density of $3x10^5$ cell/cm^2 on the apical side of Transwell® polyester cell culture inserts (6.5 mm, 0.4 µm pore size) in 100 µl medium. The basolateral compartment was filled with 700 µl medium. After 72 h of incubation (day 3), medium was removed from the apical side while the medium on the basolateral side was replaced with PneumaCult™ ALI medium (Stemcell technologies, Vancouver, Canada) to obtain air-liquid interface conditions. Medium in the basolateral chamber was replaced every two days. To monitor the development of the polarized epithelial layer, transepithelial electrical resistance (TEER) was measured every day starting from day 1 after air-lift, using an EVOM epithelial volt/ohm meter (World Precision Instruments, Sarasota, USA). TEER values were corrected by subtracting the background of an empty Transwell® insert and medium. For the measurement, 200 µl and 700 µl of medium were added to the apical and basolateral side of the insert respectively, and TEER values were recorded using an STX2 electrode following the manufacturer's instructions.

To evaluate the secretion of mucus by 16HBE14o- cells under ALI conditions, an alcian blue staining was performed. 7 days after air-lift, the cell layer was washed three times with PBS and fixed using 4% (v/v) paraformaldehyde for 15 min. Afterwards, the cell layer was washed again with PBS, incubated with 100 µL of alcian blue solution (1% in 3% acetic acid, pH 2.5) (Sigma-Aldrich) for 15 minutes and then washed again 3 times with PBS. The membrane was cut with a sharp point scalpel, mounted on glass slides using FluorSave™ reagent (Merck Millipore, Billerica, USA) and analyzed with a BZ-8100 (Biozero) fluorescence microscope (Keyence, Osaka, Japan).

To confirm the development of tight junctions under ALI conditions, the expression of zonula occludens protein-1 (ZO-1) was investigated by immunohistochemical staining. On day 7 after air-lift, the cell layer was washed 3 times with PBS and fixed in 4% paraformaldehyde for 15 min. After that, the cell layer was rinsed 3 times with PBS and permeabilized with 200 µL 0.3% Tween20 for 10 min. Afterwards, 200 µL of 5% BSA blocking buffer was added to the insert and incubated for 60 min. The membrane was then cut with a sharp point scalpel, placed in a 24-well-plate and incubated overnight with 300 µL of rabbit ZO-1 antibody solution (1:100 dilution in blocking buffer) at 4°C. On the following day, the membrane was washed 3 times with PBS and incubated with 300 µL of AF488 anti-rabbit secondary antibody (1:500 dilution in blocking buffer) for 60 min in the dark. The membrane was then washed 3 times with PBS and incubated with a 0.5

µg/ml 4′,6-diamidino-2-phenylindole (DAPI) solution for 15 min. Afterwards, the membrane was rinsed 3 times with PBS, mounted using FluorSave™ reagent on glass slides and analyzed with an SP8 inverted confocal scanning laser microscope (Leica Camera, Wetzlar, Germany). The images were exported from the Leica Image Analysis Suite and processed with the Fiji distribution of ImageJ.

2.10.2 Cell uptake study

To evaluate the cellular uptake of Alveofact-coated polyplexes in ALI culture, amine-modified siRNA was labelled with succynimidyl ester (NHS) modified AlexaFluo647 dye according to the manufacturer's protocol and subsequently purified via ethanol purification as previously reported (69).

Differentiated 16HBE14o- cells were transfected with polyplexes prepared at different Alveofact:PEI coating ratios (0, 2.5:1, 5:1) with 100 pmol AF647-siRNA and incubated for 24 h at 37°C and 5% CO_2. Afterwards, cells fixed in 4% PFA for 15 min, washed 3 times with PBS and permeabilized with PBS + 0.3% Tween20 for 10 min. Cytoskeleton was then stained by incubation with rhodamine phalloidin for 60 min, followed by nuclei staining with 0.5 µg/ml solution of 4′,6-diamidino-2-phenylindole (DAPI) for 15 min. The membrane was then cut and mounted using FluorSave™ reagent on a glass slide and analyzed with an SP8 inverted confocal scanning microscope (Leica Camera, Wetzlar, Germany). The images were exported from the Leica Image Analysis Suite and processed with the Fiji distribution of ImageJ.

2.10.4 Mucus penetration study

To test the ability of Alveofact-coated polyplexes to cross the mucus layer secreted by 16HBE14o- cells, cells were transfected with Alveofact-coated polyplexes at different Alveofact:PEI ratios (0, 2.5:1, 5:1) containing 100 pmol AF647-siRNA and incubated for 24 h at 37°C and 5% CO_2. Once the incubation time was completed, AF488-wheat germ agglutinin was added to the cells and incubated for 15 min at 37°C and 5% CO_2 to stain the mucus layer. Afterwards, cells were washed 2 times with PBS and the membrane was cut and mounted on glass slides using FluorSave™ reagent. Membranes were immediately analyzed with a SP8 inverted confocal laser scanning microscope (Leica Camera, Wetzlar, Germany). The images were exported from the Leica Image Analysis Suite and processed with the Fiji distribution of ImageJ.

2.10.5 GAPDH knockdown in 16HBE14o- cells at ALI

To measure the transfection efficiency of polyplexes in a mucus-presenting environment, 16HBE14o- cells grown at ALI conditions were transfected with Alveofact-coated polyplexes at different Alveofact:PEI ratios (0, 2.5:1, 5:1) containing 100 pmol GAPDH

or scrambled siRNA and incubated for 24 h at 37°C and 5% CO_2. Positive controls consisted of Lipofectamine2000 lipoplexes while negative controls consisted of blank/untreated cells. Once the incubation time was completed, cells were detached from the membranes and RNA was extracted using PureLink RNA mini kit (Life technologies, Carlsbad, USA) according to the manufacturer's protocol. Samples were then processed for cDNA synthesis and qPCR as described above. Values are given as the mean of triplicates ± SEM.

2.11 Statistics

Statistical analysis was performed with GraphPad Prism 5 software using One-Way ANOVA with Bonferroni post-hoc test, with $p>0.05$ considered not significant (ns), and *p<0.05. **p<0.01, ***p<0.005, **** p<0.001 considered significantly different.

3. Results and Discussion

3.1 Physico-chemical characteristics of Alveofact-coated polyplexes

Size and surface charge of polyplexes regularly requires optimization to achieve efficient delivery to their target cells. In the case of pulmonary administration, the development of a delivery system able to deliver the payload to lung epithelial cells while penetrating the mucus barrier covering the epithelium is a prerequisite not only in the diseased state. In this regard, we aimed at developing Alveofact-coated polyplexes with optimized properties for pulmonary administration.

To achieve a successful coating of polyplexes, we included two sonication steps, a first one for Alveofact alone and a second one after adding Alveofact to siRNA/PEI polyplexes. In a preliminary formulation screening, we tried initially coated polyplexes with a single Alveofact sonication step prior to incubation with siRNA/PEI polyplexes. However, only polyplexes with unfavorable physicochemical properties were obtained (Supplementary Figure 1). Conversely, the inclusion of a sonication step following incubation with lung surfactant resulted indeed in polyplexes with promising physicochemical parameters (Figure 1A). An explanation for this observation could be the fact that Alveofact tends to self-assemble into multilamellar bodies and vesicles, leading to aggregation phenomena that prevent a homogeneous coating of polyplexes, consequently resulting in poor physicochemical parameters (70). The inclusion of a sonication step seemed to favor the formation of smaller and more homogeneous surfactant vesicles, which are better incorporated in the hybrid delivery system (71). First, we investigated the optimal Alveofact:PEI coating ratio required to achieve appropriate physicochemical characteristics. Polyplexes were prepared at different Alveofact:PEI

coating ratios (0, 1:5, 1:2.5, 1:1, 2.5:1, 5:1, 10:1) and investigated in terms of size, PDI and ζ-potential. An N/P ratio of 6 was kept constant throughout the formulation study as it was previously shown to be ideal for pulmonary administration of siRNA/PEI polyplexes (28). As presented in Figure 1A, polyplexes prepared with a coating ratio between 1:5 and 5:1 showed desirable values in terms of size, PDI and ζ-potential. Sizes ranged from 90 to 120 nm, while PDI presented values around 0.2, similarly to uncoated polyplexes. However, polyplexes prepared at a coating ratio of 10:1 displayed extremely increased sizes and PDI as well as a decreased zeta-potential. We hypothesized that the excess of Alveofact used led to agglomeration phenomena, which caused loss of stability of the formulation. Furthermore, we observed that Alveofact coating did not influence the encapsulation efficiency of polyplexes. At N/P 6, only negligible siRNA release less than 0.3 % of the encapsulated siRNA was detected for both coated and uncoated polyplexes (Supplementary Table 1). To confirm the presence of the Alveofact coating, TEM pictures were acquired for uncoated polyplexes and coated polyplexes at the representative Alveofact:PEI ratio of 2.5:1 (Figure 1C-D). The pictures underlined a clear difference between coated and uncoated polyplexes. While Figure 1C represents uncoated polyplexes as dark, homogenous, rounded dots, coated nanoparticles (Figure 1D) present a lighter corona around the dark polymeric core, which can be assumed to be Alveofact coating. However, the surfactant layer is not as defined as the polymeric core, probably due to irregular coating of the polyplexes. The micrographs also reflect the presence of some empty vesicles, which could be a source of increased polydispersity. Nevertheless, the implementation of microfluidics could potentially help in the future to eliminate empty vesicles and to reduce polydispersity (72). A similar experiment was performed by Mousseau *et al*, where a supported lipid bilayer from Curosurf was deposited onto silica nanoparticles (73). The latter study resulted in comparable TEM images. However, while physico-chemical features of silica nanoparticles can be accurately tuned by synthesis, resulting in analogously spherical-shaped nanoparticles, polyplexes are more dynamic in terms of size, shape and morphology due to the fact that electrostatic interaction is the main driving force for polyplex formation.

Since a sonication step was included for preparing Alveofact-coated polyplexes, any detrimental effect of sonication on siRNA integrity was assessed by a gel integrity assay. In this experiment we tested the integrity of siRNA after sonication of uncoated polyplexes and two representative coated formulations (2.5:1 and 5:1). As positive controls, free siRNA and polyplexes incubated in presence of 1 USP unit of heparin were included in the gel (Figure 1E), which was previously identified as the heparin concentration necessary to achieve a complete release of siRNA (Supplementary Figure

2). The experiment confirmed the integrity of siRNA and complete encapsulation following sonication.

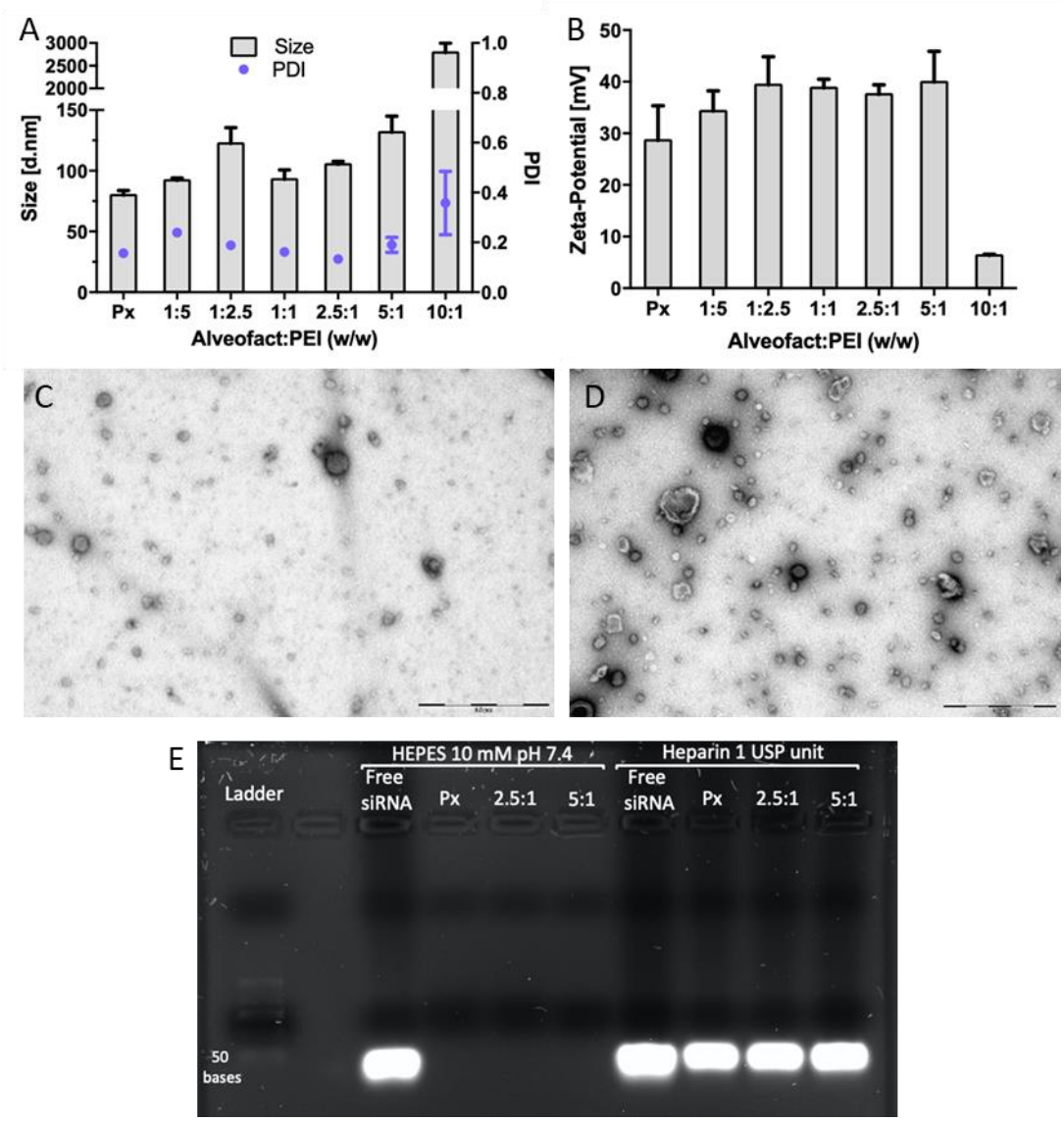

Figure 1. Physico-chemical properties of Alveofact-coated polyplexes. (A) Hydrodynamic diameter and polydispersity index, and (B) ζ-potential of Alveofact-coated polyplexes prepared at N/P 6 in HEPES 10 mM pH 7.4 at different Alveofact:PEI coating ratios. (C,D) TEM images of uncoated and Alveofact-coated and polyplexes, respectively. (E) Agarose gel electrophoresis for integrity tests of Alveofact-coated polyplexes prepared with 100 pmol siRNA. Positive controls consisted of free siRNA, uncoated polyplexes, and Alveofact-coated polyplexes (2.5:1 and 5:1) in 1 USP unit of heparin.

3.2 Stability of polyplexes

One of the main hurdles involved in local administration to the lungs is represented by the mucus barrier of the respiratory tract (74). The mucus layer, especially in chronic obstructive diseases, has a strong impact on the stability of the formulation as well as on

the efficient delivery of the cargo to the cells located below that layer. On this basis, we established a modified gel integrity assay to test the stability of Alveofact-coated polyplexes in presence of mucin, a negatively charged glycoprotein and one of the main components of pulmonary mucus (Figure 2A,B). Due to its negative charge, mucin can potentially negatively impact the stability of polyplexes by replacing siRNA in the formation of the electrostatic interactions with the polymer. In this experiment, uncoated and coated polyplexes (2.5:1 and 5:1 Alveofact:PEI, which represent the coating ratios showing the best performance in terms of activity *in vitro*) were incubated at two different mucin concentrations. As positive controls, polyplexes were incubated with 2 USP heparin to obtain a full release of siRNA. Heparin and mucin are both negatively charged macromolecules or contain such macromolecules. In the reported experiments, heparin was used as a model molecule at concentrations high enough to disrupt polyplexes, a mechanism driven by the replacement of siRNA in the formation of the electrostatic interactions with the cationic PEI (Supplementary figure 2). Therefore, while the heparin concentration was intentionally used at a concentration able to disrupt polyplexes, for mucin a physiologically relevant and not an exaggerated concentration was selected to estimate stability of polyplexes in the lung.

From this experiment, we observed that no free siRNA was detected after incubation with mucin, thereby confirming the stability of polyplexes in presence of increasing concentrations of mucin. Moreover, Alveofact coating did not negatively affect the stability of the formulation in a physiologically relevant condition, confirming the suitability for pulmonary administration.

To assess the colloidal stability of polyplexes over time, the size of polyplexes prepared at different coating ratios was measured at different time points up to 1 week. As it can be observed from Figure 2C-D, the formulations showed constant sizes and PDI over the entire period, with values ranging from 80 to 130 nm and 0.1-0.3, respectively. This experiment confirmed the stability of the formulation over a period of time suitable for formulation studies and excluded any negative influence of Alveofact coating on the stability of the formulation. The results are in line with previous studies suggesting that pulmonary surfactant coating improved the colloidal stability of polymer-based delivery systems and prevented release of siRNA in presence of competing polyanions such as mucin (63). Further studies will be intended to investigate the stability of the formulation for longer times and to develop a spray dried powder for prolonged stability and inhalation based on our previously established spray-drying methodology for siRNA polyplexes (75).

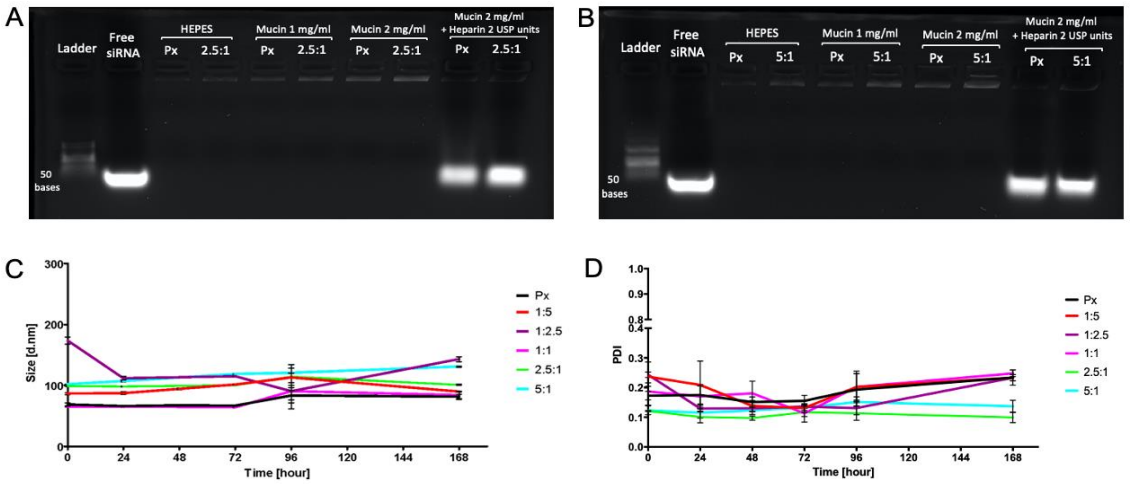

Figure 2. Stability of Alveofact-coated polyplexes. Agarose gel electrophoresis of Alveofact-coated polyplexes encapsulating 100 pmol of siRNA with Alveofact:PEI ratio of 2.5:1 (A) and 5:1 (B) in HEPES, mucin 1 mg/ml and mucin 2 mg/ml. Positive controls consisted of polyplexes in mucin 2 mg/ml and Heparin 2 USP units. (C, D) Hydrodynamic diameter and PDI of Alveofact polyplexes measured at 0 h, 24 h, 48 h, 72 h, 96 h, 168 h at room temperature with exclusion of light.

3.3 In vitro cellular uptake

To investigate the cellular internalization, a human lung epithelial cell line (H1299) was transfected with Alveofact-coated polyplexes at different Alveofact:PEI coating ratios encapsulating Alexa Fluor 488-labeled siRNA. The samples were analyzed by flow cytometry to obtain median fluorescence intensity (MFI) values of the transfected cells. Negative controls consisted of untreated cells as well as free AF488-siRNA, while positive controls consisted of Lipofectamine2000 lipoplexes. The experiment showed a slight improvement in MFI when increasing the Alveofact content for polyplex coating, approximately 10-20% higher in comparison to uncoated polyplexes, yet the differences were not significant. In this regard, De Backer *et al.* (19) reported the reduction in cellular uptake of Curosurf-coated siRNA-loaded nanogels in murine alveolar macrophage cell line due to the anionic pulmonary surfactant shell. Given that our coated polyplexes retained an overall positive charge, it can be deduced that the electrostatic interaction between coated polyplexes and cell membranes was not influenced by the presence of pulmonary surfactant shielding. Undeniably, an increased particle size hampered the internalization process, leading to a sharp drop in MFI at Alveofact:PEI ratio of 10:1. In addition, trypan blue quenching was performed to eliminate extracellular fluorescent signals resulting from siRNA bound to the cell membrane but not internalized by cells. The experiment resulted in no significant MFI differences between quenched and unquenched samples, confirming the cellular internalization of the different formulations tested.

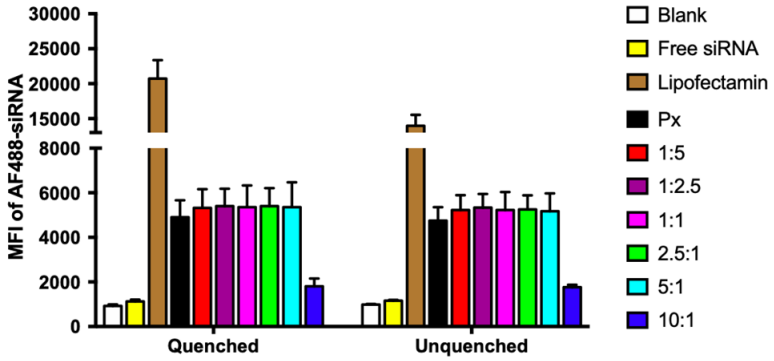

Figure 3. Cellular uptake of Alveofact-coated polyplexes in H1299 cells. Cellular uptake was evaluated after 24 h of transfection with polyplexes encapsulating 50 pmol of AF488-siRNA. Median fluorescence intensity (MFI) was determined by flow cytometry. Negative controls consisted of untreated cells and samples treated with free siRNA. Positive controls consisted of Lipofectamine2000 lipoplexes. Data points indicate mean ± SEM (n=3).

3.4 In vitro transfection efficacy in lung epithelial cells

After confirming the cellular uptake of Alveofact-coated polyplexes, we further evaluated their ability of silencing the endogenously expressed housekeeping gene GAPDH in a more relevant lung epithelial cell line. We chose the human bronchial epithelial cells (16HBE14o-) as they more closely represent the main features of the pulmonary epithelium, particularly since they present tight junction properties, which play a critical role in the barrier of airway lining (76). We anticipated that Alveofact coating might have an impact on tight junction proteins, namely Zonula occludens-1 (ZO-1) and occludin through hydrophobic and hydrophilic interaction (77,78). It is reported that phospholipid content of surfactant might increase epithelial permeability, thus opening tight junctions (79). Furthermore, the proteins present in lung surfactant, like the hydrophobic SP-B and SP-C, play also an important role in increasing cytosolic delivery (80). Consequently, the presence of lung surfactant could be beneficial for improving the internalization of our delivery system might , and siRNA could thereby reach the cytosol more efficiently. Indeed, as illustrated in Figure 4, while Lipofectamine displayed about 41% GAPDH gene silencing, polyplexes at Alveofact:PEI ratios of 2.5:1 and 5:1 significantly mediated GAPDH gene silencing capacity of 72% and 83% respectively. Interestingly, low Alveofact content (Alveofact:PEI ratios of 1:5, 1:2.5, 1:1) did not improve the downregulation efficiency in comparison to uncoated polyplexes but increased GAPDH expression. Therefore, we can conclude that well defined concentrations of Alveofact coating improved the efficiency of the delivery system by mediating a significant downregulation of the target gene.

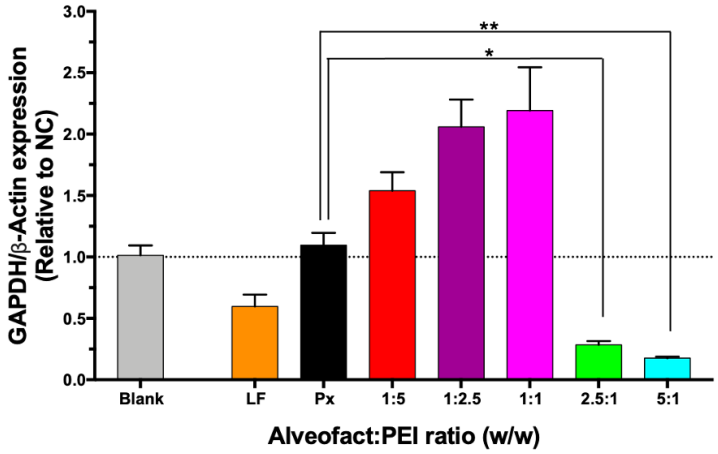

Figure 4. GAPDH gene knockdown of Alveofact coated polyplexes in 16HBE14o- cells. GAPDH gene knockdown efficiency was evaluated 24 h after transfection with polyplexes. Blank samples consisted of 16HBE14o- cells treated with HEPES 10 mM pH 7.4. Negative controls consisted of polyplexes encapsulating scrambled-sequence siRNA. Positive controls consisted of Lipofectamine2000 lipoplexes. GAPDH expression was normalized with β-Actin expression and quantified by qRT-PCR. Downregulation efficiency was displayed by the relative of GAPDH/β-Actin expression of targeting samples normalized to the GAPDH/β-Actin expression after treatment with negative control siRNA in the same formulation. Data points indicate mean ± SEM (n=3). One way ANOVA, * $p < 0.05$, ** $p < 0.01$.

3.5 In vitro cell viability on lung epithelial cells

To test the compatibility of Alveofact coated polyplexes with lung epithelial cells, an MTT assay was performed after incubation with the polyplexes prepared at the different Alveofact:PEI ratios. Viable cells can metabolize the water-soluble MTT into formazan crystals, which serves as an indicator of cell viability (81). Untreated cells and cells treated with 20% DMSO were assigned as 100% cell viability and 100% cell death, respectively. Figure 5 shows the results from the viability assay. All tested formulations showed an overall safe profile in comparison to the cells receiving no treatment. At 10:1 ratio, the large hydrodynamic diameter together with the high concentration of Alveofact, not only hampered the cellular uptake as described above, but also played a deleterious effect on cell growth, resulting in a significant reduction of cell viability. Nonetheless, the formulations with the best performance in terms of activity, 2.5:1 and 5:1 Alveofact:PEI ratio, showed safe profiles with about 85% cell viability.

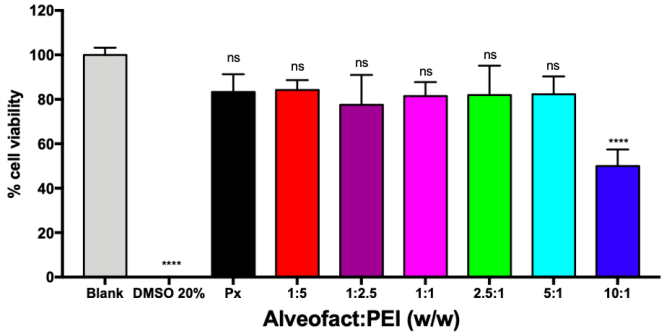

Figure 5. Evaluation of cell viability following the incubation of 16HBE14o- cells with Alveofact-coated polyplexes by MTT assay. 100% cell viability consisted of cells treated with HEPES 10 mM pH 7.4 buffer, while 0% cell viability consisted of cells treated with 20% DMSO. Data points indicate mean ± SEM (n=3). One way ANOVA, ns = not significant, **** $p < 0.001$.

3.6 In vitro delivery of Alveofact-coated polyplexes to an air-liquid interface culture system

After confirming the activity of the Alveofact-coated polyplexes on a lung epithelial cell line, we evaluated their behavior in an experimental setup more closely resembling the *in vivo* environment typical of the airways. When considering pulmonary administration, it is indeed very important to establish an *in vitro* model that includes the hurdles found in the lungs, especially regarding the mucus barrier. In this view, air-liquid interface cultures represent a valid tool for recreating the main features of the respiratory tract *in vitro*. By exposing the cells to the culturing medium on one side and to the air on the other, they can form a pseudostratified epithelium with tight junctions between cells as well as secreting mucus (82). Many studies have shown the suitability of ALI cultures as tools for mimicking healthy and diseased states of the lung, such as cystic fibrosis, asthma or viral infections (45). The 16HBE14o- cell line is also suitable for ALI culture (83). Therefore, we established an ALI 3D culture model with this cell line to test Alveofact-coated polyplexes in a more sophisticated environment. First, we confirmed the formation of the epithelial barrier by measuring TEER values. On day 2 after air-lift, TEER values as high as 1500 $\Omega*cm^2$ were observed, though slightly decreasing after 7 days (Figure 6A). This phenomenon was already reported by previous studies in literature, suggesting that the decline in TEER values did not reflect a compromised cell layer barrier, but was rather caused by increased transcellular conductance (84). Therefore, we confirmed the establishment of a stable epithelial cell layer suitable for further studies. The results were also supported by the expression of tight junctions between cells, as observed by confocal microscopy following ZO-1 staining (Figure 6B). Furthermore, we confirmed the secretion of mucus 7 days after air-lift by alcian blue staining (Figure 6C). By showing the development of high TEER values, tight junctions

and mucus secretion, we confirmed the establishment of a 3D *in vitro* model suitable for further investigation of Alveofact-coated polyplexes.

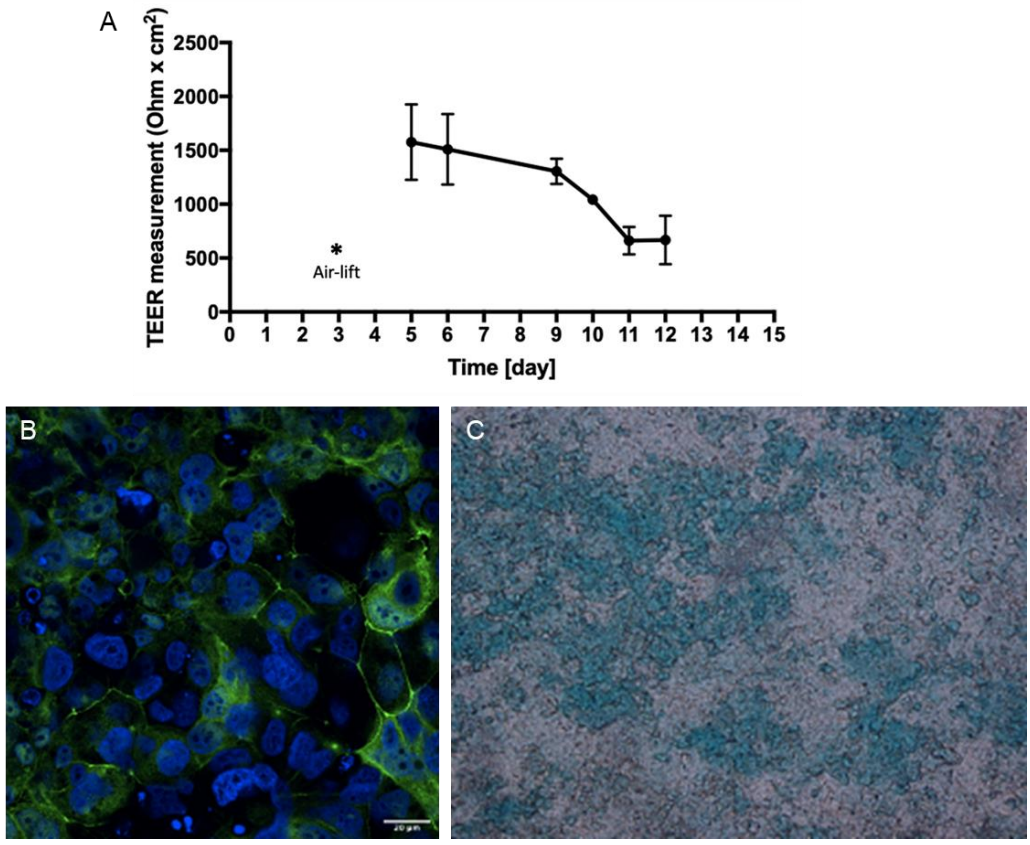

Figure 6. Characterization of 16HBE14o- cell line at the air-liquid interface. (A) TEER values of 16HBE14o- cells at ALI culture for 12 days. Cells were seeded onto Transwell at day 0, inserts were exposed to air (Air-lift) at day 3, and TEER values were measured from day 5. Data points indicate mean ± SD (n=5). (B) ZO-1 staining of 16HBE14o- cells in ALI culture after 7 days of air-lift, bar=20 µm. Green color corresponds to ZO-1 stained with rabbit ZO-1 antibody as primary antibody and AF488-anti-rabbit as secondary antibody (green), while nuclei were stained with DAPI (blue). (C) Mucus staining of 16HBE14o- cells in ALI culture after 7 days of air-lift. Blue color corresponds to mucus.

After the establishment of a 3D air-liquid interface culture of the lung epithelium, we evaluated the behavior of Alveofact-coated polyplexes in terms of cellular uptake, mucus penetration and transfection efficacy. Cell layers were transfected with the formulations showing the best performance in terms of activity in 2D culture (2.5:1 and 5:1 Alveofact:PEI coating ratio) as well as uncoated polyplexes and Lipofectamine2000 lipoplexes as controls. To test the ability of the polyplexes to diffuse through the mucus layer, polyplexes were loaded with a labelled AF647-siRNA, while mucus was stained with AF488-wheat germ agglutinin and the samples were analyzed at a confocal scanning laser microscope. In this study, Lipofectamine2000 lipoplexes as well as PEI polyplexes appeared to great extent trapped in the mucus mesh (Figure 7A-B). On the

other hand, 2.5:1 Alveofact-coated polyplexes (Figure 7C), showed the best performance in terms of mucus diffusion. In fact, while the 5:1 ratio showed a partial entrapment in the mucus mesh similarly to the samples treated with lipofectamine and uncoated polyplexes (Figure 7D), the ones treated with 2.5:1 ratio displayed only negligible entrapment in the mucus. To support these findings, a further staining was performed to better understand the fate of siRNA after crossing the mucus barrier. Here, nuclei (blue) and cytoskeleton (green) were stained, while AF647-siRNA is represented by red dots. In line with the previous results, the best cellular uptake was observed for 2.5:1 Alveofact:PEI coating ratio, followed by lipofectamine lipoplexes, which also reached the cells to some extent (Figure 7E-G). On the contrary, almost no siRNA was detected in the cells after treatment with uncoated polyplexes and 5:1 Alveofact:PEI coated polyplexes (Figure 7H).

After investigating the influence of the mucus layer on the delivery of siRNA to the cells, the consequences on the activity of the formulation were yet to be understood. Therefore, we transfected the cells with an siRNA sequence against GAPDH, as previously tested in 2D culture. Thus, we directly compared the impact of the cellular model on the activity of the formulation. As it can be observed in Figure 7J, the results were in fact quite surprising. While the activity of uncoated polyplexes and Lipofectamine2000 lipoplexes were related to the one observed in the submerged culture, that was not the case for Alveofact-coated formulations. While the 2.5:1 coating retained its activity and achieved about 50% GAPDH downregulation, the 5:1 coating, which showed the best activity in the submerged culture, showed no activity at all. This result can be explained by comparing the activity results to the mucus diffusion study. While the 2.5:1 coating ratio showed an acceptable mucus penetration, the 5:1 formulation seemed to be almost completely entrapped in the mucus mesh, therefore explaining the complete loss of activity in the 3D culture model. The discrepancy observed between the results from ALI experiments and 2D culture (Supplementary Figure 3) as well as in the physicochemical characterization can be explained by the fact that while in the latter the stability of polyplexes were tested in a more artificial and less sophisticated environment, in the former a more complex environment was established for the experiment. In this way, harsher conditions allowed to better define stability and gene silencing efficiency profiles of the different formulations. This study underlines the importance of adopting appropriate models for testing the activity of the formulations, which better predict the *in vivo* activity, such as air-liquid interface cultures (85). Nonetheless, we identified a formulation with potential for pulmonary administration of siRNA, thanks to its improved mucus penetration activity as well as transfection efficacy in a relevant *in vitro* model closely resembling the respiratory tract.

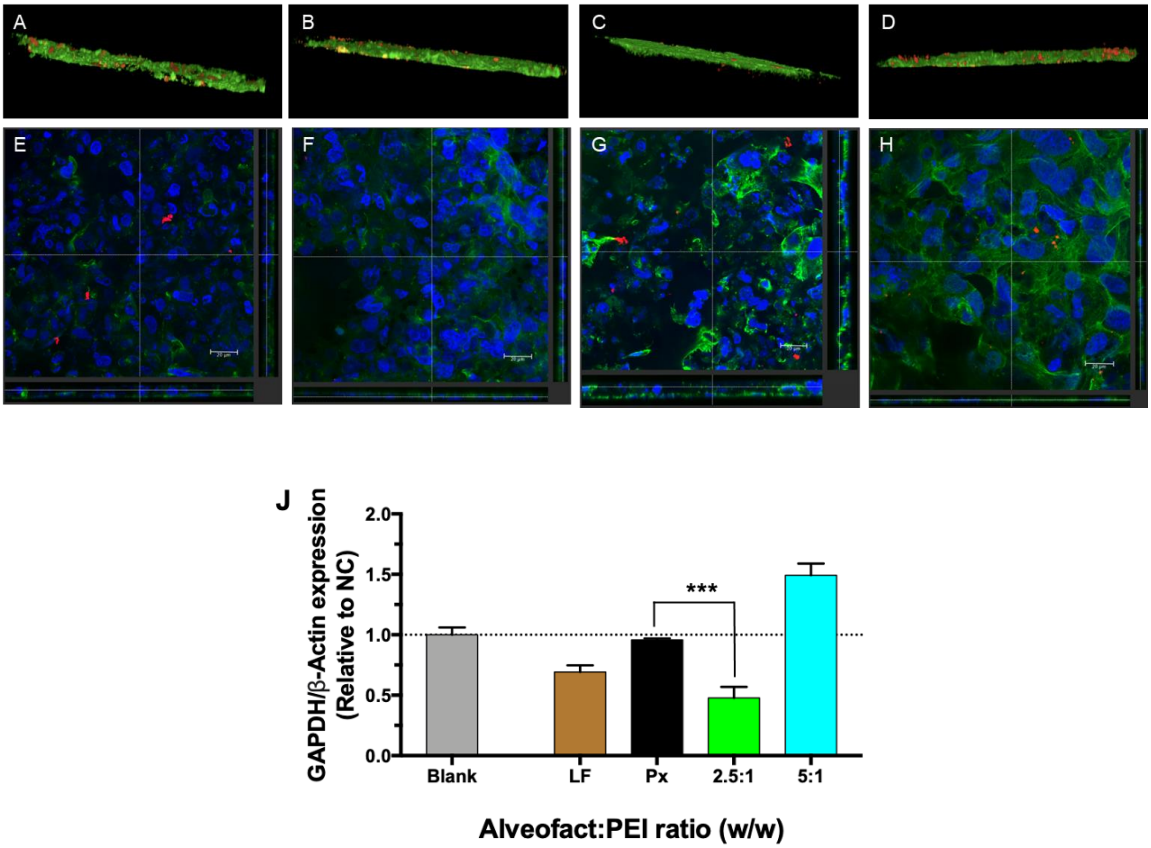

Figure 7. Evaluation of Alveofact-coated polyplexes on 16HBE14o- cells grown at air-liquid interface culture. (A,B,C,D) 3D construction of mucus penetration in 16HBE14o- cells 24h after transfection with uncoated polyplexes, Lipofectamine2000 lipoplexes, Alveofact-coated polyplexes ratio of 2.5:1 and 5:1, respectively. Green represents mucus layer stained with AF488-labeled wheat germ agglutinin, red corresponds to AF647-siRNA. (E,F,G,H) Cellular uptake in 16HBE14o- cells 24h after transfection with uncoated polyplexes, Lipofectamine2000 lipoplexes, Alveofact-coated polyplexes ratio of 2.5:1, and 5:1, respectively. Analysis was performed with confocal light scanning microscopy and images were presented in XY and XZ viewing direction, bar=20 µm. Green corresponds to actin stained with rhodamine phalloidin, red to AF647-siRNA, and blue corresponds to nuclei stained with DAPI. (J) GAPDH gene knockdown efficiency of Alveofact coated polyplexes in 16HBE14o- cells grown in ALI culture 24 h after transfection with siGAPDH and scrambled siRNA as negative controls. Blank samples consisted of 16HBE14o- cells treated with HEPES 10 mM pH 7.4. Positive controls consisted of Lipofectamine2000 lipoplexes. GAPDH expression was normalized with β-Actin expression and quantified by qRT-PCR. Downregulation efficiency was displayed by the relative of GAPDH/β-Actin expression of targeting samples over negative controls. Data points indicate mean ± SEM (n=3). One-way ANOVA, *** $p < 0.005$.

4. Conclusion

In this study, PEI polyplexes were coated with Alveofact, a commercially available pulmonary surfactant, to achieve a formulation for pulmonary administration of siRNA.

The coating process was optimized to achieve a formulation with desirable physicochemical parameters and stability. Alveofact coated polyplexes efficiently delivered siRNA to lung epithelial cells and were well tolerated. Furthermore, an ALI culture of the lung epithelium was established and used to assess the behavior of the newly developed delivery system in a more sophisticated 3D cell culture model. From this study, we identified a formulation able to penetrate the mucus layer as well as to mediate an efficient gene silencing. In summary, these findings show that Alveofact coating of cationic polymers such as PEI represents an appealing strategy to improve the delivery of siRNA to the lungs. Coating with Alveofact could in fact improve two important aspects of PEI-mediated siRNA delivery, that are mucus diffusion and gene silencing activity. The combination of these two aspects led to an overall improved outcome in comparison to uncoated polyplexes, which reinforces the rationale behind using lung surfactant for drug delivery. In conclusion, this study confirms the potential of Alveofact-coated polyplexes for targeting lung epithelial cells and it offers a new formulation strategy for efficient siRNA delivery to the lung.

Acknowledgments

The authors would like to thank Otto Berninghausen from the Gene Center Munich for help with TEM analysis.

Funding

This project was funded by the European Research Council (ERC) under the European Union's Horizon 2020 research and innovation program (Grant agreement No. ERC-2014-StG637830).

Conflict of interest

The authors declare no conflict of interest.

Supplementary information

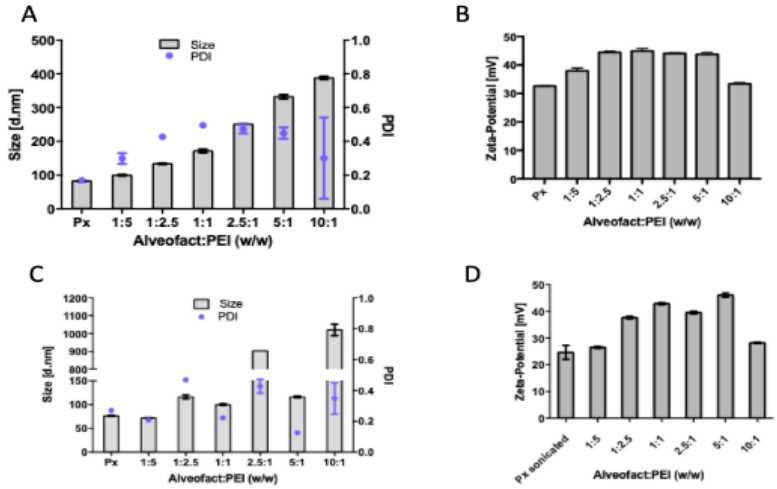

Supplementary Figure 1. Physico-chemical properties of Alveofact-coated polyplexes (A,B) without sonication and, (C,D) with a single Alveofact sonication step prior to incubation with siRNA/PEI polyplexes. (A,C) Hydrodynamic diameter and polydispersity index, and (B,D) ζ-potential of Alveofact-coated polyplexes prepared at N/P 6 in HEPES 10 mM pH 7.4 at different Alveofact:PEI coating ratios.

Alveo:PEI	Px	1:5	1:2.5	1:1	2.5:1	5:1	10:1
% Free siRNA	0.19 ± 0.010	0.18 ± 0.043	0.30 ± 0.159	0.30 ± 0.086	0.158 ± 0.025	0.03 ± 0.027	0.06 ± 0.09

Supplementary Table 1. Evaluation of siRNA condensation efficiency of uncoated polyplexes and Alveofact-coated polyplexes at Alveofact:PEI ratios of 1:5, 1:2.5, 1:1, 2.5:1, 5:1, and 10:1 by SYBR Gold assay. Polyplexes encapsulate 100 pmol of scrambled siRNA in HEPES 10 mM pH 7.4. Free siRNA represents 100% siRNA release. Data points indicate mean ± SD (n=3)

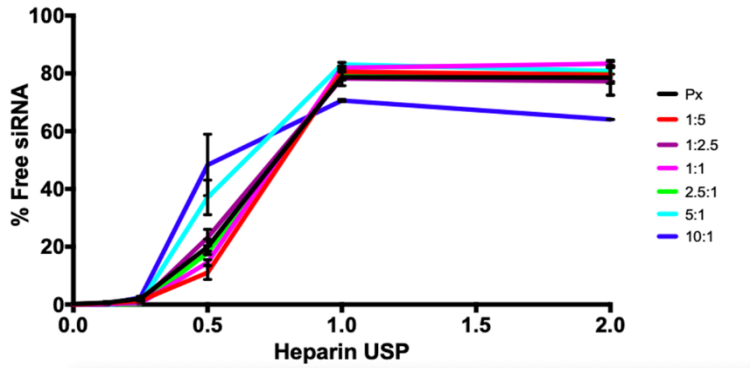

Supplementary Figure 2. Evaluation of siRNA release capacity of uncoated polyplexes and Alveofact-coated polyplexes in HEPES 10 mM pH 7.4 after 30 minutes of incubation with 0.125, 0.25, 0.5, 1, 2 USP units of Heparin by SYBR Gold assay. Free siRNA represents 100% siRNA release. Data points indicate mean ± SD (n=2).

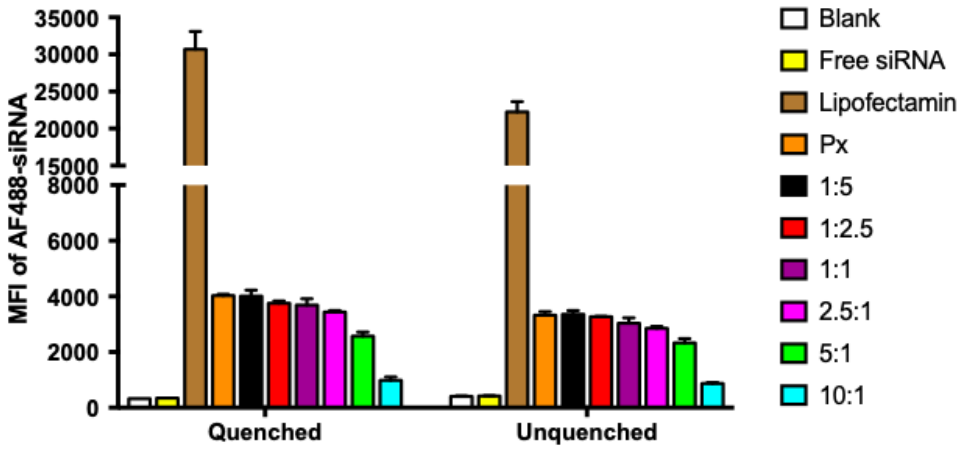

Supplementary Figure 3. Cellular uptake of Alveofact-coated polyplexes in HBEC in 2D culture. Cellular uptake was evaluated after 24 h of transfection with polyplexes encapsulating 50 pmol of AF488-siRNA.

Chapter III - On the effect of helper lipids for pulmonary administration of siRNA-loaded LNPs

Domizia Baldassi[1], Christoph Zimmermann[1], Dominik Witzigmann[2], Olivia M. Merkel[1]

[1]Department of Pharmacy, Pharmaceutical Technology and Biopharmaceutics, Ludwig-Maximilians-University of Munich, Butenandtstraße 5, 81377 Munich, German

[2]Department of Biochemistry and Molecular Biology, University of British Columbia, 2350 Health Sciences Mall, Vancouver, BC V6T 1Z3, Canada; NanoMedicines Innovation Network (NMIN), 2350 Health Sciences Mall, Vancouver, BC V6T 1Z3, Canada; NanoVation Therapeutics Inc., 2405 Wesbrook Mall 4th Floor, Vancouver V6T 1Z3, Canada.

Abstract

Lipid nanoparticles (LNPs) enabled RNA therapeutics to enter clinical practice and established themselves as a safe and effective delivery system for both siRNA and mRNA. Nonetheless, LNP-mediated siRNA delivery has been so far mainly restricted to liver targeting, limiting a broader clinical application. Consequently, research efforts have been devoted to enabling LNPs delivery beyond hepatic tissues. Lung delivery represents an advantageous route of administration as it offers a direct entry port to the lung for the treatment of several pulmonary disorders. On this basis, we investigated LNPs for siRNA delivery to the lungs. More precisely, LNPs were prepared with different helper lipids characterized by different net charges (neutral, positive and negative), and the effects on transfection efficacy and cytotoxicity were investigated in a lung epithelial cell line. LNP delivery was then tested in an air-liquid interface culture of the lung epithelium, where transfection activity and mucus penetration were studied. Furthermore, diffusion profiles as well as interactions with artificial mucus were investigated. This study confirmed that the inclusion of different helper lipids affects siRNA delivery, suggesting that lipids should be carefully selected taking into consideration not only the gene silencing activity, but also the safety and, for lung delivery, mucus diffusion of the formulation. LNPs prepared with a positively charged helper lipid displayed the best *in vitro* gene silencing activity in both 2D and 3D culture (70 and 50 % GAPDH knockdown, respectively) but mediated the highest cytotoxicity. Potency and safety should in fact be thoroughly balanced. Additionally, we emphasized the need for biomimetic models of the lungs to obtain a clearer and more comprehensive picture of the advantages and disadvantages of LNP formulations.

KEYWORDS Lipid nanoparticles, siRNA delivery, pulmonary delivery, helper lipids, air-liquid interface

1. Introduction

Pulmonary administration of siRNA holds great potential for treating several lung diseases, from genetic disorders such as cystic fibrosis to viral infections, cancer, and inflammatory conditions (13). siRNAs can in theory be designed to target and downregulate any target sequence by inducing the RNAi machinery (86). Direct administration to the lungs represents an attractive route of administration thanks to their large epithelial surface, low enzymatic activity and ease of access (22). As of today, five siRNA therapies have entered the market, however, none of them reaches the lungs as they primarily target cell populations in the liver (48,49). Although two clinical trials for intranasal delivery of siRNA were undertaken, none of them led to a successful approval of an siRNA therapy for lung diseases (57). Despite the undeniable advantages, lung delivery indeed presents some major hurdles that prevent the successful delivery and activity of the payload, particularly linked to branching of the airways, mucociliary clearance and mucus barrier (87). The latter represents a crucial obstacle that should be carefully considered when developing formulations for pulmonary administration. The major macromolecular component of mucus is represented by mucins, which are negatively charged glycoproteins that, together with the other components, create a complex, viscoelastic barrier that strongly affects the fate of the drug in the lung (88). In this view, when developing a delivery system for siRNA it is essential to take all these factors into consideration, as it should not only protect the cargo from degradation, but also overcome the barriers found in the lungs (89). In regards to this administration route, research efforts have been focused mainly on the development of polymeric delivery systems such as polyplexes and polymeric nanoparticles, as they can be easily nebulized or further processed to obtain a dry powder for inhalation (53,90,91). The past years have assisted to the rise of lipid nanoparticles as delivery system for RNA therapeutics. To begin with the approval of Onpattro® as the very first siRNA-based therapy and continuing with the approval of the first mRNA vaccines against COVID-19, lipid nanoparticles (LNPs) were established as a powerful tool for the delivery of RNA (92,93). However, their application has been so far intended only for intravenous and intramuscular routes of administration respectively. Additionally, LNP-mediated siRNA delivery has been so far approved only for targeting hepatic tissues, while delivery of LNPs beyond the liver could pave the way to various novel targets and applications (94). In a recent study of ours, we showed that siRNA-loaded LNPs can be successfully spray

dried for dry powder inhalation (32). We confirmed that LNPs retain their physicochemical characteristics as well as activity after spray-drying, highlighting their suitability for pulmonary delivery. Consequently, here we investigated biological aspects of LNPs for pulmonary delivery more deeply, with a special focus on the effect of phospholipids with different charges in LNP structure on cellular delivery and behavior in mucus. LNPs in fact consist of four lipid components: an ionizable cationic lipid, a helper lipid (a phospholipid such as DOPE or DSPC), cholesterol, and a PEG-lipid. The ionizable lipid is responsible for nucleic acid encapsulation and endosomal escape, while PEG-lipids account for LNPs stability during preparation and storage by providing a steric barrier that prevents aggregation. transfection potency. Finally, cholesterol and phospholipids have a structural role and help fusion with the plasma membrane (95). Recently, a study by LoPresti *et al*. demonstrated that altering the surface charge of LNPs with charged helper lipids directs the delivery of mRNA-loaded LNPs towards a specific organ following intravenous administration (96). In line with this observation, we further investigated how the inclusion of helper lipids with different net charges (neutral, negative and positive) in LNPs affects pulmonary delivery of siRNA and their interactions with mucus. In this study, we first analyzed how the different helper lipids affect intracellular deliver, gene silencing activity and biocompatibility *in vitro*, and then proceeded investigating the behavior of LNPs in mucus in an air-liquid interface culture that closely resembles the lung epithelium by expressing tight junctions and secreting mucus (45). Furthermore, a mucus diffusion assay was established and the interactions of LNPs with artificial as well as cellular mucus were analyzed. This study revealed that the presence of helper lipids with different net charges affects the biological behavior of LNPs, and that efficacy and toxicity in the lungs need to be carefully balanced. For instance, while on the one hand the presence of a positive net charge improved the transfection efficiency of LNPs, on the other hand it negatively affected cellular viability. Also, the use of different *in vitro* models led to different and sometimes contrasting outcomes, underlying the importance of selecting different, complementary investigation tools to obtain a clearer and more detailed picture of the LNP formulations under investigation.

2. Experimental methods

2.1 Materials

Paraformaldehyde solution, FluorSave™ Reagent, Tween20, Eagle's Minimum Essential Medium (EMEM), RPMI-1640 Medium, fetal bovine serum (FBS), Penicillin-Streptomycin solution, Dulbecco's Phosphate Buffered Saline (PBS), trypsin-EDTA solution, 200 mM L-glutamine solution, Paraformaldehyde, DMSO, G418 disulfate salt solution, methylthiazolyldiphenyl-tetrazoliumbromid (MTT), trypan blue solution, DiD' dye were purchased from Sigma-Aldrich (Darmstadt, Germany). Lipofectamine 2000, SYBR gold dye, Quant-IT Ribogreen DNA reagent, AF488-anti-rabbit secondary antibody, rhodamine phalloidin, 4′,6–diamidino–2-phenylindole dihydrochloride (DAPI), PowerSYBR Green PCR master mix, Alexa Fluor™ 647 NHS ester and Alexa Fluor™ 488 NHS ester were obtained from Life technologies (Carlsbad, California, USA). Transwell® polyester membrane cell culture inserts (0.4 µm pore size) were purchased from Corning (New York, USA). PneumaCult™ ALI differentiation medium, hydrocortisone and heparin were bought from Stemcell Technologies (Vancouver, Canada). Dicer substrate double-stranded siRNA (DsiRNA) targeting human GAPDH, the enhanced green fluorescent protein gene and non-specific DsiRNA and amine-modified siRNA were purchased from IDT (Integrated DNA Technologies, Inc., Leuven, Belgium). PEG-DMG, DSPC, DOPC, DSPG, DOPG, DSPS, DOPS, DOTAP and DOTMA were obtained from Avanti PolarLipids, Alabaster, USA.

2.2 Preparation and characterization of LNPs

LNP-siRNA formulations had a lipid composition based on the clinically approved Onpattro® formulation and were prepared as previously described (23,97). Briefly, lipid components (ionizable cationic lipid, helper lipid, cholesterol, and PEG-DMG) at molar ratios of 50:10:38.5:1.5mol% were dissolved in ethanol to achieve a concentration of 10 mM total lipid. Different helper lipids, i.e. 1,2-distearoyl-sn-glycero-3-phosphocholine (DSPC), 1,2-dioleoyl-3-trimethylammonium-propane (DOTAP), and 1,2-distearoyl-sn-glycero-3-phospho-(1'-rac-glycerol) (DSPG) were used to enable formation of LNP-siRNA systems with slightly different zeta potential as previously reported by Zimmermann *et al.* (32). Purified siRNA (siNC, siGFP and siGAPDH) was dissolved in 25 mM sodium acetate pH 4 buffer to achieve an N/P ratio of 3. The two solutions were mixed through a T-junction mixer at a total flow rate of 20 mL/min, and a flow rate ratio of 3:1 v/v (aqueous:organic phase). The resulting LNP suspension was subsequently dialyzed overnight against PBS pH 7.4, sterile filtered (0.2 µm), and concentrated to 1.0 mg/mL siRNA. Encapsulation efficiencies of siRNA in all LNP systems were above 95% measured by the Quant-iT Ribogreen Assay (Life Technologies).

LNPs were then diluted in final formulation buffer (PBS for characterizations studies, cell culture medium for *in vitro* experiments) and incubated for additional 20 min at room temperature.

2.3 *In vitro* characterization of LNPs on lung epithelial cells

2.3.1 Cell culture

The human 16HBE14o- cell line was cultivated in EMEM medium supplemented with 10% FBS and 1% P/S. The human non-small lung carcinoma cell line H1299-GFP was grown in RPMI-1640 medium supplemented with 10% FBS and 1% P/S. Cells were passaged every 3-4 days upon reaching confluence with trypsin 0.25% and 0.05%, respectively, and subcultured in 75 cm^2 flasks. Cells were maintained in a humidified atmosphere at 37°C and 5% CO_2.

2.3.2 Cellular uptake

To determine the cellular uptake of LNPs, amine-modified siRNA was labeled with succinimidyl ester (NHS-AlexaFluor488 fluorescent dye according to the manufacturer's protocol. The resulting AF488-siRNA was purified by ethanol precipitation and spin column as previously reported (69). 16HBE14o- cells were seeded in a 24-well-plate at a density of 50.000 cells/well in 500 µl medium and incubated overnight at 37°C and 5% CO_2. Afterwards, cells were transfected with AF488-siRNA loaded LNPs at a final concentration of 1 µg/mL of siRNA and incubated for 24 h at 37°C and 5% CO_2. Once the incubation time was completed, cells were harvested, washed in PBS and resuspended in PBS/2mM EDTA for analysis via flow cytometry. Positive controls consisted of Lipofectamine2000 lipoplexes, whereas untreated cells and cells treated with free siRNA were considered negative controls. For trypan blue quenching, 0.4% trypan blue was added to half of each sample to mask any extracellular fluorescence signal. The median fluorescence intensity of AF488-siRNA was measured using 488 nm excitation and a 530/30 bandpass emission filter. Samples were gated based on forward/sideward scattering of cells with a minimum of 10.000 viable cells. Results are displayed as mean values ± SD (n=3).

2.3.3. GAPDH gene knockdown

To determine the gene silencing activity of LNPs, 16HBE14o- cells were seeded in a 12-well-plate at a seeding density of 100.000/well in 1 mL medium and were incubated for 24 h at 37°C and 5% CO_2. Then, cells were transfected with the different LNP formulations (LNP1-8) loaded with scrambled or GAPDH siRNA. Each formulation was tested at the siRNA concentration of 1 µg/mL. Positive controls consisted of Lipofectamine2000 lipoplexes. After 24 h, cells were harvested and further processed to isolate RNA using the the PureLink RNA mini kit according to the manufacturer's protocol

(Life technologies, Carlsbad, USA). Next, cDNA was synthesized from total RNA using the high-capacity cDNA synthesis kit (Applied Biosystems, Waltham, Massachusetts, USA). cDNA was then diluted 1:10 in water and a qPCR was performed with the SYBR™ Green PCR Master Mix (Thermo Fisher Scientific) on a qTOWER real-time PCR thermal cycler (Analytik Jena, Jena, Germany). Primers for human GAPDH (Qiagen, Hilden, Germany) and β-actin (Qiagen, Hilden Germany) for normalization were used. Cycle thresholds were acquired by auto setting within the qPCR software (Analytic Jena AG, Jena, Germany). Values are given as mean values ± SEM. (n=3).

2.3.4 GFP protein downregulation

To evaluate the protein downregulation activity of LNPs, H1299/GFP cells were utilized. H1299/GFP cells were seeded on a 24-well-plate at a seeding density of 25.000 cells/well in 500 µL of medium. Cells were cultured for 24 h at 37°C and 5% CO_2. The day after, cells were transfected with the different LNPs (LNPs 1-8) loaded with scrambled or GFP siRNA sequences. Each condition was tested at the siRNA concentrations of 0.1 and 1 µg/mL. Cells were incubated for 48 h at 37°C and 5% CO_2. Once the incubation time was completed, cells were harvested, washed with PBS and resuspended in PBS/2mM EDTA for analysis via flow cytometry (Attune NxT, Thermo Fischer Scientific, Waltham, Massachusetts, USA). The median fluorescence intensity of GFP protein expression was detected at 488 nm excitation and with a 530/30 nm bandpass emission filter. Each sample was gated by morphology based on forward/sideward scattering with a minimum of 10.000 viable cells. Results are displayed as mean values ± SD. (n=3).

2.3.5 In vitro cytotoxicity in lung cells

2.3.5.1 Cell viability

To assess the effect of LNPs on metabolic activity, an MTT assay was performed. 16HBE14o- cells were seeded in a 96-well-plate at a density of 10.000 cells/well in 100 µl of medium and cultured for 24 h at 37°C and 5% CO_2. The day after, cells were transfected with the different LNPs (1-8) loaded with scrambled siRNA. Each formulation was tested at the siRNA concentrations of 0.1, 1 and 3 µg/mL. Cells were incubated for 24, 48 and 72 h at 37°C and 5% CO_2. Afterwards, medium was removed and replaced with 100 µl of a sterile 0.5 mg/mL 3-(4,5-dimethylthiazol-2-yl)-2,5-diphenyltetrazolium bromide (MTT) solution and incubated for 3 h at 37°C and 5% CO_2. Medium was then discarded and 200 µl DMSO were added to dissolve formazan crystals. Absorbance was read at 570 m using a microplate reader (Tecan, Männedorf, Switzerland). Results are given as mean values of triplicates ± SD. (n=3)

2.3.5.2 LDH release

The influence of LNPs on cellular membrane integrity was evaluated by determining the release of lactate dehydrogenase in the extracellular medium with a CytoTox96® Non-Radioactive Cytotoxicity Assay kit (Promega, Madison, Wisconsin, USA) according to the manufacturer's protocol. Briefly, 16HBE14o-cells were seeded in a 96-well-plate at a seeding density of 10.000 cells/well in 100 µl medium and cultured for 24 h at 37°C and 5% CO_2. Afterwards, cells were transfected with the different LNP formulations (LNP 1-8) loaded with scrambled siRNA. Each formulation was tested at the siRNA concentrations of 0.1, 1 and 3 µg/mL. Cells were incubated for 24, 48 and 72 h at 37°C and 5% CO_2. Once the incubation time was completed, 50 µl of medium was collected and transferred to a fresh 96-well-plate. To each well, 50 µl of substrate mix was then added and incubated for 30 min at room temperature protected from light. Finally, 50 µl of stop solution was added and absorbance was detected at 490 nm using a microplate reader (Tecan, Männedorf, Switzerland). Cells treated with lysis buffer were served as positive controls (100% LDH release), while untreated cells were considered negative control. Results are given as mean values ± SD. (n=3).

2.4 LNPs behavior in mucus-secreting Calu-3 cells grown at the air-liquid interface

2.4.1 Cell culture

Calu-3 cells were obtained from LGC Standards GmbH (Wesel, Germany). Cells were cultivated in EMEM medium supplemented with 10% FBS and 1% P/S. Cells were passaged once 80% confluences was reached and subcultured in 75 cm^2 flasks. Cells were maintained in a humidified atmosphere at 37°C and 5% CO_2.

For ALI experiments, Calu-3 cells were seeded on Transwell® polyester cell culture inserts (6.5 mm, 0.4 µm pore size) at a seeding density of 250.000 cells/well in 100 µl medium, while 700 µl medium were added to the basolateral chamber. After 72 h, the medium on the apical chamber was removed, while the one on the basolateral chamber was replaced with 200 µl of PneumaCult™ ALI medium (STEMcell technology, Vancouver, Canada) and exchanged every two days. Experiments were performed once TEER values ≥ 300 Ω*cm^2 were achieved and a stable, polarized epithelial layer was formed, as measured with an EVOM epithelial volt/Ω meter (World Precision Instruments, Sarasota, USA).

2.4.2 Mucus penetration study

To test the LNPs' permeation activity in cellular mucus, Calu-3 monolayers were transfected with AF647-loaded LNPs at a concentration of 3 µg/mL and incubated for 24 h at 37°C and 5% CO_2. The day after, cells were incubated with AF488-wheat germ agglutinin for 15 min at 37°C and 5% CO_2 to stain the mucus layer secreted by the cells. Cells were then washed two times with PBS and mounted on glass slides using FluorSave™ reagent and immediately analyzed with an SP8 inverted confocal scanning laser microscope (Leica Camera, Wetzlar, Germany). Images were exported from the LEICA Image Analysis Suite and processed with the Fiji plug-in of ImageJ.

2.4.3 GAPDH knockdown in Calu-3 cells at ALI

To evaluate the transfection efficacy of LNPs in ALI-cultured cells, Calu-3 monolayers were transfected with LNPs loaded with scrambled and GAPDH siRNA at a concentration of 10 µg/mL for 24 h at 37°C and 5% CO_2. Positive controls consisted of Lipofectamine2000 lipoplexes while untreated cells were considered negative controls. Cells were then harvested, and RNA was isolated using the PureLink RNA mini kit according to the manufacturer's protocol. Samples were then processed for cDNA synthesis and for qPCR as described above. Values are given as mean ± SEM. (n=3)

2.5 LNPs characterization in a lung-simulating environment

2.5.1 In vitro transport of LNPs through artificial mucus

The diffusion of LNPs through artificial mucus was tested based on a previously developed Transwell® diffusion assay (34). Briefly, 75 µl of artificial mucus were placed on the apical side of a Transwell chamber (6.5 mm, 8 µm pore size). Afterwards, the different LNPs (1-8) were prepared at a concentration of 3 µg/mL and marked with 1 µl of DiD' dye, a fluorescent lipid marker. In each well, 100 µl of the different marked LNPs were placed on top of the mucus layer, while 300 µl of simulated lung interstitial fluid (SILF) was added to the basolateral chamber. SILF was prepared based on a previously reported protocol (98)(34). At scheduled time points (0.5, 1, 2, 3, 4 and 24 h), the acceptor medium was collected and stored at 4 °C protected from light for further analysis. Non-deposited samples were stored at 4°C until analysis as reference values. The diffusion of LNPs was evaluated by spectrofluorimetric analysis of DiD' dye at λ_{ex} 644 nm/λ_{em} 665 nm using a microplate reader (Tecan, Männedorf, Switzerland). LNP diffusion was determined by normalizing values from penetrated samples to the initial dose of DiD'-LNPs. Values are given as mean ± SD. (n=3)

2.5.2 Interaction of LNPs with artificial and cellular mucus

The effect of the lung environment on LNPs stability was assessed using DLS by comparing size and PDI of LNP dispersions in PBS, SILF and artificial mucus. SILF and artificial mucus were prepared as described above. Results are reported as mean ± SD calculated on three different batches.

Cellular mucus samples were obtained by harvesting mucus secreted by Calu-3 cells grown at the air-liquid interface. Briefly, Calu-3 cells were seeded on Transwell® filters (6.5 mm, 0.4 µm pore size) and grown to achieve a differentiated muco-ciliary airway epithelium as described above. After 1 week of ALI culture, secreted mucus was collected once a week by washing the apical side with 100 µl PBS and incubating PBS and mucus for 30 min at 37 °C before removal. Mucus was then spun down at 400 g for 5 min to remove debris before it was pooled and stored at -80°C.

Harvesting of mucus was confirmed by alcian blue staining of Calu-3 cells before and after mucus removal as previously reported (35). Briefly, the cell layer was fixed with 4% PFA for 15 min, washed with PBS and incubated with 100 µl of alcian blue solution (1% in 3% acetic acid, pH 2.5) for 15 min and washed again 3 times in PBS. The membrane was then cut, mounted on glass slides using FluorSave™ reagent and analyzed with a BZ-8100 (Biozero) fluorescence microscope (Keyence, Osaka, Japan).

To evaluate the interaction between LNPs and cellular mucus, LNPs were incubated for 1 h with cellular mucus or PBS at room temperature and the resulting size distribution was evaluated by nanoparticle tracking analysis (NanoSight, Malvern Analytical, Malvern, UK).

2.6 Statistics

Statistical analysis was performed with GraphPad Prism 5 software using One-Way ANOVA with Turkey post-hoc test with $p<0.05$ considered not significant (ns) and *$p<0.05$, **$p>0.01$, ***$p>0.005$ considered significantly different.

3. Results

3.1 In vitro cellular uptake in lung epithelial cells

In this study, we investigated the effect of helper lipids on the delivery of lipid nanoparticles to the lung. We started from a library of eight different formulations, which were all prepared with the same components apart from the helper lipid. The phospholipids selected were supposed to have an overall neutral (LNP1-2), negative (LNP3-6) and positive (7-8) charge. Comparing the formulations, we investigated different *in vitro* aspect that are determine activity and safety. We investigated the cellular uptake of LNPs in a human lung bronchial epithelial cell line, which we used as a surrogate for lung epithelium due to its tight junction development (76). LNPs were loaded with AlexaFluor488-siRNA and the samples were analyzed by flow cytometry to determine intracellular uptake 24 h after transfection. Negative controls consisted of untreated cells as well as cells treated with free AF488-siRNA. Positive controls comprised samples treated with lipofectamine/siRNA lipoplexes. As shown in Figure 1, positively charged phospholipids (LNP7-8) mediated a significantly higher uptake than neutral (LNP 1-2) and negatively charged (LNP 7-8) ones, with values comparable to those reached by the positive control lipofectamine. This can be explained by the fact that the presence of a positive charge in the structure of the nanocarrier improves the electrostatic interaction with the negatively charged cellular membranes and consequently facilitates the endocytosis of the nanoparticles (99). Of note, both positively charged phospholipids, DOTAP and DOTMA, mediated a comparable cellular uptake, without major difference among the resulting MFI values. Furthermore, trypan blue quenching was performed to exclude extracellular fluorescence signals resulting from siRNA bound to the cellular membrane. The experiment showed no relevant MFI variations between quenched and unquenched samples for all tested formulations, confirming the cellular internalization of LNPs. This experiment underlined the beneficial effect arising from the inclusion of positively charged helper lipids in LNPs formulation for improving LNP internalization and thus siRNA delivery.

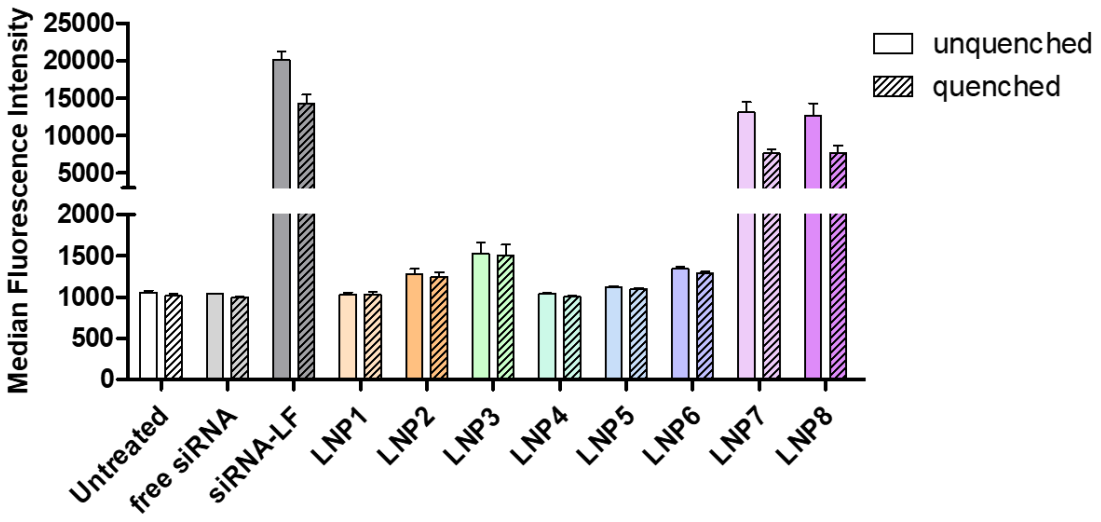

Figure 4. Cellular uptake of LNPs in 16HBE14o- cells. Cellular uptake was evaluated after 24 h of transfection with LNPs at a final concentration of 1 µg/ml of AlexaFluor488-siRNA. Median fluorescence intensity (MFI) was determined by flow cytometry. Negative controls consisted of untreated cells and samples treated with free siRNA. Positive controls consisted of Lipofectamine2000 lipoplexes. Data points indicate mean ± SD (n=3).

3.2 In vitro transfection efficacy in lung epithelial cells

After observing the effect of helper lipids on cellular uptake, we investigated if this effect was also reflected on gene silencing efficacy. To do so, 16HBE14o- cells were transfected with the different LNPs loaded with an siRNA sequence targeting GAPDH, an endogenously expressed housekeeping gene, or scrambled siRNA as negative control. Positive controls consisted of cells treated with siRNA/lipofectamine lipoplexes. Gene silencing after 24 h of incubation corroborated the findings from the uptake study. LNPs prepared with positively charged helper lipids, LNPs 7-8, showed the best downregulation activity, with knockdown values close to 75%, similarly to the one observed for the positive control lipofectamine. LNPs prepared with neutral phospholipids DSPC and DOPC (LNP 1-2), still exerted an effect, but more limited in comparison to the positively charged ones, with values not exceeding 50% of knockdown. As for LNPs prepared with negatively charged helper lipids (LNP3-6), variable outcomes were observed depending on the phospholipid employed. Here, LNPs prepared with saturated negatively charged lipids DSPS and DOPS (LNP 5 and 6) were slightly more potent in comparison to the ones containing unsaturated negatively charged lipids DSPG and DOPG (LNP 3 and 4). Although unsaturated lipids are known to improve endosomal escape (100), the presence of saturated lipids might have improved the overall stability of the formulation for more efficacious delivery and intracellular activity (Figure 2A). A similar behavior was observed also on the protein level (Figure 2B-C). For this experiment, a lung epithelial cell line stably expressing GFP

(H1299/GFP) was used, and the activity of LNPs was determined by quantifying the median fluorescence intensity of the different samples after treatment with two different siRNA concentrations, 0.1 (Figure 2B) and 1 µg/mL (Figure 2C). At the higher concentration tested, no difference among LNPs was observed, as they all showed very high gene silencing activity close to 100%. However, at the lower concentration tested, clearer differences were distinguished among the formulations. A comparable trend to the GAPDH downregulation study was observed, as positively charged LNPs exerted the best gene silencing activity, with values comparable to lipofectamine. Lipofectamine is indeed a cationic transfection reagent that takes advantage of its positive charge to encapsulate nucleic acids and then disrupt the endosomal membrane by a proton sponge effect. In a similar way, the presence of a cationic lipid in LNPs led to transfection activities comparable to lipofectamine (101). In line with the cellular uptake study, LNPs containing a cationic lipid show the best downregulation activity, with particularly high transfection efficiency even at low siRNA concentrations.

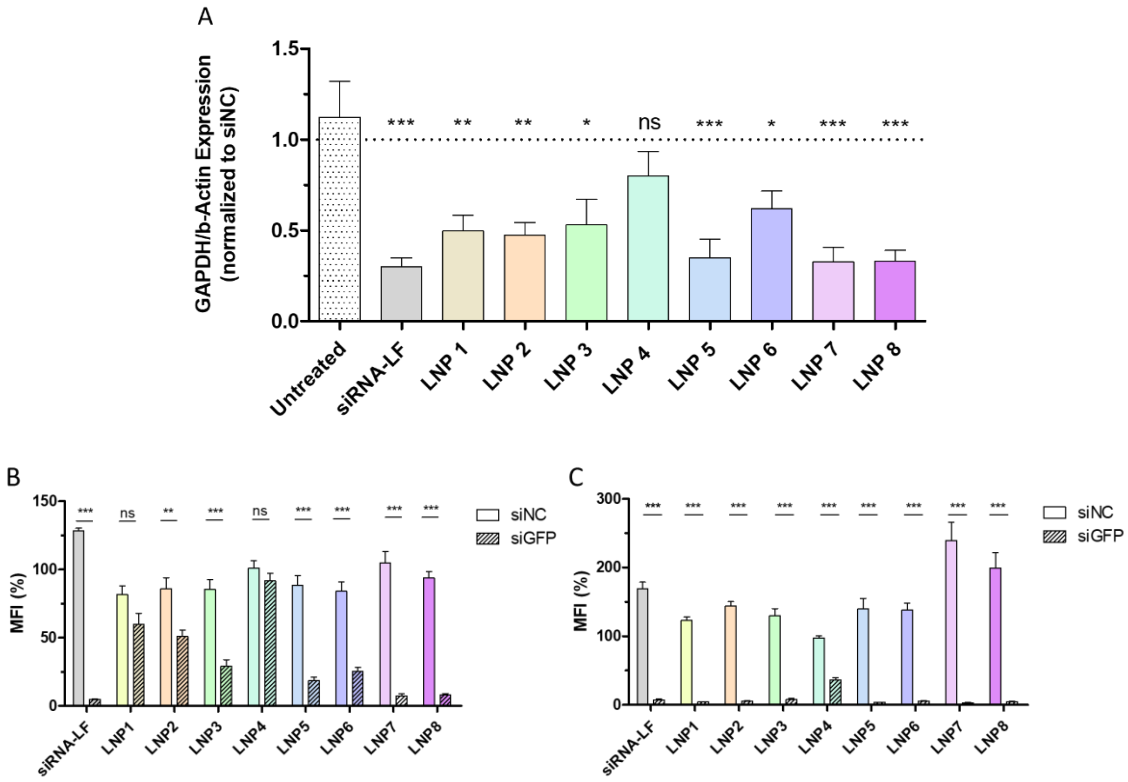

Figure 5. *In vitro* downregulation activity of LNPs. (A) GAPDH gene knockdown efficiency of LNPs in 16HBE14o- cells 24 h after transfection. Negative controls consisted of LNPs encapsulating scrambled siRNA. Positive controls consisted of siGAPDH/Lipofectamine2000 lipoplexes. GAPDH expression was normalized with β-Actin expression and quantified by qRT-PCR. Downregulation efficiency was displayed by relative GAPDH/β-Actin expression of targeting samples normalized to the GAPDH/β-Actin expression after treatment with negative control siRNA in the same formulation. Data points indicate mean ± SEM (n=3). One way ANOVA, * $p < 0.05$, ** $p < 0.01$, ***$p < 0.005$. (B-C) GFP knockdown was tested on H1299 cells

stably expressing EGFP and measured by flow cytometry 48 h after transfection with LNPs encapsulating siGFP at a final concentration of 0.1 µg/ml (B) or 1 µg/ml (C). Negative controls consisted of LNPs encapsulating scrambled siRNA. Positive controls consisted of siGAPDH/Lipofectamine2000 lipoplexes. Data points indicate mean ± SEM (n=3). One way ANOVA, * $p < 0.05$, ** $p < 0.01$, ***$p < 0.005$. SF = free siRNA. SL = lipofectamine/siRNA lipoplexes.

3.3 In vitro cytotoxicity in lung epithelial cells

A suitable nanocarrier should ensure an efficient delivery of the payload, but equally important is also for it to retain a safe, biocompatible profile. To understand if and how the incorporation of phospholipids with different net charges affected LNP biocompatibility, 16HBE14o- cells were incubated with LNPs (1-8) at distinct concentrations and incubation times. The effect on metabolic activity was evaluated in MTT assays, in which water-soluble MTT is metabolized into formazan crystals by viable cells (Figure 3A-C). Each formulation was tested at three siRNA concentrations (0.1, 1 and 3 µg/mL) as well as three incubation times (24, 28 and 72 h). The study showed that all formulations retained a safe profile over time at the lowest concentration tested, with values in the range of 100% cell viability. However, at higher concentrations, contrasting behaviors were observed for the formulations. LNPs prepared with neutral phospholipids DSPC and DOPC (LNP1 and 2) revealed the safest profile, as their addition to cells mediated viability values close to 100% at all tested concentrations and time points. LNPs comprising neutral helper lipids have been proven to retain an extraordinarily safe profile that resulted in the clinical development of Onpattro® (23). LNPs prepared with anionic lipids (LNP3-6) also retained a safe profile over time, with values slightly decreasing at longer incubation times. On the contrary, LNPs prepared with the cationic lipids DOTAP and DOTMA (LNP 7-8), revealed contrasting results depending on the concentration tested. While at the lowest concentration tested the formulations maintained high cell viability values over time, at higher concentrations the viability values decreased proportionally to incubation time. Although a positive surface charge leads to better transfection efficacy, it is also linked to higher toxicity and side effects (102). Positive charges can in fact damage the plasma membrane and lead to toxic effects. Cationic lipids are indeed known for toxicity problems, which has been the main factor limiting their application as delivery systems (103,104). This prompts the importance of properly balancing efficacy and toxicity.

To confirm the results of the MTT assay, and LDH assay was performed to evaluate the cytotoxicity derived from cellular membrane damage (Figure 3D-F). In line with the previous results, LNPs prepared with neutral and negative phospholipids reported a safe profile at the different concentrations tested over time, with values below 20% of cytotoxicity. However, LNPs formulated with cationic phospholipids also demonstrated

cytotoxic effects at higher concentrations and increasing over time in this assay. According to the results from the safety studies, it is of the essence to identify the right balance between activity and safety of the delivery system.

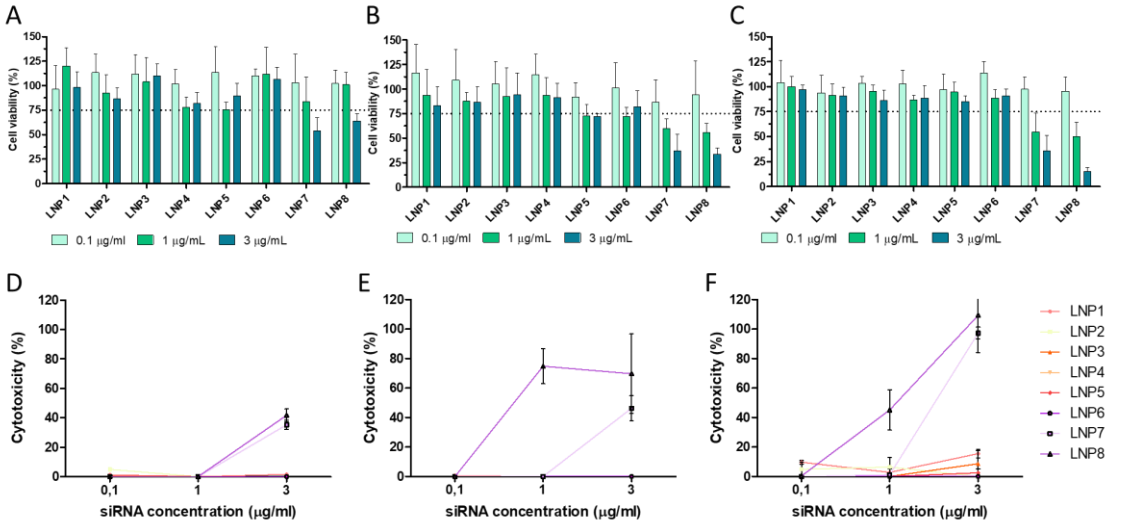

Figure 3. Evaluation of cytotoxicity following incubation with LNPs. (A-C) Evaluation of cellular viability by MTT assay in 16HBE14o- cells incubated with LNPs at 0.1, 1 and 3 µg/ml for 24 (A), 48 (B) and 72 (C) h. Data points indicate mean ± SD (n=3). (D-F) Assessment of membrane integrity by measuring lactate dehydrogenase release of cells incubated with LNPS at 0.1, 1 and 3 µg/ml for 24 (D), 48 (E) and 72 (F) h. Cells treated with lysis buffer correspond to 100% LDH release. Data points indicate mean ± SD (n=3).

3.4 LNPs delivery in an air-liquid interface culture system

To better predict the behavior of LNPs in the respiratory tract, we established an air-liquid interface cell culture model, a valid tool for reproducing *in vitro* the lung environment (82). By growing cells on Transwell® inserts, they are exposed on one side to the air and to cell culture medium on the other. This condition resembles the one found in the airways and allows the cells to differentiate and form a pseudostratified epithelium, which closely replicates the *in vivo* state typical of the lung epithelium. In this context, Calu-3 cells, an immortalized lung epithelial cell line, are considered the golden standard for ALI cultures, as they form tight junctions, reach high TEER values and secrete mucus once cultured under ALI conditions (105), which was confirmed in a previous study of ours (55). After establishing the Calu-3 ALI model, we investigated the diffusion of LNPs through the mucus layer secreted by Calu-3 cells. The mucus barrier is indeed considered one of the main factors preventing delivery to the lungs and transmucosal delivery in general (106). In this study, we selected three different LNPs among the ones screened in the previous experiments, including formulations with a neutral, negative and positive phospholipid, respectively. Thus, we studied how the presence of helper lipids with different charges affected mucus penetration. LNPs were prepared with a

fluorescently labelled siRNA and the mucus was later stained with AF488-wheat germ agglutinin 24 h after transfection. As shown in Figure 4, LNPs prepared with a positively charged phospholipid showed the best diffusion through the mucus layer (Figure 4C-F), while limited diffusion was observed for LNPs comprising neutral (Figure 4A-D) and negative (Figure 4B-E) helper lipids. Although one could suppose that the apparent better diffusion of LNP(+) could be linked to the LNPs being stuck to the mucus, the activity study confirmed that the LNPs(+) not only had the best mucus diffusion, but also performed best in terms of gene downregulation (Figure 4G). Interestingly, LNP(-) completely lost activity in this model, although demonstrating a significant downregulation in the 2D culture model (LNP5).

This finding is quite interesting, as it goes against the common assumption that negatively charged nanoparticles penetrate better though mucus (107). An explanation could be found in the fact that the mucus layer might have reduced the penetration of all LNPs tested, however, the ones presenting the cationic phospholipids proved to retain higher uptake and stronger downregulation activity even at low concentration. In this view, we can assume that the higher potency of positively charged LNPs favored the activity of LNPs in a difficult-to-transfect context where a mucus barrier restricted the delivery to the underlying epithelium.

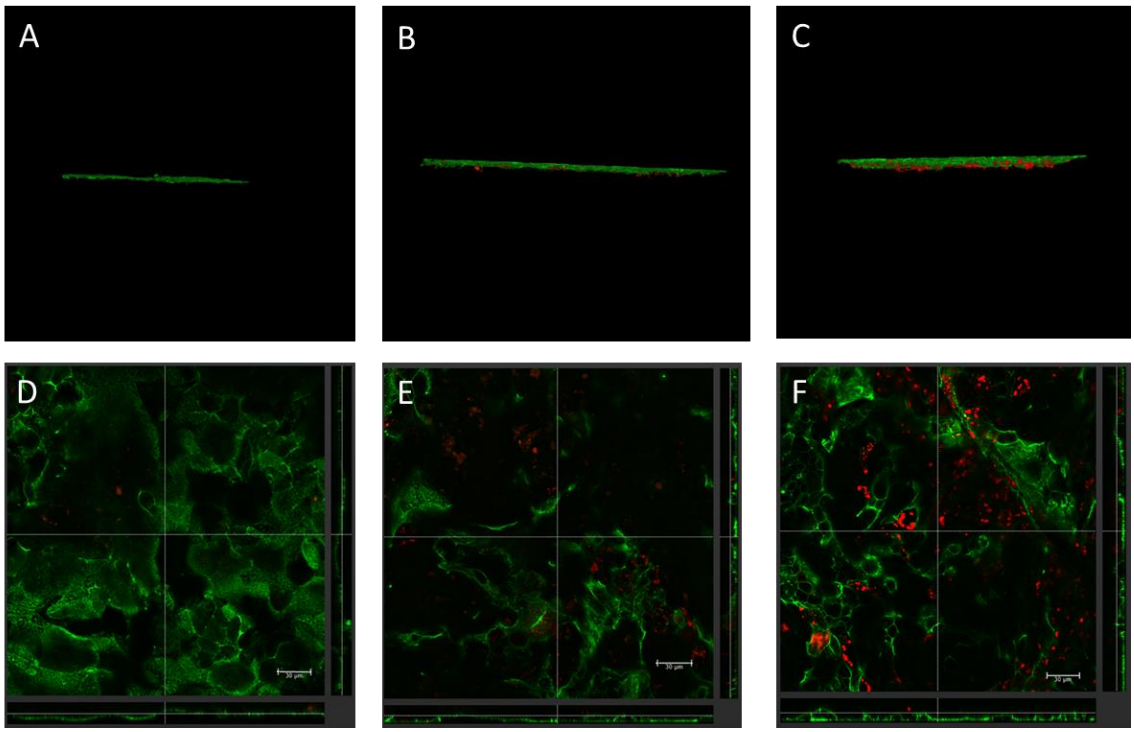

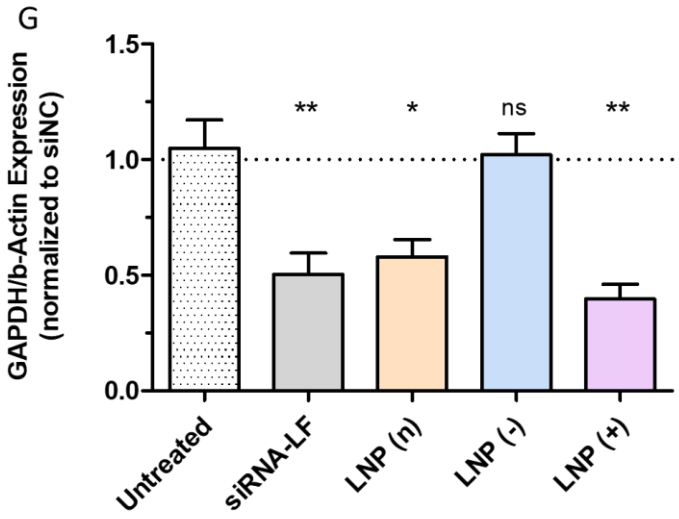

Figure 4. Evaluation of LNPs delivery to Calu-3 cells grown at the air-liquid interface. (A-F) Mucus penetration of neutral (A&D), negative (B&E) and positive (C&F) LNPs in Calu-3 monolayers 24 h after transfection. (A-C) 3D reconstruction. (D-F) XY and XZ viewing direction. Red color represents AF647-siRNA, green color the mucus layer stained with AF488-labeleled wheat germ agglutinin. (G) GAPDH gene knockdown efficiency of LNPs containing neutral, negative and positive phopholipids in Calu-3 monolayers grown under ALI conditions 24 h after transfection with siGAPDH and scrambled siRNA as negative control. Blank samples consisted of Calu-3 monolayers treated with PBS only. Positive controls consisted of Lipofectaamine2000 lipoplexes with siGAPDH. GAPDH expression was normalized with β-actin expression and quantified via qRT-PCR. Data points indicate mean ± SEM (n = 3). One-Way ANOVA, *$p < 0.05$, **$p < 0.01$.

3.5 LNPs behavior in a lung-simulating environment

To further study the behavior of LNPs in contact with mucus, we utilized a diffusion model based on Transwell® inserts to simulate the penetration of LNPs through the mucus layer. In line with previously reported data, findings suggest that negatively charged helper lipids facilitate penetration of the formulation through the mucus layer (Figure 5). Although LNPs prepared with negatively charged helper lipids show a diffusion as high as 70% (Figure 5B) and neutral ones mediate a diffusion up to 60% (Figure 5A), cationic ones do not exceed 50% (Figure 5C). These results corroborate the assumption that the inclusion of phospholipids with negative charge promote the diffusion of the delivery system through the mucus layer. However, the resulting zeta potential is only slightly different among formulations, which could explain the reason why in *in vitro* studies LNPs with positively charged helper lipids reported better mucus diffusion and activity at the air-liquid interface. An additional explanation for the behavior observed could be searched in the protein corona formed when LNPs interact with mucus. Previous studies have already demonstrated the importance of the biomolecular corona formed in serum around LNPs and how it affects stability, biodistribution and targeting (108). It is thus reasonable to think that also mucus proteins possibly form a protein corona around

LNPs, which could explain the better diffusion *in vitro* of LNPs prepared with cationic lipids. Interestingly, all tested formulations completed the diffusion process within 4 h, as almost no difference was detected between the samples withdrawn after 4 and 24 h, with most of the formulations having completed the diffusion process within the first 2 h. Diffusion time is an important aspect to consider, as the mucus layer is estimated to be replaced at a rate of 3-5 mm/min. Consequently, nanocarriers that do not rapidly penetrate the mucus layer also do not reach the underlying lung epithelium (58). Thereby, the faster the diffusion, the higher the chance to reach the target cells. To assess the effect of artificial mucus on stability, LNPs were incubated with artificial mucus and analyzed by DLS. While only a slight increase in size was observed for the formulations incubated with artificial mucus, shifted polydispersity was more evident, particularly for neutral LNPs. This observation could be linked to increased aggregation following incubation with mucus. The effect of cellular mucus on LNP stability was evaluated by NTA, to avoid any interference with globular mucus proteins using DLS. In this case, LNPs prepared with positively charged phospholipids seem to be the ones more affected by the incubation with mucus, as they exhibit more additional peaks following incubation with mucus. These findings underline the importance of adopting appropriate models for investigating the behavior of nanocarriers in a mucus-rich environment. Different models can indeed result in different outcomes and different perspectives about the formulation being investigated, and only a comprehensive study can depict a clearer picture. This aspect is very important when developing a formulation for pulmonary administration, as it can strongly impact the delivery and transfection efficiency. Further studies will be aimed at gaining a deeper understanding on the interactions between mucus and LNPs as well as on the formation of a mucus corona by proteomic analysis.

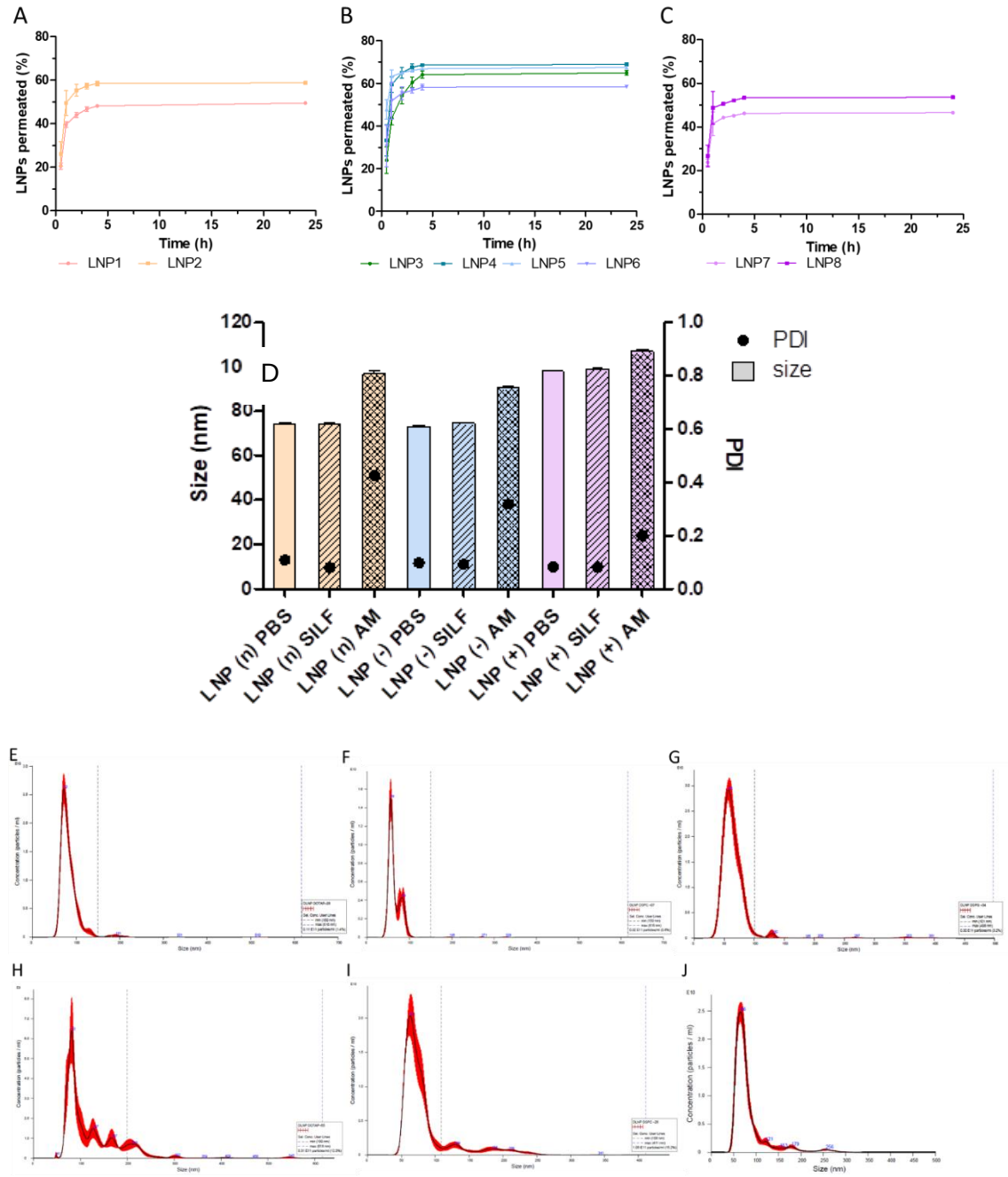

Figure 5. LNPs behavior in a lung simulating environment. (A-C) Percent amount of DiD'-labeled LNPs permeated through artificial mucus in SILF over time. (D) DLS analysis of LNPs with neutral, negative and positive helper lipids following incubation with PBS, SILF and artificial mucus. Data are presented as mean values of triplicates ± SD (n=3). (E-J) NTA analysis of LNPs containing neutral (E-H), negative (F-I) and positive (G-J) helper lipids following incubation with PBS (E-G) and cellular mucus (H-J) isolated from Calu-3 cells.

4. Conclusion

In this study, we investigated how the incorporation of helper lipids with different net charges affects siRNA-loaded LNP delivery to 2D and 3D models of the lung. The incorporation of helper lipids with a positive net charge appeared to improve cellular uptake as well as gene downregulation in a lung epithelial cell line, with activity present starting from low concentrations. On the other hand, they appeared to be the most problematic ones from the toxicity studies, underlying the importance of wisely balancing potency and safety of the formulation as well as dose. Furthermore, we considered the behavior of LNPs in presence of mucus, the main barrier found in the lungs. To this extent, formulations were screened in a 3D air-liquid interface model of the lung with Calu-3 cells. Here, LNPs prepared with cationic helper lipids showed the best activity, both in terms of mucus penetration as well as gene downregulation. Finally, the diffusion of LNPs in artificial mucus as well as the interactions of LNPs with artificial and cellular mucus were tested. In this case, LNPs prepared with cationic helper lipids were the ones to be affected the most by the presence of mucus, in disagreement with the previous study in 3D cell culture. This study underlines the importance of selecting proper and complementary models of the target organ to obtain a more comprehensive picture of the formulation. In conclusion, LNPs hold potential for pulmonary delivery of siRNA and could be advantageous for treating many lung disorders. Further studies will be aimed at clarifying the interactions of LNPs with mucus as well as at investigating LNPs pulmonary delivery *in vivo*.

Chapter IV - Inhibition of SARS-CoV-2 replication in the lung with siRNA/VIPER polyplexes

Domizia Baldassi[1], Shubhankar Ambike[2], Martin Feuerherd[2], Cho-Chin Cheng[2], David J Peeler[3], Daniel P Feldmann[4], Diana Leidy Porras-Gonzalez[5], Xin Wei[5], Lea-Adriana Keller[1,6], Nikolaus Kneidinger[7], Mircea Gabriel Stoleriu[8], Andreas Popp[6], Gerald Burgstaller[5], Suzie H Pun[3], Thomas Michler[2,9], Olivia M Merkel[1,5]

[1]Department of Pharmacy, Pharmaceutical Technology and Biopharmaceutics, Ludwig-Maximilians-University of Munich, Butenandtstraße 5, 81377 Munich, Germany
[2]Institute of Virology, School of Medicine, Technical University of Munich / Helmholtz Zentrum Munich, Trogerstr.30, 81675 Munich, Germany
[3]Department of Bioengineering and Molecular Engineering and Sciences Institute, University of Washington, Seattle, WA, United States
[4]Department of Oncology, Wayne State University School of Medicine, 4100 John R St, Detroit, MI 48201, United States
[5]Institute of Lung Health and Immunity (LHI) and Comprehensive Pneumology Center (CPC) with the CPC-M bioArchive, Helmholtz Munich, Member of the German Center for Lung Research (DZL), Munich, Germany
[6]Preclinical Safety, AbbVie Deutschland GmbH & Co. KG, Knollstrasse, 67061, Ludwigshafen, Germany
[7]Department of Medicine V, University Hospital, LMU Munich, Member of the German Center for Lung Research (DZL), Munich, Germany
[8]Center for Thoracic Surgery Munich, Ludwig-Maximilians-University of Munich (LMU) and Asklepios Pulmonary Hospital; Marchioninistraße 15, 81377 Munich and Robert-Koch-Allee 2, 82131 Gauting, Germany
[9]Institute of Laboratory Medicine, University Hospital, LMU Munich, Germany

The following chapter was published in the Journal of Controlled Release.

Baldassi D, Ambike S, Feuerherd M, Cheng CC, Peeler DJ, Feldmann DP, Porras-Gonzalez DL, Wei X, Keller LA, Kneidinger N, Stoleriu MG, Popp A, Burgstaller G, Pun SH, Michler T, Merkel OM. Inhibition of SARS-CoV-2 replication in the lung with siRNA/VIPER polyplexes. J Control Release. 2022 May;345:661-674. doi: 10.1016/j.jconrel.2022.03.051. Epub 2022 Mar 29. PMID: 35364120; PMCID: PMC8963978.

Graphical abstract

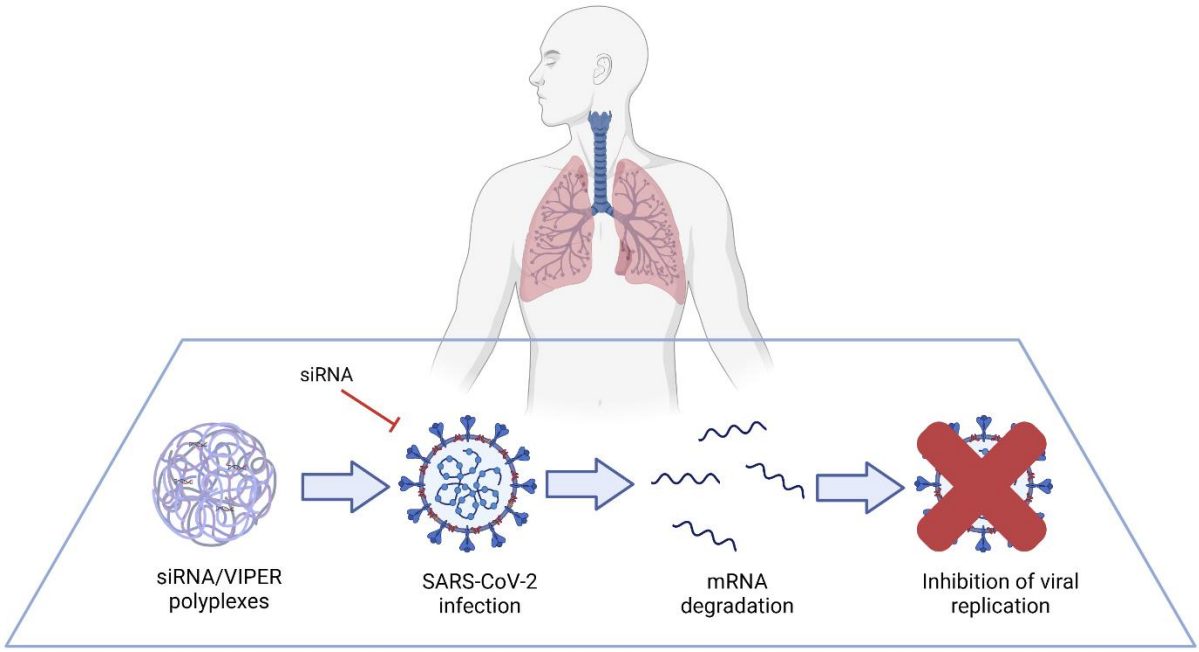

Abstract

SARS-CoV-2 has been the cause of a global pandemic since 2019 and remains a medical urgency. siRNA-based therapies are a promising strategy to fight viral infections. By targeting a specific region of the viral genome, siRNAs can efficiently downregulate viral replication and suppress viral infection. However, to achieve the desired therapeutic activity, siRNA requires a suitable delivery system. The VIPER (virus-inspired polymer for endosomal release) block copolymer has been reported as promising delivery system for both plasmid DNA and siRNA in the past years. It is composed of a hydrophilic block for condensation of nucleic acids as well as a hydrophobic, pH-sensitive block that, at acidic pH, exposes the membrane lytic peptide melittin, which enhances endosomal escape. In this study, we aimed at developing a formulation for pulmonary administration of siRNA to suppress SARS-CoV-2 replication in lung epithelial cells. After characterizing siRNA/VIPER polyplexes, the activity and safety profile were confirmed in a lung epithelial cell line. To further investigate the activity of the polyplexes in a more sophisticated cell culture system, an air-liquid interface (ALI) culture was established. siRNA/VIPER polyplexes reached the cell monolayer and penetrated through the mucus layer secreted by the cells. Additionally, the activity against wild-type SARS-CoV-2 in the ALI model was confirmed by qRT-PCR. To investigate translatability of our findings, the activity against SARS-CoV-2 was tested *ex vivo* in human lung explants. Here, siRNA/VIPER polyplexes efficiently inhibited SARS-CoV-2 replication. Finally, we

verified the delivery of siRNA/VIPER polyplexes to lung epithelial cells *in vivo*, which represent the main cellular target of viral infection in the lung. In conclusion, siRNA/VIPER polyplexes efficiently delivered siRNA to lung epithelial cells and mediated robust downregulation of viral replication both *in vitro* and *ex vivo* without toxic or immunogenic side effects *in vivo*, demonstrating the potential of local siRNA delivery as a promising antiviral therapy in the lung.

KEYWORDS siRNA delivery, RNA therapeutics, SARS-CoV-2, pulmonary delivery, human precision-cut lung slices

1. Introduction

In 2019, the severe acute respiratory syndrome coronavirus-2 (SARS-CoV-2) triggered the Covid-19 pandemic that resulted in dramatic consequences on health, politics and economics on a global scale. As of December 2021, 274 million cases were registered worldwide, and over 5 million people have died due to the consequences of viral infection (109). SARS-CoV-2 is transmitted through respiratory secretions (110) and replicates primarily in respiratory epithelial cells (111). In severe cases, the disease can lead to lung failure and death, especially in patients with pre-existing lung or cardiovascular diseases (112). Although different approaches are now available to fight Covid-19, it still represents an unmet medical need. In the last year, a number of vaccines has been approved by FDA and EMA for clinical use, two of which are based on mRNA technology (113,114). Although the introduction of vaccines has led to huge improvements in the battle against COVID-19, the pandemic is still far from an end at the time of writing this manuscript. Some antiviral drugs have been repurposed in the treatment of SARS-CoV-2 infection, such as the RNA polymerase inhibitor Remdesivir, but none of them can be considered satisfactory for the treatment of the disease (115). Only recently two novel oral antiviral therapies have been approved (116,117) The development of novel antiviral drugs is especially challenging in the case of coronaviruses as they use cellular components to replicate (118). Therefore, finding an antiviral drug able to block the viral replication without affecting the host's physiological functions remains challenging. For this reason, siRNA therapeutics represent a promising candidate. By inducing the RNAi machinery, siRNAs can, in theory, specifically downregulate any given target mRNA, whether endogenously expressed or as a product of viral infections. siRNAs can be designed to be virus-specific and, by downregulating key factors of the viral replication cycle, can prevent the replication and spreading of the virus (119). siRNA therapeutics could thus become a new ally in the fight against viral infections. After investigating the

replication steps as well as the genomic regions of SARS-CoV-2 that can be targeted by siRNA, we identified an siRNA sequence targeting the highly conserved region open reading frame 1 (ORF1), which is part of the genomic RNA of the virus and which serves as a template for the translation of polyprotein 1ab (Pp1ab) (120). Our previous study showed high efficacy of the newly developed siRNA in blocking the replication of SARS-CoV-2 as well as conservation of the target sequence in the current SARS-2 variants (120). Two major advantages of an antiviral siRNA treatment could therefore be specificity for viral factors and therapeutic index. Considering that the lungs are the entry port for the virus and that represent the main site of infection and viral replication, pulmonary delivery is a desirable route of administration, particularly for antiviral siRNA (20). Local siRNA administration to the lungs could represent an effective strategy against respiratory viral infections treatment due to the high surface area of the lungs and relatively low nuclease activity compared to systemic administration. Interestingly, a recent study by Azzi *et al*. reported that subjects who had received two doses of the COVID-19 vaccine and who presented high serum IgG antibody titers only had low saliva levels of neutralizing antibodies, indicating that local mucosal immunity at the virus entry site to the airways was not efficiently developed after vaccination. Therefore, pulmonary local administration could be beneficial to increase the immunity against viral infections (121). Despite the advantages of the pulmonary route, lungs also present some hurdles that must be overcome for achieving the desired target site and downregulation effect. Branching of the airways, mucociliary clearance and presence of mucus are the main factors hampering delivery of siRNA to target cells in the lungs (13). Therefore, formulation of siRNA with a suitable delivery system is crucial for therapeutic siRNA activity.

Several nanocarriers have been developed in the last years for siRNA, mainly based on lipids, polymers or peptides (15). Considering the pulmonary administration route, the encapsulation of siRNA in a polymer-based system appears preferable. While lipid-based systems might be affected by stability problems once nebulized for inhalation (122), polymer-based formulations can be easily nebulized or processed to produce a dry powder for inhalation (75). On this basis, we decided to formulate siRNA with VIPER (virus-inspired polymer for endosomal release), a block copolymer that showed high efficiency for both pDNA (123) and siRNA (124) delivery. In addition to protecting the cargo and enhancing cellular uptake, VIPER polymer also showed improved endosomal escape of siRNA, which is considered the bottleneck for non-viral RNA delivery systems (125). The block copolymer is composed of a hydrophilic block, responsible for the encapsulation of the negatively charged siRNA by electrostatic interactions, and a

hydrophobic, pH-sensitive block entrapping the lytic peptide melittin. Melittin is a peptide derived from bee venom with membrane-lytic activity. At acidic pH, the hydrophobic block undergoes a conformational change that leads to the exposure of the peptide, which can exert its lytic activity towards the endosome and consequently release the siRNA in the cytosol for initiating the RNAi machinery (123). Previous studies suggested the suitability of VIPER polymer for the delivery of siRNA to the lungs (124). Therefore, we further investigated this aspect to develop a formulation that can be efficiently delivered to lung epithelial cells, which are the main site of infection for SARS-CoV-2, for subsequent suppression of viral replication. To further explore the translatability of our findings, we established an air-liquid interface (ALI) culture of lung epithelial cells to understand the behavior of the polyplexes in a more sophisticated 3D culture model (45). Furthermore, to close the gap between *in vitro* and *in vivo* correlation, we tested the activity of the VIPER polyplexes against wild type SARS-CoV-2 virus in human precision-cut lung slices (PCLS), which are living 3D tissue explants that retain the main features of the lung in terms of cellular diversity as well as anatomical structure (47). Additionally, *in vivo* distribution and delivery to various cell types in the lung as well as toxicity and immunogenicity were investigated.

The aim of this study was the development of a pulmonary delivery system that can efficiently and selectively target lung epithelial cells and can efficiently block the replication of SARS-CoV-2. In this regard, VIPER polyplexes showed optimal parameters for pulmonary administration and high gene silencing efficiency *in vitro*. Additionally, the formulation was stable in presence of both lung surfactant and mucin, and penetrated the mucus layer secreted by Calu-3 cells cultured at the air-liquid interface. VIPER polyplex uptake in lung epithelial cells without toxic or immunogenic side effects was confirmed *in vivo* and their antiviral activity against SARS-CoV-2 was validated in the ALI culture model as well as *ex-vivo* human PCLS 3D lung model.

2. Experimental methods

2.1. Materials

Polyethylenimine 25 kDa was purchased from BASF (Ludwigshafen, Germany). RPMI-1640 medium, EMEM medium, DMEM-F12 medium, 0.05% and 0.25% trypsin-EDTA, heat-inactivated fetal bovine serum (FBS), penicillin/streptomycin (P/S), FluorSave, paraformaldehyde, alcian blue solution and Tween20 were purchased from Sigma-Aldrich (St. Louis, Missouri, USA). SYBR Gold dye, Lipofectamine 2000, Rhodamine Phalloidin, AF488-wheat germ agglutinin, (4′,6-diamidino-2-phenylindole (DAPI), ZO-1

rabbit polyclonal antibody, AF488-anti-rabbit secondary antibody and Alexa Fluor™ 647 NHS Ester were obtained from Life Technologies (Carlsbad, California, USA). PneumaCult ALI differentiation medium, hydrocortisone and heparin were purchased from Stemcell Technologies (Vancouver, Canada). Transwell® polyester membrane cell culture inserts were purchased from Corning (New York, USA). Dicer substrate double-stranded siRNA (DsiRNA) targeting the enhanced green fluorescent protein gene, human GAPDH and scrambled non-specific DsiRNA as well as amine-modified siRNA were purchased from integrated DNA Technologies (IDT, Coralville, Iowa, USA).

2.1.1 Design of SARS-CoV-2 targeting siRNAs

The SARS-CoV-2 specific siRNAs were previously described (120) and target highly conserved regions within ORF1 of the SARS-CoV-2 genome. Chemically unmodified siRNAs were designed as symmetric 21-mers with 2 nucleotide overhangs at 3' ends of both strands with the sense strand overhang consisting of dTdT. An siRNA targeting Firefly Luciferase (siLuc) was designed as negative control. Chemically unmodified siRNAs were purchased in desalted form (Microsynth AG, Balgach, Switzerland), resuspended and maintained in RNAse free water upon arrival. Chemically modified versions of ORF1-targeting siRNAs and siLuc were designed in an asymmetric fashion using a previously described design and chemical modification pattern (120). In brief, all nucleotides of the siRNA were subjected to a 2'-O-Methyl modification (2'OMe) except nucleotides at positions 7, and 9-11 of the siRNA sense-, as well as positions 2, 6, 8, 9, 14, and 16 of the antisense-strand (all 5'-3' direction), which contained 2'-Fluoro modifications (2'F) instead. Additionally, two consecutive nucleotides at both ends of the siRNA antisense strand, as well as at the 5' end of the sense strand were incorporated with phosphorothioate linkages (for details see table 1). Chemically modified siRNAs were synthesized by Eurogentec (Liège, Belgium) at a 40 nmol scale and purified by High Performance Liquid Chromatography (HPLC). The siRNAs were obtained in desalted form and reconstituted in RNAse free water at a concentration of 20 mM.

Name	**Sense strand (5'-3')**	**Antisense strand (5'-3')**	**Length** (nt)	
			Sense	Antisense
O1	CCAAAUGUGCCUUUCAACUTT	AGUUGAAAGGCACAUUUGGUU	21	21
O3	GGUACUUGGUAGUUUAGCUTT	AGCUAAACUACCAAGUACCAU	21	21

siLuc	CGUACGCGGAAUACUUCGATT	UCGAAGUAUUCCGCGUACGUG	21	21
O1*	[C]*-[C]*-[A]-[A]-[A]-[U]-FluoroG-[U]-FluoroG-FluoroC-FluoroC-[U]-[U]-[U]-[C]-[A]-[A]-[C]-[U]	[A]*-FluoroG*-[U]-[U]-[G]-FluoroA-[A]-FluoroA-FluoroG-[G]-[C]-[A]-[C]-FluoroA-[U]-FluoroU-[U]-[G]-[G]*-[U]*-[U]	19	21
O3*	[G]*-[G]*-[U]-[A]-[C]-[U]-FluoroU-[G]-FluoroG-FluoroU-FluoroA-[G]-[U]-[U]-[U]-[A]-[G]-[C]-[U]	[A]*-FluoroG*-[C]-[U]-[A]-FluoroA-[A]-FluoroC-FluoroU-[A]-[C]-[C]-[A]-FluoroA-[G]-FluoroU-[A]-[C]-[C]*-[A]*-[U]	19	21
siLuc*	[C]*-[G]*-[U]-[A]-[C]-[G]-FluoroC-[G]-FluoroG-FluoroA-FluoroA-[U]-[A]-[C]-[U]-[U]-[C]-[G]-[A]	[U]*-FluoroC*-[G]-[A]-[A]-FluoroG-[U]-FluoroA-FluoroU-[U]-[C]-[C]-[G]-FluoroC-[G]-FluoroU-[A]-[C]-[G]*-[U]*-[G]	19	21

Table 1. Sequences of siRNAs used in the study. nt, nucleotides; O1-3, ORF1-specific siRNAs 1-3; Luc = Firefly Luciferase; A = Adenine; C = Cytosine; G = Guanine; U = Uracil; T = Thymine; Luc, Firefly Luciferase; *, Phosphorothioate linkage; [], 2'-O-Methyl modification; Fluoro, 2' Fluoro modification; A, Adenine; C, Cytosine; G, Guanine; U, Uracil.

2.2. VIPER Synthesis

The block co-polymer p(OEGMA300$_{8,6}$-co-DMAEMA$_{50}$)-b-p(DIPAMA$_{25,3}$-co-PDSEMA$_{1}$) was synthetized via reversible addition-fragmentation chain transfer (RAFT) polymerization as described previously. The cysteine-terminated melittin peptide (cys-melittin) was conjugated to the PDSEMA side chain by disulfide exchange, purified and characterized as previously reported (123,126).

2.3. Preparation of siRNA polyplexes

Polymer/siRNA polyplexes were prepared by first dissolving polyethylenimine 25 kDa and VIPER polymer separately in RNase free water at a concentration of 1 mg/ml, and then sterilizing the solution through a 0.22 µm filter. Stocks of polymer and siRNA were further diluted in a sterile 5% glucose solution to reach the desired concentration. An equal volume of each polymer was added to a defined amount of siRNA solution and incubated for 20 min to yield polyplexes at a defined N/P ratio (N/P 6 for PEI 25 KDa, N/P 10 for VIPER, if not stated otherwise). All calculations were based on previous studies with pDNA as well as siRNA (123,124).

2.4. Hydrodynamic diameter and zeta (ζ) potential measurements of siRNA polyplexes

Hydrodynamic diameters and polydispersity indices were measured by dynamic light scattering (DLS using a Zetasizer Nano ZS (Malvern Instruments Inc., Malvern, UK). Polyplexes were prepared with scrambled siRNA in 5% glucose solution, added to a disposable micro-cuvette and measurements were performed at 173° backscatter angle running 10 runs three times per samples. Results are presented as average size (nm) ± SD. The samples were further diluted to 700 µl with 5% glucose and transferred to a folded capillary cell for ζ-potential measurements, which were analyzed by Laser Doppler Anemometry (LDA). Samples were read in triplicates, with each run consisting of 30-50 scans. Results are presented in mV ± SD.

2.5. Polyplexes stability in presence of mucin or lung surfactant

To test the stability of polyplexes in an environment that mimic the lung environment, a modified SYBRgold assay in presence of lung surfactant Alveofact or mucin was performed as previously reported (127). PEI and VIPER polyplexes were prepared with 30 pmol siRNA in 100 µl 5% glucose. Once polyplexes were formed, 50 µl of a serial dilution of Alveofact or mucin were added (final concentration: 0, 0.0005, 0.005, 0.05, 0.25, 0.5 mg/ml) and incubated for 20 minutes. Afterwards, samples were distributed in a black 96-well-plate, and 30 µl of 4x SYBRgold solution were added to each well and incubated for 10 minutes in the dark. Fluorescence was then measured on a plate reader (Tecan, Männedorf, Switzerland) at excitation wavelength of 485/20 nm and emission wavelength of 520/20 nm. To account for autofluorescence of mucin, free siRNA samples were prepared in the presence of the corresponding concentration of mucin. Fluorescence of free siRNA represents 100% siRNA release. All measurements were performed in triplicates, and results are presented as mean values ± SD.

2.6. *In vitro* characterization of siRNA/VIPER polyplexes in a lung epithelial cell line

2.6.1. Cell culture

The human non-small cell lung carcinoma cell line stably expressing the reporter gene EGFP (H1299/GFP) was cultured in RPMI-1640 medium supplemented with 10% FBS, 1% P/S and 0.4% G418. Cells were passaged every 3 days with trypsin 0.05% and subcultured in 75 cm^2 flasks. Cells were maintained in a humidified atmosphere at 37 °C and 5% CO_2.

2.6.2. In vitro GFP protein downregulation

To determine the ability of polyplexes to efficiently downregulate protein expression, H1299/GFP cells were used. H1299/GFP cells were seeded in a 24-well-plate at a

density of 25.000 cells/well in 500 µl of medium and incubated at 37°C and 5% CO_2. The day after, cells were transfected with 100 µl of VIPER or PEI polyplexes containing 100 pmol of GFP or scrambled siRNA sequence. Lipofectamine lipoplexes were used as positive control. Cells were incubated for 48 h at 37°C and 5% CO_2. Once the incubation time was completed, cells were trypsinized, washed two times in PBS and PBS/2mM EDTA respectively and analyzed via flow cytometry (Attune NxT, Thermo Fischer Scientific, Waltham, Massachusetts, USA) for the median fluorescence intensity (MFI) of GFP protein expression using 488 nm excitation and a 530/30 nm bandpass emission filter. Samples were measured in triplicates, with each sample gated by morphology based on forward/sideward scattering for a minimum of 10.000 viable cells. Results are displayed as mean values ± SD.

2.6.3. In vitro GAPDH gene knockdown

For gene silencing experiments, 24 h prior to transfection 100.000 H1299/GFP cells were seeded in a 12-well-plate and incubated at 37°C and 5% CO_2. Cells were transfected with 100 µl of VIPER or PEI polyplexes containing 100 pmol of GAPDH or scrambled siRNA. Positive controls consisted of Lipofectamine 2000 lipoplexes while negative controls consisted of blank/untreated cells. After 24 h, cells were harvested and processed to isolate total RNA using the PureLink RNA mini kit according to the manufacturer's protocol (life Technologies, Carlsbad, California, USA). cDNA was synthetized from total RNA using the high-capacity cDNA synthesis kit (Applied Biosystems, Waltham, Massachusetts, USA). Afterwards, the obtained cDNA was diluted 1:10 and a qPCR performed using the SYBR™ Green PCR Master Mix (Thermo Fisher Scientific) with primers for human GAPDH (Qiagen, Hilden Germany) and β-actin (Qiagen, Hilden, Germany) for normalization. Cycle thresholds were acquired by auto setting within the qPCRsoft software (Analytic Jena AG, Jena, Germany). Values are given as mean values ± SEM.

2.6.4. In vitro cytotoxicity in lung cells

2.6.4.1 Cell viability

Cell viability was assessed using the MTT assay. H1299/GFP cells were seeded at a density of 10.000 cells/well in 100 µl medium in a 96-well-plate 24 h prior to transfection. Cells were transfected with PEI and VIPER polyplexes containing 20 pmol scrambled siRNA at different N/P ratios (6, 10 and 15 respectively) and incubated for 24 h at 37°C and 5% CO_2. Once the incubation time was completed, medium was removed and 100 µl of a sterile 0.5 mg/ml 3-(4,5-dimethylthiazol-2-yl)-2,5-diphenyltetrazolium bromide (MTT) solution was added to the cells and incubated for 3 h at 37°C and 5% CO_2. Medium was then removed, and 200 µl of DMSO was added to each well to dissolve formazan

crystals. Absorbance was then read at 570 nm using a microplate reader (Tecan, Männedorf, Switzerland). Results are given as mean of values of triplicates ± SD.

2.6.4.2 LDH release

The effect of polyplexes on membrane integrity was assessed by measuring the release of lactate dehydrogenase (LDH) in the extracellular medium using the CytoTox96® Non-Radioactive Cytotoxicity Assay kit (Promega, Madison, Wisconsin, USA) according to the manufacturer's protocol. Briefly, 5.000 H1299/cells were seeded in a 96-well-plate in 100 µl medium 24 h prior to transfection. Cells were treated with PEI and VIPER polyplexes containing 20 pmol siRNA at different N/P ratios (6, 10 and 15 respectively) and incubated for another 24 h. Afterwards, 50 µl of supernatant was transferred to a fresh 96-well-plate and 50 µl of substrate mix was added and incubated for 30 min at room temperature protected from light. Subsequently, 50 µl of stop solution was added and absorbance was measured at 490 nm using a microplate reader (Tecan, Männedorf, Switzerland). Untreated cells were used as negative control, while cells treated with lysis buffer represented 100% LDH release. Results are given as mean values of triplicates ± SD.

2.7. Polyplexes behavior in mucus-secreting Calu-3 cells grown at the air-liquid interface

2.7.1. Cell culture

Calu-3 cells were obtained from LGC Standards GmbH (Wesel, Germany). Cells were maintained in EMEM medium supplemented with 10% FBS and 1% P/S. Cells were passaged once 80% confluence was reached and subcultured in 75 cm^2 flasks. Cells were maintained in a humidified atmosphere at 37°C and 5% CO_2.

Calu-3 cells were seeded at a density of 250.000 cells onto uncoated Transwell® polyester cell culture inserts (6.5 mm, 0.4 µm pore size) in 100 µl medium, while 700 µl medium were added to the basolateral chamber. After 72 h, the apical medium was removed to obtain air-liquid interface conditions, while the medium from the basolateral chamber was replaced with 200 µl of PneumaCult™ ALI medium (STEMcell technology, Vancouver, Canada) and replaced every two days. Experiments were performed once TEER values ≥ 300 Ω*cm^2 were reached and a stable polarized epithelial layer was formed, as measured with an EVOM epithelial volt/ohm meter (World Precision Instruments, Sarasota, USA).

To confirm the secretion of mucus by Calu-3 cells grown under ALI conditions, an alcian blue staining was performed. Briefly, cells were incubated for 15 min with 100 µl alcian blue solution and washed 3 times with 200 µl PBS. Cells were then mounted on glass

slides using FluorSave (Merck Millipore, Darmstadt, Germany) reagent and analyzed using a BZ-8100 (Biozero) fluorescence microscope (Keyence, Osaka, Japan). Images were processed with Fiji distribution of ImageJ.

To verify the expression of tight junctions when cells were cultured at ALI, the expression of zonula occludens protein-1 (ZO-1) was evaluated. Briefly, 7 days after air-lift, cells were fixed in 4% PFA for 15 min, blocked for 1 h in 5% BSA blocking buffer and then incubated overnight with a 1:100 dilution of ZO-1 rabbit polyclonal antibody (Life Technologies, Carlsbad, California, USA). Afterwards, cells were incubated for 1 h with a 1:200 dilution of AF488-anti-rabbit secondary antibody (Life Technologies, Carlsbad, California, USA). Once the incubation time was completed, cells were washed two times with PBS, and nuclei were stained with a 0.5 µg/ml solution of 4′,6-diamidino-2-phenylindole (DAPI) for 15 min. Finally, cells were washed two times with PBS and mounted on glass slides with FluorSave reagent. Samples were analyzed with a SP8 inverted confocal scanning confocal microscope (Leica Camera, Wetzlar, Germany). The images were exported and processed with the Leica Image Analysis Suite software.

2.7.2. Cell uptake study

For microscopy experiments, amine-modified siRNA was labeled with succinimidyl ester (NHS) modified AlexaFluor647 fluorescent dye according to the manufacturer's protocol and purified via ethanol purification to obtain AF647-siRNA as previously reported (69).

To evaluate the delivery of polyplexes to Calu-3 monolayers, cells were transfected with PEI and VIPER polyplexes containing 100 pmol AF647-siRNA for 24 h. Once the incubation time was completed, monolayers were fixed in 4% PFA for 15 min, washed 3 times with PBS and permeabilized with PBS + 0.3% Tween20 for 10 min. Cells were then incubated with rhodamine phalloidin for 60 min. Nuclei were stained with a 0.5 µg/ml solution of 4′,6-diamidino-2-phenylindole (DAPI) for 15 min. Finally, cells were washed two times with PBS, mounted on glass slides using FluorSave reagent and analyzed with a SP8 inverted confocal laser scanning microscope (Leica Camera, Wetzlar, Germany). The images were exported from the Leica Image Analysis Suite and processed with the Fiji distribution of ImageJ.

2.7.3. Mucus penetration study

The ability to overcome the mucus barrier was assessed by transfecting Calu-3 monolayers with PEI and VIPER polyplexes containing 100 pmol AF647-siRNA for 24 h. Afterwards, cells were incubated for 15 min with AF488-wheat germ agglutinin at 37°C and 5% CO_2 to stain the mucus layer. Cells were then washed two times with PBS and mounted on glass slides using FluorSave reagent and immediately analyzed with a SP8

inverted confocal laser scanning microscope (Leica Camera, Wetzlar, Germany). The images were exported from the Leica Image Analysis Suite and processed with the Fiji distribution of Image J.

2.7.4. GAPDH knockdown in Calu-3 cells at ALI

In order to measure the transfection efficiency of polyplexes in a more sophisticated *in vitro* model, Calu-3 monolayers were transfected with PEI and VIPER polyplexes containing 100 pmol GAPDH or scrambled siRNA for 24 h at 37°C and 5% CO_2. Positive controls consisted of Lipofectamine 2000 lipoplexes while negative controls consisted of blank/untreated cells. Cells were then detached, and RNA was extracted using the PureLink RNA mini kit according to the manufacturer's protocol. Samples were further processed for cDNA synthesis and qPCR as described above. Values are given as mean of triplicates ± SEM.

2.7.5 Immunofluorescence staining and confocal imaging of ACE-2 receptor on Calu-3 Cells

To evaluate the ACE-2 receptor expression on Calu-3 cells, the membranes were cut out of the transwells in circles and embedded on the basolateral side with Cryomatrix embedding medium (Shandon Cryomatrix, Thermo Fisher Scientific, Waltham MA, USA) on dry ice. Calu-3 cells were then covered on the apical side with Cryomatrix. Embedded cells were frozen on dry ice and stored at -80°C for further processing. Later, the embedded cells were cut into cryosections (7 µm) using a Kryostat CM3050S (Leica Biosystems, Nussloch, Germany). Cryosections were dried for 4 h on SuperFrost plus glass slides (Menzel-Glaeser, Germany) and were then fixed with ice cold methanol and acetone (1:1) for 10 min. Glass slides were washed three times for 5 min with cold 1x Wash Buffer (WB) (medac diagnostika, Wedel, Germany) with shaking. Unspecific binding sites were blocked with 10% BSA for 20 min. Slides were then incubated with a primary antibody against human ACE-2 receptor ((AF933), R&D systems, Minneapolis, MN, USA) at a concentration of 5x103 µg/ml in 1x WB, containing 1% BSA for 1 h. Cells were washed three times for 5 min with cold WB before slides were treated with a 1:500 dilution of a donkey anti goat IgG H&L Alexa Fluor® 647 preadsorbed (ab150135, Abcam, Cambridge, MA, USA) antibody in WB/BSA for 30 min in the dark. Slides were counterstained and embedded with ProLong Gold Antifade Moutant with DAPI (4′,6′-diamidino-2-phenylindole) (Life Technologies, Thermo Fisher Scientific, Waltham MA, USA) solution overnight in the dark. For control sections, only the secondary antibody was used. Fluorescence imaging was performed using a laser scanning confocal microscope LSM700 (Carl Zeiss, Wetzlar, Germany) with the Axio Imager 2 and the Software ZEN 2.3 lite (Carl Zeiss, Wetzlar, Germany). Images were taken with a Zeiss

63x oil immersion objective. The pictures were analyzed and modified regarding contrast and intensity, using ZEN 2.3 lite (blue edition). Nucleus staining (DAPI) was illustrated with the emission color blue, while Alexa Fluor 647 was shown in magenta. Scale bars were added using the free software ImageJ.

2.7.6 siRNA/VIPER polyplex activity against SARS-CoV-2 at the air-liquid interface

To test the activity of siRNA/VIPER polyplexes against wild-type SARS-CoV-2 virus, Calu-3 monolayers were transfected with 100 pmol of VIPER polyplexes containing 100 pmol ORF1#3 or luciferase siRNA as negative control 6 h before infection with 0.1 MOI wildtype SARS-CoV-2. After 24 h, RNA was extracted as described under 2.10.

2.8 *Ex vivo* activity of siRNA/VIPER polyplexes in human precision-cut lung slices

2.8.1 Human tissue, ethics statement and human precision-cut lung slices (hPCLS)

Human tissue was obtained from the CPC-M bioArchive at the Comprehensive Pneumology Center (CPC), from the University Hospital Groβhadern of the Ludwig-Maximilian University (Munich, Germany) and from the Asklepios Biobank of Lung Diseases (Gauting Germany). Participants provided written informed consent to participate in this study, in accordance with approval by the local ethics committee of the Ludwig Maximilian University Munich, Germany (Project 19-630). Precision-cut lung slices (PCLS) were prepared as described before (128,129). Briefly, PCLS were prepared from tumor-free peri-tumor tissue. The lung tissue was inflated with 3% agarose solution and solidified at 4°C. afterwards, 500 µm thick slices were cut from tissue blocks using a vibration microtome (HyraxV50) (Karl Zeiss AG, Oberkochen, Germany). PCLS were cultured in DMEM F-12 medium supplemented with 0.1% FBS. Prior to experiments, PCLS cut by means of a biopsy puncher into 4 mm in diameter PCLS punches.

2.8.2 Establishment of wild-type SARS-CoV-2 infection in hPCLS

PCLS samples were prepared as described above and cultured with Dulbecco's Modified Eagle Medium (DMEM) F-12 supplemented with L-Glutamine, HEPES, 10,000 IE Penicillin, 10,000 IE Streptomycin and 0.1% fetal bovine serum. For each sample, three PCLS were placed in a 48 well plate in 500 µl medium and infected with 300.000 (pure), 30.000 (0.1x) or 3.000 (0.01x) plaque-forming units (PFU) SARS-CoV-2. PCLS were washed with PBS after 1h and RNA extracted as described under 2.10 after 24, 48 and 72h.

2.8.3 Polyplexes activity against wild-type SARS-CoV-2 in hPCLS

PCLS samples were prepared as described above and cultured with Dulbecco's Modified Eagle Medium (DMEM) F-12 supplemented with L-Glutamine, HEPES, 10,000 IE Penicillin, 10,000 IE Streptomycin and 0.1% fetal bovine serum. For each sample, three PCLS were placed in a 48 well plate in 500 µl medium and transfected with VIPER polyplexes containing 60 pmol siRNA against ORF1 as well as non-targeting siRNA six hours before being infected with wildtype SARS-CoV-2. For infection, 300.000 plaque-forming units (PFU) SARS-CoV-2 were added to each well, which contained PCLS with an estimated cell number of 300.000 cells, resulting in an approximated MOI of 1.0. After 24 h, RNA was extracted as described under 2.10.

2.9 Nucleic acid extraction and qPCR

Nucleic acid was extracted from ALI cultures using the NucleoSpin RNA kit (Macherey-Nagel; Düren, Germany). To isolate RNA from PCLS, samples were first homogenized using the TissueLyzer LT (Qiagen, Order # 85600) and then RNA was isolated using TRIzol (ThermoFischer Scientific) according to instructions. cDNA was synthesized with the Superscript™ III First-Strand Synthesis System (Thermo Fisher Scientific; Dreieich, Germany). SARS-CoV-2 RNA was quantified by qPCR performed on a LightCycler® 480 (Roche Holding AG; Basel, Switzerland) using primers specific for the N region (total viral RNA) or the RNA dependent RNA polymerase (Rdrp) region (as measure of genomic viral RNA [gRNA]) of SARS-CoV-2 and beta-actin as a house-keeping gene. For primer sequences and cycling conditions, see table 2.

PCR name	**Primer/probe sequences (5'-3') and cycling conditions**
Beta-actin	Fw: CCACGAAACTACCTTCAACTCCAT Rev: TGTGTTGGCGTACAGGTCTTTG
N	Fw: GACCCCAAAATCAGCGAAAT Rev: TCTGGTTACTGCCAGTTGAATCTG
RDRP	Fw:CGTCTGCGGTATGTGGAAAG Rev: TAAGACGGGCTGCACTTACA
	Cycling conditions 95°C - 5 min 45 Cycles: 95°C - 15 s 55°C - 10 s 72°C - 25 s

Table 2. Oligonucleotides and cycling conditions used for polymerase change reaction. A = Adenine; C = Cytosine; G = Guanine; T = Thymine; Rev = reverse; s = second; RDRP = RNA-dependent RNA polymerase

2.10. *In vivo* polyplex distribution in the lung and pro-inflammatory effects following pulmonary delivery

All animal experiments were approved by a Wayne State University Institutional Animal Care and Use Committee (IACUC). Female BALB/c mice were purchased from Charles Rivers Laboratories (Wilmington, Massachusetts, USA) and used at 5 weeks of age. Mice were intratracheally instilled (under ketamine/xylazine anesthesia) with PEI and VIPER polyplexes containing 2 nmol AF647-sIRNA. Control groups were administered with 5% glucose only. After 48 h, mice were sacrificed under i.p. ketamine/xylazine anesthesia, exsanguinated and perfused with PBS. BALF and lung cell suspensions were prepared as reported before (130). Serum was obtained from clotted blood. Lung cell suspensions were counterstained with BB515 labeled rat anti-mouse CD45 (30-F11, 1:40, BD Biosciences), pacific orange labeled F4/80 (1:100, Invitrogen), BV421 labeled anti-tubulinβ3 (1:100, Biolegend), anti-prosurfactant protein C (1:100, Abcam), mouse anti-rabbit PE-Cy7 (1:200, Santa Cruz Biotechnology), anti-uteroglobin antibody (1:100, Abcam) and mouse anti-rabbit AF594 (1:200, Invitrogen) following the manufacturer's protocol. The analysis was performed on a BDLSR Fortessa flow cytometer. The different populations of leukocytes (CD45+), macrophage/monocytes (F4/80+), Type II pneumocytes (proSPC+), ciliated cells (tubulin beta +) and club cells (CD31 +) were gated, and the MFI of siRNA-AF647 in the different cell populations was quantified. The concentration of proinflammatory cytokines in BALF and serum was determined using the mouse LEGENDplex ELISA kit (BioLegend, San Diego, California). Values are given as mean ± SEM with n=4.

2.11. Statistics

Statistical analysis was performed with GraphPad Prism 5 software using One-Way or Two-Way ANOVA with Turkey post-hoc test, with $p > 0.05$ considered not significant (ns) and $*p < 0.05$, $**p < 0.01$, $***p < 0.005$ considered significantly different.

3. Results and discussion

3.1. Characterization of polyplexes

Size and surface charge are among the most important parameters that need to be considered when designing an efficient drug delivery system. The parameters should be optimized for the intended route of administration and tuned towards the right size and zeta potential. Considering that the lungs are the organs mainly affected by SARS-CoV-

2 infection, we aimed at achieving a formulation optimized for pulmonary administration. In previous work, we identified N/P 6 and 10 as optimal for pulmonary PEI and VIPER polyplex delivery, respectively, and have thus used these formulations throughout this study (28,124). siRNA/PEI and siRNA/VIPER polyplexes were analyzed via dynamic light scattering for size and polydispersity index, and by Lased Doppler Anemometry for zeta potential. Both PEI and VIPER polyplexes showed desirable hydrodynamic diameters for pulmonary delivery of 85.52 nm and 55.78 nm (intensity-weighed) respectively (Table 3). Nanoparticles formed with VIPER polymer, however, showed smaller sizes, which could help avoid clearance by macrophages and enhance diffusion though the mucus mesh (131). In terms of PDI, PEI and VIPER polyplexes showed values of 0.25 and 0.39 respectively. The higher PDI values observed for VIPER are possibly linked to the presence of the peptide melittin in the structure of the polymer, which could lead to an increase in PDI. Nonetheless, PDI could be reduced by introducing a microfluidic approach in future development (72,132). Similar zeta potential values were observed for PEI and VIPER polyplexes. Both formulations presented a positive zeta potential of about 10 mV in line with expectations, due to the cationic nature of the polymers being tested.

Formulation	Size (nm ± SD	PDI (± SD)	ζ potential (mV ± SD)
siRNA_PEI	85.5 ± 6.8	0.25 ± 0.01	12.4 ± 6.2
siRNA_VIPER	55.8 ± 9.5	0.39 ± 0.03	9.5 ± 2.4

Table 3. PEI and VIPER polyplexes hydrodynamic diameter, polydispersity index and zeta potential

3.2. Stability of polyplexes in presence of mucin and lung surfactant

When treating lung diseases, pulmonary delivery is the preferred route of administration due to the large surface area of the lungs, absence of serum proteins and limitation of systemic side effects (133). Especially in the case of respiratory viral infections, such as in the recent pandemic caused by SARS-CoV-2, pulmonary administration ensures that the payload will directly reach the site of infection, the lung epithelium, avoiding problems related to systemic administration. Nonetheless, biological barriers should be carefully addressed when considering pulmonary delivery. The lung epithelium is covered by a mucus layer that hampers the delivery of the cargo to the underlying cell layer. The negatively charged mucin glycoproteins represent the main component of the lung mucus layer and they are thought to be responsible for instability of polyplexes in mucus (58). Additionally, deeper lungs are covered by lung surfactant, which contains high concentration of phospholipids. Therefore, we tested the stability of VIPER and PEI polyplexes in the presence of increasing concentrations of mucin and Alveofact®, a

commercially available lung surfactant, by a modified SYBR gold assay (127). As it can be observed in Figure 1, VIPER showed increased stability at increasing concentrations of mucin in comparison to PEI. At a concentration of mucin as high as 0.5 mg/ml, VIPER showed only negligible release of siRNA, while PEI polyplexes released about 60% of their load. Both polymers showed better stability in lung surfactant compared to mucin, but VIPER outperformed PEI, with a release of 4 vs. 10% of the siRNA load. A possible explanation for the increased stability of VIPER polyplexes in mucus and surfactant could be the presence of the hydrophilic OEGMA-co-DMAEMA block (134).

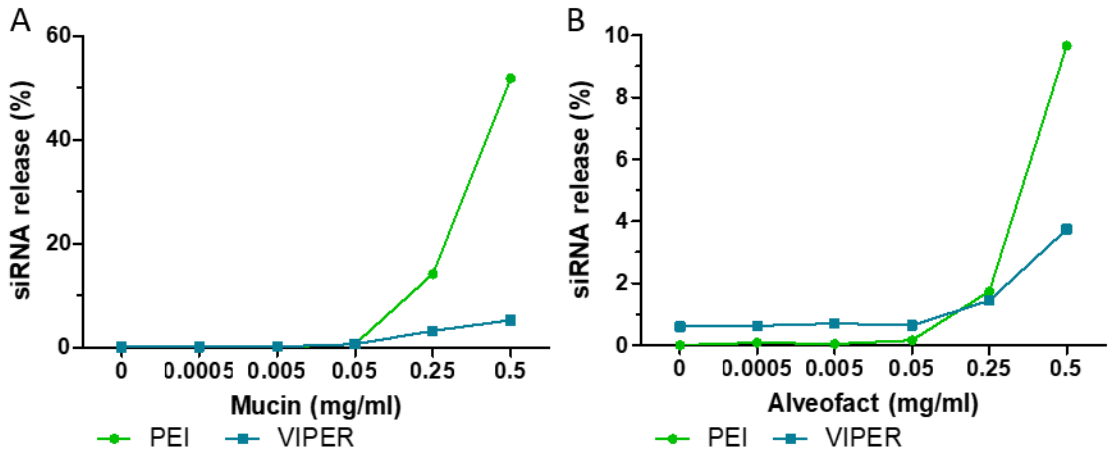

Figure 6. Stability of polyplexes at increasing concentration of (A) mucin and (B) lung surfactant was tested by modified SYBR gold assay after 20 min incubation. Free siRNA represents 100% siRNA release. (Mean ± SD, n03). Green square: siRNA release from PEI polyplexes. Blue circle: siRNA release from VIPER polyplexes.

3.3. *In vitro* transfection efficacy in lung epithelial cells

The gene silencing activity of PEI and VIPER polyplexes was tested at the mRNA and protein level in a human non-small lung carcinoma cell line stably expressing GFP (H1299/GFP cells). PEI and VIPER polyplexes were prepared with 100 pmol siRNA at N/P 6 and N/P 10 respectively. To test the activity at the mRNA level, PEI and VIPER polyplexes were prepared with siRNA specific for the human GAPDH, an endogenously expressed housekeeping gene, as well as with scrambled siRNA as negative control. Positive controls consisted of lipofectamine/siGAPDH lipoplexes. The expression of GAPDH was measured via quantitative real time PCR and normalized to β-actin expression. The experiment showed that both PEI and VIPER polyplexes mediated a gene knockdown at the mRNA level, but VIPER showed the more robust activity, reaching about 80% gene silencing (Figure 2B). A similar trend was also observed at the protein level, where the activity of the polyplexes was evaluated by quantifying the median fluorescence intensity (MFI) of the different samples and normalized for the

untreated samples (100%). Also in this case, VIPER polyplexes achieved high gene silencing activities of about 90%, similarly to the one showed by the positive control lipofectamine. PEI polyplexes instead only suppressed about 40% of the GFP expression (Figure 2A). This difference in activity is probably linked to the presence of melittin in the structure of VIPER, which is an endosomolytic peptide that has been studied for improving the activity of siRNA delivery agents (135). By disrupting the endosomal membrane, melittin helps to release the siRNA in the cytosol and consequently improves the RNAi activity of the siRNA formulation (136).

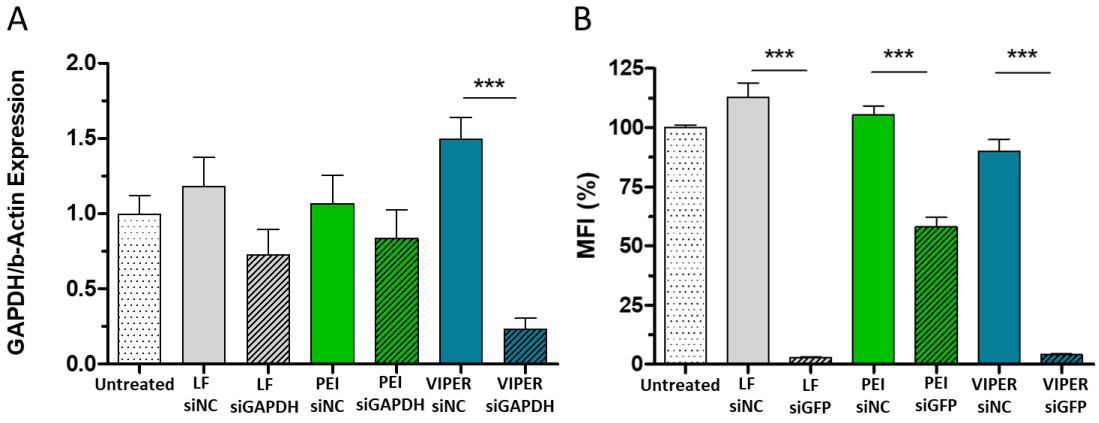

Figure 7. *In vitro* downregulation activity of PEI and VIPER polyplexes in a H1299 cell line stably expressing EGFP. (A) GAPDH gene knockdown efficiency of PEI and VIPER polyplexes 24 h after transfection with polyplexes. Blank samples consisted of H1299GFP cells treated with 5% glucose only. Negative controls consisted of polyplexes encapsulating scrambled siRNA. Positive controls consisted of Lipofectamine2000 lipoplexes with 100 pmol siGAPDH. GAPDH expression was normalized with β-actin expression and quantified by qRT-PCR. Data points indicate mean ± SEM. (B) GFP knockdown was measured by flow cytometry 48 h after transfection with PEI and VIPER polyplexes with 100 pmol siGFP. Blank samples consisted of H1299GFP cells treated with 5% glucose only. Negative controls consisted of samples treated with polyplexes encapsulating scrambled siRNA. Positive controls consisted of Lipofectamine2000 (LF) lipoplexes with 100 pmol siGFP. Data points indicated mean ± SD (n=3). One-Way ANOVA, ***p<0.005.

3.4. *In vitro* cytotoxicity in lung epithelial cells

To test the compatibility of the formulations with living cells, PEI and VIPER polyplexes were incubated with H1299/GFP cells at different N/P ratios. The viability of the cells was measured via the MTT assay, a colorimetric assay used to measure the metabolic activity of the cells as an indicator of cell viability. The experiment showed that both PEI and VIPER present an overall safe profile, with no reduction in cell viability in comparison to the untreated control for N/P 6 and 10, and a reduction by about 20% for VIPER at the highest N/P ratio tested of 15. The difference in cell viability for the two different polymers was not significant for any of the N/P ratios tested (Figure 3A).

To further investigate the effect of the formulation on cell membrane integrity, an LDH assay was performed at the same conditions as the MTT assay. By measuring the release of lactate dehydrogenase enzyme in the supernatant, the assay gives a measure of the impact of the formulation on the membrane integrity. The cytotoxicity was measured by comparing the results to a 100% LDH release considered as maximal cytotoxicity as well as to untreated cells as negative control. PEI and VIPER showed a similar trend, with only negligible LDH release detected for N/P 6 and 10 with values similar to the ones observed for untreated cells, while higher release was observed for the highest N/P ratio tested. PEI and VIPER showed a similar trend in terms of LDH release, confirming that the presence of melittin in the formulation did not results in higher membrane damage nor increased toxicity (Figure 3B). These results are in line with previously reported hemolysis data for plasmid/VIPER polyplexes and were explained by their pH-responsive behavior (123).

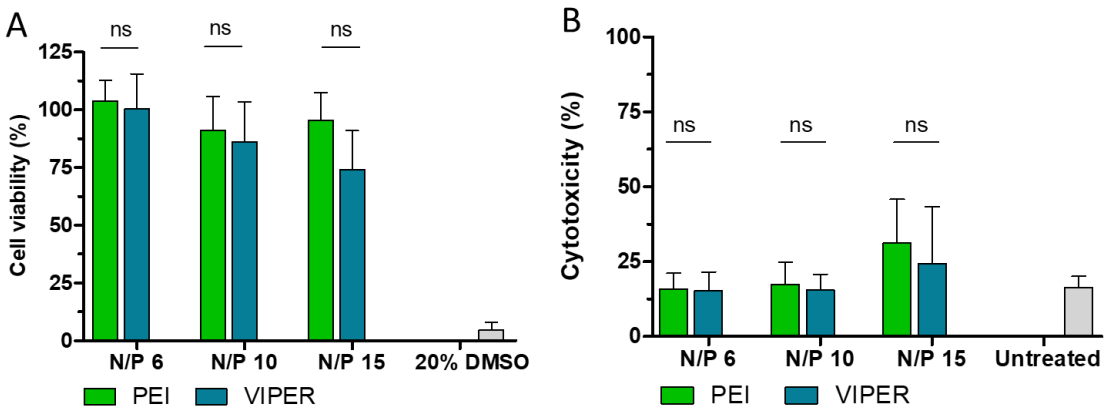

Figure 8. Evaluation of cytotoxicity following incubation with PEI and VIPER polyplexes. (A) Evaluation of cellular viability by MTT assay of H1299/GFP cells incubated with PEI and VIPER with different N/P ratios: 6, 10 and 15. Positive controls consisted of cells treated with 20% DMSO. Data points indicate mean ± SD (n=3). One-Way ANOVA, ns = not significant. (B) Assessment of membrane integrity by measuring lactate dehydrogenase release of cells incubate with PEI and VIPER polyplexes at different N/P ratios: 6, 10, 15. Cells treated with lysis buffer correspond to 100% LDH release. Data points indicate mean ± SD (n=3). One-Way ANOVA, ns = not significant.

3.5. siRNA/VIPER polyplexes delivery in an air-liquid interface culture system

Air-liquid interface cultures represent a valid tool for reproducing *in vitro* the typical aspects of the respiratory tract. In this configuration, cells can form a pseudostratified epithelium and differentiate towards a mucociliary phenotype better resembling *in vivo* conditions (137). Calu-3 cells are considered as the gold standard of ALI cultures since under these culture conditions they express tight junctions, show high TEER values and secrete mucus (105,138). In this study, we used the 3D culture model with Calu-3 cells, and monolayer formation was confirmed by tight junction staining visualized with

confocal laser scanning microscopy as well as alcian blue staining of the mucus layer visualized with fluorescence microscopy (Supplementary Figure 1). Due to their ability to secrete mucus under ALI conditions, Calu-3 cells represent a good model to investigate the mucus penetration of nanocarriers (139). Calu-3 monolayers were stained with AF488-wheat germ agglutinin 24 h after transfection with AF647-siRNA/VIPER polyplexes, mounted on glass slides and directly analyzed by confocal microscopy without fixing. As it can be observed in the 3D reconstruction of Figure 4(A-B), green fluorescence represents the mucus layer, while red dots correspond to the labeled siRNA penetrating though the mucus layer. Polyplexes efficiently diffused through the mucus layer and reached the underlying cell layer. To confirm the cellular internalization of the polyplexes after mucus penetration, an additional staining of the Calu-3 monolayer was performed to visualize cellular nuclei (blue), cytoskeleton (green) and AF647-labeled siRNA. As shown in Figure 4(C-D), VIPER polyplexes, after overcoming the mucus layer, delivered siRNA to the underlying cells, confirming the potential of this polymer as delivery system in a challenging environment such as the respiratory tract.

Although the uptake of polyplexes was confirmed, its activity in the ALI culture model was still to be investigated. The activity of the polyplexes was studied by measuring the downregulation of the housekeeping gene GAPDH 24 h after transfection as previously described. In line with the 2D culture experiments, VIPER performed best, reaching about 75% downregulation of GAPDH expression (Figure 4F). PEI showed similar results to lipofectamine, with about 40% reduction in GAPDH expression besides potential off-target related upregulation of gene expression as reflected by the samples transfected with the negative control siRNA (siNC) (140). This study confirmed the efficient delivery of siRNA to the Calu-3 monolayer by VIPER in a sophisticated culture system, which more closely mimics the *in vivo* conditions. In contrast, PEI polyplexes and Lipofectamine lipoplexes showed decreased efficacy (Supplementary Figure 3) which can be understood as a result of hampered diffusion and “stickiness” in mucus caused by larger particles sizes and higher zeta potentials of PEI complexes than VIPER complexes. This observation is in line with the reported role of particle size in mucus diffusion (141).

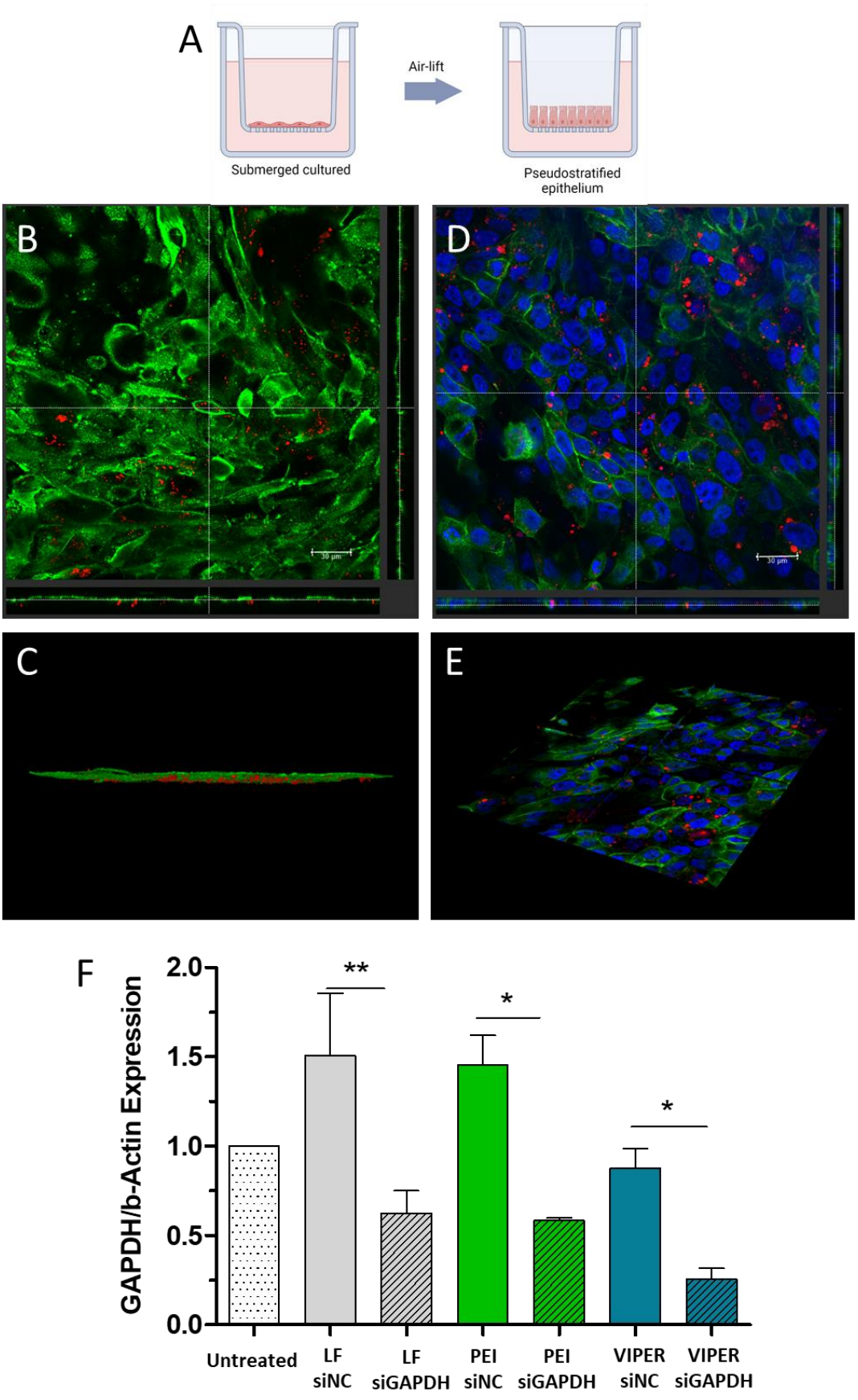

Figure 9. Evaluation of AF647-siRNA/VIPER polyplexes delivery to Calu-3 cells grown at the air-liquid interface. (A) Schematic of the air-liquid interface culture model. Figure created with BioRender.com (B,C)

Mucus penetration of AF647-siRNA/VIPER polyplexes in Calu-3 monolayers 24 h after transfection. (B) XY and XZ viewing direction. (C) 3D reconstruction. Red color represents AF647.siRNA, green color to the mucus layer stained with AF488-labelel wheat germ agglutinin. (D,E) Cell uptake of AF647-siRNA/VIPER polyplexes 24 h after transfection analyzed by confocal light scanning microscopy. (D) XY and XZ viewing direction. (E) 3D reconstruction. Red color corresponds to AF647-siRNA, green color to actin stained with rhodamine phalloidin and blue color corresponds to nuclei stained with DAPI. (F) GAPDH gene knockdown efficiency PEI and VIPER polyplexes in Calu-3 monolayers grown under ALI conditions 24 h after transfection with siGAPDH and scrambled siRNA as negative control. Blank samples consisted of Calu-3 monolayers treated with 5% glucose only. Positive controls consisted of Lipofectaamine2000 lipoplexes with siGAPDH. GAPDH expression was normalized with β-actin expression and quantified via qRT-PCR. Data points indicate mean ± SEM (n=3). One-Way ANOVA, *p<0.05, **p<0.01.

3.6 siRNA/VIPER polyplexes activity against wild-type SARS-CoV-2 on Calu-3 cells grown at ALI

After confirming the knockdown activity of siRNA/VIPER polyplexes in ALI cultures, we studied their activity against SARS-CoV-2 virus. The ACE-2 receptor is used by SARS-CoV-2 to infect human lung epithelial cells (142). Since mouse ACE-2 does not bind efficiently to SARS-CoV-2, alternative *ex vivo* and *in vivo* models need to be considered for studying the activity of antiviral COVID drugs (143). Although genetically engineered mouse models have been developed, they often present limitations in terms of accessibility. Therefore, the development of suitable *in vitro* and *ex vivo* models is critical for evaluating new antiviral candidates. Once cultured under ALI conditions, Calu-3 cells are known to express the ACE-2 receptor on the apical side, making them a suitable model for SARS-CoV-2 infection studies (137). To confirm the expression of ACE-2 receptor by differentiated Calu-3 cells, cryosections of Calu-3 cells grown at ALI were prepared and stained with a goat anti-human ACE-2 antibody (magenta) and counterstained with DAPI (blue) (Figure 5B). On the apical side, a strong signal was detected for the sections treated with the anti-ACE-2 primary antibody. On the contrary, no signal could be observed for control sections stained only with the secondary antibody (Figure 5A). The staining of the receptor was homogeneous on the apical side of the monolayer while no signal could be detected on the basolateral side of the cells.

After confirming the presence of the ACE-2 receptor on the apical side of Calu-3 monolayer cells and therefore validating its suitability as infection model for SARS-CoV-2, cells were transfected with VIPER/siRNA polyplexes 6 hours before infection with wild-type SARS-CoV-2 virus and readout performed after additional 24 h. The prophylactic siRNA application was established based on the observation that an early therapy start might be crucial for antiviral efficacy (120). The siRNA sequence chosen for blocking the viral replication was described in a recently published work. The selected siRNA sequence targets a highly conserved region of the ORF1, and it was shown to efficiently

inhibit the replication of the virus. ORF1 is a highly conserved region, suggesting a limited likelihood of escape mutations that could make the virus resistant to therapy (120). Based on our previous studies, we tested two different siRNA sequences targeting ORF1, O1 and O3. Polyplexes prepared with these sequences showed comparable characterization parameters to the siRNA sequence used for characterization and *in vitro* 2D activity experiments (Supplementary Table 1).

Indeed, infected ALI cells replicated SARS-CoV-2 at high levels, reaching extents that are only found in lungs of COVID-19 patients (144). However, such high levels were only observed in cells that had received the control siRNA or which were only infected (Figure 5C), while siORF1/VIPER polyplexes achieved a 50% and 75% reduction, for O1 and O3 respectively, of viral replication in comparison to the control groups, confirming the specific activity of the polyplexes against SARS-CoV-2. Most importantly, this study confirmed the activity of siRNA/VIPER polyplexes against SARS-CoV-2 in a relevant *in vitro* model incorporating the presence of mucus, which is one of the main barriers limiting the delivery of polyplexes to target cells in the respiratory tract.

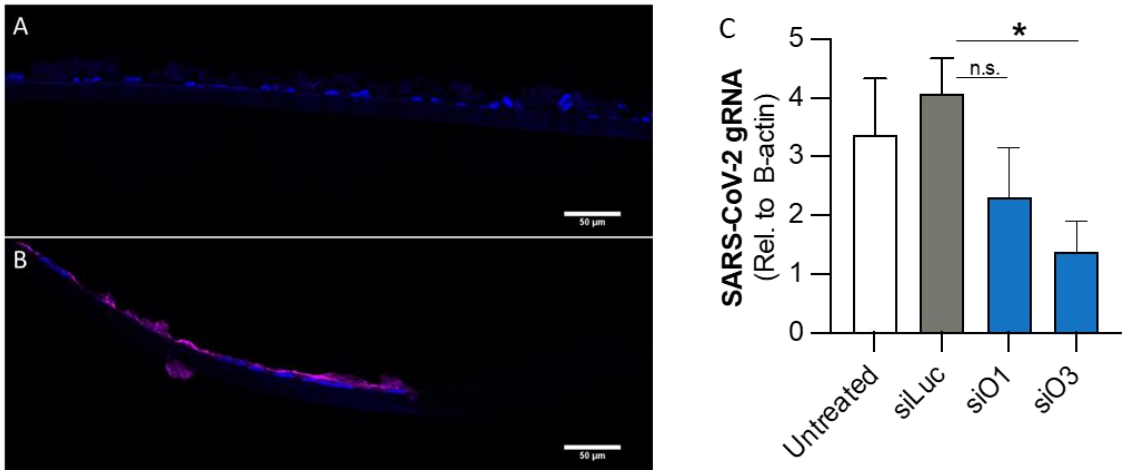

Figure 10. Evaluation of siORF/VIPER polyplexes activity against wild-type SARS-CoV-2 infection in Calu-3 cells grown at the air-liquid interface. (A, B) The expression of ACE-2 receptor on the apical side of Calu-3 cells was confirmed by preparing sections of Calu-3 monolayers. Pink color represents AF944 staining of ACE-2 receptor, blue color represents nuclei staining with DAPI. (C) SARS-CoV-2 downregulation in Calu-3 monolayers after treatment with SARS-CoV-2 specific siRNAs O1 and O3/VIPER polyplexes and siLuc/VIPER polyplexes as negative control. Calu-3 cells were infected with wild type SARS-CoV-2 (MOI 0.1) 6 h after transfection with polyplexes. Data points indicate mean ± SEM (n=3). Statistical significance was calculated using One-way Anova with Dunnett's multiple comparisons correction.

3.7. *Ex vivo* activity in human precision-cut lung slices (PCLS)

Human PCLS are complex *ex vivo* 3D tissue culture models that closely mimic the anatomy and physiology of the lung. By maintaining the 3D architecture as well as the cellular diversity found in the lung, they represent a highly relevant model closing the translational gap between *in vitro* and *in vivo* models to study respiratory viruses and to evaluate siRNA delivery to the lung (47,145). Previous studies confirmed their suitability as models for viral infections (146) as well as for testing the activity of siRNA-based formulations (147).

After titrating SARS-CoV-2 infection in PCLS (Supplementary Figure 3), the activity of siORF/VIPER polyplexes was tested in a prophylactic setup resembling the one described in the ALI model above. Infection with 1.0 MOI was performed 6 hours after polyplex transfection. qRT-PCR was performed 24 h after infection. In this experiment, chemically modified siRNA sequences of O1 and O3, namely O1* and O3*, were used. Chemical modification of siRNA is a common practice to improve its stability, which becomes particularly relevant in a clinical setup (20). Therefore, siRNA sequences were modified with the same modification pattern chosen for the recently approved Lumasiran (148). Considering that the hPCLS model contains a variety of cell types and closely mimics *in vivo* condition, we decided to use the chemically modified siRNA for testing siRNA/VIPER polyplexes in 3D human lung explants. As shown in Supplementary Table 1, polyplexes prepared with the modified siRNA showed comparable characterization parameters to the ones prepared with the unmodified version. The results confirmed an siRNA-mediated decrease of viral replication of about 50% for O1* O3*in comparison to the negative control. While the titration of the SARS-CoV-2 MOI amount in PCLS reflected a clear picture and confirmed infectability and dose-response in explanted human lung tissue (Supplementary Figure 3), the additional parameter of transfection introduced increased variability. While, to the best of our knowledge, we are the first to report SARS-CoV-2 infection and therapeutic siRNA transfection in PCLS, we can only compare our results to PCLS transfections where endogenous genes were silenced. Ruigrok *et al*. reported approximately 50% gene silencing of GAPDH in PCLS (147). However, we decided to silence viral factors rather than host factors with siRNA to avoid potential side effects. Therefore, our results of 50-75% gene silencing of coronaviral RNA levels in two different advanced models for SARS-CoV-2 infection emphasize the relevance of our approach as a promising therapy for the treatment of viral infections, particularly for COVID-19 (Figure 6).

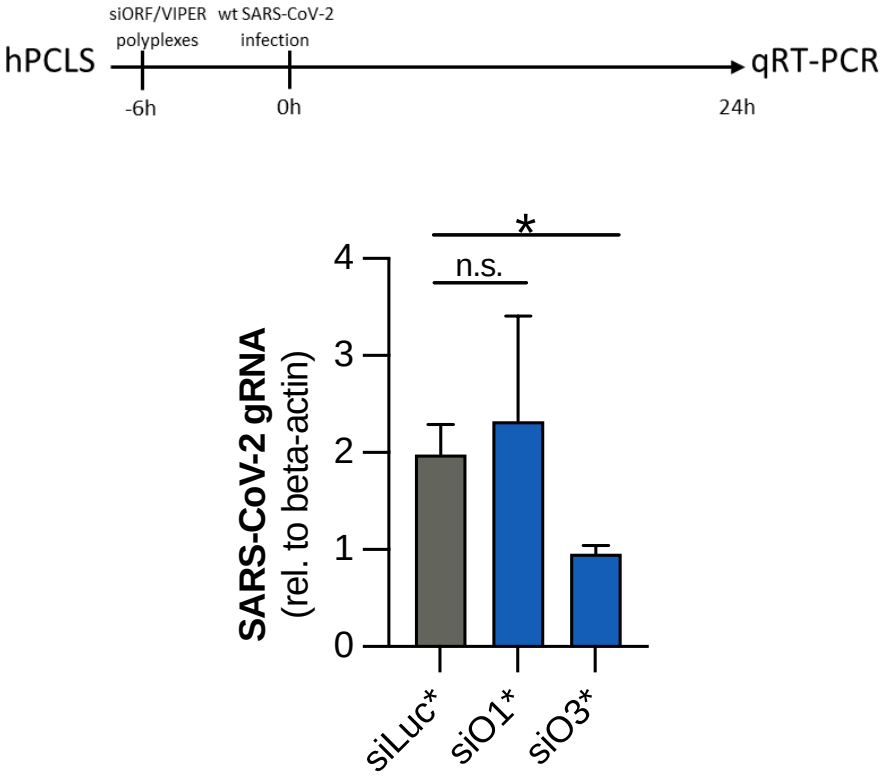

Figure 11. Evaluation of siRNA/VIPER polyplexes against wild-type SARS-CoV-2 in human PCLS. PCLS were transfected with chemically modified versions of SARS-CoV-2 specific and luciferase control siRNA (see Table 1) formulated as VIPER polyplexes 6 h before infection with wild-type SARS-CoV-2 (MOI 1). The readout was performed 24 h after infection via qRT-PCR. Significant differences (*p=0.019) were observed between the treatment with the unrelated luciferase vs. the O3* siRNA sequences. Data points indicate mean ± SEM (n=3).

3.8. *In vivo* delivery of polyplexes

Epithelial cells are considered the main site for SARS-CoV-2 replication in the lungs (149). Therefore, BALB/c mice were intratracheally administered with 2 nmol of VIPER as well as PEI polyplexes loaded with AF647-labeled siRNA to further assess pulmonary delivery of siRNA/VIPER polyplexes to epithelial cells. Two days after administration, bronchoalveolar lavage fluid (BALF) and blood were collected, while lungs were further processed to obtain a single cell suspension. Lung cells were counterstained with specific markers to identify different cellular populations present in the lung and to consequently understand the fate of polyplexes after pulmonary administration. As it can be observed in Figure 7, both siRNA/PEI and siRNA/VIPER polyplexes were found mainly in two cellular subsets: type II pneumocytes and macrophages. This experiment confirmed the delivery of siRNA to one of the main sites of viral replication - epithelial cells. Additionally, the cellular uptake observed in type II pneumocytes was surprisingly higher than the one observed in macrophages. Alveolar macrophages represent the first line cellular defense in the deep lung against foreign particulates, and their phagocytic

activity could result in clearance of the administered polyplexes (150). The ability to circumvent total macrophage clearance could be explained by the physicochemical characteristics of the formulation. Both PEI and VIPER polyplexes show sizes below 100 nm, while macrophages are known to most efficiently take up particles with sizes above 200 nm (151). Additionally, the large surface area covered by type II pneumocytes as well as the corona of adsorbed biomolecules (152) could favor the contact with the aerosolized polyplexes. Ultimately, the increased uptake of polyplexes by type II pneumocytes and in ciliated and club cells strengthens the rationale for using VIPER polymer for the delivery of siRNA to target the sites of viral replication in the lung (153,154). Both VIPER and PEI polyplexes efficiently reached type II pneumocytes, ciliated and club cells, although no significant differences were observed between both nanocarriers. The aim of this experiment is a qualitative analysis of which cell types are passively targeted in the lung rather than a quantitative assessment of *in vivo* efficacy. In a previous study of ours (124), we demonstrated that VIPER polyplexes can outperform PEI polyplexes in terms of gene silencing *in vivo*. The current study together with our previous finding confirms the potential of VIPER polyplexes as potential delivery system for siRNA against SARS-CoV-2 in the lung.

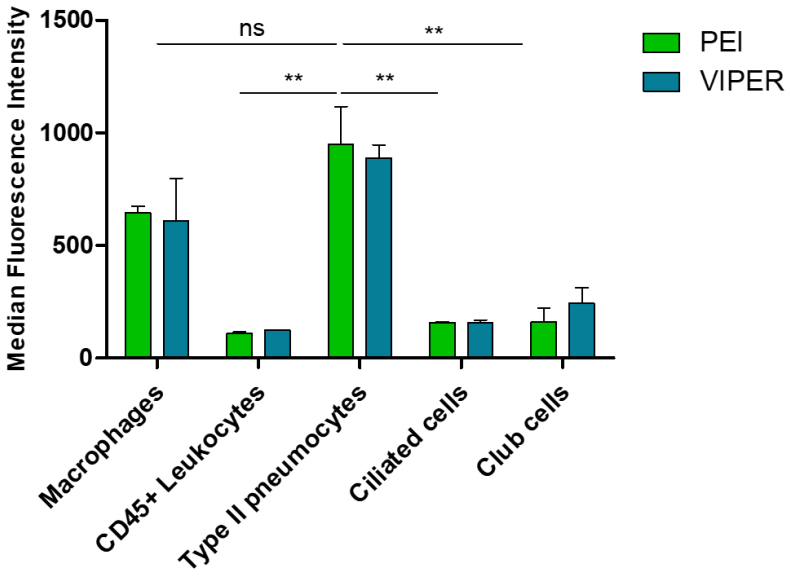

Figure 12. *In vivo* siRNA/VIPER polyplexes distribution in lung epithelial cells. BALB/c mice were intratracheally administered with 2 nmol AF647-siRNA complexed with either VIPER or PEI polymers. Negative control consisted of animals that received 5% glucose only. Cellular uptake of VIPER and PEI polyplexes in different lung cell populations was quantified by flow cytometry. One-Way ANOVA, ns = not significant, *p<0.05, **p<0.01.

An important factor to be taken into consideration when studying *in vivo* delivery is the proinflammatory effect in response to the i.t. administration of polyplexes. Both PEI and VIPER are positively charged polymers that could trigger an inflammatory response in the lung (155,156). Therefore, BALF and serum were analyzed with a LEGENDplex ELISA (BioLegend, San Diego, CA, USA) for inflammatory markers. As it can be observed in Figure 8, 13 different inflammatory cytokines were analyzed simultaneously to detect any proinflammatory effects. Only two cytokines showed an increase after i.t administration of polyplexes; namely IL-23 and MCP-1, which act as monocyte chemoattractant and T_h17 expander, respectively. However, cytokine production was limited and not statistically significant. A previous study by Beyerle *et al.* showed that PEI-PEG polyplexes can induce a 9-fold increase of MCP-1 production in BALF in comparison to the control animals three days after intratracheal administration (156). On the contrary, VIPER polyplexes induced only a 3-fold increase of MCP-1 expression in comparison to the control group which was not statistically significant. Furthermore, the proinflammatory effects following polyplexes administration where also analyzed in serum, to exclude systemic side effect (Supplementary Figure 4). Out of the 13 cytokines tested, a slight increase was observed only for IL-1α and IFN-β, 3-fold and 2-fold the control groups respectively. In line with the results from BALF analysis, no significant production of inflammatory cytokines was observed in serum.

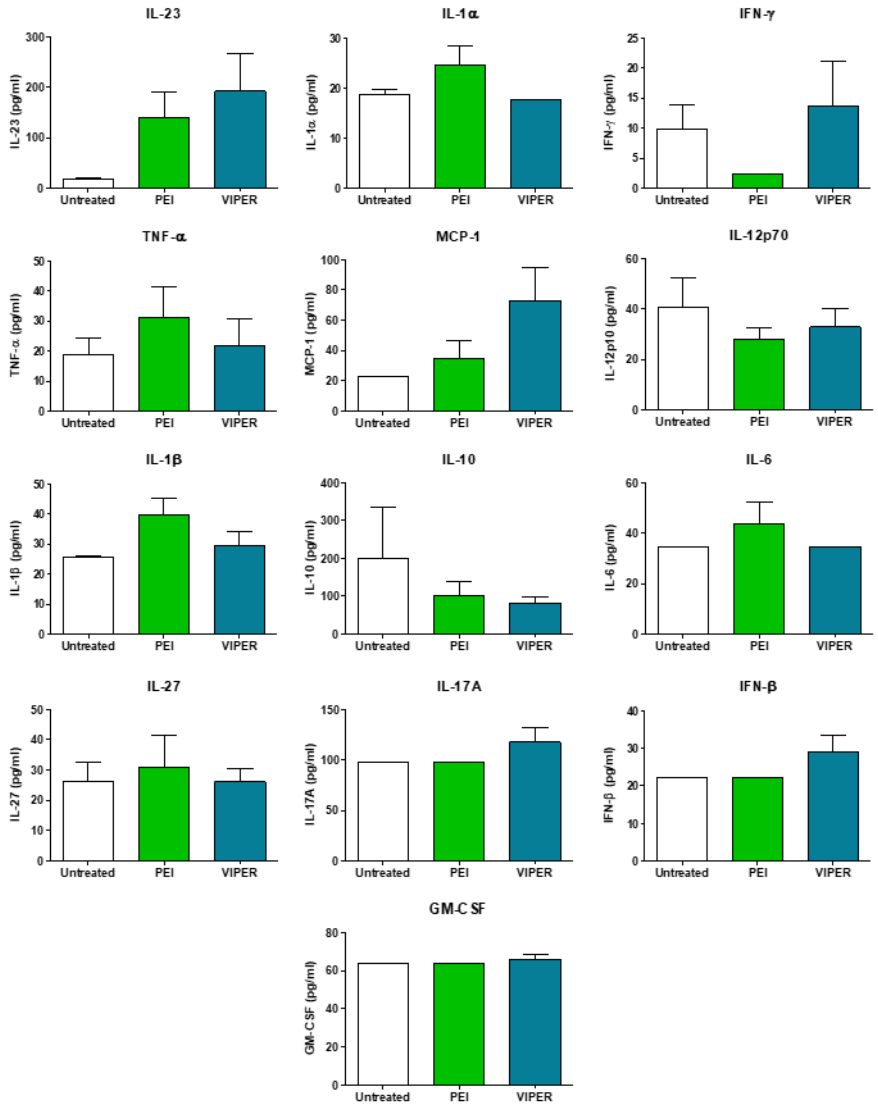

Figure 13. *In vivo* cytokines release was measured in bronchoalveolar lavage fluid (BALF) by LEGENDplex ELISA technique. Values are given in pg/ml as mean ± SEM (n=4). Value below detection limit were set as the value corresponding to the minimum detection limit. One-Way ANOVA, only non-significant differences were observed.

4. Conclusion

In this study, we present a formulation for pulmonary delivery of siRNA for the treatment of respiratory viral infection with a focus on SARS-CoV-2. Our present works demonstrates the ability of the block copolymer VIPER to form polyplexes with optimal properties for pulmonary administration, as well as improved stability in the challenging environment typical for the lungs compared to PEI polyplexes. siRNA/VIPER polyplexes reached lung epithelial cells *in vitro* and *in vivo* and penetrated through the mucus layer typical of the airways in an air-liquid interface 3D culture model. Additionally, polyplexes showed good tolerability both *in vitro* and *in vivo*. The activity against SARS-CoV-2 was

confirmed both *in vitro* in a 3D air-liquid interface cell culture model and *ex vivo* in 3D explants from human lungs. Collectively, these findings based on *in vitro* cell culture models, *ex vivo* human lung tissues and an *in vivo* animal model demonstrate the ability of siRNA/VIPER polyplexes to reach lung epithelial cells, the main site of viral replication in the lungs, and to suppress viral replication in mucus-covered cells as well as in human lung tissue. In conclusion, this study confirms the potential of siRNA-based therapies as antivirals and offers a new treatment option to tackle SARS-CoV-2 infection.

Acknowledgments

The authors thank Prof. Dr Ulrike Protzer for general support such as providing the *wildtype* SARS-CoV-2 virus. We gratefully acknowledge the provision of human biomaterial and clinical data from the CPC-M bioArchive and its partners at the Asklepios Biobank Gauting, the Klinikum der Universität München and the Ludwig-Maximilians-Universität München. The Core Facility Flow Cytometry at the Biomedical Center, LMU Munich is gratefully acknowledged. Funding by the Bavarian State Government for Förderprogramm Corona-Forschung (to T.M.), by the Volkswagen Foundation (to O.M.M., T.M., G.B.), by the European Research Council [ERC-StG 637830 to O.M.M.], by the National Institute of Health (grant numbers 1R01CA257563 and 2R01NS064404 to S.H.P.) and by the German Academic Exchange Service (DAAD to S.A.) are gratefully acknowledged.

Conflict of interest

T.M. is an ad hoc advisor for VIR Biotechnology and received research grants by Alnylam Pharmaceuticals and Gilead Sciences. M.F. is a consultant for Dr Hönle AG. O.M.M. is a consultant for AbbVie Deutschland GmbH, for PARI Pharma GmbH and an advisory board member for Coriolis Pharma GmbH. L.A.K. and A.P. are employees of AbbVie and may own AbbVie stock.

Supplementary materials

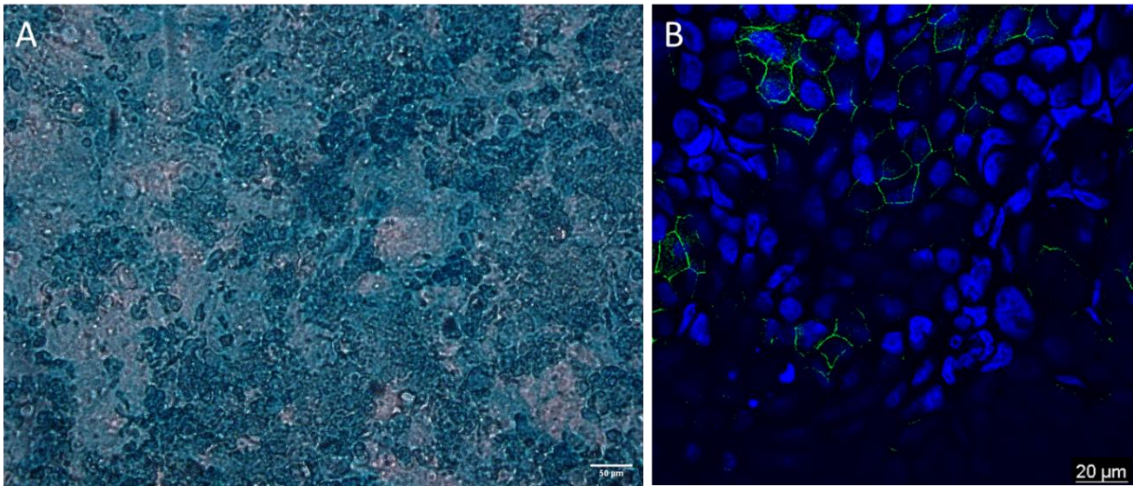

Supplementary Figure 1. Characterization of Calu-3 cells cultured at the air-liquid interface. (A) Alcian blue staining of the mucus layer secreted by Calu-3 cells. (B) Tight junctions staining of Calu-3 cells. Green color represents zonula occludens protein-1 staining with AF488 secondary antibody, blue color corresponds to nuclear staining with DAPI.

Formulation	Size (nm ± SD	PDI (± SD)	ζ potential (mV ± SD)
siO1_VIPER	69.9 ± 9.9	0.43 ± 0.14	6.6 ± 1.3
siO3_VIPER	49.5 ± 2.3	0.40 ± 0.08	13.2 ± 0.5
siO1*_VIPER	54.9 ± 1.2	0.52 ± 0.08	13.3 ± 1.8
siO3*_VIPER	38.7 ± 1.7	0.32 ± 0.02	12.5 ± 3.3

Supplementary Table 1. Hydrodynamic diameter, polydispersity index and zeta potential of VIPER polyplexes loaded with unmodified and modified siORF sequences.

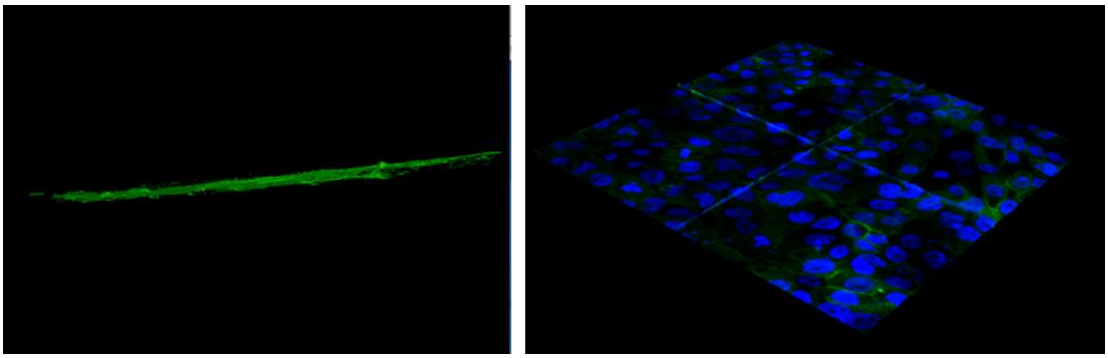

Supplementary Figure 2. Evaluation of siRNA/PEI polyplexes delivery to CAlu-3 cells grown at the air-liquid interface. (A) 3D reconstruction of mucus penetration of AF647-siRNA/PEI polyplexes in Calu-3 monolayers 24 h after transfection. (B) 3D reconstruction of cell uptake of AF647-siRNA/VIPER polyplexes 24 h after transfection analyzed by confocal light scanning microscopy.

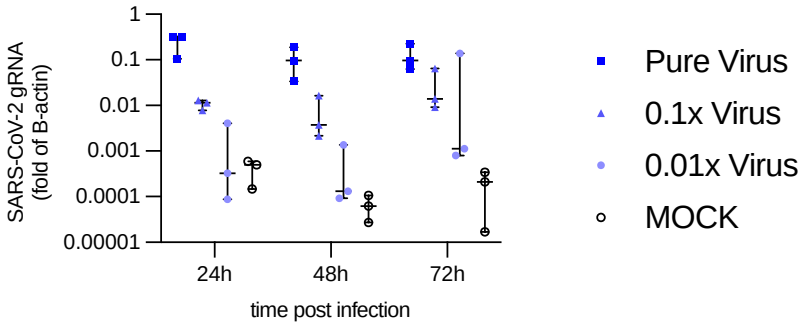

Supplementary Figure 3. Titration of SARS-CoV-2 in human PCLS.

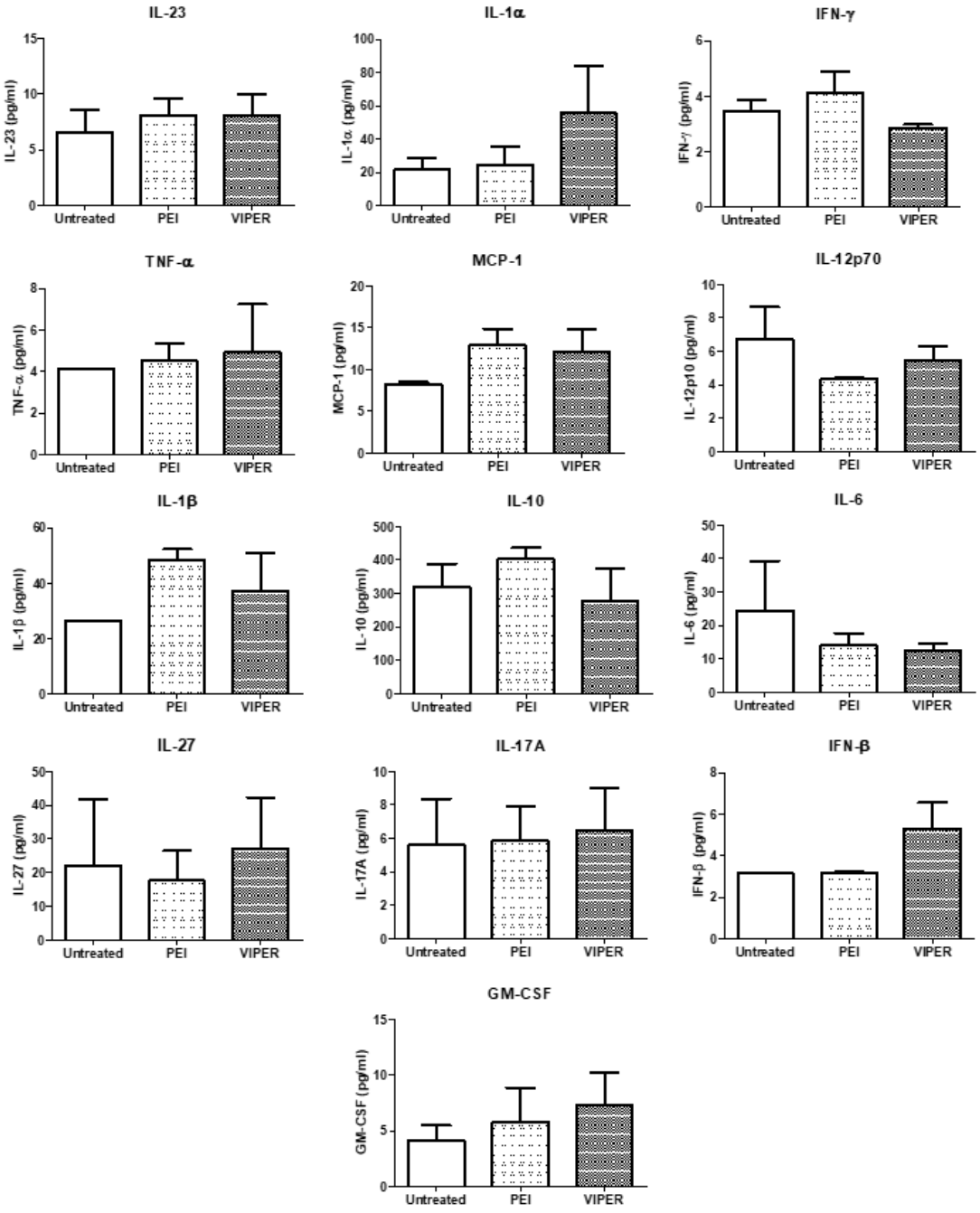

Supplementary Figure 4. *In vivo* cytokine release was measured in serum by LEGENDplex ELISA technique. Values are given in pg/ml as mean ± SEM (n=4). Values below detection limit were set as the value corresponding to the minimum detection limit. One-Way ANOVA, ns = not significant.

Chapter V - Methicillin-resistant *Staphylococcus aureus* and its intracellular infections: *in vitro* and *in vivo* efficacy of a novel antibiotic

Gabriella Costabile[a,b†], Domizia Baldassi[b,†], Christoph Müller[c], Birgit Groß[d], Franz Bracher[c,] Sören Schubert[d], Steven M. Firestine[e], Olivia M. Merkel[b,*]

[a]Department of Pharmacy, University of Napoli Federico II, Via Domenico Montesano 49, 80131 Napoli, IT
[b]Department of Pharmacy, Pharmaceutical Technology & Biopharmaceutics, Ludwig-Maximilian University of Munich, Butenandtstr. 5-13, 81377 Munich, DE
[c]Department of Pharmacy, Center for Drug Research, Ludwig-Maximilian University of Munich, Butenandtstr. 5-13, 81377 Munich, DE
[d]Max von Pettenkofer-Institut Munich für Hygiene und Medizinische Mikrobiologie, Elisabeth-WinterhalterWeg 6, D-81377 Munich, DE
[e]Department of Pharmaceutical Sciences, Eugene Applebaum College of Pharmacy and Health Sciences, Wayne State University, Eugene Applebaum College of Pharmacy and Health Sciences, 259 Mack Ave, Detroit, MI 48201, USA

[†]These authors contributed equally.

*Corresponding author: Olivia M. Merkel Department of Pharmacy, Pharmaceutical Technology & Biopharmaceutics, Ludwig-Maximilian University of Munich, Butenandtstr. 5-13, 81377 Munich, DE
Email: olivia.merkel@cup.uni-muenchen.de

Abstract

Antimicrobial resistance is considered as one of the biggest threats to the public health worldwide. Methicillin-resistant *S. aureus* is the causative agent of a number of infections and lung colonization in people suffering from cystic fibrosis. In this view, the development of novel antibiotics is of the essence and SV7, a novel antibiotic active at low concentrations against MRSA, represents a promising candidate. However, the low aqueous solubility of SV7 hampers its therapeutic translation. In this study, SV7 was encapsulated in PLGA nanoparticles to improve the solubility profile and to ensure a sustained release. Furthermore, PLGA NPs can be easily formulated for pulmonary administration and could be advantageous also to target intracellular infections. After

identifying a formulation with suitable characterization parameters, SV7-loaded NPs were investigated *in vitro* in terms of inhibitory activity against MRSA and safety profile in lung epithelial cells. Afterward, the activity against MRSA intracellular infections was investigated in a co-culture model of MRSA and macrophages. To test the translatability of our findings, SV7-loaded NPs were tested *in vivo* in a *G. mellonella* infection model showing the ability to prevent the establishment of the infection as well as higher survival rates without inducing any toxic effect. In conclusion, SV7-loaded NPs showed desirable characterization parameters for pulmonary delivery, a safe profile and activity against MRSA already at low concentrations. Furthermore, their activity was confirmed against intracellular infections and was retained also *in vivo*, establishing themselves as a promising candidate for the treatment of MRSA infections.

KEYWORDS PLGA nanoparticles; benzophenone antibiotics; sustained release; *G. mellonella*

1. Introduction

Staphylococcus aureus and its methicillin-resistant phenotype (MRSA) are the causative agent of a wide variety of infections, ranging from minor skin infections, nosocomial infections to life-threatening diseases. Notably, MRSA represents a harmful pathogen for other pathologies such as cystic fibrosis (CF). In fact, it has been demonstrated that *S. aureus* is one of the first bacteria able to colonize the airways of CF patients. Here, *S. aureus* produces the conditions for later infections sustained for example by Pseudomonas aeruginosa, which dramatically worsen the clinical outcome and result in an increased rate of lung function decline (1). In the era of antimicrobial resistance crisis, to support the battle against *S. aureus* infections as well as its early eradication, the development of new antibiotics, preferably with new targets in the bacterial cells, is pivotal.

In this work, a novel active compound discovered by Firestine and co-workers, namely SV7, has been taken into account. SV7 has indeed shown a very promising activity not only against methicillin-sensitive *S. aureus* (MSSA), but also against MRSA strains without inducing AMR phenomena (2,3). This compound is a novel benzophenone-based membrane-targeting antibiotic that has similarities to the structure and function of antimicrobial peptides (AMPs) and synthetic ion channels (2,3). From a technological point of view, there are two major obstacles to its translation into the clinics: low aqueous solubility, which can affect its dissolution in the physiological fluid, and the ability of *S. aureus* to generate intracellular infections. The treatment of *S. aureus* is indeed

particularly challenging as this pathogen can escape the immune response through invasion of both non-professional and professional host phagocytes such as endothelial and epithelial cells as well as monocytes, macrophages, and polymorphonuclear leukocytes. As a consequence, most therapies result completely ineffective against intracellular infections since many conventional antimicrobials show restricted intracellular penetration or low retention and considering that, once internalized, the pathogen will be protected up to 4-7 days without affecting host cell viability (4–6).

In order to overcome these limitations, our proposed approach has been the development of a PLGA-based delivery system, which could serve the dual purpose of increasing SV7 bioavailability but also help the delivery of SV7 inside the host cells to treat the intracellular infections (7). Thus, the general aim of this work has been the development and preclinical evaluation of SV7-loaded PLGA NPs to demonstrate, first *in vitro* and then *in vivo*, the high potential of SV7 in the treatment of infection sustained by MSSA and MRSA strains even when intracellularly established. For successful delivery of the drug to the site of action, an interesting approach is represented by the development of a nanoparticle-based formulation for direct administration to the lungs. In fact, among all the other advantages expected, avoiding the systemic route, a consequent reduction of the administered dose may be useful to reduce the patients' exposure to antibiotics resulting in a delay of eventual AMR induction (Zhou et al. 2015). Additionally, it is expected that the number of administrations can be reduced, increasing patient adherence to complex therapeutic regimens required by chronic lung diseases (8).

Very unique anatomical and physiological features make pulmonary delivery particularly advantageous in terms of drug adsorption allowing for a better control of the administrated dose. This aspect is particularly welcomed for antibiotics therapy considering the direct correlation between the onset of AMR phenomena and the drug dose (9).

In this project, NPs were produced through a single evaporation emulsification method and the composition has been optimized based on size, polydispersity index, surface charge and especially on the enhancement of SV7 loading, to achieve a formulation with desirable physicochemical parameters for pulmonary administration.

The formulations were characterized for morphology, residual amount of organic solvents and stability over time, evaluating the possibility to extend the shelf-life of the formulation through freeze-drying. In order to evaluate how the manufacturing process could alter the SV7 release in a physiological environment, the antimicrobial activity and

the potential cytotoxic effect were tested *in vitro* in suitable models. cytotoxic effects on human epithelial lung cells (A549, 16HBE14o-). Furthermore, the potential of the NPs in the treatment of intracellular infection was evaluated in terms of cellular uptake as well as activity against MRSA intracellular infection on a macrophage cell line (J774A.1) in presence of fluorescently labelled NPs and SV7-loaded NPs, respectively. Finally, preliminary activity data on the *in vivo* performance to better support further translation into clinics, were collected in a *Galleria Mellonella* infection model, a valid tool for studying the antimicrobial activity of antibiotics encapsulated in polymeric nanoparticles (10,11).

2. Experimental methods

2.1 Materials

SV7 was synthesized as described previously (2,3,12). Resomer® RG 502 H, Poly(D,L-lactide-co-glycolide) (PLGA) 50:50 (molecular weight 7kDa) was purchased from from Evonik Nutrition & Care GmbH (Essen, Germany). Polyvinyl alcohol (PVA) (Mw ~205 kDa), mannitol, trehalose, 2-hydroxypropyl-β-cyclodextrin (HP-β-CD), acetone and dichloromethane were purchased from Sigma-Aldrich (St Louis, MO, USA). All solvents used were ACS grade solvents.

Human lung adenocarcinoma epithelial cells (A549) and mouse BALB/c monocyte macrophages (J774A.1) were obtained from ATCC (LGC Standards GmbH, Wesel, Germany) human bronchial epithelial cell line (16HBE14o-) were a kind gift from the Comprehensive Penumology Center of Munich. Minimum Essential Medium (MEM), Roswell Park Memorial Institute (RPMI) 1640 Medium, Dulbecco's Modified Eagle Medium (DMEM), fetal bovine serum (FBS), L-glutamine, MEM non-essential amino acid solution and penicillin-streptomycin (P/S) for cell culture were purchased from Sigma-Aldrich (St Louis, MO, USA). 3-(4,5-Dimethylthiazol-2-yl)-2,5-Diphenyltetrazolium Bromide (MTT), Lysotracker™ red and Trypsin 0.25% EDTA were purchased from Thermofisher scientific (Waltham, MA). All other chemicals were standard chemicals required for cell and bacterial culture.

Microscope slides were purchased from VWR (Radnor, PA, USA). FluorSave™ reagent was purchased form Merck Millipore (Burlingtone, MA, USA). 13 mm Karl Hecht™ Assistent™ Circular Cover Glasses for Microscopy were purchased from Fischer Scientific (Hampton, NH, USA).

2.2 SV7 Analytical determination

The amount of SV7 in the samples was measured via UV spectroscopy at 265 nm using a microplate reader with quartz 96 well plate (FLUOstar Omega, BMG Labtech, Ortenberg, Germany) as previously reported (13). Briefly, a known amount of SV7 was placed into microcentrifuge tubes, then 500 µL of dichloromethane (DCM) and 1 mL 50 mmol HCl were added. The samples were vortexed and the two phases were left to separate. Protonated SV7 is present in the aqueous phase. A calibration curve was obtained by plotting absorbance versus the concentration of SV7 standard solutions prepared in DCM. The linearity of the response was verified over a concentration range of 0.5-25 µg/mL (r2 = 0.999). The extinction coefficient determined from the standard curve was 0.050.

2.3 Production of SV7-loaded PLGA nanoparticles

PLGA nanoparticles as well as SV7-loaded PLGA (PLGA_SV7) were prepared through a single evaporation emulsification method, adapting a protocol previously published (13). Briefly, the organic phase was prepared by dissolving PLGA in acetone. When needed, SV7 was added to the organic phase. Then, the organic solution was added dropwise to the aqueous phase of Polyvinyl alcohol (PVA) (1, 1.5 and 2% w/v) under magnetic stirring (1200 rpm). The emulsion formed was treated for 10 min with an ultrasound probe sonicator (heat flux density 8.5 W/cm2) and left under stirring overnight to evaporate the organic solvent. Nanoparticles were recovered and washed with Milli-Q water by centrifugation at 16900 g and 4 oC for 30 min, the supernatant was discarded and the procedure was repeated twice. The NPs were then suspended in 10 mL of Milli-Q water.

2.4 Characterization of SV7-loaded PLGA nanoparticles

2.4.1 Nanoparticle size, polydispersity index, surface charge through DLS and size through TRPS

The hydrodynamic diameter (D_H), the polydispersity index (PDI), and zeta potential (ζ) of the freshly prepared nanoparticles were measured by dynamic light scattering Zetasizer (Nano ZS, Malvern Instruments, Grovewood, UK). In particular, the nanoparticles suspension was diluted 10-fold with Milli-Q water for size and polydispersity index determination, while it was diluted 100-fold for zeta potential determination. All the measurements were performed in triplicate (n=3) and the results are expressed as mean value ± standard deviation (SD).

The particle size was confirmed using a qNano size analyzer (iZON Sciences, Christchurch, New Zealand) with a nanopore 200 (iZON NP 200) and a calibration particle 200 nm (CP 200). Buffer containing sodium chloride (NaCl), Tris (pH 8),

ethylenediaminetetraacetic acid, and triton in deionized water was used as the electrolyte to suspend the NPs sample and the calibration particles. Each recorded measurement was based on 500 nm particles and the size was measured using the iZON control suite 2.2 software.

2.4.2 Nanoparticle surface morphology

Surface morphology of the nanoparticles was evaluated using scanning electron microscope (SEM) (FEI, Helios G3 UC Dual beam Thermofisher scientific, Waltham, MA, USA). For sample preparation, prior observation 10 □L of nanoparticles in suspension were deposited on a metal stub and, after drying, the sample was coated with gold under vacuum for 120 s. The SEM images were analyzed using the free software ImageJ to calculate the particles size.

2.4.3 Drug loading and entrapment efficiency

The drug loading of SV7 in the NPs was assayed by dissolving 100 µL of SV7-loaded PLGA nanoparticles in 500 µL of DCM and then following the analytical procedure described above. The drug loading is reported as the percent of the amount of SV7 in relation to 10 mL of NPs suspension ± SD of value collected from three different batches. The entrapment efficiency (EE) is reported as percent of the ratio between the drug loading and the theoretical loading ± SD of value collected from three different batches.

2.4.4 Residual organic solvent after nanoparticles production

At the end of the NPs preparation, the residual amount of organic solvents in the formulation was evaluated through static headspace gas chromatography-mass spectrometry (HS-GC-MS) (14). An Agilent Technologies 7890B gas chromatograph (Waldbronn, Germany) was coupled with an Agilent Technologies 7010B triple quadrupole detector. The MS was operated in scan mode (m/z 50 -150; EI 70 eV). The corresponding autosampler, PAL RSI 85, came from the company CTC Analytics (Zwingen, Switzerland). An Agilent J&W GC column DB-624 Ultra Inert (6% cyanopropyl phenyl and 94% polydimethylsiloxane) 30 m × 0.25 mm × 1.4 µm from Agilent Technologies (Waldbronn, Germany) was used as stationary phase. The carrier gas used was helium 99.999% from Air Liquide (Düsseldorf, Germany). The conditions of the headspace sampler and the GC-MS system are summarized in Supplementary Table 1. 100 mg of sample were weighted into a 20 mL headspace vial, 5 mL deionized water, 2 g NaCl and 10 µL of stable isotope–labelled internal standard solution (100 µg/mL acetone d6, SIL-IS) was added, and the vial was closed tightly. After sealing, the sample was analyzed by static HS-GC-MS. The molecule peaks of acetone and acetone D6 (SIL-IS) (m/z 58.1 and 64.2) were used as qualifier ions and the base peaks m/z 43.2 and 46.2 as quantifier ions.

2.4.5 Nano-embedded dry powder production through freeze-drying

Nano-embedded dry powders were produced through freeze-drying. The optimized SV7-loaded PLGA nanoparticles were shock frozen in liquid nitrogen and lyophilized overnight using a VirTis BenchTop Pro freeze dryer (SP Scientific, Warminster, PA, USA). To improve the dry powder properties after freeze-drying, different cryoprotectants, such as mannitol, trehalose and 2-hydroxypropyl-β-cyclodextrin (HP-β-CD), in different concentrations were tested. The dry powders were then stored in closed vials at room temperature in a desiccator. To evaluate the redispersibility of the freeze-dried powder, particle size analysis of the reconstituted liquid dispersion was performed through dynamic light scattering Zetasizer (Nano ZS, Malvern Instruments, UK) and the results are expressed as mean value ± SD of value collected from three different batches.

2.4.6 In vitro release profile

The *in vitro* drug release behavior of SV7 from SV7-loaded PLGA nanoparticles, before and after freeze drying, was determined. Phosphate buffer saline (PBS) (120 mM NaCl, 2.7 mM KCl, 10 mM Na2HPO4) at pH 7.2 with 0.2% Tween 80 was used as buffer (15). During the study the samples were kept at 37 °C with shaking. At scheduled time intervals, samples were centrifuged at 15700 g for 10 min at 4 °C to isolate the NPs while the release medium was withdrawn and analyzed by UV spectroscopy for SV7 content as previously described. The medium was replaced by the same amount of fresh PBS at pH 7.2. Experiments were carried out in triplicate and results expressed as cumulative release of SV7 from NPs ± SD.

2.5 In vitro antimicrobial activity

The minimum inhibitory concentration (MIC) of SV7 as free compound and after encapsulation in PLGA NPs was determined by the broth microdilution method in 96-well microplates (Falcon). Both gram-positive and gram-negative strains were used for the experiments (Methicillin sensitive *Staphylococcus aureus* (ATCC 29213), Methicillin resistant *Staphylococcus aureus* (ATCC 43300), *Pseudomonas aeruginosa* (ATCC 10145), *Escherichia coli* (ATCC 25922), *Klebsiella pneumoniae* (ATCC 700603) as well as Pseudomonas aeruginosa, Enterobacter cloacae, Serratia marcescens, *Klebsiella oxytoca*, *Citrobacter freundii* and *Proteus vulgaris* from clinical isolates). Briefly, every strain was grown in Luria Bertani (LB) broth at 37 °C. The bacterial suspension to be used as the inoculum was diluted to yield an optical density (OD) around 0.5 at 600 nm (corresponding to about 1×109 CFU/mL). Afterwards, the bacterial cell suspension was further diluted 100-fold to produce a bacterial cell suspension of 10×104 CFU/mL. SV7 encapsulating PLGA nanoparticles were serially diluted 2-fold in Brain Heart Infusion (BHI) broth to achieve final concentrations ranging from 50 µg/mL to 0.1 µg/mL in a final

volume of 200 µL (including 100 µL of bacterial suspension). Free SV7, ciprofloxacin, tobramycin and erythromycin (Amdipharm) were used as controls in the same concentration range used for SV7 encapsulating PLGA NPs. The bacterial suspension alone was used as the positive control while the negative controls were the antibiotics at the highest concentrations and BHI broth alone. After 24 h of incubation the plates were visually inspected. The MIC is defined as the lowest concentration of the tested antibiotic at which no growth of the inoculum was observed.

2.6 *In vitro* cytotoxicity on lung cells

2.6.1 Cell culture

Human adenocarcinoma alveolar based lung cancer cells (A549) were cultured in RPMI 1640 cell culture medium and supplemented with 1% penicillin/streptomycin and 10% fetal bovine serum (FBS). Human epithelial bronchial cells (16HBE14o-) were cultured in EMEM cell culture medium supplemented with 1% L-glutamine, 1% penicillin/streptomycin and 10% FBS. Cells were grown in 75 cm2 cell culture flasks and passaged every 3 days with 0.05% and 0.25% trypsin, respectively. Cells were maintained in a humidified atmosphere at 37 °C and 5% CO2.

2.6.2 Cell viability and lactate dehydrogenase (LDH) release

When confluent, A549 and 16HBE14o- cells were trypsinized and seeded at a density of 10000 cells per well in 100 µL of medium in 96-well plates. Twenty-four hours after seeding, the medium was removed and 100 µL of fresh medium containing different amounts of PLGA_2.5SV7 nanoparticles corresponding to a certain amount of SV7 entrapped (1.6, 8, 16, 40, 80 and 160 µg/mL of SV7), or their corresponding controls were added to each well. After the NPs addiction, the plates were incubated for 24 h, 48 h and 72 h respectively at 37 °C and 5% CO_2. At each time point, the medium from the wells was collected to assess the LDH release assay while 100 µL of a 0.5 mg/mL MTT sterile solution were added to each well. After 3 h of incubation each well was washed PBS and then 200 µL of acidic isopropanol (0.04 M HCl in absolute isopropanol) were added and the plates placed on orbital shaker for 15 minutes. The absorbance was read at 570 nm using a microplate reader (FLUOstar Omega, BMG Labtech). Control groups included cells treated with blank nanoparticles and free SV7 dissolved in DMSO. The percentage of viable cells was calculated by the ratio of absorbance of treated cells compared with untreated cells. Results are given as mean values of triplicates ± SEM.

CytoTox 96® non-Radioactive Cytotoxicity Assay (Promega, Madison, WI, USA) according to the manufacturer's guidelines was used to quantify the LDH release. The absorbance was read at 490 nm using a microplate reader (FLUOstar Omega, BMG

Labtech). Control groups included cells treated with blank nanoparticles. The percentage of cytotoxicity was calculated by the ratio of absorbance of treated cells compared with lysed cells (maximum LDH release control). Results are given as mean values of triplicates ± SEM.

2.7 *In vitro* cellular uptake

2.7.1 Cell culture

Mouse BALB/c monocyte macrophages (J774A.1) were cultured in DMEM cell culture medium supplemented with 1% glutamine, 1% pencillin/streptomycin and 10% FBS. Cells were grown in 75 cm^2 cell culture flasks at 37 °C and 5% CO_2.

2.7.2 Cellular uptake by flow cytometry

To evaluate the cellular uptake of nanoparticles by macrophages, the fluorescent dye coumarin-6 was incorporated in SV7-PLGA formulation. J774A.1 macrophages were seeded at a density of 50.000 cells/well in a 24-well-plate and incubated for 24 h at 37 °C and 5% CO_2. Cells were then transfected with 100 µl of coumarin-6-loaded PLGA (PLGA_C6) nanoparticles suspension for 2, 4, 24 and 48 h. At different time points, cells were harvested and washed two times at 400 xg for 5 minutes and resuspended in PBS/2 mM EDTA. Cells were analyzed using an Attune NxT flow cytometer (Thermofisher Scientific, MA, USA) with 488nm excitation and 530nm emission filter. Cells were gated based on morphology resulting from forward/sideward scattering and 10.000 events were analyzed per sample. Results are given as mean values of triplicates ± SEM.

2.7.3 Confocal microscopy

J774A.1 macrophages were seeded in a 24-well-plate containing a cover glass at a density of 50.000 cells/well in 500 µL of medium and incubated for 24 h at 37°C and 5% CO2. The day after, cells were transfected with 100 µl of coumarin-6 loaded nanoparticles and incubated for 2, 4, 24 and 48 h. One hour before the incubation time was completed, cells were washed with PBS two times and incubated with 300 µl of a 75 nM LysoTracker® red (Thermofisher Scientific, MA, USA) solution, an organelle-specific labelling dye. Cells were then washed two times with PBS and fixed with 4% paraformaldehyde for 15 minutes. After three washing steps, cells were finally incubated with DAPI (4',6-diamidino-2-phenylindole) at a final concentration of 1 µg/mL for 20 minutes. Cells were then washed again two times and mounted using FluorSave™ (Merck Millipore, Billerica, USA) reagent for confocal microscopy. Fluorescent images were acquired using a SP8 inverted scanning confocal microscope (Leica Camera, Wetzlar, Germany).

2.8 SV7-loaded nanoparticles against MRSA intracellular infection

To evaluate the activity of SV7-loaded NPs against intracellular infections, J774A.1 macrophages were seeded in a 24-well-plate at a density of 50.000 cells/well in 500 µl of medium and incubated for 24 h at 37°C and 5% CO_2. Afterwards, MRSA was added to the cells at a concentration of $2.5*10^5$ CFU/well and co-cultivated for 1 h. Cells were then washed with PBS and the medium was replaced with fresh medium containing 1 µg/ml gentamicin to remove extracellular MRSA. After 30 min, plates were washed with PBS and fresh medium containing free SV7 in DMSO, SV7-loaded NPs and empty NPs was added at final SV7 concentrations of 8.5, 17, 42.5 and 85 µg/ml. After 24 h, cells were lysed with ice-cold 0.1% Tryton-X for 15 min and collected in Eppendorf tubes. The lysates were serially diluted in PBS for colony count in blood agar plates. Bacterial colonies were counted after overnight incubation at 37°C. The results are expressed as X-fold reduction in comparison to the cells that received only MRSA infection and no treatment.

2.9 *In vivo* antimicrobial activity

2.9.1 In vivo toxicity and survival of G. mellonella larvae

The antimicrobial activity of SV7-loaded nanoparticles was tested *in vivo* on TruLarv™ *Galleria mellonella* (Biosystems Technology, Exeter, UK) model. The safety of the formulation was evaluated by injecting larvae with 10 µL of the different samples (8.5 µg/mL) and the survival percentage was observed for the following 96 h.

In a pre-treatment study, larvae received a 10 µL injection of SV7-loaded NPs or the respective unloaded control (8.5 µg/mL), 24 h before the infection with LD50 *S. aureus* methicillin-sensitive ($2.5*10^5$ CFU/ml) or *S. aureus* methicillin-resistant ($7.5*10^5$ CFU/ml). Larvae were incubated in the dark at 37 °C and the survival percentage was monitored 24, 48 and 72 h post-infection. Each experiment consisted of 10 larvae per group. Control groups consisted of untreated larvae, PBS-only injected larvae and infected-only larvae.

2.9.2 G. mellonella bleeding for residual bacterial load

In a following study, the residual bacterial load from larvae was evaluated by harvesting the hemolymph of 3 larvae per group (untreated, infected-only, PLGA NPs and SV7-PLGA NPs) 72 h post-infection. The hemolymph was serially diluted in PBS and 15 µL of each sample were plated on blood agar. Bacterial colonies were counted after overnight incubation at 37 °C.

2.9.3 Statistical analysis

Percent survival of G. *mellonella in vivo* study was shown as Kaplan-Meier plots and statistical significance was determined using the log-rank (Mantel-Cox) test (GraphPad

Prism 5.0). Statistical significance of the residual bacterial load in G. *mellonella* was analyzed by One-way ANOVA with Turkey post-test (GraphPad Prism 5.0). Statistical significance values were indicated as *P<0.05, **P<0.01, ***P<0.005.

3. Results and discussion

3.1 Production and characterization of SV7-loaded PLGA nanoparticles

SV7 is a novel benzophenone-based membrane-targeting antibiotic which is able to release potassium ions resulting in the disruption of the bacterial membrane. The major obstacle for its clinical application is its low aqueous solubility that can affect its dissolution in physiological fluid such as the lung lining fluid where the bacteria are located. Thus, SV7-loaded PLGA nanoparticles were prepared through a single evaporation emulsification method in order to encapsulate and deliver SV7. In our group, this approach has been already exploited for controlled release purposes (16). With special regard to SV7, in order to increase the reported encapsulation efficiency (EE) of 33.3 ± 5.13%, an in-depth formulation study was carried out (13). At first it was evaluated the best ratio between PLGA and a fixed amount of PVA. Smaller NPs could be fabricated using a PLGA:PVA ratio equal to 0.1% w/v. (Supplementary Figure 1).

A.

	PLGA (% w/v)	PVA (% w/v)	PLGA:SV7 (w:w)
PLGA_10SV7_1PVA	0.1	1.0	1:1
PLGA_5SV7_1PVA	0.1	1.0	2:1
PLGA_2,5SV7_1PVA	0.1	1.0	4:1
PLGA_5SV7_1.5PVA	0.1	1.5	2:1
PLGA_2.5SV7_1.5PVA	0.1	1.5	4:1
PLGA_5SV7_2PVA	0.1	2.0	2:1
PLGA_2.5SV7_2PVA	0.1	2.0	4:1

B.

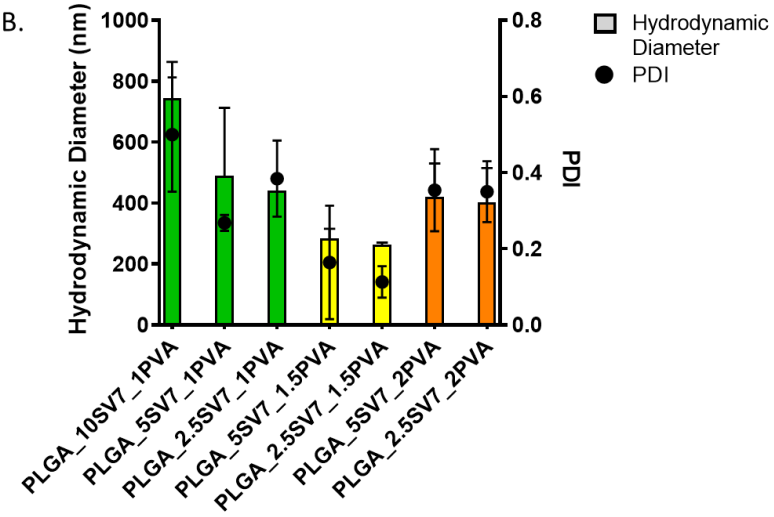

Figure 1. SV7-loaded PLGA nanoparticles (A) composition and (B) hydrodynamic diameter (DH) and polydispersity index (PDI) characterized by dynamic light scattering.

Then SV7 was added to the formulation varying parameters such as the amount of payload added to the formulation or the surfactant concentrations (Fig. 1A). Through this approach, we determined that keeping the ratio between PLGA:SV7 at 4:1 (PLGA_2.5SV7) and 2:1 (PLGA_5SV7), in presence of 1.5% w/v of PVA, it is possible to produce NPs characterized by an hydrodynamic diameter around suitable for lung administration purpose (9,17,18) (Figure 1B).

In particular, the NPs suspension analyzed through Dynamic Light Scattering (DLS) showed dimensions of 277.19 ± 37.14 and 253.65 ± 16.79 nm respectively for PLGA_2.5SV7 and PLGA_5SV7 (Table 1). The NP suspensions are characterized by a very homogenous nature with a polydispersity index (PDI) of 0.100 ± 0.050 and 0.090 ± 0.040 (Table 1). Both formulations presented a negative surface with a ζ-potential around -17 mV (Table 1).

Finally, the freshly prepared SV7-loaded PLGA nanoparticles produced respectively with 2.5 and 5 mg of SV7 were characterized also for their encapsulation efficiency (EE) (Table 1).

	PLGA_2.5SV7	**PLGA_5SV7**
D_H (nm ± SD)	253.65 ± 16.79	277.19 ± 37.14
PDI (± SD)	0.090 ± 0.040	0.100 ± 0.050
ζ Potential (mV ± SD)	-16.96 ± 6.76	-17.53 ± 6.18
SV7 drug loading* (mg ± SD)	1.48 ± 0.060	2.14 ± 1.14
Entrapment efficiency (%)**	59.40 ± 2.4	42.82 ± 22.8

Table 1. Overall characterization of PLGA_2.5SV7 and PLGA_5SV7

*mg SV7 / 10 ml SV7-loaded PLGA nanoparticles suspension

**Entrapment efficiency is calculated as percent of the ratio between drug loading and theoretical loading

EE is calculated as the ratio between the actual and the theoretical loading × 100 and resulted respectively of 59.40 ± 2.4% and 42.82 ± 22.8%, corresponding to a bulk loading of 1.48 ± 0.060 and 2.14 ± 1.14 mg of SV7 for batch. These results are considerably improved compared to the first report in which the EE was 33.3 ± 5.13% (13). Based on the higher entrapment efficiency the formulation PLGA_2.5SV7 was selected for further characterizations.

An in depth particle diameter measurements was performed by tunable resistive pulse sensing (TRPS) (19–21). In this case, the collected data displayed an even smaller mean diameter of 188 ± 65 nm supported by a nanoparticles size distribution that shows how the majority of the particles population has a size lower than 250 nm (Supplementary Figure 2). This difference could be attributed to the difference in the working principle between the DLS and TRPS technique. In fact, TRPS performing a particle-by particle-measurements is able to provide a finest measurement which has been confirmed through SEM observation. SEM images show particles with spherical shape and a size of 142.06 ± 7.93 (Figure 2) as verified with manual size counting through ImageJ (20).

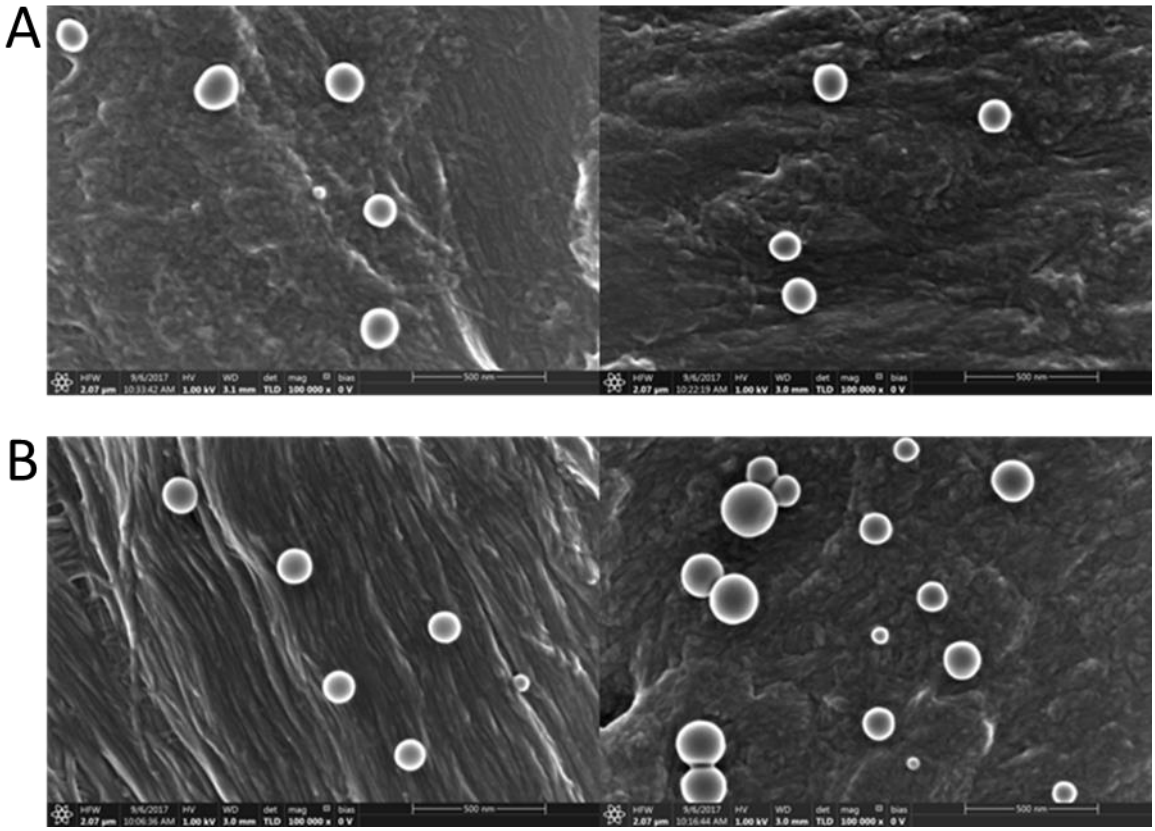

Figure 2. SEM images of PLGA_5SV7 (A) and PLGA_2.5SV7 (B).

Considering that the production of PLGA_2.5SV7 nanoparticles has involved a single evaporation emulsification method, a residual amount of organic solvents could be find in the final NPs suspension. Because of the potential risk for the human health the acceptable amount of residual solvent is strictly regulated from the authorities. In particular, acetone is classified in class 3 which includes solvent considerate as less toxic and of lower risk. Nevertheless, the European medicines agency says that it would be acceptable, without further justification, a residual solvent amount of 50 mg per day or less (corresponding to 5000 ppm or 0.5%) (Ph.Eur. 11th Ed.). In order to evaluate if the formulation responds to this required standard, the residual acetone has been quantified through gas chromatography-mass spectrometry after nanoparticles production. The mean residual content of acetone was 0.45 µg per 100 mg sample (w/w) corresponding to 0.0005% ± 0.0001% (± SD, n=3) assuring in this way the tolerability of the formulation.

After production the NP suspension was stored at 4 °C to test the stability over time (Supplementary figure 3). After 60 days of storage, almost a 0.5-fold increase in the particle hydrodynamic diameter was observed compared to the original value, while in the same time frame, the PDI showed a 4-fold increase. This instability is not surprising and is given by hydrolytic degradation of PLGA in the aqueous environment, as well as

the aggregation phenomena arising from its storage (22). However, in a translational perspective the need to extend the storage stability was highlighted. Thus, to enhance the shelf life of the formulation and avoid the loss of native nanocarrier characteristics, a strategy commonly used by pharmaceutical industries with an easy industrial scale-up such as the lyophilization was used (23,24). The optimized formulation PLGA_2.5SV7 was further processed to achieve a solid long-term stable lyophilized powder which can be reconstituted in saline solution and, in order to prevent particles from degradation and aggregation during freeze-drying, cryoprotectants were added to the NPs suspension. Among the possible others, were preferred excipients already used for lung administration or that could add a functionality to the NPs suspension as airways rehydrating agents (i.e. mannitol, trehalose and 2-hydroxypropyl-β-cyclodextrin) (25).

The selected cryoprotectants have been added to the SV7-loaded PLGA nanoparticles suspension at different concentrations. After the solidification process, the hydrodynamic diameter and the polydispersity index of PLGA_2.5SV7 NP reconstituted through saline solution addition after lyophilization has been performed through dynamic light scattering analysis and the results are reported in Figure 3.

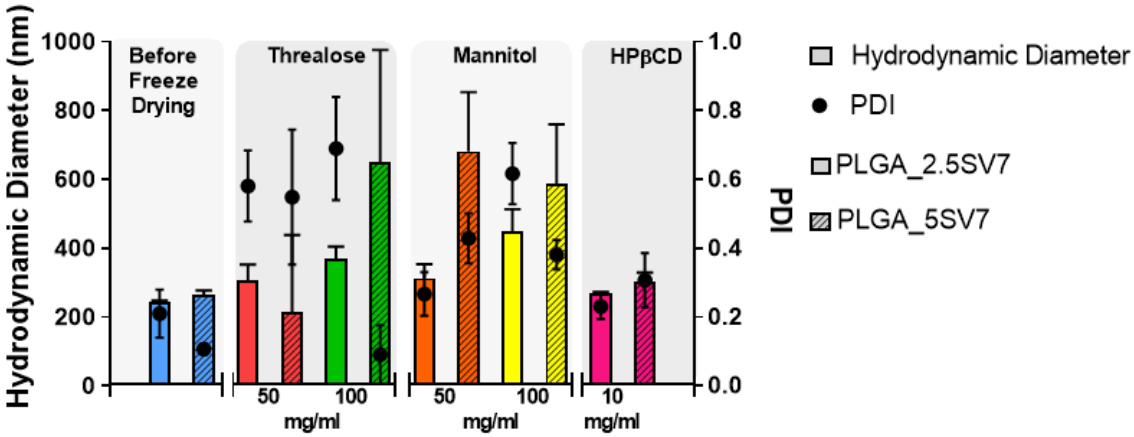

Figure 3. Hydrodynamic diameter and polydispersity index of PLGA_2.5SV7 NP reconstituted through saline solution after lyophilization.

The redispersibility index (RDI), defined as:

$$RDI = D/D_0$$

where D0 represents the size of the nanoparticles prior to drying, and D represents the corresponding value post rehydration of the dried sample in water was calculated. A redispersibility index whose value is as close as possible to 1 indicates that the powders obtained by lyophilization can be completely reconstituted in the initial formulation for size and PDI (26). The best performance was obtained in presence of 100 mg/ml of

HPβCD, which showed for PLGA_2.5SV7 a RDI of 1.10, a RDI of 1.15 and for PLGA_2.5SV7 a RDI of 1.10. Overall, considering the better performance of PLGA_2.5SV7, this formulation was selected for further experiments.

The ability of PLGA_2.5SV7 to release SV7 in physiological condition was evaluated showing a typical two-stage release profile (Figure 4). In particular, the freshly prepared PLGA_2.5SV7 NPs, after a burst effect in the first 6 hours during which 11.3±2.6% of the encapsulated SV7 was released, display a sustained release of the payload lasting about 50 days that reach a final release of 42.7±6.0% of the loaded drug. The release of SV7 has been evaluated also after converting the NPs suspension in nanoembedded dry powder using HPβCD as cryoprotectant. The presence of HP□CD increases the rate and amount of SV7 released and causes a release of 22.1±1.1% and 52.0±3.6% respectively after 6 h and 50 days. This effect could be explained considering that CD offer many benefit, not only as cryoprotectant but are already used for their ability to improve the drug solubility of low-water soluble compound such as SV7 (27,28).

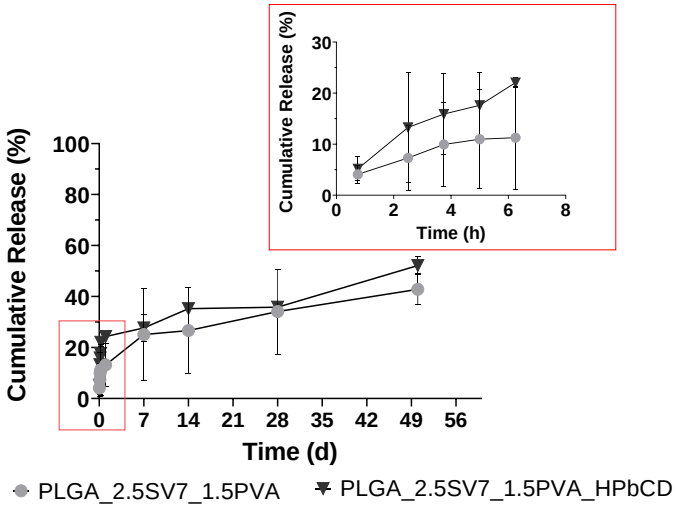

Figure 4. *In vitro* release profile of freshly prepared and HPβCD-nanoembedded PLGA_2.5SV7 NP.

3.2 *In vitro* antimicrobial activity

In order to evaluate if the encapsulation process caused a loss in efficacy of SV7, the inhibitory activity of SV7 after encapsulation in PLGA NPs was determined on methicillin-sensitive *Staphylococcus aureus* (MSSA), methicillin-resistant *Staphylococcus aureus* (MRSA), *Pseudomonas aeruginosa, Escherichia coli, Klebsiella pneumoniae*, as well as *Pseudomonas aeruginosa, Enterobacter cloacae, Serratia marcescens, Klebsiella oxytoca, Citrobacter freundii and Proteus vulgaris* from clinical isolates. Only the MIC collected on MSSA, MRSA and P. *aeruginosa* are reported in table 2 while results are not shown for the other gram-negative strains since, in the range of concentration tested,

SV7 did not show any observable effect on the inoculum growth. As comparison the MIC observed for conventional antibiotics (i.e. ciprofloxacin, tobramycin and erythromycin) and their break point from the "The European Committee on Antimicrobial Susceptibility Testing" are reported (29).

SV7 as free compound showed a MIC of 1.7 mg/L and 1.8 mg/L respectively against MSSA and MRSA. After encapsulation in the PLGA NPs, SV7 was able to exert its antimicrobial effect but with an increase in the MIC, respectively 9.4 mg/L against MSSA and 12.5 mg/L against MRSA. This indicated that the potency of SV7 had been adversely affected by the formulation process, or could also be related to the slow release of SV7 from the NPs. At equivalent NP polymer concentrations examined, blank NPs had no discernible effects on the visible growth of the bacteria.

MINIMUM INHIBITORY CONCENTRATION (MIC) (mg/L)			
	MSSA	MRSA	*P. aeruginosa*
Ciprofloxacin (**Break point)***	0.7 (S ≤ 1)	1.7 (S ≤ 1)	0.2 (S ≤ 0.5)
Tobramycin (**Break point)***	n.d.**	n.d.**	0.4 (S ≤ 4)
Erythromycin (**Break point)***	n.d.**	n.d.**	(-)
SV7	1.7	1.8	n.d.**
PLGA_2.5SV7	9.4	12.5	n.d.**

Table 2. Minimum inhibitory concentration of SV7, SV7-loaded NPs, ciprofloxacin, tobramycin and erythromycin

*Break point reported by the "The European Committee on Antimicrobial Susceptibility Testing". Breakpoint tables for interpretation of MICs and zone diameters. Version 8.1, 2018. http://www.eucast.org (29).

**n.d: no effect detected in the concentration range tested (100 and 0.05 mg/L)

3.3 *In vitro* cytotoxicity on lung cells

The effect of SV7-loaded PLGA NPs on cell viability was evaluated through the 3-(4,5-dimethylthiazol-2-yl)-2,5-diphenyltetrazolium bromide (MTT) assay and LDH release assay.

MTT assay is one of the common assays used to study cell viability and proliferation. It depends on the ability of viable cells to reduce the yellow MTT dye to insoluble purple formazan crystals (30,31). With this experiment, we aimed at evaluating the safety of our formulation at increasing concentrations of SV7 and over an extended time period. We tested the effect of PLGA_2.5SV7 NPs, the respective unloaded control and free SV7 dissolved in DMSO at different concentrations (1.6, 8, 16, 40, 80 and 160 µg SV7/ml) on two different lung epithelial cell lines. All concentrations tested are higher than SV7 active concentration. Cell viability was monitored up to 72 h. As shown in Figure 5, PLGA_2.5SV7 NPs showed a safe profile up to the highest concentrations tested, decreasing in viability only at a concentration 100-fold higher than the MIC value at the longest exposure time. Moreover, this experiment confirms that encapsulation in PLGA NPs represents a valid strategy to improve biocompatibility and bioavailability (32). In fact, the viability of cells treated with free SV7 dissolved in DMSO is much lower than SV7 encapsulated in PLGA NPs due to the toxic effect of the solvent on cells. This finding reinforces the value of PLGA-based nanosystems as a tool for increasing biocompatibility of small molecules, in our case of a newly developed antibacterial agent.

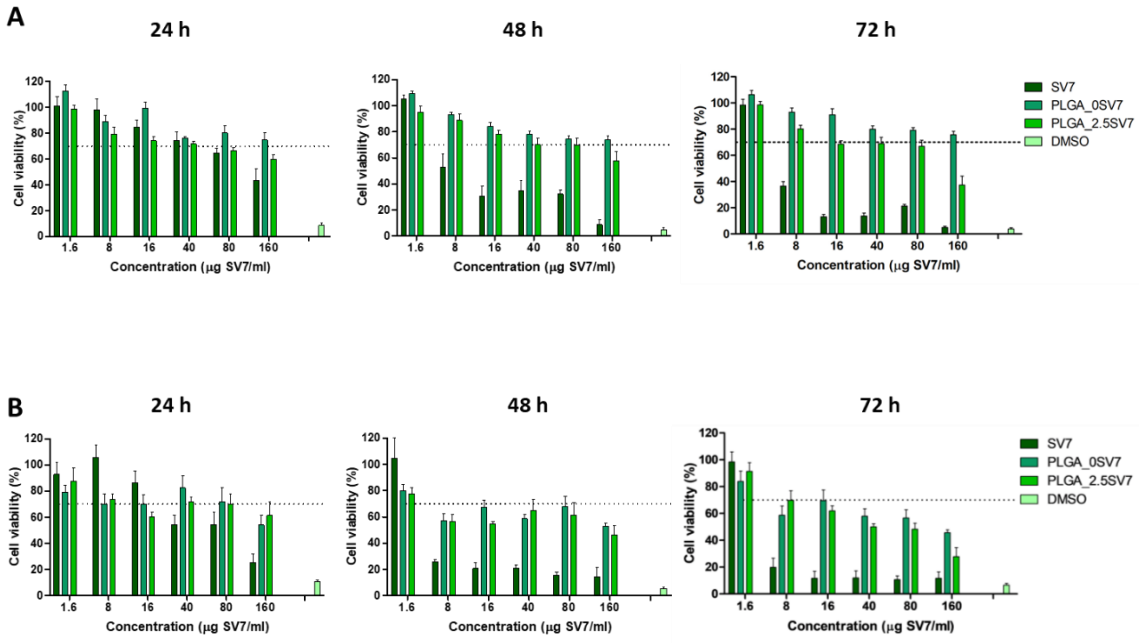

Figure 5. Evaluation of cellular viability in A549 (A) and 16HBE14o- (B) cells after incubation with increasing amounts of PLGA_SV7 NPs and respective controls for 24, 48 and 72 h.

The effect of different nanoparticle concentrations in terms of disruption of the cellular membrane was determined through the release of lactate dehydrogenase (LDH) in cells supernatant (33). The LDH release was tested in 16HBE14o- cells after incubation with different NPs concentrations, corresponding to the MIC value, 10-fold and 100-fold MIC.

In agreement to what was previously observed for the MTT assay, SV7-loaded NPs retained a safe profile at all concentrations and time points tested (Supplementary figure 4). Moreover, higher cyototoxicity was observed for free SV7 dissolved in DMSO, confirming the leading role of PLGA NPs as a safe and biocompatible delivery system.

3.4 *In vitro* cellular uptake

3.4.1 Cellular uptake by flow cytometry

Notably, there is a growing body of evidence demonstrating that *S. aureus* survives inside macrophages *in vitro* and *in vivo* (34), making it essential to target this intracellular population to clear infection. In order to evaluate if and for how long the NPs are internalized in J774A.1 macrophages, the cellular uptake was determined by flow cytometry. To this purpose, PLGA NPs were loaded with Coumarin-6 (PLGA_C6), a fluorescent dye soluble in organic solvents and commonly used to evaluate cellular uptake of nanoparticles (16,35). PLGA_C6 NPs retained the same properties of PLGA_SV7 NPs in terms of size and ζ-potential (supplementary table 2). Considering the extended release profile of SV7_PLGA NPs, we investigated the uptake of Coumarin-6 loaded NPs at different time points (2, 4, 24 and 48 h). The median fluorescence intensity values resulting from the flow cytometry analysis are presented in Figure 7. The results indicate that at each time point tested a significant uptake was observed in comparison to the respective untreated control group. Moreover, the uptake proved to be sustained over time, since the median fluorescence intensity values were comparable at all time points or slightly increased at longer time intervals. Additionally, this analysis also confirmed that the cellular uptake was homogenous in the cell population under investigation, since most of the cells resulted positively stained by coumarin-6 (data not shown).

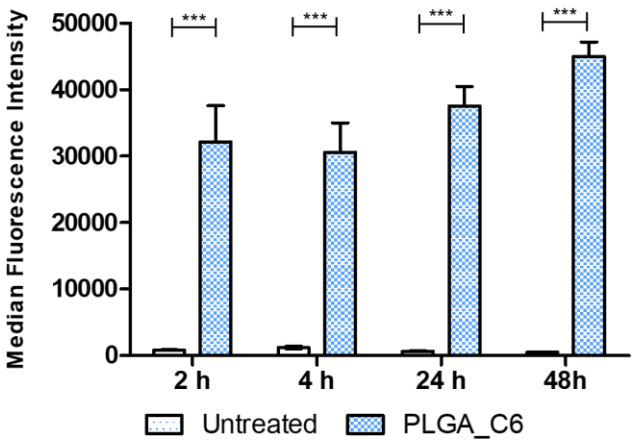

Figure 6. Cellular uptake of Coumarin-6 loaded NPs in J774A.1 murine macrophages measured by flow cytometry and presented as median fluorescence intensity. Cells were analyzed after incubation with PLGA_C6 NPs for 2, 4, 24 and 48 h. Cellular uptake significance was measured using one-way ANOVA analysis in comparison to the untreated group.

Our formulation retains optimal parameters for macrophage targeting. Nanoparticles in the size range of 200-500 nm, which are generally considered too big to be taken up by most cellular types, are indeed optimal to be recognized and phagocytized by macrophages (36). Our NPs, which have a hydrodynamic diameter of about 250 nm, well fit this observation and can be easily internalized by macrophages.

3.4.2 Confocal microscopy

To confirm the cellular internalization of PLGA_C6 NPs in J774A.1 macrophages, fluorescence images were acquired using an inverted scanning confocal microscope and the results are presented in Figure 8. In this experiment, nuclei were stained with DAPI (blue); lysosomes with LysoTracker® Red (red) and coumarin-6 is shown in green. At each time point tested, co-localization between the green fluorescence of coumarin-6 and the red fluorescence corresponding to the lysosomal staining can be observed. The overlap of the two fluorescence channels results in a yellowish color, confirming that the PLGA_C6 NPs could be efficiently internalized by the macrophages and therefore represent a promising tool for the treatment of intracellular infections.

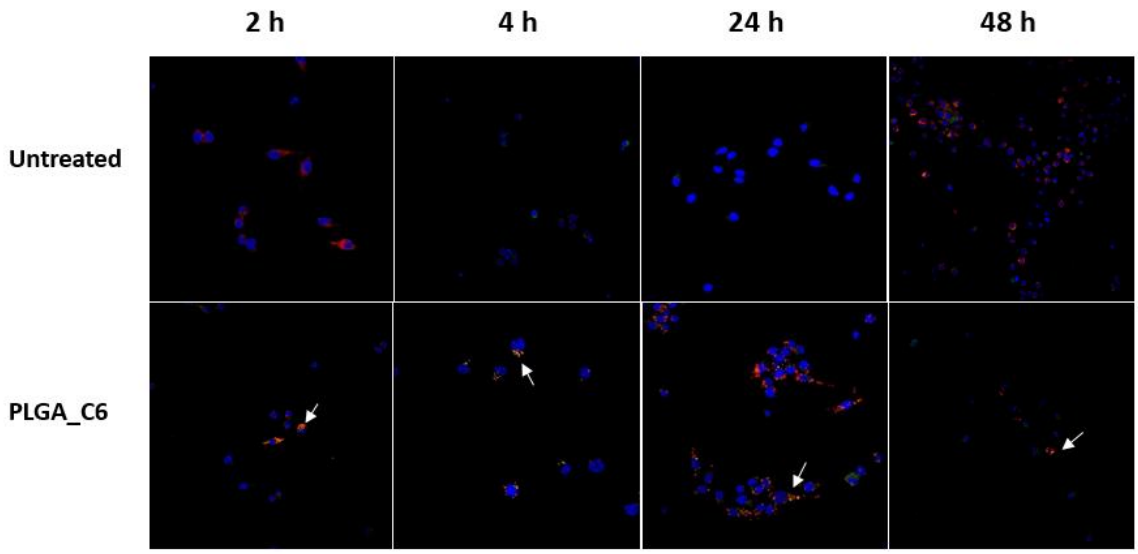

Figure 7. Fluorescence microscopy of J774A.1 macrophages after transfection with PLGA_C6 NPs and staining with DAPI and LysoTracker® Red at different time points with respective untreated controls. White arrows indicate co-localization between lysosome and PLGA_C6 NPs.

3.5 Inhibition of MRSA intracellular infection

After confirming the internalization of NPs by macrophages, the activity of the formulation against intracellular MRSA was investigated in a co-culture of J774A.1 macrophages and MRSA. After establishing the co-culture, cells were treated with different concentrations of SV7-loaded NPs as well as empty NPs and free SV7 as controls. As it can be observed in Figure 8, SV7-loaded NPs retained about 50% activity against intracellular MRSA at the MIC for extracellular MRSA. This is not surprising as higher concentrations of antibiotics are generally required to eradicate intracellular infections (37). Indeed, at a concentration 5 times the extracellular MIC, SV7-loaded NPs could inhibit bacterial growth almost completely, therefore confirming the potential of the formulation as a valid ally against intracellular MRSA infections. Free SV7 showed higher activity against intracellular MRSA at a lower concentration than SV7-loaded NPs, in line with the results from the MIC study. This can be explained by the encapsulation of the antibiotic in the PLGA matrix, that leads to longer times or higher concentrations required to achieve comparable activity as the free drug. Nonetheless, the encapsulation in PLGA NPs assures an improved safety profile of the formulation and a sustained release over time, which could be particularly important to prevent the establishment of intracellular infections in macrophages as well as decrease the risk of recurrence of infection, while reducing the frequency of administration that could favor the development of antimicrobial resistance (38).

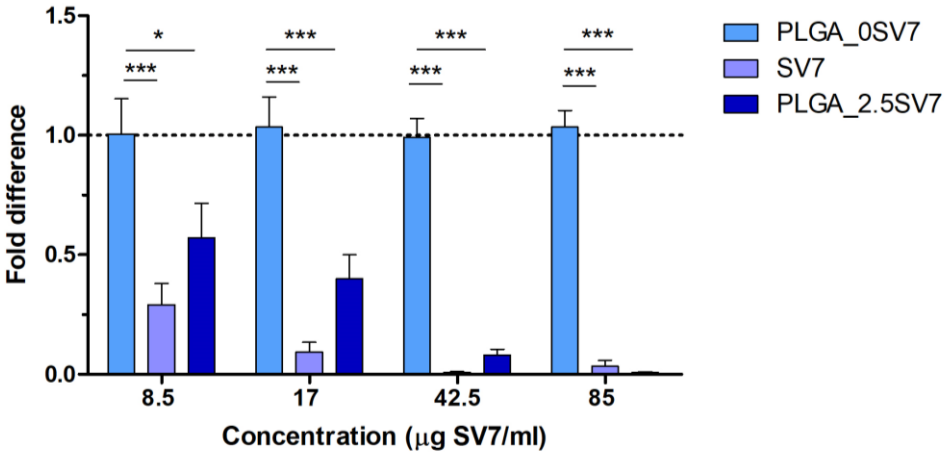

Figure 8. Activity of SV7-loaded NPs against intracellular MRSA infection in J774A.1 macrophages. Data significance was measured using One-Way ANOVA.

3.5 *In vivo* antimicrobial activity

SV7, as raw compound, has shown the capability of curing mice of a lethal MRSA infection (3). The efficacy of SV7-loaded NPs against *S. aureus* infections was examined *in vivo* in G. *mellonella* wax moth larvae, a well-characterized animal model suitable for the screening of novel antimicrobial agents (39). This animal model retains several advantages in terms of ease of handling and maintenance. Additionally, it also presents an innate response with many similarities to the human one as well as being able to survive at 37°C. These properties make G. *mellonella* an ideal model for high antimicrobial screenings, allowing a more accurate candidate selection for further studies (39).

3.5.1 Safety study

To investigate any potential toxic effect of the formulation, a safety study was conducted by injecting SV7-loaded NPs and the respective unloaded control in G. *mellonella* at the working concentration of 8.5 µg/mL. The percentage of survived animals was observed over the following 96 h. The formulation underlined a safe profile, resulting in the survival of all the treated animals, showing the same profile as the control group treated with PBS (Figure 9A).

3.5.2 Pre-treatment study

Based on the controlled release nature of the formulation, a prophylactic treatment protocol was established to test the ability of SV7-loaded NPs to prevent the bacterial infection in G. *mellonella* and to extend the protection over time. In a preliminary experiment, in fact, it was observed that higher survival rates were achieved in the groups where NPs were administered before the bacterial infection in comparison to the groups receiving both injections at the same time (data not shown). Consequently, larvae

were injected with LD50 MSSA (2.5*10^5 CFU/ml) which was determined in a preliminary experiment (Supplementary figure 6), 24 h after the treatment with 8.5 µg/mL SV7-loaded NPs and the respective unloaded NPs as control. As it can be observed in Figure 9B, SV7-loaded NPs mediated a significant improvement in the percentage of survived animals, with an increase of almost 40% in comparison to both the group received only the infection and the one treated with the unloaded NPs. Similar results were observed also for MRSA-infected larvae (Figure 9C). In this case, SV7-loaded NPs allowed for the survival of 70% of the animals while without treatment the survival was only 30%.

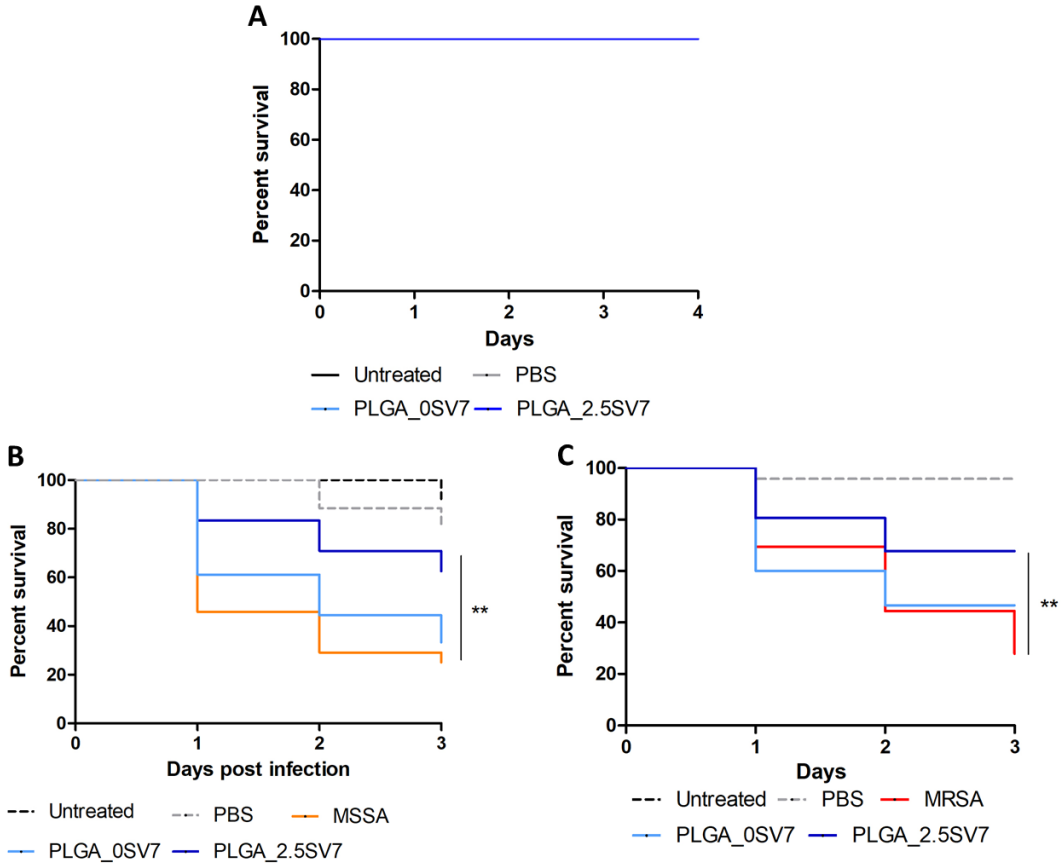

Figure 9. Antibacterial activity and safety of SV7-loaded NPs in *G. mellonella* infection model. (A) PBS, PLGA NPs and PLGA_SV7 NPs were administered to uninfected larvae and the survival was followed for the following 96 h. *G. mellonella* larvae were infected with MSSA (B) and MRSA (C) after 24 h pre-treatment with PLGA_SV7 NPs and the respective unloaded control. Percentage survival was monitored for the following 72 h. Statistical significance of survival was determined using the log-rank (Mantel-Cox) test.

3.5.3 G. mellonella bleeding for residual bacterial load

To confirm the results observed in the *in vivo* pre-treatment study, three larvae from each group were further analyzed for the residual bacterial load after 72 h from the infection as shown in Figure 10. The results confirmed that the number of colonies detected for the group treated with SV7-loaded NPs was significantly decreased in comparison to

both control groups that received only the infection with *S. aureus* or were treated with unloaded NPs.

Similar observations were made also from the bleeding of MRSA-infected larvae. In this case, a consistent reduction of the residual bacterial load could be observed for the animals treated with SV7-loaded NPs in comparison to both control groups. Interestingly, both MSSA and MRSA-treated groups showed an increased bacterial load after the injection of unloaded PLGA NPs in comparison to the group that received only the infection. This might be explained due to the acidification of the environment following the degradation of PLGA NPs, which might have favored bacterial growth (40). S. *aureus*, in fact, has an optimal growth at slightly acidic pH. However, animals treated with SV7-loaded NPs showed a marked reduction of bacterial load in comparison to both control groups. This experiment proved that PLGA_SV7 NPs could prevent the establishment of *S. aureus* methicillin sensitive as well as *S. aureus* methicillin resistant infection in G. *mellonella*, supporting the observations suggesting that the antimicrobial agent retains its activity after the encapsulation in PLGA nanoparticles. Moreover, thanks to the sustained release profile of the formulation, the protection against infection could be retained over time.

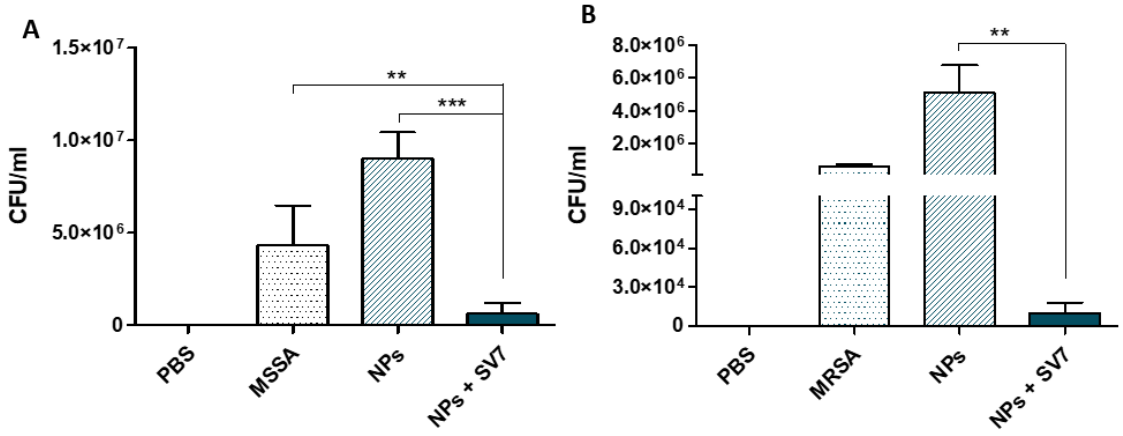

Figure 10. Residual bacterial load in *G. mellonella* was determined 72 h after the infection with MSSA (A) and MRSA (B). Bacterial load reduction was measured using One-Way ANOVA analysis of significance.

4. Conclusion

In this study we have shown the development of a long term stable PLGA nanoparticle carrier to deliver a novel benzophenone antibiotic, namely SV7, which has been fully characterized for dimension, morphology and ability to mediate sustained release of the payload. The safety of the formulation was demonstrated *in vitro* in lung cell lines and *in vivo* in the *G. mellonella* model. The efficacy against methicillin sensitive *S. aureus* and

methicillin resistant *S. aureus* strains was demonstrated respectively *in vitro* in several bacteria strains and *in vivo* in the *G. mellonella* model. We further showed the ability of the NPs to be efficiently internalized by macrophages to target intracellular MRSA infection, which represents one of the biggest hurdles in the fight against being limited by the bacterial resistance process. Overall, the results support the use of nanoformulation systems for the clearance of intracellular infection, thanks to the overall safe profile of the formulation as well as a sustained release of the drug, that could avoid triggering antimicrobial resistance. Finally, to confirm the translatability of the findings, an *in vivo G. mellonella* infection model was established. Here, the safety of the formulation as well as the activity of SV7-loaded NPs against MRSA in a prophylactic setup were confirmed. The pre-treatment with NPs in fact prevented the establishment of the infection and assured higher survival rates than control groups. Further mouse *in vivo* studies will focus on the optimization of post-infection treatment regimes. To exploit the advantageous features of the NPs developed here, an interesting approach could be the direct administration to the lungs, for which a dry powder formulation was developed.

Supplementary information

Headspace sampler parameters	
Headspace vial size	20 mL
Agitator cycle	5 sec on, 2 sec off
Agitator speed	350 rpm
Agitator temperature	80 °C
Sample incubation time	10 min
Syringe size	2.5 mL
Syringe temperature	85 °C
Injection volume	0.25 mL
Syringe flush time	5 min
GC-MS parameters	
Carrier flow rate	1.2 mL min-1
Split ratio	50 : 1
Oven profile	30 °C for 10 min 30 to 150 °C at 30 °C min-1 150 to 240 °C at 75 °C min-1 for 1min
Transfer	250 °C

line temperature	
Inlet temperature	140 °C
Ion source temperature	230 °C
Quadrupole temperature	150 °C

Supplementary Table 1. Conditions of static HS-GC-MS.

A.

	PLGA (% w/v)	PVA (% w/v)
10PLGA_1PVA	0.10	1
25PLGA_1PVA	0.25	1
50PLGA_1PVA	0.50	1

B.

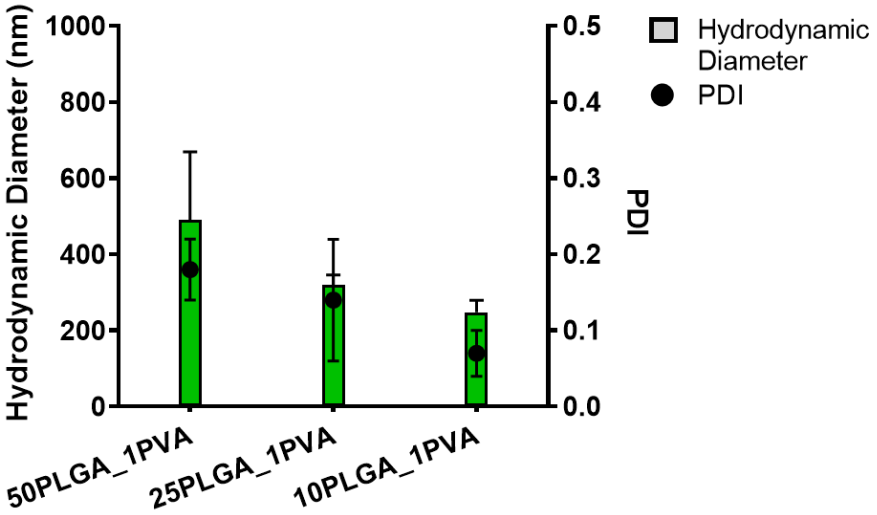

Supplementary Figure. 1. Composition (A), and characterization though hydrodynamic diameter (DH) and the polydispersity index (PDI) of empty PLGA_PVA Nanoparticles (B).

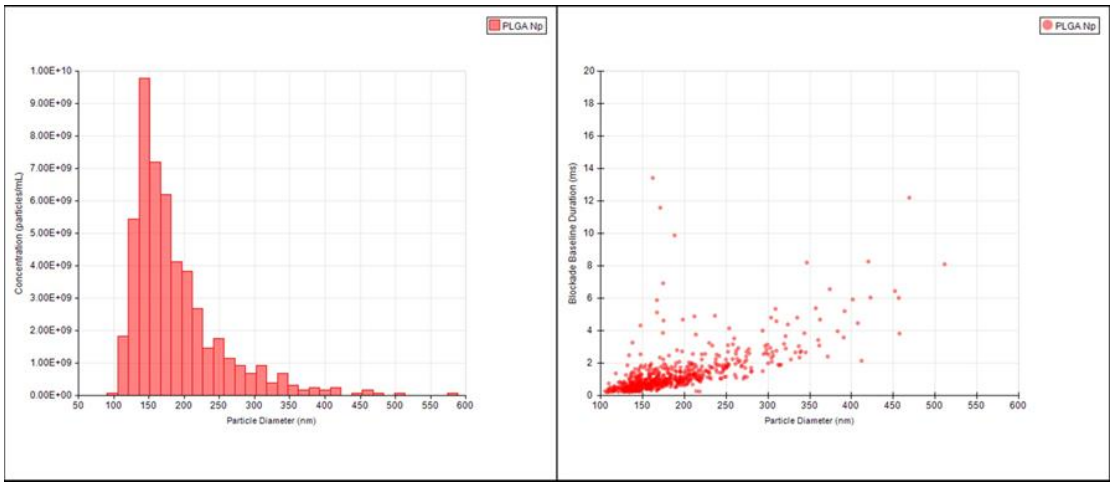

Supplementary Figure 2. Nanoparticles size distribution through TRPS.

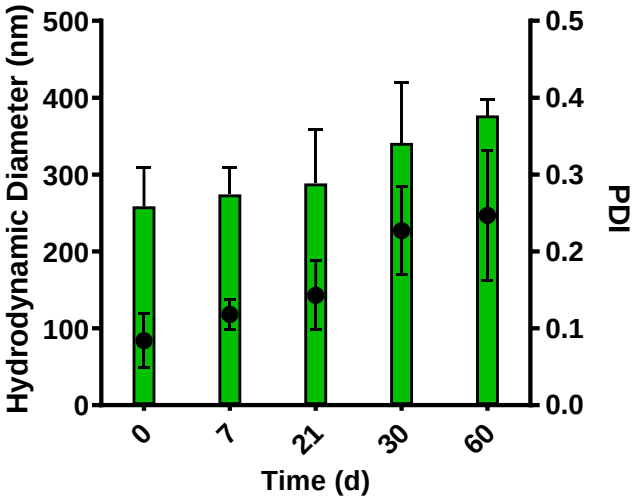

Supplementary Figure 3. Stability study. After production, SV7-loaded PLGA nanoparticles were stored in polypropylene conical tubes at 4 C°. Particle stability was assessed by measuring size and PDI over a period of 60 days. All the measurements were performed in triplicate (n=3) and the results are expressed as mean value ± SD

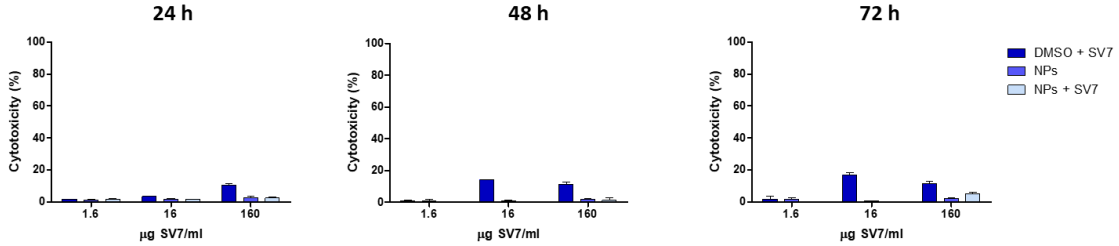

Supplementary Figure 4. Evaluation of lactate dehydrogenase release in cell supernatant of 16HBE14o- cells after incubation with different amounts of PLGA_SV7 NPS and respective controls for 24, 48 and 72 h.

Parameters	PLGA_C6
D_H (nm ± SD)	234.4 ± 7.1
PDl (± SD)	0.04 ± 0.02
ζ Potenzial (mV ± SD)	-24.2 ± 0.5

Supplementary Table 2. Characterization through hydrodynamic diameter (DH), polydispersivity index (PDI) and ζ potential of PLGA_C6 NPs.

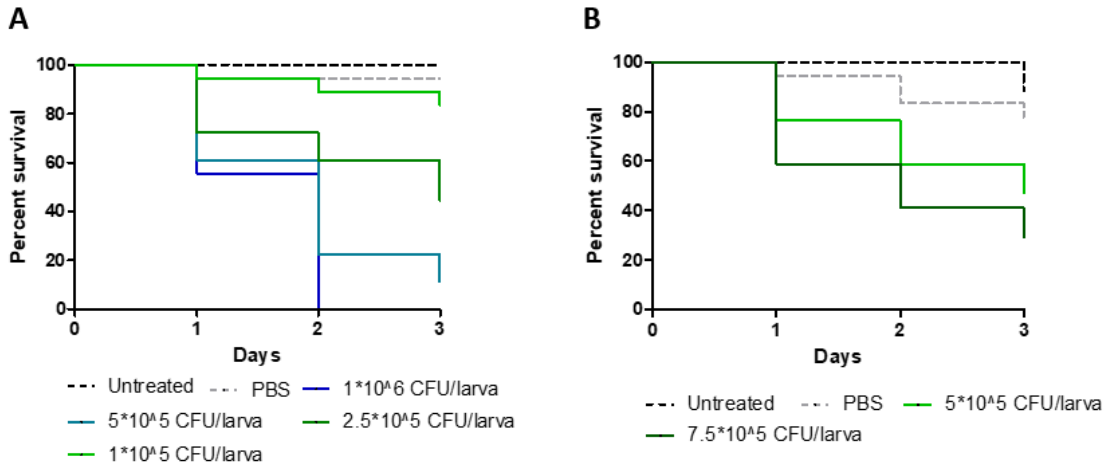

Supplementary Figure 6. LD50 determination in *G. mellonella* infected with MSSA (A) and MRSA (B) at different concentrations. Control groups consisted of untreated animals as well as injected with PBS.

Acknowledgement

Olivia M. Merkel acknowledges Fondazione Ricerca Fibrosi Cistica, grant FFC#23/2017 and the European Research Council, grant ERC-2014-StG – 637830 for financial support.

Gabriella Costabile acknowledges UniNa and Compagnia San Paolo as recipient of a mobility fellowship in the frame of Programme STAR (CALL 2016) and Fondazione Umberto Veronesi for the postdoctoral fellowships (CALL 2019, CALL 2020).

Birgit Groß at the Max von Pettenkofer-Institut is sincerely acknowledged for precious technical assistance.

Chapter VI - T_H2-cell targeted pulmonary siRNA delivery for the treatment of asthma

Tobias W.M. Keil[1†], Domizia Baldassi[1†], Olivia M. Merkel[1*]

[1]Pharmaceutical Technology and Biopharmaceutics, LMU Munich, Munich, Germany

[†]These authors contributed equally.

The following chapter was published in WIREs Nanomedicine and Nanobiotechnology.

Keil TWM, Baldassi D, Merkel OM. T-cell targeted pulmonary siRNA delivery for the treatment of asthma. Wiley Interdiscip Rev Nanomed Nanobiotechnol. 2020 Sep;12(5):e1634. doi: 10.1002/wnan.1634. Epub 2020 Apr 8. PMID: 32267622; PMCID: PMC7116616.

Graphical abstract

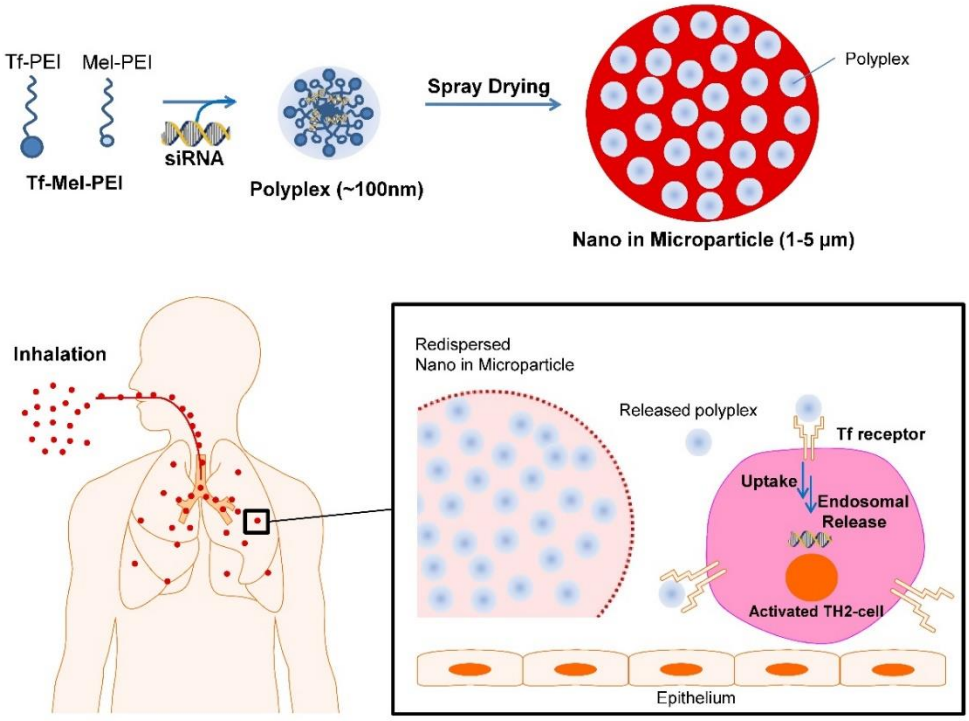

Abstract

Despite the large number of drugs available for the treatment of asthma, in 5-10% of the patients this disease is not well controlled. While most treatments palliate symptoms, those suffering from severe and uncontrolled asthma could benefit more from a therapeutic approach addressing the root problem. An siRNA-based therapy targeting the transcription factor GATA3 in activated T helper cells subtype 2 (Th2 cells), one of the key upstream factors involved in asthma, could therefore represent a promising strategy. However, the difficult-to-transfect cell type has not extensively been explored for nucleic acid therapeutics. In this regard, our group first identified a suitable pathway, i.e. transferrin receptor mediated uptake, to target efficiently and specifically activated Th2 cells with a transferrin-polyethyleneimine (PEI) conjugate which forms polyplexes with siRNA. This system, despite efficient uptake in activated T cells *in vivo*, suffered from poor endosomal release and was later improved by a combination with a melittin-PEI conjugate. The new formulation showed improved endosomal escape and gene silencing efficacy. Additionally, in order to develop a clinically relevant dosage form for pulmonary delivery of siRNA we have lately focused on a dry powder formulation by spray drying for the production of inhalable nano-in-microparticles. In proof-of-concept experiments, DNA/PEI polyplexes were used in order to implement analytics and engineer process parameters to pave the way for spray drying also siRNA containing polyplexes and more sophisticated systems in general. Ultimately, our efforts are devoted to the development of a novel treatment of asthma that can be translated from bench to bedside and are reviewed and discussed here in the context of the current literature.

KEYWORDS asthma, inhalation, siRNA, T cells

1. Introduction

Amongst chronic inflammatory diseases of the airway, asthma is still considered a great medical and socioeconomic burden under which nearly 340 million people suffer worldwide(199). The disease hallmarks, besides persistent lung inflammation, are shortness of breath, mucus hypersecretion, broncho obstruction with enhanced reactivity to spasmogens (airway hyperactivity) and airway remodeling (199–202). The current asthma treatment algorithm is based on bronchodilating and anti-inflammatory agents (inhaled and/or systemic glucocorticoids) targeting symptoms only. However, in a small subset of patients these symptoms cannot be controlled even with high doses of the recommended drugs (203).

The origin of these symptoms, amongst others is the activation, infiltration and accumulation of T cells positive for the cluster of differentiation 4, also known as T helper cells (Th2 cells), of subtype 2 (CD4+Th2 cells) into major airways and mucosa of small airways, and the subsequent release of proinflammatory cytokines (IL-4, IL-5, IL-9 and IL-13) (200–202,204). After it was found that the release of these interleukins is triggered by an upregulation of the GATA-binding protein 3 (GATA3) in Th2 cells upon activation (205), GATA3, a transcription factor regulating T cell differentiation into Th2 cells, emerged as a powerful therapeutic target (206). Considering that the effect of silencing only single cytokines can be overcompensated by others (207), therapeutic downregulation of GATA3, preventing downstream release of all Th2 cytokines and concomitant symptoms in parallel holds great promise.

A powerful tool for post-transcriptional gene silencing is RNA interference (RNAi): Fire and Mello who earned the Nobel Prize, discovered a nuclease complex known as RNA induced silencing complex (RISC) which recognizes and destroys target mRNAs. The target is specifically identified by small interfering RNAs (siRNA) which are RNA strands of 21-25 base pairs with base-complementarity to the target mRNA. Upon pairing of the activated RISC with single-stranded siRNA and the complementary mRNA site, cleavage of mRNA is initiated and the translation of the protein alongside the degraded mRNA is prevented (208). Accordingly, targeting mRNA coding for GATA3 with siRNA could enable post-transcriptional gene silencing of the transcription factor which is overexpressed in activated Th2 cells. Subsequently, downregulating the overexpressed level towards a more physiologic one could therapeutically be exploited towards a new asthma treatment without general immunosuppressive side effects. Delivering siRNA exogenously into activated Th2 cells, however, is not a simple task.

Considering the macromolecular nature of siRNAs which are highly negatively charged and the lack of nucleic acid specific active transporters on cell membranes in combination with ubiquitously present nucleases which quickly degrade siRNA in the body, intracellular siRNA delivery requires formulation of the latter. Compared to viral vectors, non-viral vectors are more advantageous regarding safety, manufacturability and immunogenicity (16). Positively charged polymers are one class of non-viral vectors where polyethyleneimine (PEI) and its derivatives are the most studied representatives. These polymers form so called polyplexes on the nano-scale by electrostatic interaction with siRNA protecting it on the one hand from nucleases and enabling internalization and release into cells on the other (209). However, in case of intracellular delivery into T cells, additional barriers, such as endosomal release, need to be considered (210).

In addition to avoiding nucleases which are present in high concentrations in blood but in very low concentrations in lung lining fluids, pulmonary administration of nucleic acids also avoids the rapid distribution within the body upon systemic delivery which comes with possible side effects (211). Local pulmonary delivery can be achieved by inhaling particles (liquid or solid) of an aerodynamic size between 1 and 5 µm. Greater particles are deposited in the throat and upper airways unable to reach the area of interest. Smaller particles can undergo insufficient sedimentation and are exhaled. For optimal lung deposition, dry powder formulations are favored for siRNA delivery despite more complex formulation and preparation as compared with aerosolization (90). The advantages can be easily explained by increased physical and chemical stability and the resulting prolonged shelf life due to the absence of water and nucleases (31). Typical procedures to produce inhalable powders are spray drying or a combination of spray drying and lyophilization – spray freeze drying – of drug only or drug-excipient combinations (212). For the latter, solutions or suspensions are sprayed into liquid nitrogen resulting in frozen particles which are lyophilized afterwards to remove residual water. However, this process requires high energy and time consumption due to long lyophilization cycles. A more straight forward process is spray drying where droplets are generated and dried by hot air (213). This technique leads to microparticles where polyplexes or other nanoparticles are embedded in an excipient matrix resulting in nano-in-microparticles which ideally resuspend into nanoparticles upon impaction on lung fluid.

This Focus Article highlights our previous and ongoing research regarding polyplexes designed for pulmonary delivery for the treatment of lung diseases in general, and of asthma specifically in the context of the current literature.

2. T_H2-cell targeting

In the pathogenesis of asthma, Th2 cells play a central role in orchestrating the allergic reaction. Upon activation and concomitant upregulation of GATA3, Th2 cells secrete IL-4, IL-5, IL-9, IL-13 and tumor necrosis factor alpha (TNFα) (214,215). As shown in Figure 1, these cytokines stimulate different cell types resulting in further downstream effects and symptoms known for asthma. Although symptoms were shown to be reduced by i.v. application of antibodies against single interleukins in mice, their use is limited due to whole body distribution after systemic administration resulting in various side effects (6) and due to lack of compliance if administered clinically.

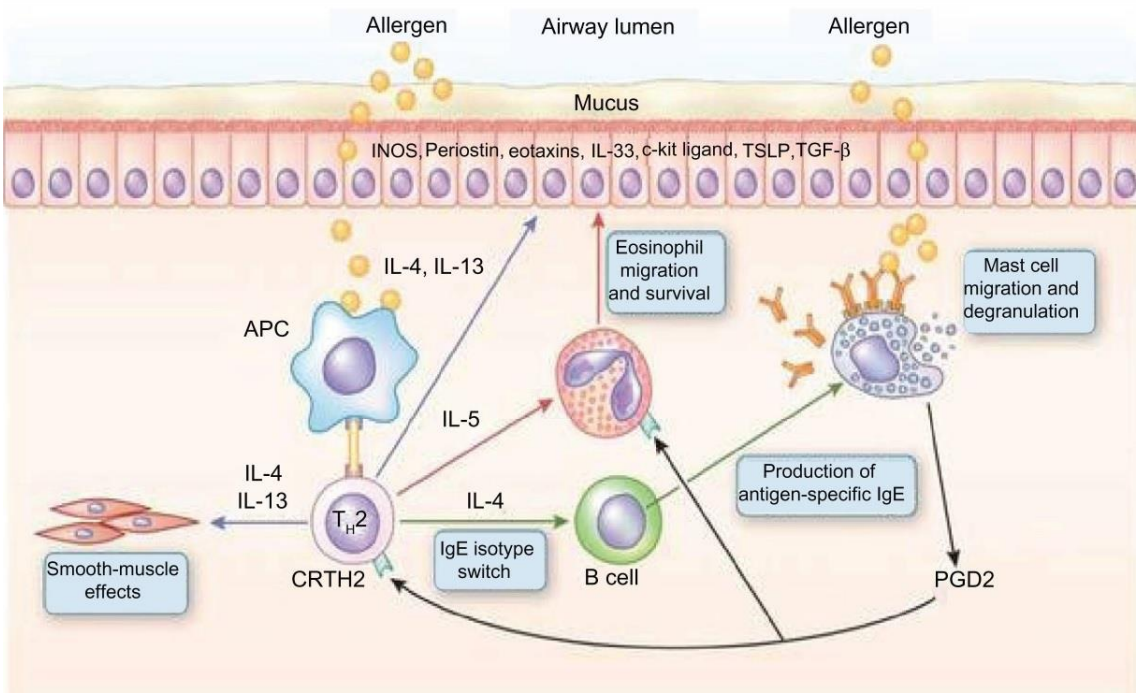

Figure 1. T helper-2 (Th2) cells in asthma pathogenesis. Inhaled allergens are thought to be processed by two mechanisms in asthmatic airways. Allergens either: (1) activate mast cells through cross-linking with IgE on their cell surfaces through the high-affinity type 1 IgE receptor (FcεR1) to release mediators that induce bronchoconstriction, such as histamine, cysteinyl leukotrienes, and prostaglandin D2 (PGD2) or (2) are processed by dendritic cells, which are induced to secrete the CC chemokine ligand (CCL) 17 and CCL22 by thymic stromal lymphopoietin (TSLP). Dendritic cells then attract and activate Th2 cells by the binding of CCL17 and CCL22 with CC chemokine receptor 4 (CCR4) on the Th2 cell surface. IL-33 is produced by airway epithelial cells and activates dendritic cells and Th2 by inducing the release of tumor necrosis factor-alpha from mast cells. Th2 secretes cytokines, including IL-4 and IL-13, which switch B cells to produce IgE, IL-5, which promotes the development and survival of eosinophils, and IL-9, which activates mast cells. Once IL-13 is produced, it can increase the survival and migration of eosinophils, and it promotes activation of macrophages to create an M2, or an allergic cell phenotype. Airway epithelial cells are stimulated, and through mediators such as periostin and transforming growth factor β1 (TGF-β1), they can increase airway inflammation and lead to the increased permeability of airway epithelial cells and mucous hypersecretion. IL-13 also has direct effects on airway smooth muscle, leading to increased contraction to agonists such as acetylcholine and decreased relaxation with beta-agonists. Reproduced with permission from Thomson, Patel, & Smith, 2012, Copyright 2012 Dove Medical Press Ltd.

Rather than blocking or downregulating single cytokines, post-transcriptional interference with GATA3 expression has been reported to be a promising approach using intratracheal instillation with a bolus of GATA-3 shRNA lentiviral vector (216) or intranasal treatment with GATA-3 DNazyme (217). In those experiments, however, the therapeutic nucleic acids were administered as unstable, free DNA and were not specifically targeted towards Th2 cells.

The downregulation of GATA3 in activated Th2 cells via pulmonary administration is therefore preferred as the secretion of Th2 cytokines is ideally only downregulated in the activated T cells in the lung, preventing side effects of general immune suppression. However, the transfection of T cells is challenging since they do not express caveolin and are devoid of caveolae, preventing them from active endocytosis of nanoparticles. Primary T cells are thus known to be resistant to common non-viral delivery vectors (218).

Since viruses efficiently transduce T cells, we sought to find a virus-like tool to target activated Th2 cells specifically and efficiently in a receptor-mediated manner. While in the 1980s, an overexpression of transferrin receptor (CD71) in activated T cells was found whereas naïve T cells lacked the expression of CD71 (219), this finding had so far not been exploited for nucleic acid delivery to T cells. This idea was picked up by our group in the early 2010s. First experiments were conducted to confirm differential receptor expression in naïve vs. activated T cells and to test whether receptor mediated uptake was possible *ex vivo* in primary T cells exploiting transferrin (Tf) as a targeting ligand (220). Therefore, in proof-of-concept experiments, low molecular weight (LMW) PEI was conjugated to Tf (Tf-PEI) and complexed with fluorescently labelled siRNA into polyplexes at different ratios. These formulations were initially only tested regarding intracellular delivery in primary T cells *ex vivo*. As seen in Figure 2a, Tf-PEI polyplexes were significantly more efficiently taken up by activated T cells (ATCs) compared to blank, compared to unmodified PEI and even compared to the positive lipofectamine control. Also, no efficient uptake was observed in naïve T cells for either formulation (Figure 2b), which was expected based on the lack of caveolae in T cells (218). The activation dependent expression of CD71 in both activated and naïve primary T cells was confirmed by anti-CD71 antibody binding assays (see Figure 2 insets). These results confirmed our hypothesis that specific targeting of activated T cells via transferrin is possible and further research was conducted.

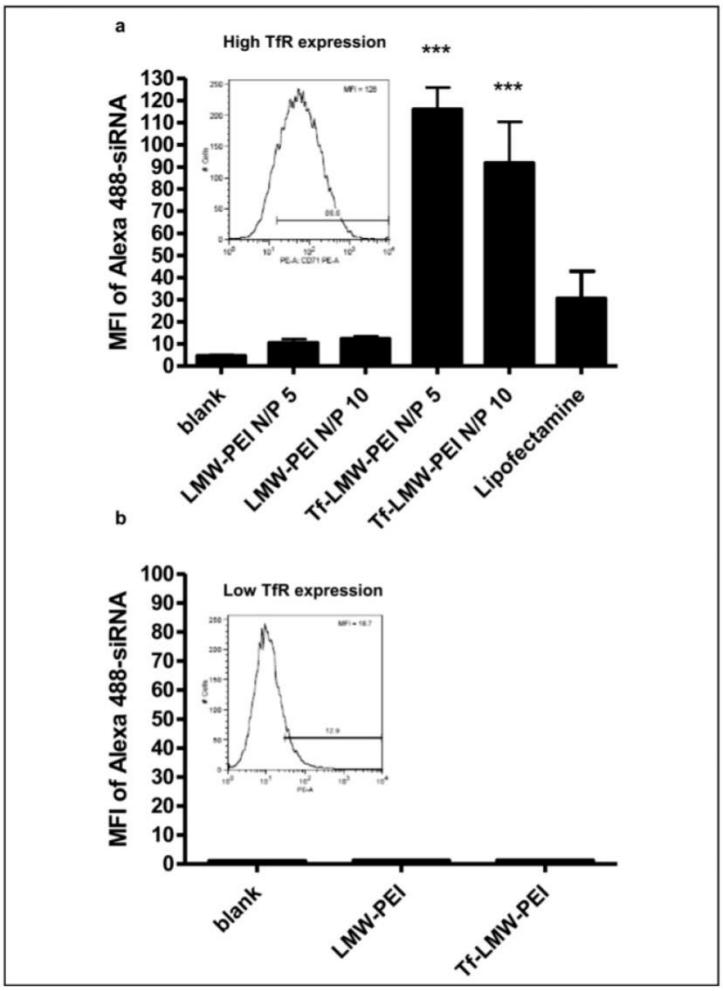

Figure 2. Specific Uptake of siRNA in activated T cells with a Tf-PEI conjugate. Uptake of Alexa488-labaled siRNA a) at different N/P ratios into fully activated T cells with high TfR expression (inset 2a), and b) lack of uptake into T cells with low TfR expression (inset 2b). The expression of TfT in the T cells was confirmed by anti-CD71 antibody binding assay. The siRNA taken up into T cells was analyzed by flow cytometry. Lipofectamine was used as a positive control. Reproduced with permission from (220). Copyright 2013 Elsevier B.V.

While successful targeting of T cells was also shown by Ramishetti *et al*. after systemic administration of lipid nanoparticles which were surface functionalized with an CD4+ antibody (221), no differentiation between resting and activated T cells was made as the intention was to target and downregulate T cell specific genes systemically. In contrast, CD71 targeting results in the benefit of addressing only activated T cells which are strongly involved in asthma.

To test specificity of Tf-PEI polyplexes toward activated T cells in the complex environment of the lung, an *in vivo* biodistribution study was performed in a murine asthma model in comparison to healthy control groups: Mice were intratracheally administrated on four consecutive days with Tf-PEI or PEI polyplexes. After euthanizing

animals, bronchoalveolar lavage (BAL) cells were collected to investigate the distribution of siRNA in different cells types (macrophages, eosinophils, type II pneumocytes, B and T cells). We observed a specific uptake in T cells in comparison to the other investigated cell types.

In line with the previous *ex vivo* study, the uptake in Th2 cells was also significantly higher in asthmatic than in healthy mice (127). In healthy animals, only macrophages took up siRNA independent of the formulation, and non-targeted PEI mediated uptake in type II epithelial cells and macrophages in both inflamed and healthy animals. However it has been described that macrophages do not express GATA3 (222), which leads us to hypothesize a lack of severe side effects due to nanoparticle delivery to macrophages. Type II pneumocytes, however, do express GATA3 and are involved in Th2 cytokine production. Therefore, non-specific delivery to lung epithelial cells is expected to have a positive, anti-inflammatory effect. Since GATA3 does however have a protective effect, for example in mammary luminal cells (223), we will investigate biodistribution of siRNA after pulmonary delivery to assess potential risks and side effects of the treatment.

3. Optimization of Endosomal Release: Tf-Mel-PEI

After confirming effective targeting and uptake of Tf-PEI polyplexes in Th2 cells in the lung, their therapeutic efficacy was tested *in vivo* by evaluating the knockdown of GATA3 and subsequent downstream effects. Despite significantly higher gene silencing rates of Tf-PEI compared to PEI *ex vivo* in primary Th2 cells (127), a single treatment with Tf-PEI polyplexes did not result in significant gene silencing of GATA3 in lung tissue or of IL13 in pulmonary T cells, as determined by qRT-PCR and intracellular cytokine staining, respectively (224). The reason for the lack of significant gene silencing was hypothesized to depend on the single administration and/or on insufficient endosomal escape of the nanocarrier after endocytosis.

Endosomal escape represents a crucial factor and is considered the rate-limiting step in cytoplasmatic delivery of nanoparticle-based therapies. In fact, a failure of escape would result in a probable degradation of the cargo in the lysosome which merges with the late endosome, leading to a loss of therapeutic activity (225). Several strategies have been proposed to overcome this problem, such as including positively charged or pH-sensitive moieties able to disrupt the endosomal membrane (226). In this respect, it is to be noted that endosomal acidification, leading to the so-called proton sponge effect and osmotic rupture of polyamine-loaded endosomes, is slower and less robust in T cells as compared to epithelial cell lines (227). In this view, the use of melittin, a pore-forming

peptide, was hypothesized to yield more efficient endosomal escape. Melittin is a peptide derived from bee venom and consisting of 26 amino acids that has an inherent capacity to disrupt cell membranes also at acidic pH. Moreover, this peptide was shown to be effective as a delivery system for siRNA itself, being able to reach significant transfection efficiencies (228). Additionally, a virus-inspired polymer for efficient *in vitro* and *in vivo* gene delivery, called VIPER (123), containing melittin, had been shown to efficiently mediate gene silencing in the lung of healthy mice and had been tolerated very well after pulmonary delivery (124). Based on these observations, we decided to include melittin in our Tf-PEI conjugate to improve the endosomal escape. However, melittin was modified by 2,3-Dimethyl-maleic anhydride (DMMAn) to reduce side effects by directing its activity to acidic pH and hence to the endosomal membrane only. Thus, general membrane activity was reduced, and this melittin derivative was conjugated to PEI and blended with different ratios of Tf-PEI. As a result, we obtained a delivery system which retained its selectivity toward activated T cells due to the presence of transferrin at improved endosmolytic activity (65). The new blend composed of Tf-PEI and Mel-PEI (Tf-Mel-PEI, 50:50) displayed optimal characterization parameters, showing particle sizes below 200 nm, low polydispersity indices and stability in lung lining fluids. In line with the results obtained with the Tf-PEI conjugate, we achieved significant cellular uptake results in both Jurkat and human primary activated T cells in comparison to both free siRNA and siRNA/lipofectamine. Moreover, after determining binding kinetics of the different formulations with CD71 using Surface Plasmon Resonance technique, we observed that Tf-Mel-PEI stably bound the transferrin receptor and also showed superior affinity over Tf-PEI (65).

In the next step, the effect of melittin on the endosomal membrane was investigated via acridine orange staining of living cells. This technique is based on a differential fluorescence emission of the cell-permeable nucleic acid binding dye which emits red light if trapped in the endosome and green light if located within cytoplasmic pH. As shown in Figure 3A, chloroquine, as positive control for successful endosomal release, as well as transfection with melittin-containing conjugates resulted in efficient endosomal escape, reflected in a color change of the dye from red to green. Positive and negative controls in fluorescence based assays with chloroquine treatment are especially important as chloroquine is a mild base used to neutralize endosomal and lysosomal pH, and pH dependent dyes used to visualize these compartments can potentially render a negative result in the presence of this drug. After transfection with the Tf-PEI conjugate, only few green dots were detected while in PEI transfected cells, only red dye was found, supporting the findings by Olden *et al*. describing a lack of endosomal acidification in T

cells (210) resulting in endosomal entrapment of PEI. Regarding endosomal escape, Tf-Mel-PEI clearly showed superior characteristics over the previously used Tf-PEI formulations (65).

To determine whether the effect of improved endosomal escape was also reflected on higher mRNA downregulation, the knockdown of GAPDH was evaluated via qRT-PCR (Figure 3B). Indeed, in human primary activated T cells the Tf-Mel-PEI blend achieved higher gene silencing levels than Tf-PEI with 76% gene knockdown compared to 43%, respectively X. Most importantly, however, the increased endosomal escape was not paralleled by increased cytotoxicity or membrane destabilization (65).

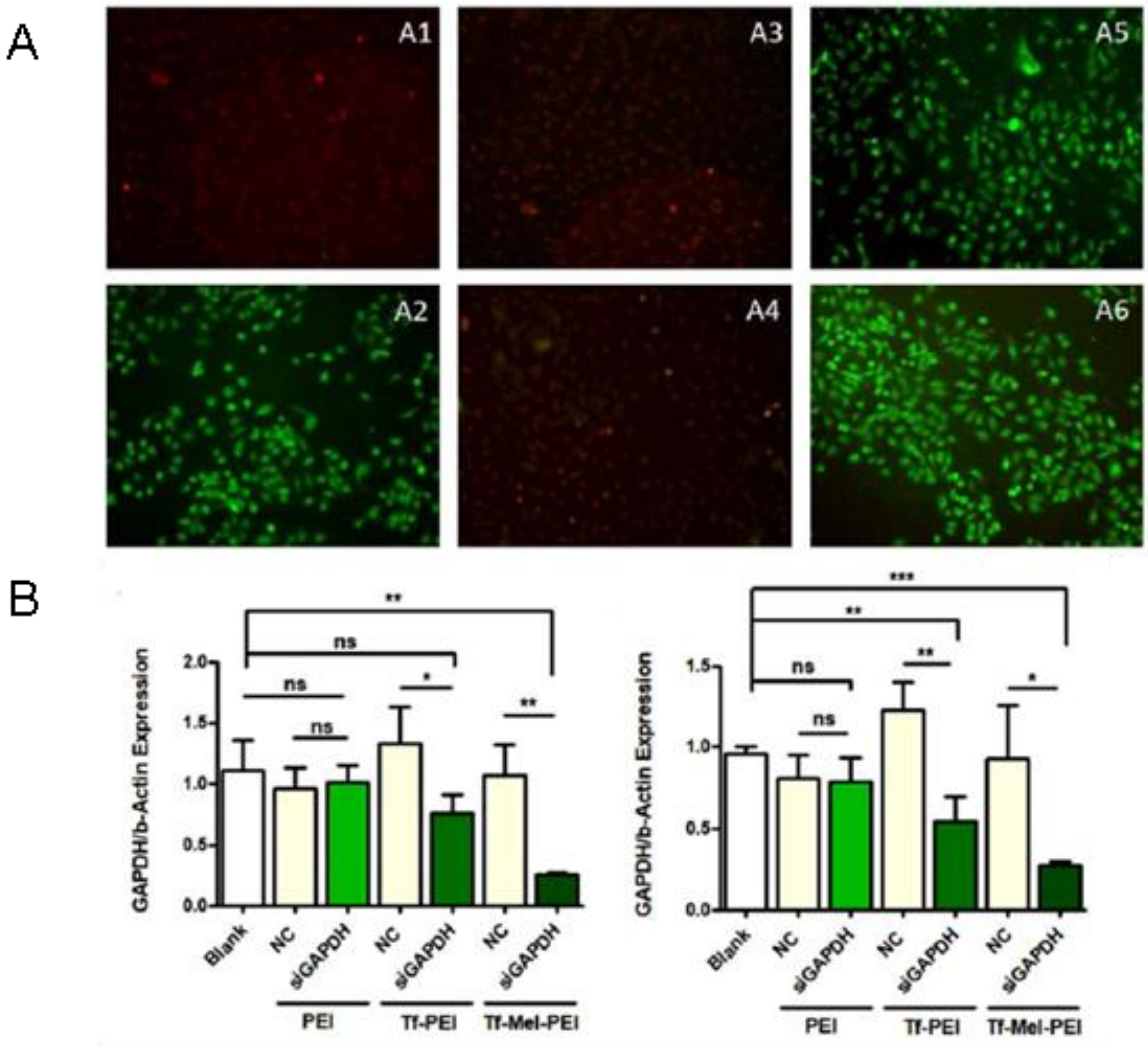

Figure 3. A) Acridine orange staining of untreated A549 cells (A1) and of A549 cells after incubation of polyplexes with Chloroquine (A2), PEI (A3), Tf-PEI (A4), Mel-PEI (A5) and Tf-Mel-PEI (A6). B) GAPDH knockdown in Jurkat cells (B1) and human primary activated T cells (B2) after treatment with GAPDH-siRNA

or scrambled siRNA as negative control. Data points indicate mean ±SD, n = 3; One-way ANOVA, *P<0.05, **P < 0.01, *** P < 0.001. Reproduced with permission from (65). Copyright 2019 Wiley.

Our published efforts so far describe a formulation of Tf-Mel-PEI polyplexes with optimal particle characteristics able to selectively target activated T cells and improved endosomal escape and gene silencing efficacy. Tf-Mel-PEI was therefore considered a suitable tool for follow up *in vivo* studies concerning *in vivo* specificity for activated T cells, biodistribution and therapeutic gene silencing efficiencies in a murine asthma model. Despite the fact that LMW-PEI and its Tf-PEI conjugate have been tolerated well in healthy and asthmatic mice (127), we are currently developing oligospermine derivatives to replace the PEI block in our approach (229). It is expected that in the inflamed lung, even Tf-shielded LMW-PEI is not well tolerated, especially intracellulary where the disulfide bond between Tf and PEI will be reduced. Therefore, non-biodegradable PEI is not a promising approach for the treatment of a chronic disease, and biodegradable alternatives are currently developed by us and others. By mimicking PEI with a polyamine that endogenously acts as nucleic acid condenser, we believe that similar condensation efficacy of siRNA will be obtained at reduced toxicity and immunogenicity but at increased biodegradability (229). In parallel, inhalable dry powder formulations are being developed to pave the way for translation from bench to bed side.

4. Pulmonary delivery of nucleic acids

Therapeutic approaches of delivering nucleic acids to the lung via inhalation benefit from direct accessibility and the ease of its administration route. However, several barriers, such as the architecture of the lung, the presence of mucus and surfactant, mucociliary clearance and phagocytosis by cells of the immune system, need to be overcome in the lung for successful delivery of nucleic acids to their target cells and sites of action (22,230). After carefully optimizing our formulations for gene silencing in T cells over the past years, we are currently assessing their efficacy in 3D cell culture models (Zscheppang *et al*., 2018) and in mucus mobility assays based on Fluorescence Correlation Spectroscopy (FCS) (231). Current clinical trials for inhalable gene-based therapies have been focused mainly on the use of viral and liposome-based vectors, such as in the case of cystic fibrosis, to deliver cDNA for the CFTR gene (232,233). However, the results obtained were not as good as expected in terms of transfection efficiency. The study and the development of new formulation strategies for inhalable gene therapies is therefore of paramount importance.

5. Dry powder formulation

Spray drying (SD) is the most straight forward technique to produce inhalable particles. Although several groups have applied SD to obtain dry powder formulations of their nucleic acid formulations, analytics for characterizing nanoparticles before and after spray drying have been very scarce. However, an understanding of changes between freshly prepared and redispersed nanoparticles is needed to fully understand effects of tubing material, pump stress, shear forces and heat stress which are applied to the particles during production (213,234). Loss of nucleic acid and or polymer could ultimately lead to decreased *in vitro* and *in vivo* performance. Hence, we successfully developed and set up protocols for nucleic acid as well as amine based polymer quantification to easily quantify the components of dried formulations and redispersed suspensions (235). Additionally, the effect of mannitol and trehalose on the redispersability of polyplexes consisting of 25k PEI and bulk DNA (bDNA) after SD was investigated. Both materials were chosen as they are generally recognized as safe (GRAS) substances, known for their lyo-and desicco-protection and commonly applied in SD (236). We found that a distinct concentration of excipient was needed to preserve PEI-bDNA polyplex size and particle distribution, independent of the excipient's nature. Initial changes in zeta potentials of the formulations after SD and redispersion could also be eliminated. Furthermore, it was confirmed by cascade impaction analysis that particles were prepared with an aerodynamic diameter between 1 and 5 µm, which is a conducive size range for pulmonary administration. SEM revealed round smooth microparticles for mannitol based formulations and also round but partly fused trehalose based microparticles. These findings were explained by the state of mannitol and trehalose via x-ray powder diffraction and differential scanning calorimetry revealing that mannitol crystallized upon spray drying while trehalose formulations dried without forming a crystalline but an amorphous state. This most probably led to the high residual moisture content of 3.2% of trehalose formulations compared to 0.4% of mannitol formulations and hence the fusion of trehalose microparticles. However, crystallinity and water content did not affect aerodynamic properties on short term. After establishing and ultimately applying the new set of analytical methods to SD powders, important changes to the initial formulations were detected: trehalose formulations showed ~32% nucleic acid loss at low N/P ratios reaching a plateau of ~20% at higher N/P ratios of the polymer/nucleic acid polyplexes, suggesting a stabilizing effect of excess polymer (Figure 4A). Considering the measured polymer loss of the different formulations after SD (Figure 4B), N/P ratios of the redispersed formulations overall increased (Figure 4C). It was therefore hypothesized that the N/P increase at least partially explained the improved uptake and transfection efficiency of redispersed formulations *in vitro*

compared to their freshly prepared counterparts with and without excipient as control (Figure 4D and 4E) (235).

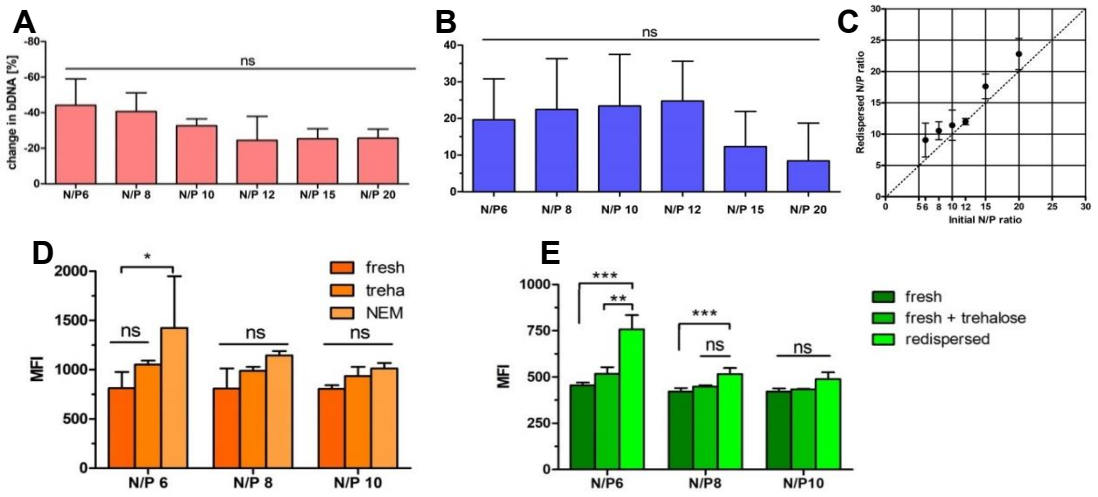

Figure 4. Polymer and nucleic acid quantification. Quantification of A) bulk DNA and B) PEI in the 10% trehalose nano in microparticle formulations following spray drying; C) Comparing the redispersed N/P ratio with the initial N/P ratio of the PEI polyplexes loaded with bulk DNA; D) Uptake and E) Transfection efficiency of redispersed nano in microparticle formulations in A549 cells. Median fluorescence intensity (MFI) was determined by flow cytometry to evaluate efficiency of D) fluorescently labeled bDNA or E) pEGFP in a human non-small cell lung carcinoma cell line (A549) of fresh or redispersed polyplexes from 10% trehalose NEM formulations at N/P ratios of 6, 8 and 10 with D) 0.5µg of bDNA or E) 0.75 µg of GFP plasmid in comparison to freshly prepared formulations in presence of trehalose. Blank samples consisted of A549 cells treated with 5% glucose only. Data points indicate mean ± SD (n=3). Two-way ANOVA, Bonferroni post-test, *P<0.05, **P < 0.01, *** P < 0.001, ns = non-significant. Reproduced with permission from (235). Copyright 2019 Elsevier B.V.

Even if both DNA and RNA are nucleic acids, we have more than once shown that circular plasmid DNA, for example, behaves very differently from rigid, short double-stranded siRNA when condensed with cationic polymers (237). Therefore, our current research on dry powder formulations focuses on the preparation of polyplexes consisting of siRNA and different PEI based delivery vectors with the goal of developing a platform technology for inhalable nucleic acid formulations.

6. Conclusion

siRNA-based therapies offer the chance to potentially target any single mRNA specifically and efficiently and mediate its downregulation. In the treatment of asthma, this technique could be exploited to target GATA3 in activated Th2 cells, one of the main factors involved in the pathogenesis of asthma. Almost 10 years ago, our group started a journey aimed to find a suitable delivery system able to downregulate GATA3 and to

produce a final spray dried powder formulation to be administered to patients via inhalation. After identifying transferrin as a targeting ligand for activated T cells, we developed the Tf-PEI conjugate, a delivery system that displayed high cellular selectivity and intracellular uptake with high transfection efficiencies *ex vivo*. Due to insufficient *in vivo* gene silencing, however, this formulation was then improved in terms of endosomal escape by blending it with the Mel-PEI conjugate. The new formulation showed optimal particle characteristics and *ex vivo* parameters. In parallel, we have also focused on the development of a dry powder formulation, an essential step to produce a final formulation that could be transferred from bench to bedside. We successfully produced nano-in-micro particles with ideal characteristics while retaining high transfection efficacies after redispersion.

Current research is therefore focusing on the *in vivo* testing of Tf-Mel-PEI in a murine asthma model and the dry powder formulation of siRNA based polyplexes. Ultimately, both research fields will be combined and hopefully result in a new therapy for the treatment of severe, uncontrolled asthma.

Funding Information

This project has received funding from the European Research Council (ERC) under the European Union's Horizon 2020 research and innovation programme (Grant agreement ERC-2014-StG637830)

Acknowledgments

The authors like to thank all former and current lab members both in Detroit and Munich who made this research progress possible.

Chapter VII - Targeted GATA-3 knockdown in human PCLS by siRNA polyplexes as a novel therapy for allergic asthma

Rima Kandil [a,†], Domizia Baldassi [a,†], Sebastian Böhlen [b], Joschka T. Müller[a], David C. Jürgens[a], Tonia Bargmann[b], Susann Dehmel[b], Yuran Xie[c], Aditi Mehta[a,d], Katherina Sewald[b], Olivia M. Merkel[a,d,*]

[a]Department of Pharmacy, Pharmaceutical Technology and Biopharmaceutics, Ludwig Maximilians-University of Munich, Butenandtstraße 5, 81377 Munich, Germany

[b]Fraunhofer Institute of Toxicology and Experimental Medicine, Biomedical Research in Endstage and Obstructive Lung Disease Hannover (BREATH) of the German Center for Lung Research (DZL), Hannover, Germany

[c]Department of Oncology, Wayne State University School of Medicine, 4100 John R St, Detroit, MI 48201, United States

[d]Comprehensive Pneumology Center (CPC) with the CPC-M bioArchive, Helmholtz Munich, German Center for Lung Research (DZL), Munich, Germany

[†]These authors contributed equally.

The experiments performed in this chapter were included in the following publication "Targeted GATA3 knockdown in activated T cells via pulmonary siRNA delivery as novel therapy for allergic asthma" and published in the Journal of Controlled Release.

Kandil R, Baldassi D, Böhlen S, Müller JT, Jürgens DC, Bargmann T, Dehmel S, Xie Y, Mehta A, Sewald K, Merkel OM. Targeted GATA3 knockdown in activated T cells via pulmonary siRNA delivery as novel therapy for allergic asthma. J Control Release. 2023 Feb;354:305-315. doi: 10.1016/j.jconrel.2023.01.014. Epub 2023 Jan 13. PMID: 36634709.

Abstract

Asthma is one of the most common inflammatory diseases of the lung affecting millions of people worldwide and, in some cases, it still remains poorly controlled. siRNA-based therapies give the chance to specifically and efficiently silence a target gene linked to a

certain disease. In the case of asthma, siRNA can be designed to inhibit the expression of GATA-3 in T helper 2 cells, which is a transcription factor involved in the inflammatory cascade of allergic asthma. In our previous studies we developed a delivery system for siRNA, Tf-Mel-PEI, composed of polyethylenimine (PEI) as polycationic carrier, transferrin (Tf) as targeting ligand and melittin (Mel) as endosmolytic agent, and we confirmed its activity in primary T cells. In this study, we developed an *ex vivo* model based on precision-cut lung slices (PCLS) to get deeper knowledge of the translatability of our findings. We were able to induce inflammation and upregulate GATA-3 expression in PCLS, confirming their ability to closely mimic *in vivo* conditions. In this model, our formulation was well tolerated and delivered siRNA efficiently to the cells. Furthermore, GATA-3 expression was successfully downregulated. These findings support the suitability and translatability of Tf-Mel-PEI siRNA delivery to T cells in the lungs and therapeutic GATA-3 silencing as a potential novel treatment for allergic asthma.

KEYWORDS siRNA therapy, pulmonary delivery, asthma, T cell targeting, cytokines, PCLS

1. Introduction

Asthma is considered as the most prominent inflammatory disease affecting the respiratory tract, with about 340 million people affected worldwide (199). Hallmarks of the disease are represented by shortness of breath, mucus hypersecretion, lung inflammation and bronchoconstriction. Although available therapies are effective in controlling the symptoms in most cases, 5-10 % of all patients have poor control over their disease with risks for severe consequences (5). Therefore, the development of novel therapeutics for handling severe forms is essential. Allergic asthma, in particular, is a form of the disease that develops in about 50-80% of all patients who are affected by severe illness (6). In this case, the immune-inflammatory response is driven by T helper 2 (Th2) cells that function as a bridge between the innate and adaptive immunity. After being taken up and processed by dendritic cells, allergens are presented to naïve T helper cells, which are consequently activated and stimulated to produce Th2 cytokines, namely IL-4, IL-5 and IL-13 – the major players in the asthmatic inflammatory cascade. Their release is triggered by the upregulation of a transcription factor, namely GATA-3, that could hence represent a therapeutic target for upstream blocking the inflammatory cascade, which would prevent the release of Th2 cytokines (205). Silencing of GATA-3 was already demonstrated to help controlling asthma by means of a DNAzyme therapy targeting GATA-3 (238,239)**.** On this basis, RNAi could be employed

to post-transcriptionally downregulate the expression of GATA-3 (53). siRNAs can in principle be developed to silence any target gene specifically and efficiently. Nonetheless, siRNAs are susceptible to degradation by nucleases and cannot penetrate the cell membrane on their own, and should therefore be formulated with a suitable carrier. Moreover, an appropriate nanocarrier system is also required to overcome the biological barriers encountered in the lung when considering the pulmonary route of administration (22). Polyethylenimine (PEI) is a cationic polymer that has been widely studied as a delivery system for nucleic acids. Thanks to its cationic nature, it can complex the negatively charged siRNA to form the so-called polyplexes and deliver the payload to the target cells (240). However, T cells are particularly challenging to transfect as they do not do not express caveolin and do not present caveolae, therefore, the most common entry port to cells for non-viral vectors (241). Another limiting factor is represented by the endosomal escape, which is considered the bottleneck of most non-viral delivery systems. Therefore, we have developed an optimized delivery system, namely Tf-Mel-PEI, that should overcome these two major obstacles (65). Tf-Mel-PEI is a blend of two conjugates, transferrin (Tf)-PEI and melittin (Mel)-PEI. Transferrin is used as a targeting ligand for T cells, as they overexpress the transferrin receptor in the activated state (220). Thus, Tf-PEI efficiently and selectively delivers siRNA to activated T cells (127). Melittin is a cationic peptide with endosmolytic properties, that supports the release of the therapeutic cargo from the endosome (135,242). In our previous work, we showed that the formulation efficiently delivered siRNA to primary T cells as well as mediated a significant downregulation of GATA-3 in immortalized as well as primary T cells, outperforming the results obtained with the first generation conjugate Tf-PEI thanks to the improved melittin-mediated endosomal escape (65). To gain a better understanding of the translatability of our findings, in this study an *ex vivo* model of asthma was established using human precision-cut lung slices (PCLS) from lung explants. PCLS are living tissues that retain the anatomical as well as cellular structure of the lung and thus represent a sophisticated *ex vivo* model for drug screening. They can be used to better mimic the diseased environment as well as to get a deeper understanding of the translatability of a drug (47). Previous studies already confirmed their potential also for investigating siRNA-based therapeutics (55,147). Here, hPCLS were stimulated with CD3/CD28 beads to activate T cells and to induce the release of inflammatory cytokines. PCLS were then used for investigating the formulation in terms of cellular uptake, tolerability of the formulation and GATA-3 downregulation activity. Overall, the results confirm the potential of Tf-Mel-PEI/siGATA-3 polyplexes as a promising approach to treating allergic asthma.

2. Experimental methods

2.1 Materials

5kDa PEI (Lupasol® G100) was purchased from BASF (Ludwigshafen, Germany). Cysteine modified melittin was obtained from Pepmic (Suzhou, China). HEPES, NaCl, glucose, SPDP, human transferrin, DMMAn, DMSO, EDTA, low gelling temperature agarose, Earle's Balanced Salt Solution (EBSS), were purchased from Sigma Aldrich (Darmstadt, Germany). PEG4-SPDP, Dulbecco's modified Eagle's medium/nutrient mixture F-12 Ham (DMEM, pH 7.2–7.4) were purchased from Thermo Fisher Scientific (Waltham, USA). Alexa Fluor™ 647 NHS ester was obtained from Life Technologies (Carlsbad, California, USA). Penicillin-streptomycin solution and Dulbecco´s phosphate-buffered solution without Ca2+ and Mg2+ (DPBS) were purchased from Lonza (Basel, Switzerland). 2000, 3000 and 10000 MWCO centrifugal filters were obtained from Sartorius (Göttingen, Germany). siRNA sequences against GATA-3 (GATA-3_7 and GATA-3_8), human GATA-3 and β-actin primers were purchased from Qiagen (Hilden, Germany). Scrambled non-specific DsiRNA and amine-modified siRNA were purchased from Integrated DNA Technologies (Leuven, Belgium).

2.2 Synthesis of conjugates and preparation of polyplexes

Tf-PEI and Mel-PEI were prepared as previously reported (65). For Tf-PEI, 5kDa PEI (1 mg/ml) was dissolved in HEPES buffered saline (HBS) (20 mM HEPES, 150 mM NaCl, pH = 7.5) and mixed with a 10-fold molar excess of SPDP (20 mM) in DMSO and stirred overnight at room temperature. The day after, transferrin was dissolved in HBS at a concentration of 10 mg/ml and stirred with a 5-fold molar excess of SPDP for 2 hours. Purification of PEI-SPDP and Tf-SPDP were performed with 3000 or 10,000 MWCO centrifugal filters with HBS/1mM EDTA (pH 7.1). The estimation of the SPDP concentration in PEI-SPDP was done by reacting 100 µl of 50-fold diluted PEI-SPDP with 1 µl of a 150 mM DTT solution for 30 min. the release of pyridon-2-thion was then measured at a plate reader at 343 nm (Tecan, Männedorf, Switzerland). A 10-fold excess of DTT was then added to PEI-SPDP and reacted for 2 h under nitrogen protection. The reduced PEI-SPDP was then purified with 3000 MWCO centrifugal filters with HBS/20mM EDTA (pH 7.1). Tf-SPDP was then added dropwise to PEI-SPDP and stirred overnight at 4 °C. Purification of Tf-PEI was performed through an ÄKTA FPLC system (GE healthcare) equipped with 2 connected 1 ml HiTrap SP HP cation exchange column (GE healthcare). Further purification and desalinization were performed by 10.000 MWCO centrifugal filters with HBS. The concentration of Tf was measured spectrophotometrically at 280 nm, while the concentration of PEI was determined with a

TNBS by measuring the absorbance of the sample with respective standard curve at 405 nm (Tecan, Männedorf, Switzerland) (243).

For Mel-PEI, 5k PEI (5 mg/ml) was dissolved in in HBS and mixed with an excess of PEG-SPDP in dry DMSO and stirred overnight at room temperature. Cysteine-modified melittin (3 mg/ml) was dissolved in HBS and mixed with a 150 mM solution of DTT for 2 h with shaking. Reduced melittin was purified with a 2000 MWCO centrifugal filter using 100 mM HEPES, 125 mM NaOH and was subsequently mixed with 1 mL of 2,3-Dimethyl-maleic anhydride solution (DMMAn, 1.5 mg/mL in EtOH) and stirred for 1 h. PEI-SPDP and Mel-DMMAn were purified with 3000 MWCO centrifugal filter and HBS or 2000 MWCO centrifugal filter and 20 mm HEPES, 0.5 m NaCl, 1 m Guanidine hydrochloride (pH = 8), respectively. PEI-SPDP and Mel-DMMAn were then mixed and stirred overnight at room temperature. The conjugate was then purified and desalted with a 10,000 MWCO centrifugal filter and HBS as buffer. The concentration of PEI was measured via TNBS assay at 405 nm (Tecan, Männedorf, Switzerland) (243).

For Tf-PEI or Tf-Mel-PEI (which corresponds to a 50:50 mixture of Tf-PEI and Mel-PEI) polyplexes preparation, conjugates were diluted in 5% glucose and defined amount of siRNA were added to achieve an amine to phosphate (N/P) ratio of 10. The formulations were mixed by pipetting and incubated for 20 min to yield polyplexes.

2.3 Human donors and ethics statement

Human lung lobes were acquired from patients who underwent cancer lobe resection at Hannover Medical School (MHH, Hannover, Germany) or KRH Klinikum Siloah-Oststadt-Heidehaus (Hannover, Germany). Experiments were approved by the ethics committee of the Hannover Medical School (MHH, Hannover, Germany) and are in compliance with “The Code of Ethics of the World Medical Association” (renewed on 2015/04/22, number 2701–2015). All patients gave written informed consent for the use of their lung tissue for research.

2.4 Preparation of hPCLS

Human PCLS were prepared as previously described (244). Briefly, a 1.5% agarose-DMEM solution was gently inflated into the lung explant and solidified at 4°C. Sections of 8 mm in diameter were sliced into approximately 250-300 µm slices using a Krumdieck tissue slicer. PCLS were cultured in DMEM medium (2 slices per 500 µl) under submerged conditions in a humidified atmosphere at 37 °C and 5% CO_2.

2.5 Activation of hPCLS (Stimulation of PCLS for cytokine release)

Two PCLS per well were treated in duplicates with anti-CD3/CD28 coupled magnetic beads, (Dynabeads™ Human T-Activator CD3/CD28 for T Cell Expansion and

Activation, Thermo Fisher Scientific), to activate tissue resident T cells at a bead:cells ratio of 1:1 in 500 µl DMEM for 48 h under standard cell culture conditions. Once the incubation time was completed, the supernatant was collected and stored for further analysis. Changes in T cell cytokines were measured in PCLS supernatants using multiplex assays (Pro-Inflammatory Panel 1 Human V plex (IFN-γ, IL-1β, IL-2, IL-4, IL-6, IL-8, IL-10, IL-12p70, IL-13, TNF-α; Meso Scale Diagnostics) according to the manufacturer's instructions. Negative controls consisted of unstimulated samples.

2.6 Cell viability and lactate dehydrogenase (LDH) release

2.6.1 Cell viability

Viability of the formulation following activation as well as incubation with Tf-PEI ad Tf-Mel-PEI polyplexes was assessed via the metabolic WST-1 assay according to the manufacturer's protocol and as described before (244). After 48 h of stimulation with beads and 24 h of polyplex treatment, PCLS were incubated with 1:10 diluted WST-1 solution for 1 h at 37°C. Absorbance was then measured at 420-480 nm with a reference wavelength at 690 nm using a plate reader (Tecan, Männedorf, Switzerland).

2.6.2 LDH release

The effect of bead stimulation as well as polyplexes transfection on membrane integrity of PCLS cells was evaluated by measuring the release of lactate dehydrogenase (LDH) using the Cytotoxicity Detection Kit (Th. Geyer, Renningen, Germany) according to the manufacturer's protocol. Briefly, 5 days after stimulation with beads and 24 h after incubation with Tf-PEI and Tf-Mel-PEI polyplexes, 50 µl of the supernatant were collected and incubated with 50 µl of the substrate mix for 20 min at room temperature protected from light. Absorbance was measured at 490 nm with a reference wavelength at 690 nm using a microplate reader (Tecan, Männedorf, Switzerland).

2.7 Microscopic assessment of siRNA delivery in hPCLS

PCLS were fixed overnight in 2% PFA and subsequently washed with PBS. DAPI staining was performed for 45 minutes, and the PCLS were embedded in Ibidi mounting medium on two thin coverslips. The fluorescence labeled siRNA was detected in the Cy5 channel while autofluoresence of the tissue was recorded in the Cy3 channel. Z stacks of the tissue slide were imaged with a confocal microscope (Zeiss 880) and reconstructed in three dimensions using IMARIS® Software (Bitplane).

2.8 GATA-3 downregulation

Two PCLS/well were stimulated with anti-CD3/CD28 coupled magnetic beads in DMEM/F-12 to activate tissue resident T cells. PCLS were placed in 24-well-plates in 500 µl complete medium and transfected with Tf-PEI and Tf-Mel-PEI polyplexes

encapsulating 50, 100 and 250 pmol siRNA against GATA-3 or scrambled negative control. The tissue slices were incubated for 5 days at 37°C and 5% CO_2 in technical biological duplicates. Experiments were conducted with tissue from three human donors. Five days post treatment, supernatants of technical replicates were pooled, supplemented with 0.2% protease inhibitor cocktail P1860 (Sigma-Aldrich), and aliquots were stored at 80 °C for cytokine analysis and LDH release assay. PCLS were stored in RNAlater® (Thermo Fisher Scientific) at 4°C overnight and subsequently frozen at -80°C until RNA was isolated.

Afterwards, RNA was isolated according to an optimized protocol for PCLS (245). cDNA was synthesized from total RNA with a high-capacity cDNA synthesis kit (Applied Biosystems, Waltham, Massachusetts, USA). cDNA was then diluted 1:10 and qPCR was performed using the SYBR™ Green PCR master mix (Thermo Fisher Scientific) with primers for GATA-3 (Qiagen, Hilden, Germany) and β-actin (Qiagen, Hilden, Germany) for normalization. Amplification and data analysis was performed using a QuantStudio 3 Real-Time PCR (Thermo Fisher Scientific, Waltham, Massachusetts, USA). Cycle thresholds were acquired by autosetting with the qPCR software (Thermo Fisher Scientific, Waltham, Massachusetts, USA). Values are given as mean values ± SEM.

3. Results and discussion

3.1 Activation of PCLS

The activation of T cells in PCLS was optimized with Dynabeads™, magnetic ferric oxide beads covalently coupled to anti-CD3 and anti-CD28 antibodies. Dynabeads™ have a size of 4.5 µm to resemble the size of antigen presenting cells. They are chemically inert and supermagnetic, allowing them to be easily removed from culture medium with a magnet. Here, CD3 and CD28 were chosen as target for the coupled antibodies as these epitopes are typically used to induce T cells activation and to partially mimic the *in vivo* stimulation pattern via antigen presenting cells (246). The effect on cytokine production was measured by ELISA after 3 days and 5 days of incubation with Dynabeads™. As shown in Figure 1, each condition was compared to the respective non-stimulated PCLS. The incubation with Dynabeads™ successfully induced an inflammatory state in PCLS. Cytokines typical of general inflammation (IL-12p70, IL-8, IL-6 and IL1b) as well as mediated by Th1 response (TNF-α, IFN-γ and IL-2) and Th2 cells (IL-4, IL-13 and IL-10) were upregulated following the activation process. Th2 related cytokines are directly affected by GATA-3 expression, since it promotes and upregulates their secretion (205). The consistent upregulation of the different inflammatory cytokine secretion confirmed

that the activation procedure was successful in establishing an inflammatory environment, resembling the one typical of asthma, where a mixture of different inflammatory cytokines is found. Commonly, GATA-3 related non-related cytokines contribute to the pathogenesis of allergic asthma. The observation of activation and inflammation was confirmed by the upregulated expression of GATA-3 in PCLS after 5 days of incubation with beads (Figure 2). The expression of GATA-3 was measured by qRT-PCR in PCLS obtained from 3 different patients. The activation with Dynabeads™ led to an increased expression of GATA-3, confirming activation response at both the upstream and downstream level of the inflammatory cascade.

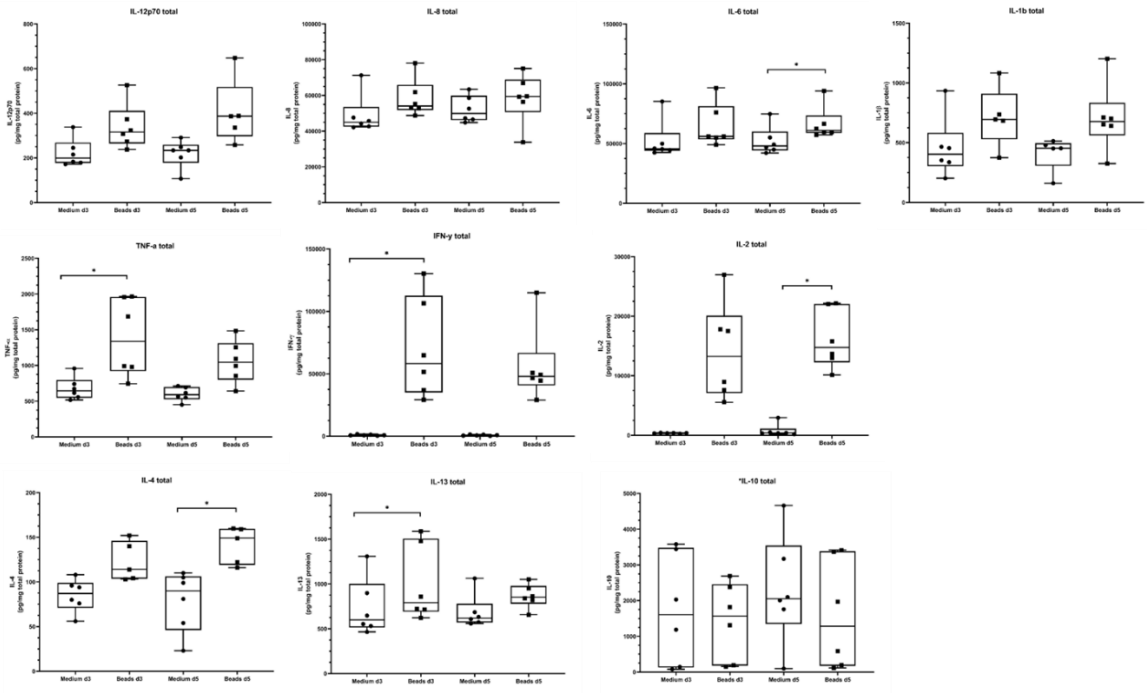

Figure 1. Cytokine concentrations (IL-12p70, IL-8, IL-6, IL-1b, TNF-α, IFN-γ, IL-2, IL-4, IL-13 and IL-10) in the supernatant of human PCLS after 72 h and 120 h of activation with beads as measured by ELISA.

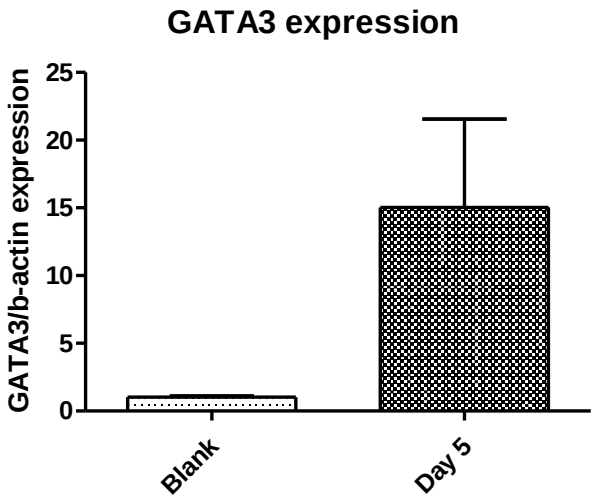

Figure 14. GATA-3 expression as measured by qRT-PCR in human PCLS 5 days after activation with beads, normalized to β-actin expression. Blank represents untreated PCLS.

3.2 Effect of activation and transfection on metabolic activity and LDH release

The effects of incubation with Dynabeads™ as well as with polyplexes on metabolic activity was evaluated by WST-1 assays. Activated or non-activated PCLS were incubated for 5 days with Tf-PEI or Tf-Mel-PEI polyplexes encapsulating siGATA-3 or a siNC negative control to observe if any of the different factors influenced cell viability. As it can be observed in Figure 2A, the treatment with Dynabeads™ negatively affected cell viability, with a decrease of 40 to 50%. This result is to be expected considering that sites with ongoing inflammation and triggered immune response present alterations of metabolic activity (247). Nevertheless, the treatment with the Tf-PEI and Tf-Mel-PEI did not induce any relevant change in cell viability, with values close to the samples receiving no additional treatment. To confirm the results, LDH assays were performed to detect any detrimental effect on membrane integrity. In line with the metabolic activity results, non-activated samples showed only negligible membrane impairment, reflected in LDH release values below 20%. On the other hand, samples incubated with beads indicated an increase in membrane disturbance, with a maximum of 40% of LDH release. The increase in membrane leakiness can be linked to the inflammatory state induced by the beads. The transfection with the different formulation did not increase the LDH release, in both stimulated and unstimulated samples, confirming the safety of Tf-PEI and Tf-Mel-PEI as nanocarriers for siRNA. The results are in line with our previous studies in cell culture, where no significant cytotoxicity was observed for any of the different formulations, even at higher N/P ratios (65).

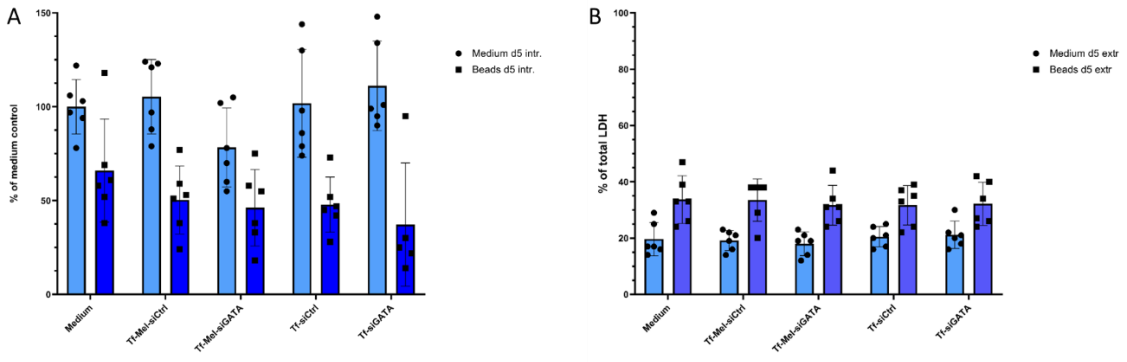

Figure 15. Tolerability of Tf-PEI and Tf-Mel-PEI polyplexes in activated and non-activated PCLS after 5 days of incubation. (A) evaluation of cellular viability by WST-1 assay. (B) Assessment of lactate dehydrogenase release by LDH assay following incubation with polyplexes. Data points indicate means ± SD.

3.3 siRNA delivery to PCLS

Confocal scanning laser microscopy was utilized to evaluate the ability of Tf-PEI and Tf-Mel-PEI polyplexes to deliver siRNA to PCLS. The encapsulated fluorescently labelled siRNA, AF647-siRNA, is presented in red, and nuclei were stained with DAPI, shown in blue. The typical green autofluorescence observed in lung tissue is shown in yellow (Figure 3). From the qualitative assessment of this experiment, it appears that siRNA reaches the epithelium and, more importantly, more siRNA shown as red dots seems to be delivered with Tf-Mel-PEI polyplexes compared to samples transfected with Tf-Mel-PEI. This observation is in line with our previous studies in immortalized and primary T cells, where the presence of melittin improved not only the endosomal escape, but also the uptake of siRNA (65). Melittin is indeed a positively charged peptide that, in addition to endosmolytic activity, can also deliver nucleic acids. This specific property could explain the superior siRNA delivery observed for Tf-Mel-PEI polyplexes (135).

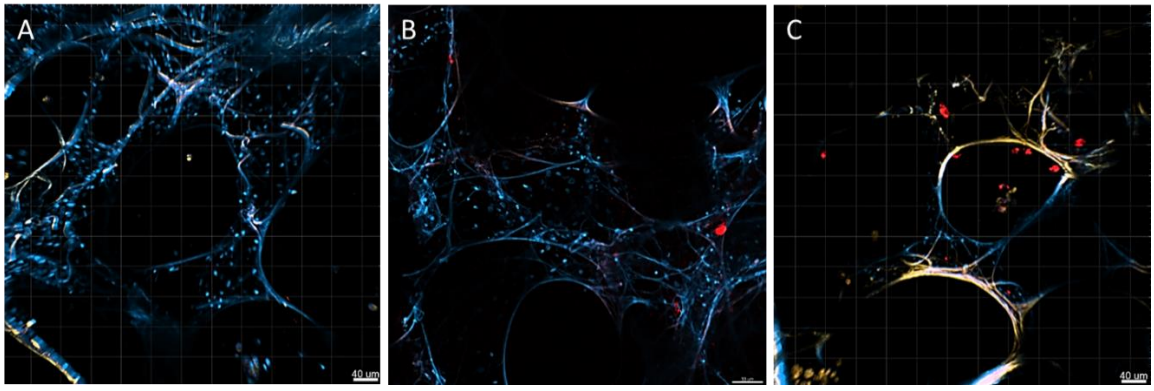

Figure 4. Delivery of Tf-PEI (B) and Tf-Mel-PEI ((C) polyplexes loaded with AF647-siRNA to human PCLS analyzed by confocal scanning laser microscopy. Red dots represent AF647-siRNA, blue corresponds to nuclei stained with DAPI and yellow reflects autofluorescence of PCLS. (A) represents a control PCLS receiving no treatment.

3.4 siRNA-mediated RNAi of GATA-3 in PCLS

The GATA-3 gene silencing activity of the polyplexes was measured by qRT-PCR 5 days after activation and 2 days after transfection. For this experiment, a 50:50 blend of two siRNA sequences, GATA-3_8 and GATA-3_9 was selected, as they showed the best silencing activity in a preliminary experiment using Lipofectamine as transfection reagent. PCLSs were incubated with Tf-PEI or Tf-Mel-PEI polyplexes encapsulating different amounts of siGATA-3. For comparison, untreated samples as well as samples transfected with scrambled siRNA were included as negative controls. Both Tf-PEI and Tf-Mel-PEI polyplexes mediated a significant downregulation of GATA-3. Interestingly, the downregulation was observed for both activated and non-activated samples, with silencing activity in the same range. This observation could be explained by the fact that activated samples retained a higher basal expression of GATA-3 and, considering that the readout was performed 5 days after treatment with polyplexes, this continued activation could have led to a higher expression of mRNA and thus a lower therapeutic effect of the siRNA in comparison to the non-activated PCLS. Nonetheless, also in the activated samples a significant downregulation of GATA-3 was observed for both Tf-PEI and Tf-Mel-PEI polyplexes. Here, Tf-Mel-PEI polyplexes achieved better downregulation of GATA-3 in comparison to Tf-PEI at the highest concentration tested, with values of 45% and 25% gene silencing, respectively. In line with our previous findings, the inclusion of melittin in the formulation improves the endosomal escape and consequently the RNA interference activity of the formulation. This experiment confirmed the potential of Tf-PEI and Tf-Mel-PEI polyplexes as delivery systems for siRNA. To the best of our knowledge, we are the first to attempt GATA-3 downregulation in human lung explants. In an unrelated study by Ruigrok *et al*., the downregulation of GAPDH was tested by qRT-PCR in mouse PCLS 48 h after transfection with siRNA. In that study, siRNA was delivered with a commercially available transfection reagent and achieved 50% reduction of mRNA expression (248). Tf-Mel-PEI polyplexes here reached 75% downregulation, thus confirming that our formulation represents a valid option for delivering siRNA to lung tissues and as a promising strategy to treat allergic asthma.

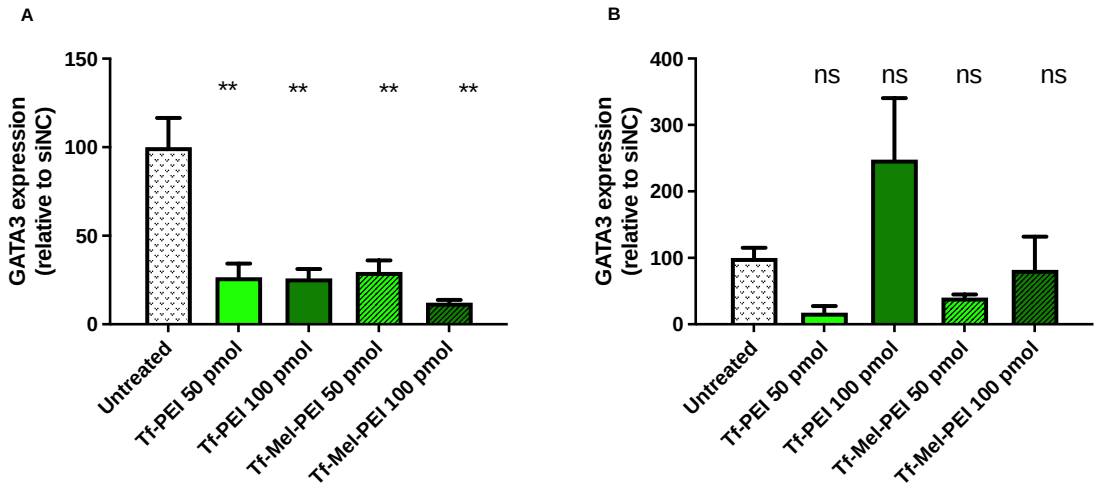

Figure 5. GATA-3 knockdown in activated (A) and non-activated (B) human PCLS transfected with Tf-PEI and T-Mel-PEI polyplexes encapsulating different amount of GATA-3 siRNA as measured by qRT-PCR and normalized to β-actin expression. Each value is normalized to the GATA-3/β-actin expression after treatment with negative control siRNA at the same conditions. Data points indicate mean ± SEM. One way ANOVA, *p<0.05, **p<0.01, ***p<0.005.

4. Conclusion

In this study, we developed a sophisticated *ex vivo* model of the lung resembling the inflammatory pattern found in patients suffering from allergic asthma. PCLS prepared from lungs of human donors were treated with T cell activating beads to stimulate the release of inflammatory cytokines from tissue resident cells. PCLSs were then used to test the translatability of our previous findings regarding T cell transfection with Tf-PEI and Tf-Mel-PEI polyplexes. Tf-PEI and Tf-Mel-PEI demonstrated a safe profile when incubated with PCLS and efficiently delivered siRNA to the tissues. Furthermore, the downregulation activity of Tf-PEI and Tf-Mel-PEI polyplexes against GATA-3, a transcription factor involved in asthma pathogenesis, was confirmed, with Tf-Mel-PEI showing the best activity results, in line with our previous findings. In conclusion, this study confirms the potential of siRNA-based therapies for the treatment of inflammatory diseases and offers a new treatment option for asthmatic patients.

Chapter VIII - hNPs for the treatment of inflammation in cystic fibrosis

Domizia Baldassi[1], Gabriella Costabile[2], Gemma Conte[3], Ivana D'Angelo[3], Francesca Ungaro[2], Olivia M. Merkel[1]

[1]Department of Pharmacy, Pharmaceutical Technology and Biopharmacy, Ludwig-Maximilians-Universität, München, Munich 81377, Germany

[2]Department of Pharmacy, University of Napoli Federico II, Napoli 80131, Italy

[3]Di.S.T.A.Bi.F., University of Campania Luigi Vanvitelli, Caserta 81100, Italy

The experiments described in this chapter were included in the following publication "Hybrid Lipid/Polymer Nanoparticles to Tackle the Cystic Fibrosis Mucus Barrier in siRNA Delivery to the Lungs: Does PEGylation Make the Difference?" and published in ACS Applied Materials and Interfaces.

Conte G, Costabile G, Baldassi D, Rondelli V, Bassi R, Colombo D, Linardos G, Fiscarelli EV, Sorrentino R, Miro A, Quaglia F, Brocca P, d'Angelo I, Merkel OM, Ungaro F. Hybrid Lipid/Polymer Nanoparticles to Tackle the Cystic Fibrosis Mucus Barrier in siRNA Delivery to the Lungs: Does PEGylation Make the Difference? ACS Appl Mater Interfaces. 2022 Feb 16;14(6):7565-7578. doi: 10.1021/acsami.1c14975. Epub 2022 Feb 2. PMID: 35107987; PMCID: PMC8855343.

Abstract

Inhaled therapy with short interfering RNA (siRNA) holds the exceptional potential to treat severe lung disease such as cystic fibrosis. siRNA can in theory be designed to specifically target and silence any given target gene. In the case of cystic fibrosis, siRNA can be used to downregulate the nuclear factor-κB (NFκB), one of the main mediators involved in inflammation, to reduce the inflammatory state and improve patients' condition. Nonetheless, different barriers need to be overcome in the lung before reaching the target cells, above all the mucus layer, making the formulation of siRNA with a suitable delivery system essential for exerting its activity. In this view, hybrid lipid-polymer nanoparticles (hNPs) were developed, comprising a poly(lactic-co-glycolic) acid (PLGA) core and lipid shell of dipalmitoyl phosphatidylcholine (DPPC) or (1,2-distearoyl-sn-glycero-3-phosphoethanolamine-poly(ethylene glycol) (DSPE-PEG). Resulting formulations were investigated in terms of physicochemical characterization, *in vitro*

behavior and mucus permeation. Overall, the results indicate the potential of hNPs, particularly the non-PEGylated hNPs as carriers for local delivery of siRNA to the lungs for the treatment of inflammation in cystic fibrosis.

KEYWORDS siRNA therapy, hybrid nanoparticles, cystic fibrosis, pulmonary delivery, air-liquid interface

1. Introduction

Cystic fibrosis is the most prevalent autosomal recessive disease affecting 100.000 people worldwide. The disease arises as a consequence of mutations in the Cystic Fibrosis Transmembrane Conductance Regulator (CFTR) gene, which causes an impaired transport of chloride and bicarbonate ions across epithelial cells (249). Despite being a multiorgan disorder, the organ mainly affected by the disease is the lung. CFTR loss of function leads to impaired mucociliary clearance, recurring bacterial infections and chronic inflammation, with respiratory failure being the primary cause of death and morbidity (3,250). One of the main traits of cystic fibrosis is airway inflammation, which seems to be strictly associated to an increase in NFκB expression due to altered CFTR function. For this reason, a therapy downregulating the expression of NFkB could be beneficial for reducing inflammation in the lungs and improving the quality of life of patients (251). Small interfering RNA (siRNA) holds great potential for the treatment of severe diseases, since it can in theory be designed to target any gene of interest, such as NFκB (252). Furthermore, the pulmonary route of administration offers the possibility to directly deliver the therapeutic the region of interest, such as the epithelium of the lungs in the case of cystic fibrosis, thus improving patients' compliance and reducing systemic side effects (253). Nevertheless, siRNAs are susceptible to RNase degradation and cannot permeate through the cell membrane. Additionally, siRNAs need to overcome the mucus barrier found in the lungs, which is particularly viscous and adherent in the case of cystic fibrosis (58,74). Therefore, formulation with a suitable delivery system is of the essence (14). In this study, we developed hybrid lipid-polymer nanoparticles (hNPs), that bring together features from both polymer and lipid-based systems. hNPs are composed of a poly(lactic-co-glycolic) acid (PLGA) core and coated by either non-PEGylated or PEGylated lipid shells, dipalmitoyl phosphatidylcholine (DPPC) or N-(carbonyl-methoxypolyethyleneglycol-2000)-1,2-distearoyl-sn-glycero-3-phosphoethanolamine (DSPE-PEG) respectively. The lipid shell should confer muco-inertia to the formulation, hence helping the transport of the cargo through the mucus to the underlying epithelium (254). Furthermore, polyethylenimine (PEI) was included as an

additional component to the formulation due to its ability to complex siRNA and consequently improve its loading inside hNPs (254). The resulting hNPs were investigated in terms of physicochemical characterization as well as biological behavior in a lung epithelial cell line in regards of cellular uptake, downregulation activity and biocompatibility. To further explore the translatability of our findings, an air-liquid interface (ALI) culture was established to evaluate hNPs in a more sophisticated, mucus-rich environment (45).

2. Experimental methods

2.1 Materials

ResomerRG 502H (uncapped PLGA 50:50, inherent viscosity 0.16 0.24 dL/g) was purchased from Evonik Industries AG (Germany). 1,2-dipalmitoyl-sn-glycero-3-phosphocholine (DPPC) and N-(carbonyl-methoxypolyethyleneglycol-2000)-1,2-distearoyl-sn-glycero-3-phosphoethanolamine (DSPE-PEG) were a kind gift from Lipoid GmbH (Switzerland). ON-TARGETplus siRNA was purchased from Dharmacon (Germany). Ethanol 96% was supplied by Carlo Erba (Italy). Branched polyethyleneimine (PEI; 25 kDa), RPMI-1640 medium, EMEM medium, penicillin/streptomycin, foetal bovine serum, L-glutamine, 3-(4,5-dimethylthiazol-2-yl)-2,5-diphenyltetrazolium bromide (MTT) powder, Dulbecco's phosphate buffer saline, Tween20, 20% paraformaldehyde, DAPI, RIPA buffer, phosphatase inhibitor, protease inhibitor and Ponceau S solution were purchased from Sigma-Aldrich (Germany). Alexa-Fluor647, Quant-IT™ RiboGreen® reagent, 96-well-plates, 24-well-plates, 6-well plates, Trypsin 0,25% EDTA, LysoTracker™ green, Lipofectamine2000, Pierce™ BCA Protein Assay Kit, Tris-buffered saline, SuperSignal™ West Pico PLUS Chemiluminescent Substrate and Restore™ Western blot Stripping Buffer were supplied by Thermo Fisher Scientific (Germany). T-25 and T-75 cell culture flasks, Laemmli loading buffer, TG buffer UltraPure were provided by VWR (Germany). Rotiphorese® 10x SDS-page, methanol and Bovine Serum Albumin - IgG free were purchased from Carl-Roth GmbH (Germany). 10% Tris-Glycine Gel and the electrophoresis chamber were supplied by Invitrogen (Germany). The transfer chamber was provided by BioRad (Germany). 8-well-plates were purchased from Ibidi (Germany). CytoTox96® Non-Radioactive Cytotoxicity Assay kit was purchased from Promega (Germany) and Human TNF-α ELISA MAX Deluxe Sets kit was purchased by BioLegend (Germany). FluorSave™ reagent was provided by Merck (Germany). Primary and secondary antibodies (NFkB p65 mouse monoclonal

antibody, Actin goat polyclonal IgG, mIgG BP-HRP secondary antibody, Donkey anti-goat IgG-HRP) were purchased from Santa Cruz Biotechnology (Germany).

2.2 Production of hNPs

1,2-Dipalmitoyl-sn-glycero-3-phosphocholine_poly(lactic-co-glycolic) acid (DPPC_PLGA) and N-(carbonyl-methoxypolyethyleneglycol-2000)-1,2-distearoyl-sn-glycero-3-phosphoethanolamine_poly(lactic-co-glycolic) acid (DSPE-PEG_PLGA) hNPs were prepared by an emulsion/solvent diffusion technique as previously reported (254). The first step consisted in a water-in-oil emulsion (w/o) by adding 100 µL of water to 1 mL of methylene chloride containing PLGA (10 mg; 1% w/v) and either DPPC or DSPE-PEG under vortex mixing. When required, poly(ethylenimine) (PEI) was added to the internal water phase at the theoretical loading of 0.016 mg per 100 mg of PLGA. Just after mixing, the w/o emulsion was added to 12.5 mL of ethanol 96% (v/v) under moderate magnetic stirring, leading to immediate nanoparticle precipitation. Afterwards, the formulation was diluted with 12.5 mL of Milli-Q water under stirring for 10 minutes. The residual organic solvent was then removed by rotary evaporation under vacuum at 30°C and hNPs were isolated form the resulting hNP colloidal dispersion by centrifugation at 7000 rcf for 20 minutes at 4°C and dispersed in Milli-Q water. siRNA-loaded hNPs were prepared at a theoretical loading of 1 nmol/100mg of PLGA by adding siRNA to the internal water phase. For cellular uptake studies and confocal microscopy experiments, hNPs were encapsulated with AlexaFluor647-labelled siRNA. For lyophilization, trehalose was used as cryoprotectant at a hNPs/cryoprotectant ratio of 1:25 w/w.

2.3 Characterization of hNPs

Hydrodynamic diameter (D_H), polydispersity index (PDI) and the zeta potential (ζ potential) of hNPs were determined by dynamic light scattering with a Malvern Zetasizer Nano ZS (Malvern Instruments). Results are expressed as mean value ± standard deviation (SD) of triplicate measurements in different batches.

The actual siRNA loading was measured indirectly by quantifying the amount of unencapsulated siRNA. After production, hNPs were collected by centrifugation (7000 rcf for 20 minutes at 4°C) and the supernatant was analysed for siRNA content using Quant-IT™ RiboGreen® reagent according to the manufacturer's instructions. Quantitative analysis was performed by spectrofluorometry at λ_{ex} 480 nm/λ_{em} 520 nm. Results are reported as actual loading (nmol of encapsulated siRNA per mg of yielded hNPs) and encapsulation efficiency (actual loading/theoretical loading x100) ± SD of values collected from three different batches.

2.4 Cell culture

Human epithelial bronchial cells (16HBE14o-) and Calu-3 cells were cultured in EMEM cell culture medium supplemented with 1% L-glutamine, 1% penicillin/streptomycin and 10% fetal bovine serum. Cells were grown in 75 cm^2 cell culture flasks at 37°C and 5% CO_2 and passaged when they had reached confluency.

2.5 Quantification of cellular uptake

For flow cytometry and microscopy experiments, amine-modified siRNA was labeled with succinimidyl ester (NHS) modified AlexaFluor647 fluorescent dye according to the manufacturer's protocol and purified via ethanol purification to obtain AF647-siRNA (siFluo) as previously reported (69).

16HBE14o- cells were seeded in 24-well-plates at a density of 100.000 cells per well and incubated overnight at 37°C and 5% CO_2. Cells were transfected for 5 h or 24 h at 37°C and 5% CO_2 with 100 µL of hNPs suspension containing 0.5, 1 and 2.5 pmol AlexaFluor647-labelled siRNA respectively, within a total volume of 500 µL of serum containing cell culture media. Positive controls consisted of lipofectamine lipoplexes, while negative controls consisted of free siRNA. Cells were then detached from the well surface and spun down at 350 rcf for 5 minutes. After centrifugation, the supernatant was decanted, and the cells were washed with 1x PBS first and then with PBS-EDTA 2 mM. Samples were analyzed via flow cytometry (Attune® NxT Acoustic Focusing Cytometer, Thermo Fisher Scientific) and the median fluorescence intensity (MFI) was collected and recorded. Samples were run in triplicates, with each sample consisting of a minimum of 50.000 viable cells. Negative control samples consisted of untreated cells. Analysis and presentation of data was performed by GraphPad Prism 5.0 software calculating mean values and standard deviation. Significance was measured by One Way ANOVA analysis (**$p<0.01$, ***$p<0.005$).

2.6 Immunofluorescent staining

16HBE14o- cells were seeded in 8-well-plates at a density of 15.000 cells per well and incubated overnight at 37°C and 5% CO_2. Cells were transfected for 24 h at 37°C and 5% CO_2 with 100 µL of DSPE_PEG, PEI_DSPE_PEG, DPPC and PEI_DPPC hNPs suspension containing 2.5 pmol AlexaFluor647-labelled siRNA respectively, within a total volume of 400 µL of serum containing medium. After 24 h, medium was discarded, plates were washed two times with 200 µL PBS and 300 µL/well of LysoTracker™ green was added, which was previously diluted in medium (final concentration = 75 nM) and incubated 1 h at 37°C and 5% CO_2. Afterwards, the medium was removed, plates were washed twice with PBS and 100 µL/well of 4% paraformaldehyde was added and incubated for 15 min. Cells were then washed twice with PBS and 300 µl/well of DAPI at

a final concentration of 1 µg/mL diluted in blocking buffer was added and incubated for 20 min. Finally, wells were washed again with PBS and mounted using FluorSave™ reagent. The samples were analyzed using the TCS SP8 confocal microscope (Leica) and Leica LAS-X software.

2.7 *In vitro* NFκB gene silencing in LPS-stimulated 16HBE14o- cells

16HBE14o- cells were seeded in 6-well-plates at a density of 250.000 in 2.5 mL of medium and incubated overnight. Before transfection, cells were stimulated with LPS (25 µg/mL) to induce NFκB gene expression. After 4 h, the medium was removed, and the cells were transfected with hNPs containing 20 nM siNFκB or non-coding siNC for 72 h at 37 °C in a 5% CO_2 humidified atmosphere. siRNA/lipofectamine complexes were used as positive controls. After transfection, cells were lysed using RIPA Buffer with a 1× cocktail of protease/phosphatase inhibitors (Roche, Basel, Switzerland). The samples were analyzed for the expression of NFκB p65 subunit (NFκB p65 mouse monoclonal antibody, 1:500, sc-1008, Santa Cruz Biotechnology) by Western blot analysis, following a published protocol(255). Actin (actin goat polyclonal IgG, 1:500, Santa Cruz Biotechnology) was used as housekeeping protein. Mouse IgG binding protein conjugated to horseradish peroxidase (mIgG BP-HRP) and donkey anti-goat IgG-HRP were used as secondary antibodies (1:5000, Santa Cruz Biotechnology). Membranes were treated with SuperSignal West Pico PLUS chemiluminescent substrate (Thermo Fisher Scientific) immediately before analysis at the ChemiDoc MP imaging system (Bio Rad). Cell studies were performed in triplicate, and results are expressed as mean value ± SD, n = 3. One-way ANOVA was performed to assess statistical significance of differences between mean values (**$p < 0.01$, ***$p < 0.005$).

2.8 *In vitro* cytotoxicity in lung cells

2.8.1 Cell viability

The effect of siRNA-loaded hNPs on cell viability was tested using the 3-(4,5-dimethylthiazol-2-yl)-2,5-diphenyltetrazolium bromide (MTT) colorimetric assay on the 16HBE14o- cell line. 16HBE14o- cells were seeded at a density of 5000 cells per well in 100 µL of medium in 96-well plates and incubated overnight at 37°C and 5% CO_2. Each formulation was diluted to varying concentrations (0.5, 1 and 2 mg hNPs/mL) and added to the cells. Plates were incubated for 24 h, 48 h and 72 h respectively at 37°C and 5% CO_2. Once the incubation time had been completed, medium was removed and 100 µL of a sterile 0.5 mg/mL 3-(4,5-dimethylthiazol-2-yl)-2,5-diphenyltetrazolium bromide (MTT) solution was added to the cells and incubated for 3 h at 37°C and 5% CO_2. Medium was then removed and each well was washed with 100 µL sterile PBS and 200 µL of acidic isopropanol (0,04 N HCl in absolute isopropanol) was added to each well and

plates were placed on an orbital shaker for 15 minutes. Absorbance was measured at 570 nm using a microplate reader (FLUOstar Omega, BMG Labtech). Control groups included cells treated with empty nanoparticles. The percentage of viable cells was calculated by the ratio of absorbance of treated cells compared with untreated cells. Results are given as mean values of triplicates ± SEM.

2.8.2 LDH release

The effect of siRNA-loaded hNPs on membrane integrity was assessed by measuring the release of lactate dehydrogenase (LDH) into the extracellular medium. 16HBE14o- cells were seeded in 96-well-plates at a density of 5000 cells per well 24 h before their treatment with hNPs suspensions at different concentrations (0.5, 1 and 2 mg/mL). Plates were incubated for 24 h, 48 h and 72 h respectively at 37°C and 5% CO_2. The experiment was performed using the CytoTox96® Non-Radioactive Cytotoxicity Assay kit following the manufacturer's instructions. Once the incubation time had been completed, 50 µL of each supernatant was transferred into a fresh 96-well-plate and 50 µL of a mixture of substrate mix and assay buffer were added into hNPs containing medium and incubated for 30 min at room temperature. Afterwards, 50 µL of stop solution was added. Lactate dehydrogenase (LDH) release was determined by measuring wavelength absorbance at 490 nm in a FLUOstar OMEGA microplate reader (BMG Labtech). The results were evaluated by comparing the LDH release of transfected cells to the cells treated with Triton-X lysis solution as positive control (100%). Results are given as mean values of triplicates ± SEM.

2.8.3 Evaluation of hNPs pro-inflammatory effect

The pro-inflammatory effect of hNPs was tested using an ELISA kit for the quantification of TNF-α release in the extracellular medium. Briefly, 16HBE14o- cells were seeded in a 96-well-plate at a density of 5000 cells per well 24 h before they were treated with hNPs suspensions at different concentrations (0.5, 1 and 2 mg/mL). Plates were incubated for 24 h at 37°C and 5% CO_2. The experiment was performed according to the instructions reported on the Human TNF-α ELISA MAX Deluxe Set kits (Biolegend, San Diego, CA, USA). Absorbance was read within 15 minutes at 450 nm using a FLUOstar Omega microplate reader (BMG Labtech). Results are given as mean values of triplicates ± SEM.

2.9 hNPs uptake in mucus-covered Calu-3 cells at the air-liquid interface

Calu-3 cells were seeded in a clear polyester cell culture insert (growth area 1.12 cm^2, pore size 0.4 µm) on Transwell® permeable supports. Per sample, 500.000 cells were seeded in 500 µL of medium in the apical chamber, while 1.5 mL of the medium was added to the basolateral chamber. After 72 h, the medium in the upper and basolateral

chamber was removed and replaced by fresh Pneumacult ALI medium (Stemcell Technologies GmbH, Germany) in the basolateral chamber to air-lift the culture. Once TEER values ≥300 $\Omega \cdot cm^2$ were reached and a stable polarized epithelial layer was formed, cell layers were used for cell uptake experiments and mucus transport studies. For cell uptake experiments, Calu-3 monolayers were incubated with 500 µL of PEI/siFluo_DPPC or PEI/siFluo_DSPE-PEG resuspended in medium corresponding to a 20 nM siRNA final concentration (10 pmol siFluo per well). After 24 h, monolayers were washed, cells were detached from the inserts and the dispersion was analyzed by flow cytometry on an Attune NxT flow cytometer (Thermo Fisher Scientific) with 638 nm excitation and a 670/14 nm emission filter. All cells were gated according to morphology based on forward/sideward scattering, and 10.000 events were evaluated per sample to determine the median fluorescence intensity (MFI) and siFLuo uptake per cell. Controls consisted of cells transfected with free siFluo and lipofectamine/siFluo complexes as negative and positive controls, respectively. For transport experiments across the mucus layer, differentiated mucus-covered Calu-3 cells were exposed for 24 h to PEI/ siFluo_DPPC or PEI/siFluo_DSPE-PEG amounts corresponding to 10 pmol siFluo per well. Monolayers were then washed with PBS, and the mucus layer was stained by incubation with AlexaFluor488-labelled wheat germ agglutinin (10 µg/mL) (Invitrogen, Thermo Fisher Scientific, USA) for 10 min at 37 °C. After washing with PBS, the membranes of the Transwell® inserts were cut, mounted on microscope slides, covered with coverslips, and immediately analyzed by confocal laser scanning microscopy (CLSM) (SP8 inverted scanning confocal microscope, Leica Camera, Wetzlar, Germany). Z-stack pictures were taken, and optical sections were processed to create a 3D view, which allows observing the diffusion of the hNPs through the mucus and their cellular internalization.

3. Results and discussion

3.1 Characterization of hNPs

hNPs were successfully prepared by an emulsion/solvent diffusion technique. hNPs consisted of a polymeric core of PLGA and a surface corona of either DPPC or DPSE-PEG, each of them formulated with or without the pre-complexation of siRNA with PEI, a cationic polymer that can efficiently encapsulate the negatively charged siRNA, for a total of four different formulations being investigated. hNPs were investigated first in terms of size and PDI by dynamic light scattering and of zeta potential by Laser Doppler Anemometry. As it can be observed in Table 1, formulation conditions did not significantly

affect hNPs' properties. All formulations showed hydrodynamic diameters below 180 nm, low PDI and negative zeta potential, independently of the lipid shell type and of the presence of PEI. Considering that hNPs were developed for direct administration to the lungs, the obtained parameters are suitable for pulmonary administration. Sizes below 200 nm should in fact assure internalization of the formulation within the lung epithelium while avoiding macrophage clearance (131). Furthermore, the negative surface charge should help to overcome the mucus layer found in the lung, particularly in disease states as found in cystic fibrosis (107). The presence of PEI improved siRNA encapsulation inside hNPs, with a 30% increase for DPPC-containing hNPs (256).

Formulation	D_H (nm ± SD)	PI (mean ± SD)	ζ potential (mV ± SD)	Actual loading (nmol/100mg)	Entrapment Efficiency (%)
siNFκB_DPPC	177.6 ± 9.2	0.193 ± 0.039	-28.7 ± 1.6	0.599 ± 0.004	60 ±1
PEI-siNFκB_DPPC	161.3 ± 3.8	0.170 ± 0.042	-23.3 ± 0.7	0.914 ± 0.038	91 ±4
siNFκB_DSPE-PEG	159.1 ± 5.1	0.062 ± 0.017	-28.6 ± 1.7	0.796 ± 0.022	80 ±4
PEI-siNFκB_ DSPE-PEG	165.5 ± 14.1	0.105 ± 0.069	-28.9 ± 6.9	0.894 ± 0.064	89 ±4

Table 1. hNPs hydrodynamic diameter, polydispersity index, zeta potential and actual loading.

3.2 In vitro cellular uptake of hNPs

To test the ability of hNPs to deliver siRNA to cells, a cellular uptake study by flow cytometry was performed using a lung epithelial cell line. The final goal of the formulation is in fact to deliver an siRNA against the inflammatory mediator NFkB and downregulate its expression in lung epithelial cells. For uptake studies, hNPs were loaded with an AlexaFluor647-labelled siRNA. The experiment was performed at different siRNA concentrations and at two different time points, after 5 h and 24 h of incubation, respectively. As it can be observed in Figure 1(A-B), no significant uptake was observed after 5 h of incubation. Nonetheless, after 24 h significant uptake was observed for both PEI-containing formulations (Figure 1(C-D)). This can be explained by the fact that siRNA is encapsulated in the PLGA matrix and therefore requires longer time to reach the cells. Also, healthy epithelial cells retain slower endocytosis metabolism in comparison to other cell lines, such as cancer cells, which generally show faster uptake kinetics (257). Notably, in this experiment only PEI-containing formulations efficiently

delivered siRNA to the cells, while almost no siRNA was detected for samples treated with hNPs without PEI, independently of the lipid present in the outer layer. This can be explained by the cationic nature of PEI, which can in fact encapsulate and deliver siRNA very efficiently (258). To confirm the delivery of siRNA to the cells, the experiment was repeated by incubating cells either at 4 °C or 37 °C for 24 h to discriminate between internalized fluorescent siRNA and siRNA attached to the cell membrane. Here, we confirmed that PEI-containing formulations efficiently delivered siRNA into the cells (Figure 1E).

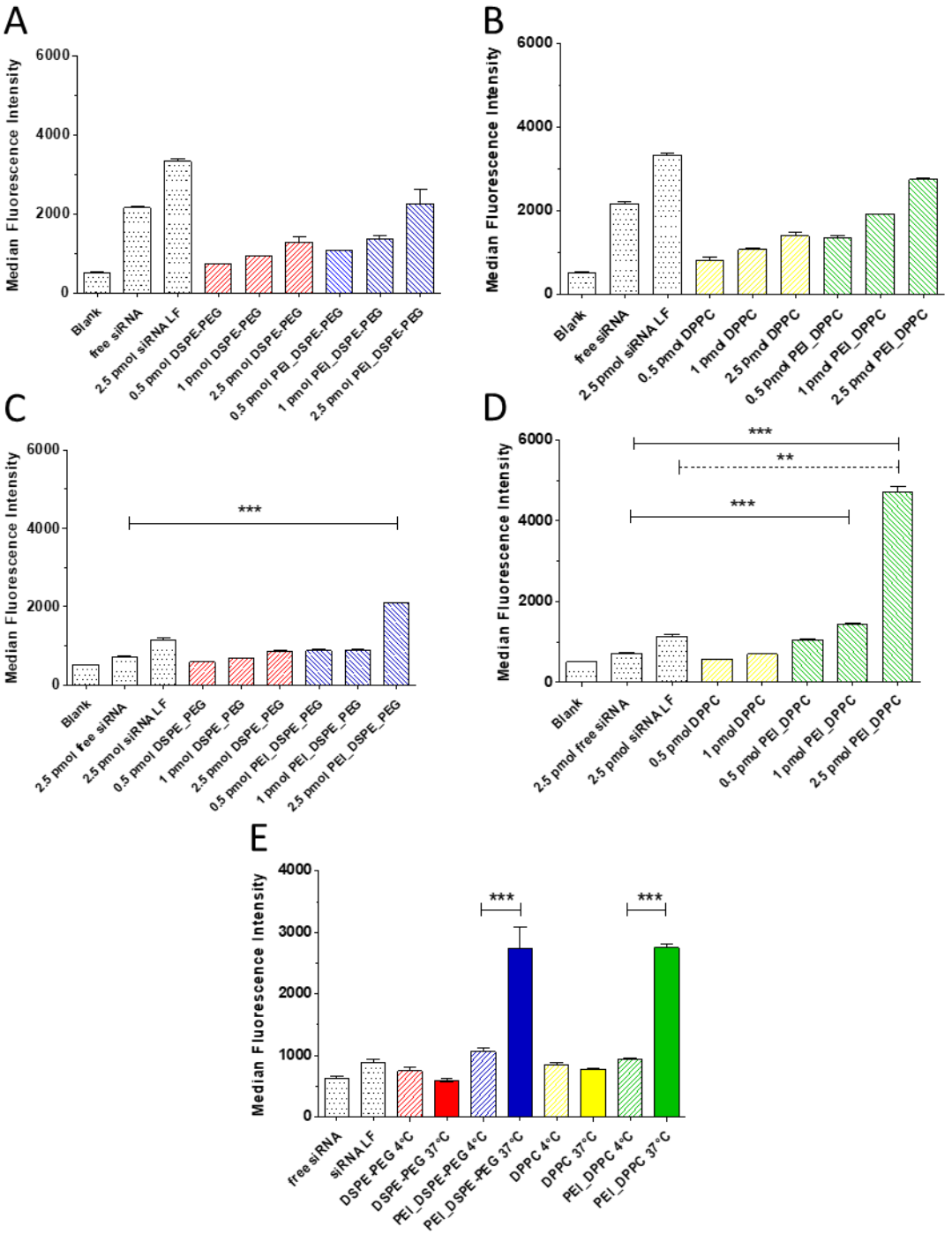

Figure 16. Cellular uptake in 16HBE14o- cells after transfection for 5 h (A-B) and 24 h (C-D) with AF647-siRNA-loaded hNPs. Positive controls consisted of siRNA/lipofectamine lipoplexes. Free siRNA was used as negative control. € Cellular uptake in 16HBE14o- cells following transfection at 4°C and 37°C for 24 h with AF647-siRNA-loaded hNPs. Results are expressed as mean values ± SEM. ***p<0.005.

To further validate cellular internalization of siRNA-loaded hNPs following transfection, microscopy pictures were acquired from cells treated with hNPs following staining of the nuclei (DAPI, shown in blue) and of the lysosomes (Lysotracker™ green, shown in green). As it can be observed in Figure 2, formulations without PEI resulted in insignificant presence of siRNA inside the cells. On the other hand, the ones including PEI, displayed a consistent amount or red dots corresponding to AF647-siRNA, partially colocalizing with lysosomes. This study confirmed hNPs as a promising delivery system for siRNA to the lungs as well as PEI as a key element of the formulation to achieve successful delivery of siRNA to the cells.

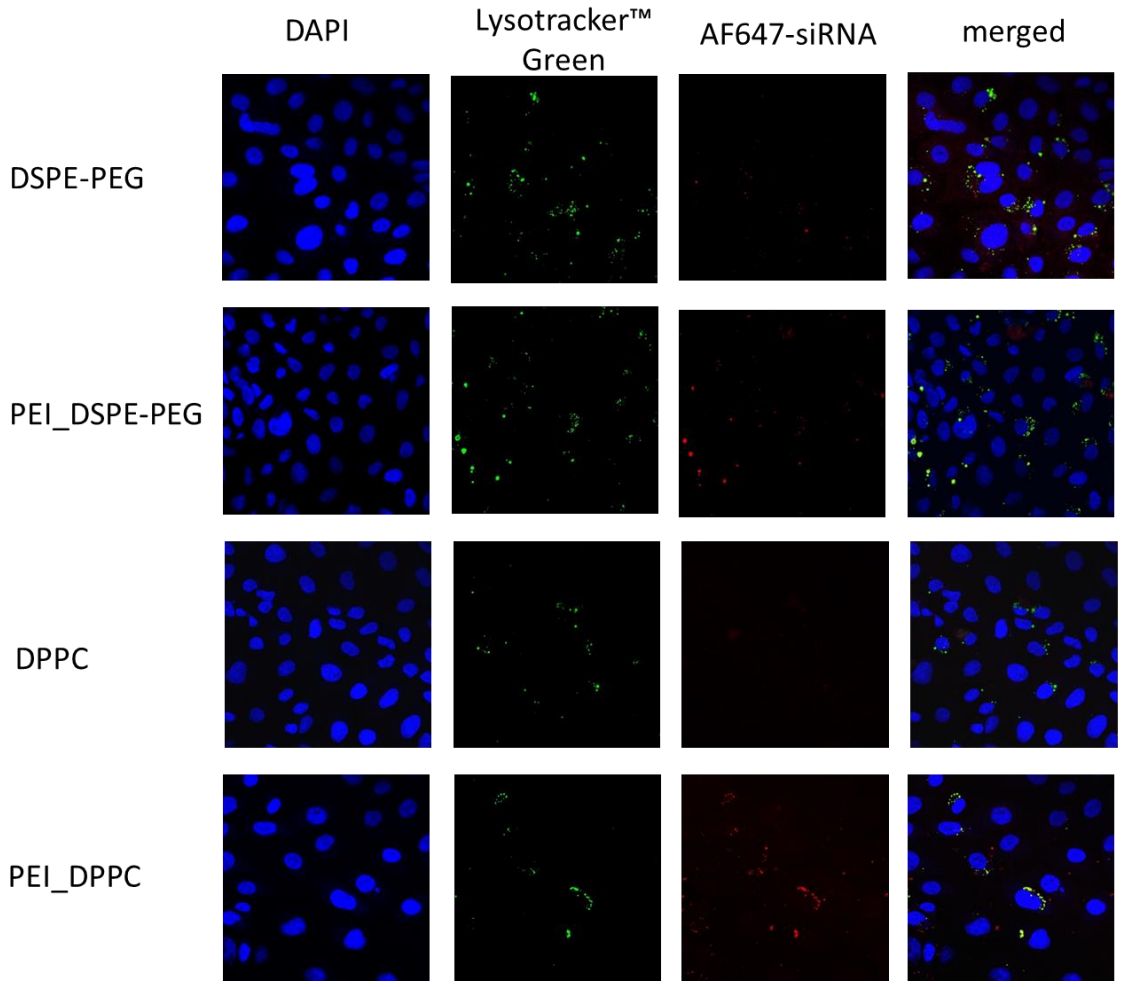

Figure 17. Confocal microscopy images of 16HBE14o- cells after 24 h incubation with AF647-siRNA-loaded hNPs. Red color corresponds to AF647-siRNA, green color to Lysotracker™ green staining and blue color to DAPI staining of nuclei.

3.3 In vitro gene silencing activity

The gene silencing effect of siRNA-loaded hNPs against NFκB was tested on the protein level by western blot analysis on LPS-stimulated 16HBE14o- cells. Cells were pre-stimulated with LPS from *E. coli* to induce an increase in NFκB expression and better reproduce the inflamed state of the epithelium. After identifying 20 nM siNFκB as the concentration necessary to inhibit NFκB expression (Figure 3(A-B)), we performed the *in vitro* inhibitory experiments at the corresponding concentration of siNFκB-loaded hNPs. Considering that only PEI-containing formulations showed cellular uptake of siRNA, we considered only these two formulations for silencing experiments. As it can be observed in Figure 3(C-D), both formulations achieved a significant silencing effect in comparison to samples treated with a non-targeting sequence. Furthermore, the downregulation activity was comparable to the one achieved by the commercially available reagent lipofectamine. In line with the cellular uptake experiments, DPPC-coated hNPs displayed a slightly better activity than DPSE-PEG-coated hNPs, probably due to the faster release kinetic of the formulation (34).

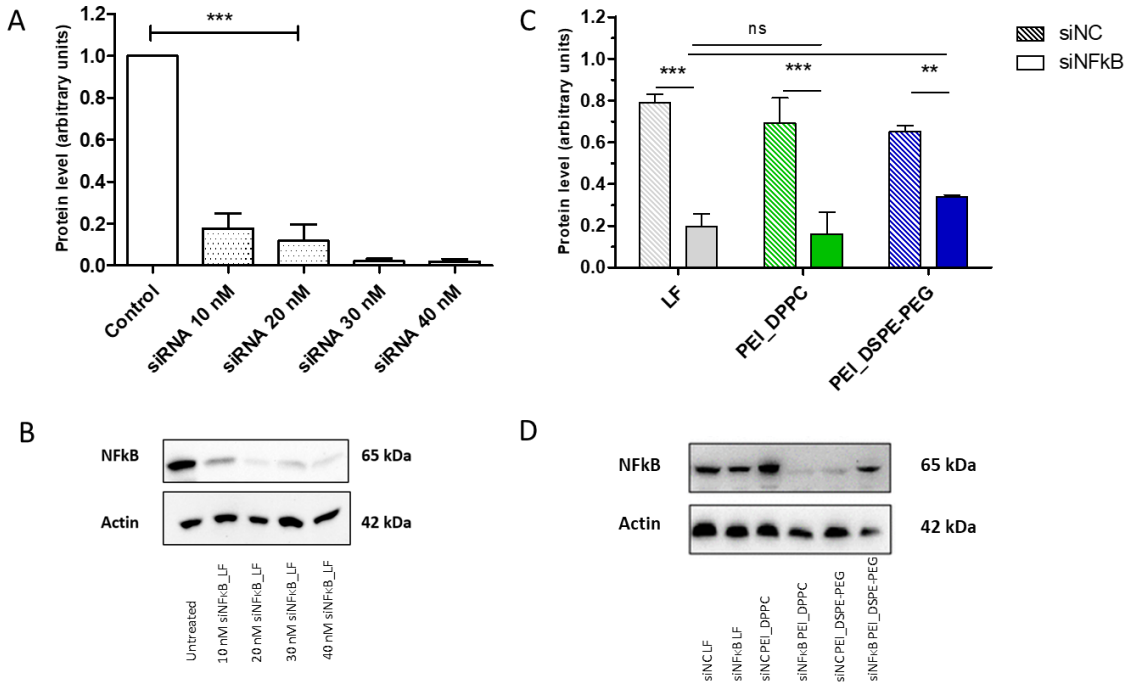

Figure 3. Western blot analysis of protein extracts from 16HBE14o- cells. Before transfection, cells were stimulated with LPS (25 µg/ml) to induce NFκB expression. Cells were treated with different amounts of siNFκB/lipofectamine to identify the best siRNA working concentration (A-B). Afterwards, transfection was performed with 20 nM of siNFκB loaded hNPs as well as siNC-loaded hNPs as negative control for 72 h. Positive controls consisted of cells treated with siNFκB/lipofectamine lipoplexes(C-D). Results are reported as mean ± SEM. ***p<0.005.

3.4 Nanoparticle permeation in mucus covered Calu-3 cells grown at the air-liquid interface

Cystic fibrosis is a debilitating disease characterized by mucus hypersecretion and reduced mucociliary clearance in the lungs. Therefore, the delivery system needs to overcome a mucus barrier before to the underlying epithelium where the cargo should be released. Calu-3 cells cultivated at the air-liquid interface are a widely used model for studying delivery systems for cystic fibrosis due to the high transepithelial resistance, mucus secretion, and mutated CFTR expression on the apical side (259). Furthermore, they can form a pseudostratified epithelium that resembles the *in vivo* structure and secretory pattern of the lungs (260). Calu-3 monolayers were transfected with hNPs loaded with fluorescently labelled siRNA and stained with wheat germ agglutinin to visualize the mucus layer by confocal scanning laser microscopy (Figure 4(A-D)). Thus, it was possible to determine which formulation penetrated the mucus layer. In line with previous results, PEI_DPPC hNPs displayed the best performance. The results were confirmed by quantifying the cellular uptake in Calu-3 cells by flow cytometry (Figure 4E). Also in this case, PEI_DPPC hNPs showed the best activity, outperforming even siRNA/lipofectamine lipoplexes used as positive control. hNPs were indeed developed to exert their action in harsh conditions such as in a mucus-rich environment. The lipid layer, together with the negative charge of the formulation and the small sizes of the hNPs, should help in overcoming this major barrier that hampers the delivery of the cargo to the epithelium. The better activity demonstrated by DPPC-coated hNPs may be explained by the fact that the presence of PEG in DSPE-PEG is known to limit the uptake by cells although being advantageous for mucus penetration (261).

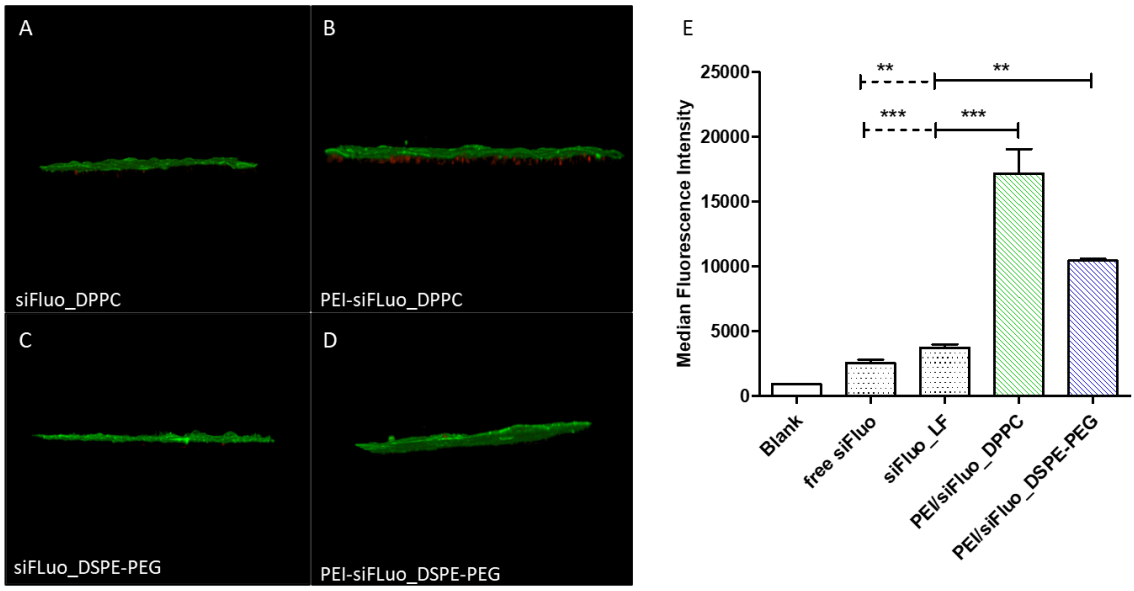

Figure 4. Evaluation of AF647-siRNA-loaded hNPs delivery to Calu-3 cells grown at the air-liquid interface. (A-D) 3D view created from confocal laser scanning microscopy sections of confluent Calu-3 cells exposed to siFLuo_DPPC (A), PEI-siFluo_DPPC (B), siFLUO_DSPE-PEG (C), PEI-siFLUO_DSPE-PEG (D) hNPs for 24 h and stained with AF488-labeleed wheat germ agglutinin. Red dots correspond to AF647-siRNA, while green color shows the stained mucus covering the cells layer. (E) Cellular uptake in Calu3 cells grown at ALI following 24 h with AF647-siRNA-loaded hNPs. siRNA/lipofectamine lipoplexes were used as positive control and free siRNA as negative control. Results are reported as mean values ± SEM. ***p<0.005.

3.5 Safety of the formulation

To estimate the compatibility of the different formulations with epithelial cells, hNPs were incubated with 16HBE14o- cells at different concentrations and for different incubation times. The viability of the cells was evaluated by means of the MTT assay, a colorimetric assay that indicates the cell viability by measuring the metabolic activity of the cells (Figure 5). To include all the different factors that could have an impact on cell viability, all four formulations were tested at 3 different concentrations and 3 different time points (24, 48 and 72 h). Furthermore, each formulation was tested with and without the encapsulation of siRNA. Trehalose was also included as control since it was used as cryoprotectant during the lyophilization step. Up to 48 h, all formulations tested showed an overall safe profile, with viability values above 70%. After 72 h, slightly lower values were detected, probably due to the longer time in which cells were exposed to trehalose. Interestingly, samples treated with 2 mg/ml of DPPC hNPs showed extremely high values of cell viability. Here, high concentrations and long exposure times of hNPs together with trehalose could have interfered with the metabolic activity of the cells and increased the amount of formazan produced (262).

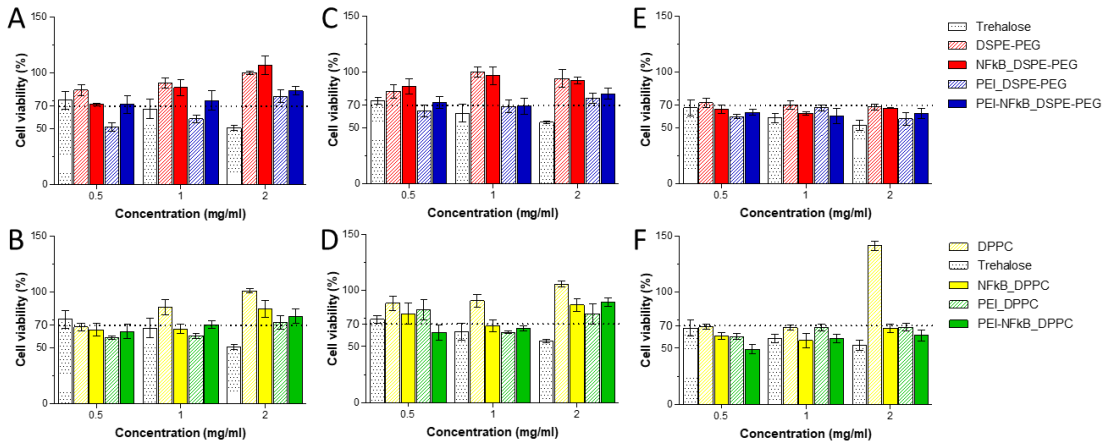

Figure 5. Evaluation of cell viability by MTT assay in 16HBE14o- cells following incubation with hNPs for 24 h (A-B), 48 h (C-D) and 72 h (E-F). Results are expressed as mean ± SEM.

To further investigate the effect of the different formulations on cell membrane integrity, an LDH assay was performed at the same conditions established for the MTT assay (Figure 6). The LDH assay detects the release of lactate dehydrogenase in cells supernatant as a consequence of loss of membrane integrity following incubation with the formulations. The results were compared to a 100% LDH release as positive control. No cytotoxicity was detected for any of the formulations tested, with values never exceeding 20% of LDH release even after 72 h of incubation. Taken together, these results confirm the *in vitro* safety of the formulation.

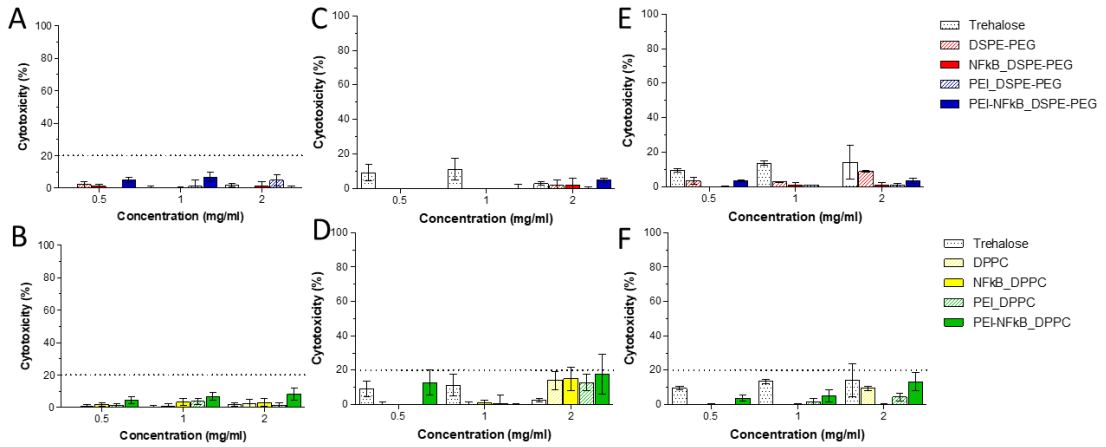

Figure 6. Evaluation of cytotoxicity in 16HBE14o- cells by LDH assay following incubation with hNPs after 24 h (A-B), 48 h (C-D) and 72 h (E-F). Cells treated with lysis buffer correspond to 100% LDH release. Results are expressed as mean ± SD.

Finally, the pro-inflammatory effect of hNPs was evaluated by measuring the release of TNF-α in cell culture supernatant 24 h after incubation of hNPs at different concentrations by an ELISA assay (Figure 7). In this experiment, generally low TNF-α release was

detected, with a significant release in comparison to untreated cells only for DPPC and PEI-NFκB_DPPC at the highest concentration tested. Nonetheless, taking all the results from the safety studies together, none of the formulations tested negatively affected cell viability, and the presence of PEI nor the different lipids tested were found to be the cause of increased cytotoxicity.

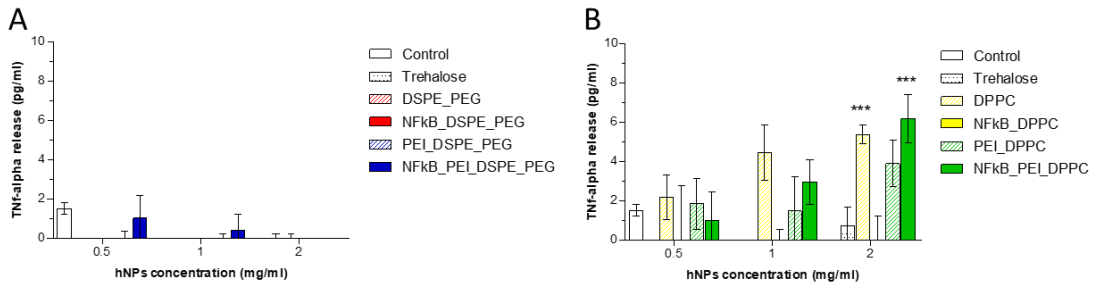

Figure 7. Pro-inflammatory effect of hNPs on 16HBE14o- cells following incubation with hNPs for 24 h measured by ELISA technique. Values are given in pg/ml as mean ± SEM. ***p<0.005.

4. Conclusion

The development of nanocarriers able to efficiently deliver siRNA to the lungs remains one of the main challenges for the RNA delivery field. Despite the unquestionable advantages offered by the pulmonary route of administration, many hurdles need to be overcome, with the mucus layer representing the major barrier that limits the delivery to the lung epithelium. Here, non-PEGylated and PEGylated hNPs were evaluated as a delivery system for siRNA targeting NFκB, one of the main factors involved in the inflammatory cascade. Due to the presence of an inert lipid shell, hNPs are presented as a possible strategy to tackle the mucus barrier present in the lung, particularly for cystic fibrosis. hNPs displayed optimal parameters for pulmonary delivery and a safe *in vitro* profile. Only formulations containing PEI efficiently delivered siRNA to lung epithelial cells and mediated NFκB protein downregulation. Furthermore, DPPC-coated hNPs showed better activity than DSPE-PEG hNPs. This was confirmed also in a 3D model of the lung, where DPPC-coated hNPs better permeated through the mucus layer and delivered siRNA to the underlying cells. The results confirm the potential of hNPs as carriers for pulmonary delivery of siRNA against NFκB for local treatment of inflammation in cystic fibrosis and encourage towards *in vivo* investigation of their therapeutic activity.

Chapter IX - Air-liquid interface cultures of the healthy and diseased human respiratory tract: promises, challenges and future directions

Domizia Baldassi[1†], Bettina Gabold[†] and Olivia Merkel[1*]

[1]Pharmaceutical Technology and Biopharmacy, LMU Munich

[†]These authors contributed equally to this work

The following chapter was published in Advanced NanoBiomed Research.

Baldassi D, Gabold B, Merkel O. Air-liquid interface cultures of the healthy and diseased human respiratory tract: promises, challenges and future directions. Adv Nanobiomed Res. 2021 May 6;1(6):2000111. doi: 10.1002/anbr.202000111. PMID: 34345878; PMCID: PMC7611446.

Graphical Abstract

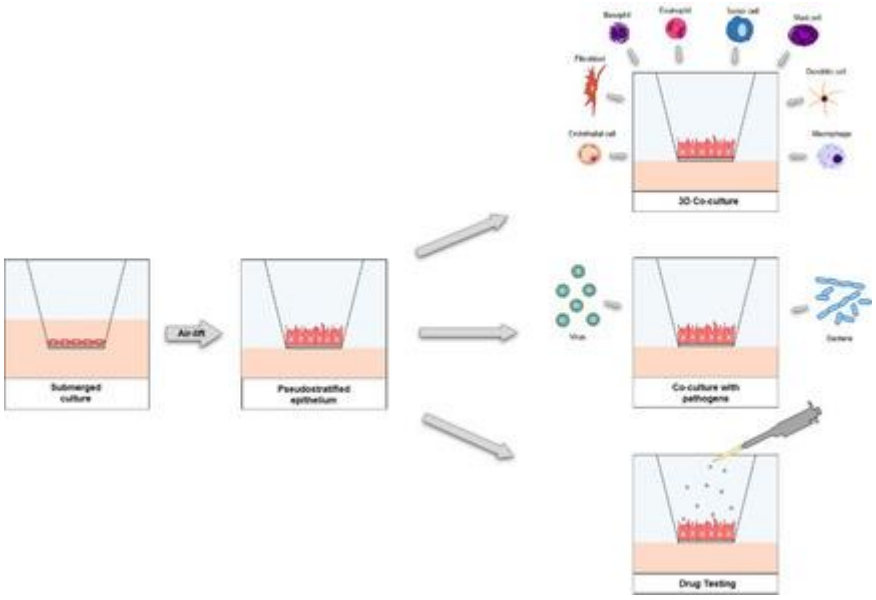

Abstract

Air-liquid interface (ALI) culture models currently represent a valid tool to recreate the typical aspects of the respiratory tract *in vitro* in both healthy and diseased state. They can help reducing the number of animal experiments, therefore, supporting the 3R principle. This review discusses ALI cultures and co-cultures derived from immortalized as well as primary cells, which are used to study the most common disorders of the respiratory tract, in terms of both pathophysiology and drug screening. The article displays ALI models used to simulate inflammatory conditions of the lung such as asthma and chronic obstructive pulmonary disease (COPD), lung cancer, cystic fibrosis and also viral infections, including a focus on ALI cultures described in literature studying respiratory viruses such as SARS-CoV-2 causing a global Covid-19 pandemic at the time of writing this review. Additionally, commercially available models of ALI cultures are presented. Ultimately, this review aims at giving an overview of ALI models currently available and critically discussing them in the context of the most common diseases of the respiratory tract.

KEYWORDS: air-liquid interface, lung, 3D co-culture models, pulmonary administration, respiratory tract, SARS CoV-2

1. Introduction

Chronic respiratory diseases such as asthma, cystic fibrosis and COPD are leading causes of death and morbidity worldwide.(263) Besides, lung cancer and respiratory infections, including the global COVID-19 pandemic in the year 2020, are frequent causes of mortality. Therefore, more efficient treatment strategies are urgently sought for, particularly for diseases causing irreversible tissue damage and loss of function in the lung. The complex cellular composition of the respiratory tract and its location at the air-liquid interface hamper an accurate mimicking of the physiological situation. Many different models have been used in the past ranging from *in vivo* animal experiments to *in vitro* models using lung cells.(264) In this field of research, animal models are routinely used since all *in vitro* models lack one or another aspect of lung anatomy or physiology, hampering validation of research results. Consequently, animal models are widely regarded as the only reliable option available. However, the anatomical differences between rodents and humans emphasize a significant lack of functional homology regarding various biomolecules, drug deposition rates and localization of particulate drug delivery systems.(265) For example, the alveolar and the airway architecture show fundamental differences.(41,266) Mice only have 6-8 levels of branching airways while humans have up to 20 or more. Furthermore, mice do not have typical respiratory

bronchioles with characteristic interruptions on their walls projecting into the alveoli. They only have short terminal bronchioles opening directly into several alveolar ductules.(267) Therefore, interpretation of data derived from rodent models cannot easily be translated into human context. Furthermore, the strong support to reduce, refine and replace the use of animals (3R) in experimental testing is constantly increasing.(268) These key facts have driven the development of alternative *in vitro* methods aimed at mimicking the respiratory tract, the most promising being the ALI approaches derived from the domain of inhalation toxicology.(269) The defining feature of ALI culture is that the basal surface of cells is in contact with liquid culture medium while the apical surface is exposed to air. This configuration allows cell differentiation towards a mucociliary phenotype, simulating *in vivo* conditions better than it is possible in conventional cell culture. ALI systems have the potential to provide relevant data of the respiratory tract since they can be constructed from human-derived cells and are therefore capable to model scenarios close to what might occur *in vivo*.(270) Another advantage is that drugs administered as aerosols and particles are not altered by contact with cell culture medium before they impact on the epithelium, as would happen in a submerged model. Furthermore, dosing can be exactly controlled in contrast to *in vivo* administration, giving ALI the potential to reduce the number of experimental animals required, due to a better optimization of parameters *in vitro*. Besides, these lung models cannot only be used to help understand pathophysiological processes and perform drug screening. They also support the mechanistic understanding of the interaction of xenobiotics at the cellular level in healthy and diseased tissue, complementing findings gained from *in vivo* studies. However, for many applications, ALI mono-culture platforms fail to represent the cellular arrangement thoroughly, e.g. by lacking direct cell-cell interactions. Hence, co-culture models constituted of more than one cell type are widely being developed.(271) For many applications, they are beneficial over ordinary ALI culture models because they provide more *in-vivo*-like morphology, function, and intercellular interactions enabling greater similarity to physiological conditions.

This review focuses on the different types of ALI cell culture models resembling the human respiratory tract including the commonly used cell types and applications. Hereby, importance is given to models mimicking not only the healthy but also the diseased states of the lung, e.g., in patients suffering from asthma, cystic fibrosis or COPD. Especially advanced systems using multiple cell types or even culturing cells with viruses or bacteria for pathogen-host interaction studies will be presented in detail.

2. Anatomical and cellular structure of the respiratory tract

The respiratory tract is part of the respiratory system that also includes parts of the central nervous system, the chest wall and the pulmonary circulation.(12) One can picture the respiratory tract as an upside-down tree with a complex network of bifurcations getting thinner and thinner with every branching step. Generally the respiratory tract can be divided into three main regions: (a) the extrathoracic (ET) region which includes the oral and the nasal cavity, the pharynx and the larynx to the trachea entrance, (b) the tracheobronchial (TB) or conducting region ranging from the trachea to the terminal bronchioles, and (c) the alveolar (Al) region, where gas exchange takes place.(11) Within the airways, several structural and cellular mechanisms help to protect the organ against harmful materials and potential pathogens. First, a continuous layer of epithelial cells lines the entire respiratory tree. These cells form specific tight junction complexes keeping the structural integrity of the epithelial layer, and they play a vital role in maintaining the normal functions of the respiratory system. Furthermore, the surfactant film coating the lower airways and the mucociliary escalator of the upper airways join forces to transport unwanted matter up the airways, where it can subsequently be swallowed.(272) Also, dendritic cells reside inside and underneath the airway epithelium, and other innate cell populations such as macrophages are constantly present in airways and alveoli to phagocytose foreign material. (273,274)

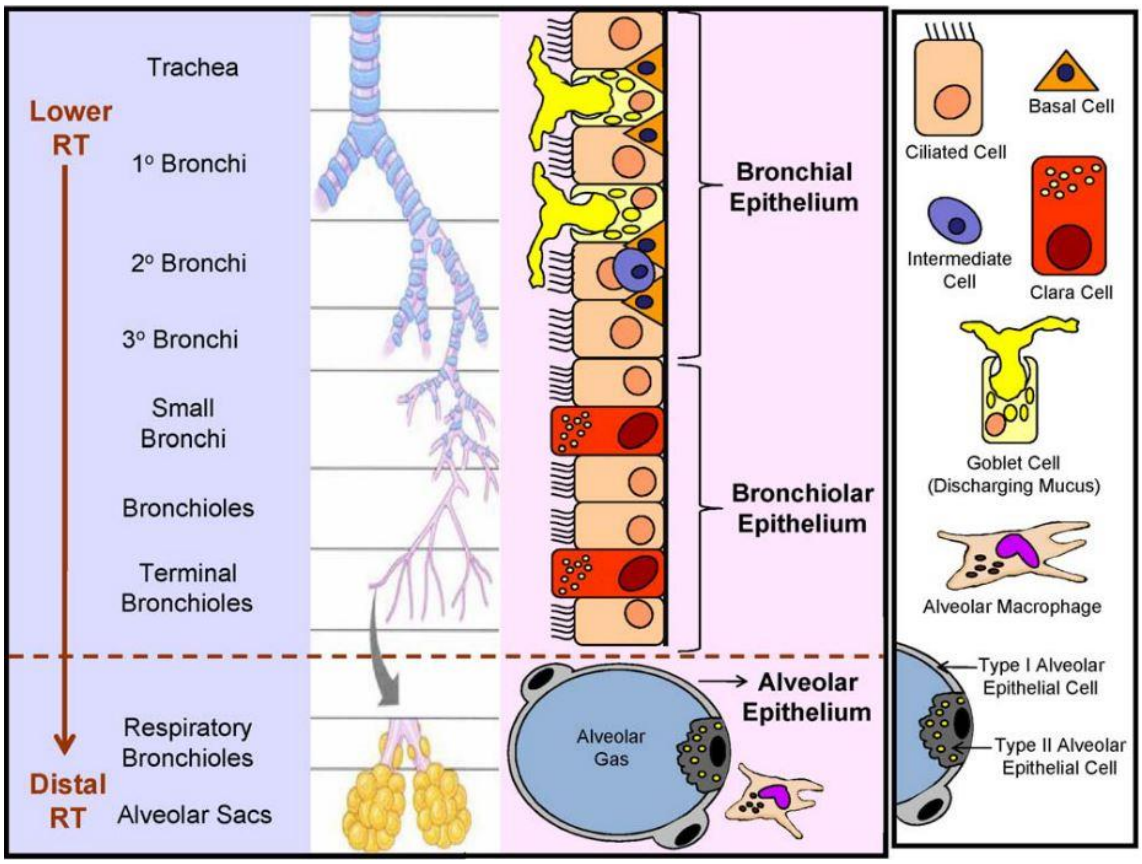

Figure 1. Principle cell types found alongside the human respiratory tract varying in functions and defense mechanisms. Reproduced with permission.(275) Copyright 2010, Elsevier**.**

Cell types present in the different regions alter while moving from the conducting to the respiratory zone of the airways, accommodating the respective specific functions and defence mechanisms (Figure). The ET epithelium constitutes predominantly of ciliated columnar cells and goblet cells, whereas the TB region is lined by a pseudostratified, columnar epithelium consisting of goblet cells, basal cells and ciliated cells, supporting the mucociliary clearance. The epithelium of the bronchioles is dominated by cuboidal ciliated cells together with secretory Clara cells.(276) Apart from these tissue-specific epithelial cells, many non-epithelial migratory cells can be found such as lymphocytes, leukocytes and mast cells. The AI region further down the respiratory system is constituted of alveolar type I and II pneumocytes forming the alveolar epithelium. Type I pneumocytes account for about 95% of the internal lung surface and are mainly responsible for gas exchange, whereas type II cells fulfill many other functions including regulation of the lung surfactant system, the alveolar fluid content and secretion of antimicrobial and surface-active components. Besides, alveolar cells attach to endothelial cells via their basal membranes to form the gas exchange barrier. Additionally, a resident population of alveolar macrophages removes inhaled debris.

3. Cellular composition of ALI models

In vitro cell culture systems create simplified biological systems that offer controllable, versatile and reproducible setups compared with *in vivo* and *ex vivo* systems. Numerous epithelial cell models have been cultured at the ALI with the aim of mimicking distinct parts of the respiratory tract. Compared to submerged culture, differences in cell morphology, biochemistry and response to tested materials was detected showing a good resemblance to the actual *in vivo* situation. ALI models can be established with primary material or with immortalized cell lines, both offering pros and cons. In general, primary cultures isolated from tissue represent a heterogenous population of several different types of epithelial cells. Primary cells from patient populations suffering from respiratory disorders such as cystic fibrosis,(277) asthma,(278) and COPD(279) have been isolated for research purposes. Moreover, primary epithelial cells were used to study virus-host-interactions.(280) Cells from different sections of the respiratory tract are cultured at ALI and can reproduce many features of the diseased state.(281) Each isolate, however, is unique and impossible to fully reproduce. Moreover, cell number is a limiting factor when isolating from normal human airway tissue.(282) Epithelial immortalized cell lines, as presented in Table 1**Errore. L'origine riferimento non è stata trovata.**, are more homogenous with less phenotypic differences compared to primary cells making them more stable during culturing and hence, relatively easy to work with. This is the reason why immortalized human cell lines are very commonly utilized in ALI cultures of the respiratory tract. However, it is important to emphasize that due to the transformation process and clonality, they can potentially lack important molecules that are usually encountered *in vivo*. In general, primary epithelial cells better represent the native microenvironment and in principle are optimal candidates for mimicking *in vivo* conditions.

For the ET region of the respiratory system, only very few cell lines are suitable. The only immortalized cell line of human origin frequently used in nasal drug delivery research is the RPMI2650 cell line.(283) This epithelial cell line is derived from an anaplastic squamous cell carcinoma of the human nasal septum and shows high stability throughout continued *in vitro* culturing without phenotype alteration exhibiting superior differentiation under ALI conditions.(284,285) RPMI2650 cells grow in sheets of non-ciliated cells instead of polarized monolayers, and transepithelial electrical resistance (TEER) values range from 41-270 $\Omega \cdot cm^2$.(283,286) Due to the lack of suitable immortalized cell lines of normal nasal tissue, many applications of drug delivery research use primary epithelial cells from nasal brushings or from nasal polyps.(287,288)

One of the most widely used human bronchial epithelial cell lines, 16HBE14o-, was

developed by the transformation of normal bronchial epithelial cells. They are used to mimic the TB region and have a cuboidal shape expressing tight junction proteins and develop proper TEER values.(289) While there are conflicting reports whether this cell line is ciliated or not, it has been shown that 16HBE14o- cells express several transport proteins.(290) Furthermore, although bronchial epithelial cells are normally located at an air interface, these cells sometimes fail to polarize under ALI conditions.(291) The exact mechanism or reason for this is currently still unknown but improvements in culture conditions were shown to enable 16HBE14o- cell polarization at ALI, as described for the RPMI 2650 cell line.(83,284) Apart from 16HBE14o-, another cell line derived from healthy human epithelial cells, the BEAS-2B cell line, is also commonly used. It is particularly described in co-culture models to evaluate the influence of epithelial cells on co-cultured immune cells after exposition to tobacco smoke or diesel exhaust.(292,293) However, at the ALI this cell line does not appear to polarize, form tight junctions or produce mucus and only reaches very low TEER values of < 100 Ω cm^2.(294)

Another widely used bronchial cell line is the Calu-3 cell line derived from a bronchial epithelial adenocarcinoma.(295) This cell line shows an excellent polarized monolayer formation at ALI together with high levels of tight junction proteins and mucus production.(105) Depending on the culture conditions, TEER values of Calu3 cells at ALI are usually bigger than 300 Ω cm^2, sometimes even exceeding 1000 Ω cm^2.(294) However, also for this cell line the ability to express cilia appears to be highly inconsistent, which might be related to the number of cell passages.(295–297) Due to high stability, robustness, *in vivo* resemblance and easy culture, the Calu-3 cell line is often described as a suitable model for the respiratory epithelium.(298)

The most frequently used alveolar cell line mimicking the Al region of the respiratory tract is the A549 cell line, which is derived from human pulmonary adenocarcinoma. Many studies suggest that these cells are unable to polarize and functionally deficient in tight junctions, although they seem to express certain tight junction proteins such as Occludin and E-cadherin.(299) Despite these limitations, the A549 cell line contains multilamellar cytoplasmic inclusion bodies, which are typically seen in human alveolar type II cells.(300) The cells additionally release surfactant to reduce surface tension, similarly to what is observed *in vivo*. (301,302) Therefore, A549 cells are still used in ALI co-culture models, mostly in presence of other epithelial cell lines in order to facilitate cell layer polarization but also together with immune cells and endothelial cells to simulate the alveolar barrier in the lung.(303–305) Besides A549, the NCI-H441 human alveolar cell line from lung adenocarcinoma has been used in some studies. This cell line has been described to have characteristics of both bronchiolar Clara cells and alveolar type II cells.(306,307) It can form polarized monolayers with TEER values of around

300 Ω cm^2 and has mainly been employed to study the air-blood barrier in co-cultures with endothelial cells.(308,309)

In general, the regulation mechanisms of airway responses to allergens, pathogens and other antigens are extremely complex, and the different cell types and cytokines present in the airways have a great influence on the microenvironment. Therefore, it is obvious that such a complex system cannot be mimicked by just one cell type, and the reproduction of this microenvironment as a field of research is still progressing. Depending on which part of the respiratory tract and, above all, which disease should be analyzed, there are multiple options for designing a suitable model.

Cell type	Derivation	Phenotype	TEER [Ω·cm^2]	Reference
RPMI 2650	Nasal squamous cell carcinoma	Multilayered, non-ciliated, mucin expression, exhibiting tight junction formation	41-270	(283)(286)
16HBE14o-	Immortalized healthy tissue	Cuboidal monolayer, non-ciliated but microvilli present tight junction formation, transporter protein expression	~ 250	(83)
Calu-3	Adenocarcinoma	Columnar monolayer, mucin expression, tight junction formation, microvilli formation	> 300	(105)(294)(310)
BEAS-2B	Immortalized healthy tissue	Monolayer formation, cytokine secretion, antioxidant expression, no mucin secretion or tight junction formation	< 100	(294)
A549	Alveolar adenocarcinoma	Monolayer formation, membrane bound inclusion, alveolar type II-like, surfactant secretion, no tight junction formation	n.a.	(282)(301)(302)
NCI-H441	Papillary adenocarcinoma	Polarized monolayer formation, alveolar type II-like, Clara cell-like	~ 300	(308)

n.a. = not applicable

Table 1. Phenotypic characteristics of cell lines used in ALI cultures to mimic different parts of the respiratory tract.

4. ALI models in health and disease state

4.1. Respiratory viruses

Acute respiratory diseases account for an estimated 75% of all acute morbidities in developed countries. The majority of these are caused by viruses. For the evaluation of

virus-host interactions and the development of antiviral treatments, specific models capable of high-throughput screening in physiologically relevant conditions are required. In many other fields, animal experiments are used for this purpose but in virology, small animal models are often not suitable. Some animal models are naturally not permissive to human viral infections or need virus adaption, thereby, potentially affecting viral pathogenicity. Often, transgenic expression of human receptors is needed and, in many cases, the clinical course of the disease in humans is not reflected properly. Therefore, it is advantageous to make efforts towards establishing advanced human *in vitro* models for a reliable analysis of virus-host interactions.

Immortalized human cell lines, such as Calu-3, are invaluable tools for the evaluation of virus replication cycles in lung epithelial cells.(311) However, the natural target cells of viruses in the respiratory tract are differentiated cells, whose characteristic features sometimes differ widely from immortalized cells. Hence, experimental infection of continuous cell lines does not address all aspects of the viral pathogenesis. In recent years, models using well-differentiated epithelial cells from airway tissue have been established to assess respiratory virus infections under more clinically relevant terms. The cells are cultured under air-liquid interface conditions forming a monolayered, polarized and differentiated epithelium.(312) This model closely resembles the airway epithelium *in vivo* regarding morphology and function, including mucus production and cilia movement.(313) For emerging respiratory viruses unable to proliferate in a traditional two-dimensional (2D) submerged cell culture due to the lack of expression of several entry factors, ALI models greatly facilitate virus isolation and characterization.(314,315) Ashraf *et al*. developed an ALI model to study the basic biological properties of human rhinovirus-C viruses (HRV–C).(316) This subtype of human rhinoviruses, which is considered the primary cause of the common cold, has been circulating unnoticed due to the failure of culturing under submerged conditions. The group developed a system for growing HRV-C in an ALI culture of differentiated human sinus epithelium characterized by a pseudostratified morphology, cilia and goblet cells producing mucus. Thus, they were not only able to analyze the characteristics of clinical HRV-C but also to compare the biological properties of different subtypes of rhinoviruses in the same cell culture system. Warner *et al*. strengthened the hypothesis that using physiologically relevant cell lines as well as a suitable cell culture model is fundamental. They evaluated the replication and innate immunity of rhinoviruses in highly differentiated human airway epithelial cells cultured under ALI conditions and challenged, with their experiments, older findings obtained from HeLa cells grown under conventional culture conditions.(317) Despite the potential advantages of primary cell-based models as discussed above, there are also some limitations. Ziegler *et al*. studied

the susceptibility to the Epstein-Barr virus using an ALI model with primary bronchial epithelial cells.(318) Thereby they detected significant donor differences. Results from this study indicate that host variables impact susceptibility in the nasopharynx as well as the type of EBV infection (productive or non-productive). In conclusion, studying donor-dependent infection mechanisms as well as treatment responses, but also to improving the robustness and reproducibility of *in vitro* models for interpretable results represents a clinical need. Jonsdottir *et al*. established transgenic primary ALI cultures using lentiviral vectors aiming at allowing for more combinations for virus-host interactions in different cell types and species.(319) They hypothesized that transgenesis would enable the study of viral and/or host factors, relevant for respiratory virus infections. They also expected that studying interactions between the virus and cells engineered for targeted gene knockdown or overexpression would allow the elucidation of specific mechanisms involved in virus-host interactions. This model in fact offers the potential for translation to animal cells so that viral pathogenesis can also be studied in other species in the future.

Apart from testing different virus-host interactions, ALI models can also be utilized for the screening of different therapeutically relevant agents and their effectiveness on virus inactivation.(320) Especially for respiratory coronaviruses (CoV) an immediate unmet clinical need for broad-spectrum antiviral therapies was particularly emphasized by the 2020 COVID-19 pandemic. Originally, the importance of CoVs in the burden of human disease was underestimated and therefore, no vaccine or general therapy exists to treat CoV-induced disease in humans. However, some strains of the mainly zoonotic coronaviruses can enter new host species and spread there rapidly.(321) Both the Middle East respiratory syndrome CoV (MERS-CoV) and the severe acute respiratory syndrome CoV (SARS-CoV) have recently crossed the species barrier, entered the human population and resulted in severe diseases. In 2019, a novel human infecting coronavirus (first provisionally named 2019-nCoV, later SARS-CoV-2) was first identified in Wuhan, in the Hubei province in China, and caused a worldwide pandemic, which is not yet under control by the time this article is written.(322) Scientists were able to rapidly isolate the virus from bronchial lavage fluid of patients suffering from COVID-19, the coronavirus disease caused by SARS-CoV-2. They studied its biological characteristics using ALI models of primary human bronchial epithelial cells.(323,324) Hence, well differentiated ALI cultures represented a valuable and high–throughput tool for rapidly gaining information about infection, replication and pathogenesis of the new virus.(325) The thus obtained knowledge helped scientists and clinicians to decide upon suitable containment measures for the population. At the time of writing this article, two mRNA based vaccines against SARS-CoV-2 are approved in a few countries.(326,327)

However, antiviral treatment options for patients with CoV infections are still very rare. Multiple therapeutic approaches are currently under development including commonly known antivirals, antibodies, interferons, vaccines and more recently also nucleic acid based therapeutics.(328–333) For the evaluation of this broad variety and number of new therapeutic entities, more physiologically relevant *in vitro* models are needed including not only well-differentiated primary cells but also co-cultures formed by more than a single cell type. One approach for a robust, high throughput *in vitro* screening platform is presented by Gard *et al*.(280) The group utilized a human primary airway epithelial cell-based model integrated into a high-throughput microfluidic platform where tissues are cultured at an air-liquid interface (PREDICT96-ALI). This model can be used to study virus infections and could potentially be used for fast efficacy screening of different therapeutics in a clinically relevant manner.

Nonetheless, to this day, only very few co-culture models have been used for studying virus-host interactions and possible therapies. Yoshikawa *et al*. cultured Calu-3 cells at the ALI to study the different functionalities of the apical and the basolateral domains in response to viral infection.(334) After virus inoculation of differentiated Calu-3 cells, the medium from apical and basolateral side was collected and incubated with dendritic cells or pulmonary macrophages in order to assess the potential of epithelial cytokines to modulate intrinsic factors of these cells. They found that both dendritic cells and pulmonary macrophages are capable of relaying and amplifying the early acute inflammatory response initiated by SARS-CoV-infected lung epithelial cells. In another study, a real ALI co-culture model of the human respiratory tract was established by Blom *et al*. using human bronchial epithelial cells (16HBE14o-cell line), human monocyte-derived dendritic cells and macrophage cultures.(335) Apart from establishing a reliable ALI co-culture, they aimed to study the interplay between those three different cell types as well as interactions with biomimetic nanocarriers such as liposomes and virosomes, which show a promising opportunity for vaccines and/or drug delivery systems for antiviral therapeutics. Both studies underline the need for advanced ALI co-culture models in the field of virology, not only with a differentiated epithelial layer but also in combination with other cell types that are present in the human lung tissue. With the implementation of such three-dimensional (3D) *in vitro* models, scientists will be able to gain improved insights into virus-host interactions and to obtain more reliable and

translatable results regarding antiviral therapy, thereby, reducing animal experimentation to a minimum.

4.2 Cystic fibrosis

Cystic fibrosis (CF) represents one of the disorders involving the respiratory tract where ALI culture can help unveil the molecular processes of the disease and the search for novel therapeutic strategies. Cystic fibrosis is the most common autosomal recessive disease in the Caucasian population, involving about 100,000 people worldwide. It is caused by mutations in the cystic fibrosis transmembrane conductance regulator (CFTR) gene, which encodes for a transmembrane protein responsible for the transport of chloride and bicarbonate ions across epithelial cells.(249) Despite being a monogenic disease, about 2,000 mutations have been observed at the CFTR level, resulting in different phenotypes and severity levels. The deletion of a phenylalanine in position 508 (ΔF508) is the most frequently encountered mutation, observed in about 70% of the CF population. The mutations result in a reduction of channel number, function or both, with severe consequences on the functionality of the affected tissues.(3) Although CF is a multi-organ disorder, the lung is the most affected. CFTR loss on the apical side of lung epithelium causes an imbalanced transport of ions and fluids across the cells, leading to unpaired mucociliary clearance, chronic inflammation and recurring bacterial infections. Respiratory failure certainly represents the primary cause of morbidity and mortality.(250)

From the discovery of the CFTR gene in 1989,(336) great progress was made in the understanding and treatment of CF, that resulted in improved life quality and expectancy of the patients. The development of a mouse CFTR-knockout model helped identify many characteristics of CF. However, the CF mouse model lacked the development of spontaneous lung disease, which limited its use and pushed towards the development of alternative *in vivo* models in pigs and ferrets, and *in vitro* models.(259) In the last two decades polarized *in vitro* epithelial cultures have been fundamental for the progresses made in this field, especially for studying the role of CFTR in CF pathogenesis. Air-liquid interface culture systems are an ideal instrument for growing epithelial cells *in vitro*, since they allow the production of a differentiated airway epithelium including the main features found *in vivo*, particularly in terms of cellular differentiation, mucus secretion and barrier function.(337) For this purpose, secondary as well as primary cell lines have been used. Among the immortalized cell lines, models using both CF, CFBE41o- cells, and non-CF cells, mostly 16HBE14o- and Calu-3, can be found. Calu-3 cells, in particular, are widely used due to their high transepithelial resistance, mucus secretion and high expression of CFTR protein (259). Alternatively, CFBE41o- is a CF-immortalized cell line

homozygous for the ΔF508 deletion, therefore simulating the CF epithelium with high accuracy.(338)

Despite the ease of use and accessibility, secondary cell lines are not representative of the great variety of scenarios found in CF epithelia, particularly in terms of CFTR variants. More appropriate patient-specific epithelial cell models need to be adopted. On this basis, primary cell lines are now considered the gold standard in CF research and are used for disease modeling as well as drug screening.(277) Primary human airway epithelial cells can be isolated from biopsy samples, lung explants or cadavers and, after an expansion step, they can be seeded on transwell filters and grown at ALI. This process allows the generation of a pseudostratified epithelium with mucociliary morphology displaying the key physiologic functions of CF cells.(339) Moreover, it is possible to assess CFTR channel conductance through an Ussing chamber or patch clamping.(340) Recently, primary nasal epithelial cells have also been explored for ALI studies. These cells can overcome one of the major drawbacks of primary lung cells, namely the limited accessibility associated to the invasive sampling methods. Nasal epithelial cells are obtained by non-invasive nasal brushing of patients and it was demonstrated that they show a polarization pattern well-correlating with primary lung cells. They share similar growth and structural characteristics and, remarkably, also an analogous CFTR expression.(341,342)

The development of polarized primary CF epithelia played a significant role in the progress achieved by precision medicine in the context of CF. In particular, they strongly supported the development of CFTR modulators.(343) This class of drugs directly modulates the defective CFTR channel. They function either as CFTR potentiators by opening the channel present at the cell surface or as CFTR correctors by increasing the trafficking of the protein to the cell membrane.(344) These therapeutics were a milestone in the treatment of CF, since they exert their action directly on the primary cause of the disease. However, they are not accessible to the entire CF population since they are mutation specific, meaning that they are effective only on specific CFTR mutations. The *in vitro* investigation of these modulators on patient-derived cells helped to discriminate the efficiency of each drug on the different genotypes. The potentiator Ivacaftor, for example, was shown to work on the G551D mutation,(345) while the corrector Lumacaftor worked best on the ΔF508 mutation.(346) A wider study additionally showed the different effects of Lumacaftor on primary cells from patients with different genotypes, demonstrating the great potential of this airway model in the identification of patient-specific treatments.(347) Notably, Pranke *et al*. demonstrated that the efficiency of CFTR modulators could also be evaluated on nasal epithelium by testing the effect of two CFTR correctors, Lumacaftor and Tezacaftor on primary human bronchial and nasal cells. The

results revealed only small response discrepancies in the two cell types, paving the way for using easily accessible nasal epithelial cells as predictors of CFTR modulators' effectiveness.(348)

Apart from small molecule drugs, ALI models can also be exploited to evaluate the ability of macromolecule-based therapies, including siRNA to downregulate a target gene. In the context of CF, one example for a target is the epithelial sodium channel (ENaC), which is generally responsible for the transport of sodium. In CF, this channel is upregulated causing airway liquid depletion and thickened mucus. Manunta *et al*. were able to efficiently down-regulate ENaC expression on primary CF and non-CF cells grown in both submerged and ALI cultures. Interestingly, lower transfection efficiencies were observed in ALI cultures, reinforcing the importance of using advanced culture models to better mimic the *in vivo* situation.(349) This was confirmed by another study evidencing a similar behavior in CF cells cultured at ALI and in an *in vivo* mouse model in terms of dose regimen. In both systems, siRNA mediated a significantly higher ENaC knockdown after three repeated transfections compared to a single administration.(350)

Co-culture models, as already discussed, present a promising opportunity for further alignment between *in vitro* models and the complex *in vivo* situation. The addition of immune cells, in fact, greatly improves the imitation of the airway microenvironment.(337) In a study by d'Angelo *et al.*, a triple co-culture system was established to test the cellular internalization and pro-inflammatory effect of an ENaC-targeted siRNA therapy. This model comprised 16HBE14o- cells, human-blood monocyte-derived macrophages and dendritic cells. Interestingly, in this study the formulation was applied via nebulization through the Vitrocell Cloud system, thus increasing the resemblance to inhalation under *in vivo* conditions.(254)

Moreover, co-culture models have also contributed to shed light on another important aspect of CF, namely bacterial infection of the airways. *Staphylococcus aureus* and *Pseudomonas aeruginosa* are the bacterial strains mainly involved in lung infections of patients with CF. Several studies showed that it is possible to cultivate both *S. aureus* (351,352) and *P. aeruginosa* (353) on the apical side of polarized CF epithelial cells grown at ALI to observe the infection process, biofilm formation and inflammatory responses. In this model, the bacterial infection can therefore be performed under non-submerged conditions, providing a more natural condition for the infection process.(354)

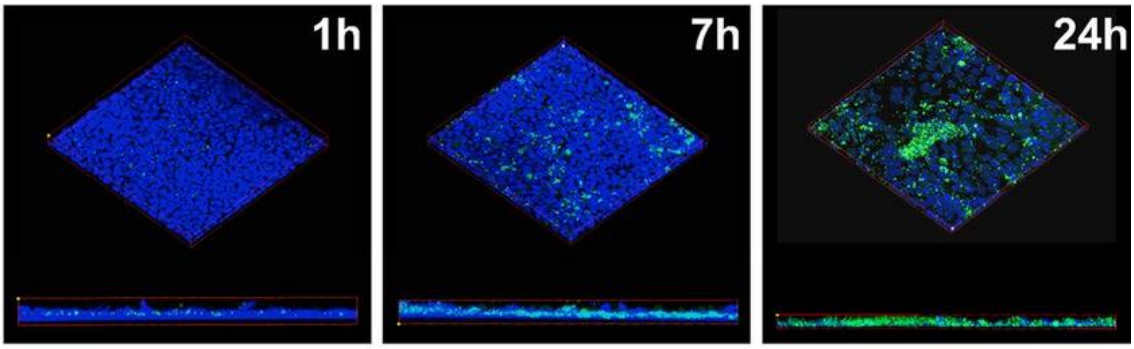

Figure 18. Polarized monolayers infected with GFP-expressing *S. aureus* USA100 (green) and then fixed and stained with Hoechst stain (blue) for confocal imaging at specified time points. (352) Reproduced with permission. Copyright 2018, mSphere.

Using a more sophisticated method, Yonker *et al*. developed a model of inflamed mucosa by co-culturing human airway basal cells and neutrophils. The group observed the migration of the latter in response to inflammation mediated by *P. aeruginosa* growth in the apical chamber of the Transwell® filter.(355) Moreover, co-culture of epithelial and bacterial cells can be a useful tool in testing the efficacy of antimicrobial agents. In case of *P. aeruginosa*, ALI co-cultures were adopted to evaluate the ability of antibiotics,(356) combination therapies (357) and antimicrobial peptides (358) to prevent bacterial infection while examining the consequences on human epithelial cells.

4.3 Asthma

Asthma is a chronic disease affecting more than 300 million people worldwide, associated with a growing burden for healthcare systems of both industrialized and developing countries. The most prominent feature of asthma is a generalized inflammation of the upper airways resulting in recurrent episodes of coughing, wheezing, chest tightness and dyspnoea.(199) In addition to a severe symptomatology, chronic inflammation has also serious consequences on lung structure and functionality, especially in terms of airway hyperresponsiveness, obstruction and remodeling as well as mucus hypersecretion.(5) The mechanisms behind the inflammatory status rely on inappropriate immunological responses to common inhaled allergens, which trigger cytokine secretion by T helper 2 (Th2) immune cells. The sustained release of inflammatory cytokines mediates a perpetuated inflammatory state.(6) In addition to Th2 cells, other immune cells such as eosinophils, mast cells and dendritic cells are involved, defining asthma as an immunological disorder.(359) Indeed, asthma involves several cell types including epithelial cells, which act as first line defense and regulators of immune responses against the environmental factors. Activated epithelial cells secrete cytokines and chemokines that recruit dendritic cells, which are responsible for the

following coordination of the inflammatory cascade. Airway epithelium functionality, however, is altered in the disease state.(360) Apart from the infiltration of immune cells, bronchial biopsies of asthmatic patients point out structural changes of airway epithelium in response to chronic inflammation. In addition to the increased number of mucus-secreting goblet cells and enhanced angiogenesis, they also display a remodeled, damaged epithelium missing tight and adherent junctions with consequent loss of apicobasal polarity.(361) This condition is strictly correlated to the breakdown of the defense mechanisms observed in asthma.

The alterations of the airway epithelium make the development of suitable experimental models essential to comprehend the ongoing immunological and structural modifications and to identify possible therapeutic targets. Mouse models of allergic asthma have been widely used to investigate asthma driving mechanisms and to screen therapeutic agents. Nonetheless, they present anatomical as well as immunological discrepancies with human airways. As described above, mouse lungs differ in terms of lobar structure and branching pattern of the bronchi.(41,267) Moreover, mice lack bronchodilatory nerves and the ability to cough, along with a different pattern of mediators secreted by mast cells.(362) The complex human *in vitro* and *ex vivo* systems now available embody a valid support to the well-established *in vivo* models. Epithelial cells grown at ALI can be used as a powerful tool to mimic the asthmatic epithelium *in vitro* with high similarity to the *in vivo* situation. The simplest way to reproduce the polarized epithelium at ALI for asthma studies is adopting common lung epithelial cell lines such as 16HBE14o-, BEAS-2B and Calu-3. They are easily accessible and relatively simple to grow on Transwell® supports. Additionally, they express tight junctions, making them suitable for barrier function studies.(362) Stewart *et al*. evaluated different immortalized cell lines in comparison to primary bronchial epithelial cells in terms of TEER values and marker expression. They observed that Calu3 cells featured a similar expression pattern of ZO-1, E-Cadherin and MUC5AC to primary cells, although lacking a localized expression of β-tubulin.(294) Nonetheless, secondary cell lines lack the genetic features and the structural changes observed in asthmatic epithelium. The improvements achieved in primary cell extraction from bronchial biopsies allowed their implementation in asthma research as *ex vivo* model of airway epithelia. Primary cells from asthmatic patients show marked differences from the ones obtained from healthy individuals due to the increased secretion of inflammatory cytokines and mucus production. Furthermore, they retain a less differentiated phenotype with diminished capability to repair injuries.(278) Additionally, they have disrupted tight junctions that lower TEER values and increase permeability.(363) ALI culture of asthmatic primary cells can therefore be considered a

suitable model to depict the morphologic and inflammatory imbalances caused by chronic inflammation. Notably, these models retain the phenotypic differences typical of the disease state. Gras *et al*. confirmed that reconstituted bronchial epithelium from mild and severe asthma patients retains a trend in inflammatory marker expression and mucus production that varies in correlation to the severity of asthma.(364) Thanks to the high resemblance to the real-life condition, ALI culture of primary airway epithelial cells has been a valuable tool for the identification of novel drug targets and screening of alternative therapeutic options. They were, for instance, used to investigate the role of transforming growth factor-β (TGF-β) (365) and histocompatibility antigen G (HLA-G) (366) in airway remodeling. Moreover, *in vitro* cultures of primary cells from asthmatic patients are also exploited to detect novel subsets of asthmatic patients, as the recently identified interleukin-6-driven asthmatic group.(367) As mentioned above, this model system plays an important role in the preclinical investigation of novel therapeutic agents and for understanding the mechanisms of action of therapies already in use. β2-adrenoreceptor agonists, for example, together with corticosteroids are first choices in the step therapy approach for the management of asthma symptomatology. Holden *et al*. cultured primary cells as well as BEAS-2B cells at ALI as a simplified version of the respiratory tract to investigate the effect on inflammatory response of the β2-agonists in epithelial cells in combination with corticosteroids.(368) Potential anti-inflammatory agents were also screened using ALI culture. An inhibitor of nuclear factor κ-B2 (IKK2i) was confirmed to mediate reduction of inflammatory mediators in corticosteroid unresponsive epithelial cells,(369) while an src-family kinase inhibitor was able to reduce TNF-α release, a key inflammatory mediator, and improved barrier properties of severe asthmatic ALI cultures.(370) Sexton *et al*. tested the ability of a human monoclonal antibody to inhibit a member of the tissue kallikrein family of serine proteases on primary cultures of bronchial epithelial cells, which induces bronchoconstriction and mucus hypersecretion in the airways. The monoclonal antibody reduced the mucus secretion and the inflammatory burden. The results from ALI cultures showed that antibody treatment restored kallikrein expression and reduced mucus sexretion. *In vivo* studies in a sheep asthma model emphasized that the monoclonal antibody decreased bronchoconstriction and hyperresponsiveness as well.(371)

As already discussed in the context of cystic fibrosis, nasal primary epithelial cells offer an attractive alternative to bronchial primary cells thanks to their higher availability and effortless extraction procedure. A study comparing primary asthmatic nasal cells with non-asthmatic and bronchial cells demonstrated that the former express higher levels of typical mediators which are commonly encountered in asthmatic patients, such as

vascular endothelial growth factor (VEGF) and TGF-β. This observation strengthened the hypothesis that nasal epithelial cells can be used as surrogate for primary lung epithelial cells.(372) Healey *et al*. utilized nasal epithelial cells from asthmatic donors in the preclinical testing of an siRNA-based therapy aimed at downregulating STAT-6 expression in epithelial cells, a gene involved in bronchial inflammation of asthma.(373) Similarly, Bequignon *et al*. investigated the ability of a monoclonal antibody to bind the neonatal Fc receptor in human nasal epithelial cells as a potential administration route in asthma-related chronic rhinosinusitis.(288) Despite the advantages offered by this alternative source of primary cells, it is important to consider that they have some intrinsic differences in comparison to the bronchial ones that might affect the reliability of the results. It is therefore important to keep in mind the implications of choosing one or the other source of cells.

The asthma research field has greatly benefited from ALI culture of epithelial cells. However, simple monoculture models cannot represent the complex cellular network typical of the disease state. Asthma is a multicellular disease involving epithelial cells as well as several immune cells. Co-culture systems more closely represent the complexity encountered in asthmatic lungs since they bring together two or three different cell types on the same Transwell® filter. Co-cultures for asthma-related studies generally present lung epithelial cells, primary or immortalized, in the apical chamber of a Transwell® to form a polarized epithelium, while the basolateral chamber hosts a subtype of immune cells, such as dendritic cells,(374) eosinophils,(375) or T cells.(376) A co-culture formed by primary epithelial cells and T cells was used by Wawrzyniak *et al*. to study the role of T cell secreted cytokines and histone deacetylases on the integrity of the epithelial barrier integrity. They demonstrated a beneficial effect on barrier integrity after treatment with a histone deacetylase inhibitor.(376) Co-cultures were also used to study airway remodeling in asthma, a typical feature of the disease. Haghi *et al*. developed an airway remodeling model by growing primary bronchial epithelial cells on the apical chamber and airway smooth muscle cells on the basolateral one.(377) In another study, Reeves *et al*. co-cultured primary human bronchial epithelial cells from asthmatic children and human lung fibroblasts to study the fibroblast-myofibroblast transition. They showed that it is possible to restore the healthy condition by using a monoclonal antibody inhibiting TGF-β, a central factor involved in airway remodeling.(378) Triple co-cultures would be an even more exemplary model of the asthmatic environment. However, studies exploiting this method are infrequent. A recent study by Paplinska-Goryca *et al*. provides a triple co-culture model formed by primary epithelial cells, macrophages and dendritic

cells that might be helpful for better understanding the pathogenesis of asthma thanks to the higher complexity of the system.(379)

4.4 Lung cancer

Lung cancer is the most common cause of cancer-related deaths, both in men and women.(380) Therapeutic advancements of the last ten years are barely reflected in the small decline of lung cancer mortality. One reason is the histologic diversity of lung cancer. It includes three major types, namely adenocarcinoma, squamous cell carcinoma and small cell carcinoma, and several less frequent types including adenosquamous carcinoma and large cell neuroendocrine carcinoma. Due to this high variability, it is necessary to examine the exact molecular mechanisms of each cellular type to further improve therapy options. Hereby, animal models are an important standard tool. Apart from known drawbacks such as high costs, species differences and limited availability, ethical issues in relation to the use of animals in tumor research are highly controversial.(381) Therefore, also in this field extensive research has been conducted in the last years to establish reliable and physiologically relevant *in vitro* models, thereby, reducing the number of animals used in tumor research and drug evaluation. Since conventional 2D cell cultures are not capable of mimicking the complex architecture and microenvironment of lung cancer *in vivo*, 3D cell cultures and co-cultures contribute greatly to the understanding of tumor cell pathophysiology and in therapeutic evaluations of anti-tumor drug discovery.(382)

Often, ALI systems are used to study the exact mechanisms of malignant transformations of different cell types because of their resemblance to the human lung physiology.(383,384) ALI systems also serve studies about how a specific signaling pathway can potentially be inhibited.(385) Horie *et al*. established a 3D co-culture model at the ALI using A549 cells and lung cancer-associated fibroblasts.(386) They found that fibroblasts enhanced A549 cell invasion into collagen gels, suggesting their tumor-promoting role through the production of various instructive signals, such as growth factors and chemokines. Due to its aggressive nature and high mortality, it is especially important to improve the early detection and chemoprevention of lung cancer. However, the pathobiology of early stages is poorly understood. To this purpose, Correia *et al*. engineered the inducible activation of oncogenes in an ALI culture of immortalized human bronchial epithelial cells overlaid on a fibroblast containing collagen layer.(387) In this work they provide direct evidence that deregulation of the putative oncogene SOX2, under the appropriate *in vivo* mimicking circumstances, is sufficient to drive bronchial dysplasia. These findings are important steps forward towards the development of agents to be used for primary and secondary chemoprevention.(385)

The most frequently found 3D *in vitro* tumor models are lung cancer spheroids constituted of one or more cell types.(388,389) Tumor spheroids are cell constructs that have self-organized to exhibit a 3D structure resembling the cancerous state. It was shown that genes expressed in 3D spheroids, especially the ones responsible for aggressive tumor growth, recapitulate the *in vivo* phenotype better than the respective 2D models.(390) Also, three dimensional models hold the potential to guide personalized medicine in the future, clearly demonstrating their superiority over conventional models.(391) However, particularly in lung cancer research, spheroid models have one critical disadvantage. Many of them lack air exposure and therefore do not reflect the physiological environment correctly. Subsequently, these cultures are unsuited models for testing the efficacy of aerosolized drugs. Meenach *et al*. compared lung tumor spheroids in air- and liquid-interface culture for treatment with paclitaxel-containing dry powder PEGylated phospholipid microparticles.(392) For the cultivation at ALI conditions, A549 cells were seeded on collagen coated transmembrane inserts in a 24-well plate and incubated for 24 h under submerged conditions. Subsequently, the medium on the apical side was removed and spheroid formation was evident after 9 days. The group showed that IC_{50} values of paclitaxel can differ substantially between treatment of a tumor spheroid grown under submerged conditions and another one cultured at ALI conditions. Moreover, they stated that the results reported in ALI evaluation were in µg/dose, in contrary to the usual µM results, thereby allowing for a simple determination of the patient dose in terms of mg/kg via direct inhalation of the drug. Gupta *et al*. developed a high-throughput model growing A549 lung adenocarcinoma cells as 3D spheroids at the air-liquid interface.(393) They found that, due to limited drug diffusion, the cytotoxic effect of paclitaxel in A549 ALI spheroids was restricted only to the outer layer of proliferating cells. However, the co-administration of a tumor penetrating peptide enhanced paclitaxel penetration depth. These results emphasize the importance of air-grown three-dimensional *in vitro* models not only to characterize tumor growth and microenvironment of different cell types, but also to understand the mechanism of resistance in lung cancer. Such models strongly improve efficacy and success of the screening process of chemotherapeutics and drug combinations and serve as a first step before conducting expensive *in vivo* pre-clinical or clinical studies.

Apart from spheroids, other ALI models have been developed. Movia *et al*. used a multilayered cell culture of A549 cells to study four anti-cancer drugs delivered by a clinical nebulizer as liquid aerosol.(394) Their results clearly demonstrated the advantages of this model: incorporation of the necessary levels of biological complexity

due to 3D architecture, closer resemblance to the patient status by modeling the multidrug resistance (MDR) observed in human patients, and applicability of aerosol administration methods due to ALI conditions. In a subsequent study, the group incorporated human fibroblasts into their multilayered cell culture (MCC) model to assess their role in MDR.(395) Indeed, cancer cell-fibroblast crosstalk led to a higher MDR than the one found in an ALI multilayered monoculture. These studies emphasize that a monoculture, even if it is three-dimensional and under ALI conditions, still does not reflect the *in vivo* conditions sufficiently. Therefore, it is crucial to integrate several other key factors, such as immune cells, extracellular matrix and genetic variability, into the *in vitro* platform in further studies. Zhang *et al*. assessed the impact of tumor microenvironment on bone marrow mesenchymal stem cells.(396) Conclusively, they found that an *in vitro* ALI lung cancer A549 microenvironment might induce stem cells to undergo changes in cell morphology, proliferation, karyotype, cytoskeleton and migration ability. This study is an important example for the versatility and flexibility of advanced ALI *in vitro* models. In lung cancer research, they can be used for the evaluation of various therapeutic approaches by simply incorporating key factors of interest.

Due to the versatile nature of lung cancer and the increasing development of multidrug resistance in tumors, new and innovative therapy options are constantly needed to improve therapeutic efficacy. In the last decade, nanotechnology emerged as a promising alternative and/or addition to conventional treatment strategies. When using these nanocarriers in pulmonary administration, the lung can be used as port of entry limiting systemic distribution and avoiding first pass metabolism.(397,398) Many attempts have been described in the literature to improve the delivery of already approved chemotherapeutics, such as paclitaxel or doxorubicin, by using nanocarriers.(399–401) Furthermore, nanocarriers are often used to encapsulate new therapeutic entities for the treatment of lung cancer such as nucleic acids,(255) and also for the co-delivery of different therapeutic agents.(402)

The huge variety and number of combinations of delivery systems with already existing or new active pharmaceutical ingredients requires testing in more complex and physiologically relevant *in vitro* models to assess and compare efficacy. By using 3D co-culture systems scientist can make reliable statements about penetration, efficacy, toxicity and other characteristics of drug formulations, thereby reducing the amount of animal experiments drastically. Conclusively, the development of these advanced cell culture systems is crucial because in combination with organ-on-a-chip models and simulation approaches they could potentially lead the way to animal-free research.

4.5 COPD

Chronic obstructive pulmonary disease (COPD), together with asthma, is considered one of the chronic respiratory diseases displaying the highest impact on healthcare systems worldwide. Based on the World Health Organization report, it affects more than 250 million people around the world, with more than 90% of the deaths occurring in low- and middle-income countries.(7) COPD is triggered by persistent exposure to toxic gases and particles, where cigarette smoke exposure was identified as a central risk factor. Tobacco smoke, in fact, mediates an abnormal chronic inflammatory status resulting in severe consequences on lung structure and functionality.(8) COPD affects small airways, lung parenchyma as well as larger airways, and it is characterized by a progressive obstruction of the airways that ultimately leads to lung failure. The clinical manifestations of COPD can be grouped into two major subsets, chronic bronchitis and emphysema, which affect large and distal airways, respectively. Chronic bronchitis is distinguished by chronic inflammation and remodeling of the large airways together with mucus secretion, while emphysema shows a progressive destruction of airway walls as well as loss of alveolar cells, which consequently impairs gas exchange.(403) The abnormal inflammatory response typical of COPD is linked to an enhanced presence of inflammatory cells in the airways, with neutrophils, macrophages and CD8+ T cells playing a prominent role. These cells secrete cytokines and chemokines, such as TNF-α, IL-1β and IL-8, which mediate a perpetuated inflammatory condition.(404) Similarly to asthma, bronchial epithelial cells retain a central function also in COPD. While at physiological condition airway epithelium acts as a defensive barrier towards external agents, the alterations of the homeostatic environment driven by toxic agents cause severe modifications of epithelium structure and functionality. This is reflected particularly in terms of reduced mucociliary clearance and increased permeability to external factors. Therefore, lung epithelium faces increased permeability, reduced cilia beat ability as well as decreased mucus clearance. Moreover, in this imbalanced status, epithelial cells are not only the target of inflammatory mediators, but they also secrete cytokines and chemokines that perpetuate and worsen the inflammatory status. The increased secretion of TGF-beta and EGF, for example, is directly linked to fibrosis and mucus secretion.(405)

Considering the central role played by epithelial cells in COPD, ALI models can grant deeper understanding of the disease driving mechanisms as well as identification of novel therapeutic options. COPD is directly correlated to lung exposure to toxic pollutants such as tobacco smoke or diesel exhaust. Therefore, ALI cultures represent a straightforward tool mimicking the *in vivo* lung environment of the disease. Several

studies have shown that after growing and differentiating cells at ALI, they can be exposed to cigarette smoke to obtain an *in vitro* model incorporating most of the effects observed also *in vivo*. Shamberger *et al*. showed that cigarette smoke exposure of healthy human primary bronchial epithelial cells alters their differentiation and functionality. Apart from impairing the epithelial barrier integrity, it also affected cellular differentiation, resulting in an increased number of mucus-secreting cells while the number of ciliated cells was decreased. These changes caused a mucus-rich lung environment.(406) Indeed, mucus hypersecretion is one of the main features of COPD. Culturing epithelial cells at ALI is essential to investigate this distinct mucus hypersecretion trait of the disease (407) along with reduced mucus clearance by ciliated cells.(408) The effect of tobacco smoke on epithelial barrier integrity has also been explored in terms of tight junction loosening (409) and airway remodeling.(410) Both factors are crucial for the pathophysiology of the disease and, similarly to the ones described above, their understanding was expanded by ALI cultures. Cells grown under this condition, in fact, form differentiated epithelia with different cellular subsets, such as ciliated cells, and can even secrete mucus, a condition not reproducible under submerged cultures. Recently, a novel protocol was established to grow primary small airway epithelial cells at the air-liquid interface. Small airways are the part of the airways mainly affected by chronic bronchitis. Gindele *et al*. showed that once primary cells from COPD patients were grown at ALI and exposed to cigarette smoke, their behavior well correlated to the *in vivo* conditions in terms of barrier integrity, mucus secretion and cellular differentiation, making them a suitable tool for further COPD treatment studies.(279) The effect of cigarette smoke on barrier integrity is reflected also in an increased susceptibility to microbial infections.(411) Co-culture of epithelial cells grown at ALI and bacteria were developed along with exposure to cigarette smoke. Amatngalim *et al*. grew primary epithelial cells from COPD and non-COPD subjects at ALI and studied the different response to *Haemophilus influenzae* after exposure to cigarette smoke. They observed that antibacterial activity was lower in primary cells from COPD patients and suppressed after cigarette smoke exposure.(412)

To further improve the translatability of ALI-based systems in COPD research, efforts have been made towards the development of exposure systems for tobacco smoke. Azzopardi *et al*. used an aerosol exposure chamber to uniformly expose lung epithelial cells grown at ALI and used it to study the consequences on cellular viability and cytokine release after the aerosolization of tobacco smoke. This system allowed the investigation of tobacco effect on cells with various exposure regimens and exposure times that well correlate with the real life parameters.(413) In another study, primary COPD epithelial

cells were exposed to diesel exhaust, another toxic agent responsible for triggering the disease, using a Vitrocell nebulization system. Instead of using suspended particles, this exposure system allowed to reproduce *in vitro* exposure conditions similar to the ones observed in everyday life.(414) As discussed above, co-culture models can fill the gap between *in vitro* and *in vivo* models thanks to the more advanced cellular complexity.

In COPD research, several studies have exploited co-culture models to study the cellular networks involved in the disease. Ladjemi *et al*. developed a co-culture model formed by primary epithelial cells from COPD patients and B-cells. They used this system to test how the bronchial epithelium influenced the humoral response in the lung. Specifically, they observed the effect of Interleukin 6 (IL-6) secreted by epithelial cells on immunoglobulin A (IgA) secretion by B cells, which is increased in COPD patients.(415) In another study, co-culture of airway epithelial cells and lung fibroblasts was developed to understand the mechanisms behind airway remodeling and inflammation in COPD. The authors observed a stronger interleukin1 α (IL-1α) mediated inflammation in co-cultures exposed to cigarette extract, confirming the connection between smoke and inflammation.(416) An additional co-culture model was established between primary small airway epithelial cells and macrophages to analyze the epithelial wound injury mechanisms in respiratory diseases.(417) COPD co-culture models could therefore represent a useful tool to obtain a deeper understanding of the driving mechanisms of the disease as well as for *in vitro* screening of potential therapeutic agents. So far, most of the treatment-related studies were carried out using ALI cultures involving only a single cell line, mostly epithelial cells. The mucus-secreting cell line Calu-3, for example, was used to test the ability of simvastatin, a drug mediating reduced mucus secretion of epithelial cells of COPD patients.(418) Calu-3 cells were also exposed to cigarette smoke extract to examine the ability of the antimicrobial peptide Cathelicidin LL-37 to prevent the disruption of tight junctions. This effect was expected to reverse the impaired activity of the epithelium typical of COPD.(419) Another study investigated the effect of the phosphodiesterase inhibitor Roflumilast on mucociliary clearance impairment. Primary human bronchial epithelial cells were exposed to cigarette smoke through a Vitrocell nebulizer after Roflumilast pre-treatment. An Ussing chamber was used to determine the recovery of mucociliary activity.(420) Primary cell-based ALI cultures were also used to test the potential of monoclonal antibody candidates to improve the COPD phenotype. ALI cells treated with an anti-TGF-β monoclonal antibody reversed the progressive de-differentiation of the epithelium typical of the disease.(421) Monoclonal antibodies directed towards IL-1α and IL-1β decreased cigarette smoke-mediated airway inflammation in primary human bronchial epithelial cells.(422) Taken together, ALI

models of mono- and co-culture have been used in a variety of pharmacological and pharmacotherapeutic studies trying to understand and treat COPD better.

5. Commercially available ALI models

As described above in detail, there is an urgent clinical need for standardized 3D *in vitro* ALI models of the respiratory tract to be used in toxicology studies and for efficient drug screening. Therefore, several companies have specialized in the fabrication of ALI models mimicking the morphology of healthy and diseased human tissue. Two of these models, available under the brand names MucilAir™ (Epithelix) and EpiAirway™ (MatTek Corporation), are made of primary human epithelial cells freshly isolated from nasal or bronchial biopsies.(423) They can accurately reproduce the biophysiology of human airway epithelia including the presence of a functional mucociliary system and the secretion of mucus in a homeostatic state.(424) It was shown that both, MucilAir™ and EpiAirway™ models, express tight and adherent junction proteins, as well as functional ABC drug efflux transporters.(425,426) Hoffmann *et al*. showed similar permeability of 30 model substances when comparing MucilAir™ to nasal and bronchial epithelium in human tissue.(427) These findings confirm the match of these ALI models with major features of a normal human nasal and bronchial epithelium.(428) Hence, these models are widely used for toxicology studies, drug efficacy and formulation screening.(429–432)

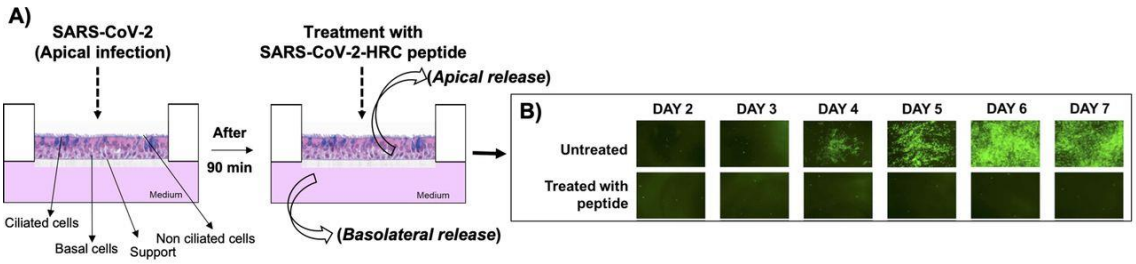

Figure 3. SARS-CoV-2-derived cholesterol-conjugated peptides block SARS-CoV-2-mNeonGreen viral spread in human airway epithelial cells (HAE). (A) HAE cells were infected with SARS-CoV-2 (2,000 PFU/well for a multiplicity of infection of ~0.02) for 90 min before adding SARS-CoV-2 peptide. Fluid was collected from the apical or basolateral surfaces daily for 7 days. (B) Spread of fluorescent virus is shown at the indicated days with or without peptide treatment. Adapted with permission.(433) Copyright 2020, American Society for Microbiology.

With two other models expressing a different phenotype, EpiAlveolar™ and SmallAir™, scientists are additionally able to study the impact of different drugs on the lower respiratory tract.(434,435) The two leading companies in this field, MatTek Corporation and Epithelix, recently also developed co-cultures of epithelial cells at the ALI and fibroblasts (EpiAirway™ FT, MucilAir™ HF) for advanced analysis of cell interaction and better mimicking *in vivo* conditions.(436,437) These commercial models open various

possibilities for further modifications with other cell types, bacteria and viruses depending on the application. Outlaw *et al*. infected cells of the EpiAirway™ model with SARS CoV-2 to study the efficacy of a lipopeptide as virus entry inhibitor (Figure).(433) As shown by Signer *et al*., MucilAir™ can readily be infected with different respiratory coronaviruses in order to evaluate the effect of new antiviral agents.(438) Another example to show the modularity of these systems is given by Mas *et al*. (Epithelix).(439,440) They combined a functional airway epithelium, primary lung fibroblasts and developing tumor nodules from a KRAS mutated Non-small Cell Lung Cancer cell line. After confirming the biological relevance of this brand named OncoCilAir™ model regarding the *in vivo* situation, the group showed reduced growth of tumors when treated with MEK inhibitors and the standard anticancer agent docetaxel. Subsequently, this model has been used in a variety of other studies including specific tumor targeting and multi organ chips.(431,441)

In general, organ-on-a-chip devices present the possibility to create artificial cellular microenvironments that closely mimic those found in the human body. This can also be exploited to mimic lung functions, which involve a complex and hierarchical milieu of fluid and solid mechanical stress.(442,443) Zamprogno *et al*. developed a lung-on-a-chip model to reconstitute the lung alveolar barrier. They used a hexagonal gold mesh with a suspended stretchable membrane to culture alveolar epithelial cells in ALI conditions mimicking physiological lung movement.(444) Huh *et al*. developed a microfluidic device replicating a functional unit of the living human lung. (445) Therefore, they constructed a compartmentalized microchannel system consisting of two chambers separated by a mesoporous elastomeric membrane. Human alveolar epithelial cells and pulmonary microvascular endothelial cells were seeded into the chambers and cultured at ALI. With this model, the group was able to simulate physiological breathing motions by stretching the mesoporous membrane. Although these particular techniques and execution are not yet optimized, there is already a microfluidic based ALI lung model on the market. The company SynVivo developed a device containing a co-culture of epithelial cells surrounded by vasculature comprised of endothelial cells. Hereby, tight junctions are formed, functional cilia are built, and airway tubules form and transport mucus.(446) These examples including many more that can be found in literature demonstrate that lung-on-a-chip models are valid tools in pharmaceutical development.(447)

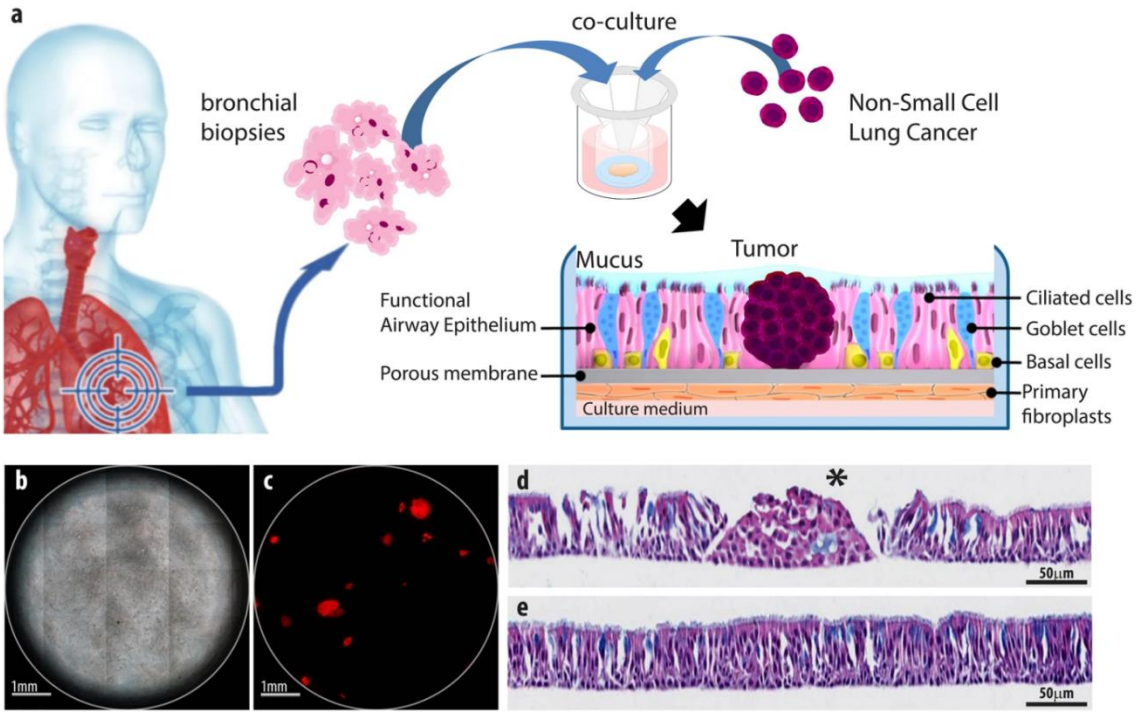

Figure 4. The OncoCilAir™ model. (a) Schematic representation of lung cancer invasion of a human functional airway modelled by OncoCilAir™ tissue. (b) Phase contrast and (c) fluorescence images showing a human airway epithelium with EGFR tumor nodules (mRFP labeled) at the air–liquid interface. (d + e) Haematoxylin eosin histological staining of differentiated healthy region of the airway (e) and with a cluster of non-polarized tumor cells (d, star) invading the epithelium (d). Reproduced with permission.(440) Copyright 2017, Nature.

6. Aerosolization systems

All the models described above demonstrate the possibility to mimic the unique nature of the lung epithelium *in vitro* with a high degree of complexity using ALI cell cultures. However, so far, the development of aerosolized drugs for inhalation therapy is hampered by the lack of a high-throughput technology for dosimetrically accurate and efficient aerosol-to-cell drug delivery. Lenz *et al*. investigated the ALICE-CLOUD system, an aerosol-to-cell exposure system with a vibrating mesh nebulizer developed for the use in standard multi-well plates.(448) The same group found that aerosolized drug delivery with the ALICE system results in a ca. 8 µm thin liquid layer, which is about 1000-fold lower than typical media heights under submerged cell culture conditions.(449) Therefore, it resembles the clinical conditions in the bronchial regime making aerosolized drug delivery to ALI cells crucial for biokinetic studies. This system can be combined with co-culture systems to study the potential effect of particles in the lung using a sophisticated *in vitro* model.(450) A commercial version of this system has been made

available by Vitrocell Systems. An interesting application of a tetra-culture in combination with the Vitrocell system was developed by Klein *et al*. to investigate the effects of particle deposition on the lung. (450) In this model, four different cell lines (epithelial cells, macrophages, mast cells and endothelial cells) were grown on the same Transwell® insert demonstrating the potential offered such ALI systems. Cells were cultured on both sides of the insert to mimic *in vivo* cellular distribution (Figure 5).

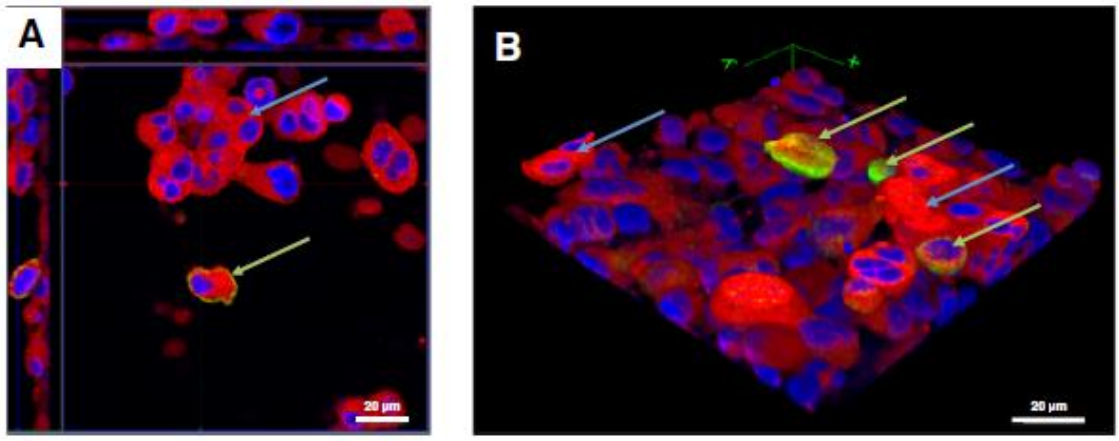

Figure 5. Z-stack image series to analyze the distribution of THP-1 macrophages and HMC-1 in the tetra-culture system present in the apical compartment of the insert. The distribution of A549, differentiated THP-1, HMC-1 and EA.hy 926 cells in the tetra-culture was analyzed via CLSM. Cellular membranes are stained with cell mask deep red dye (red), and nuclei are stained with DAPI (blue); Macrophage-like cells are counterstained with an anti-CD11b-antibody. A: x–y projection with the respective side views. B: 3D reconstruction of the tetra-culture based on the results of the z-stack from A. THP-1 (green arrows) and HMC-1 (blue arrows) cells are found on top of the epithelial cells. EA.hy 926 cells were not considered in the 3D reconstruction.(450) Reproduced with permission. Copyright 2013, BioMed Central.

Another example of a commercially available aerosolization system is CULTEX from Cultex® Technology. The company did not only develop an exposure system but also a computer-controlled long-term cultivation system.(451,452) Using these two modules together allows prolonged ALI cultivation of normal human bronchial epithelial cells for a period of 38 days exhibiting *in vivo*-like differentiation characteristics for inhalation toxicological studies. The computer-controlled system can operate independently, reducing the risk of contamination and eliminating process variability. With the CULTEX aerosolization system, the particle or gas exposure takes place for 15-60 min under humid atmosphere at 37°C. The device was extensively validated for the inhalation of airborne particles by Tsoutsoupoulos *et al*.(451) After testing the aerosolization of 24 different substances, the results demonstrated the device to be robust, transferable and predictive for *in vitro* screening. Other exposure systems with a limited number of users

have also been described.(453) Additionally, nebulizers can be used as well with the drawback of uncertain dose deposition after direct nebulization on top of ALI cultures. Many of the systems described in the literature need further modification for standardised particle deposition and dosimetry.(454–457)

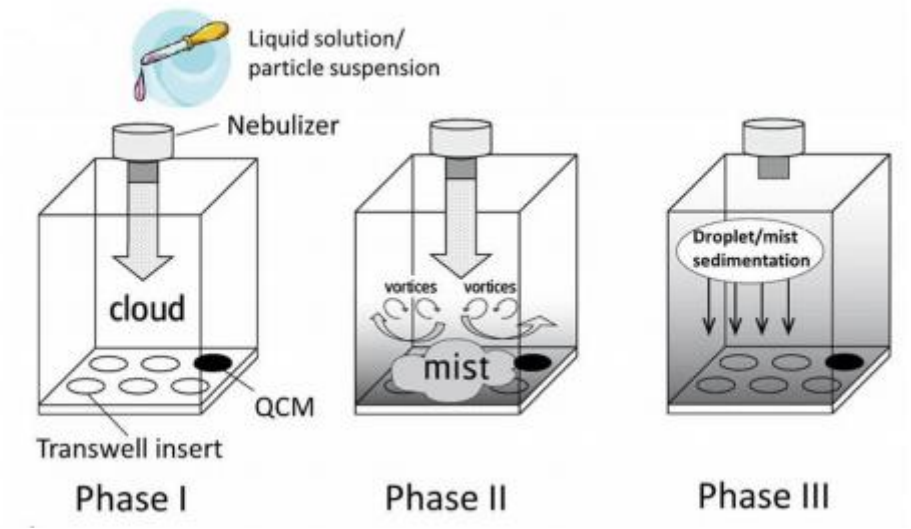

Figure 6. Nebulization and sedimentation of liquid solutions or nanoparticle suspensions using the VITROCELL® Cloud 6 system equipped with a quartz crystal microbalance (QCM). Phase 1: emission of droplet cloud from nebulizer. Phase 2: emitted cloud is transformed into a fine mist of droplets, which is distributed uniformely filling the chamber from bottom up. Phase 3: droplet deposition onto the cells via sedimentation. Reproduced with permission.(458). Copyright 2020, BioMed Central.

7. Conclusion

In the last years, the need for alternatives to *in vivo* models to reduce, refine and replace (3R) animal experiments increased drastically. Furthermore, anatomical differences between commonly used laboratory animals, such as mice or rats, and humans lead to a significant lack of functional homology, especially regarding the respiratory tract. Modeling this part of the human body *in vitro* is particularly challenging and requires multiple considerations in order to mimic *in vivo* pathophysiology as closely as possible. In this review, different *in vitro* air-liquid interface cultures mimicking the human respiratory tract were described in detail. The most frequently used cell lines for different areas of the airways were discussed together with the possibilities of replacing these with human-derived primary cells. Besides, different approaches to mimic diseases of the human respiratory tract, such as asthma, COPD or viral infections, were discussed. These can be of great use in gaining deeper understanding of disease pathophysiology and in high throughput drug screening to find new therapeutic options. Yet, recreating

such a complex environment *in vitro* using epithelial cells in combination with other cell types, such as immune cells, bacteria or even viruses, as a field of research is still progressing. Moreover, the large variety of cell sources, culture methods and exposure setups requires further evaluation on ease-of-use, complexity and robustness of the *in vitro* setup. Currently there is no golden standard model. However, a few companies have started commercializing validated and standardized ALI models from primary human respiratory epithelium. In conclusion, the use of the ALI culture technique, especially in co-culture systems, could lead to significant advances in the development of more physiologically representative tissue models for drug discovery and disease modelling, thereby reducing the number of experimental animals.

Acknowledgements

This project has received funding from the European Research Council (ERC) (Grant agreement ERC-2014-StG637830).

The authors have declared no conflicts of interest for this article.

Summary and outlook

Within this work, efforts were made to identify formulations with optimized features for lung delivery of therapeutics, with a focus on the development of siRNA delivery systems for pulmonary administration. siRNA-based therapies could indeed be exploited to treat several pathological conditions of the lung for which no resolving cure is available yet. RNAi cascade can in fact be tuned to downregulate disease-specific genes and thus target disease-related pathways specifically and efficiently. Despite the number of advantages offered by siRNA, its translatability into clinics holds some major challenges. Negative charge and susceptibility to nucleases make the formulation of siRNA with a suitable delivery system of the essence. Additionally, the formulation should be further optimized to overcome the main barriers found in the lungs, such branching of the airways, mucus layer as well as mucociliary clearance. In this view, with this work we aimed at identifying different strategies to improve the delivery of siRNA to the lungs in different pathological conditions.

Chapter 1 and chapter 2 focus on the optimization of formulations for siRNA delivery to the lungs. In Chapter 1, siRNA/PEI polyplexes were coated with a commercially available pulmonary surfactant, Alveofact. After identifying a formulation with suitable physicochemical characteristics, Alveofact-coated polyplexes were tested *in vitro* in 2D as well as 3D cell culture lung models. The results suggested that coating with Alveofact could indeed improve the activity of the formulation as well as the mucus penetration in air-liquid interface cultures. However, Alveofact coating of polyplexes must be carefully controlled to avoid instability issues. In chapter 2 lipid nanoparticles based on the well-known formulation of Onpattro® were prepared with helper lipids with different net charges to study how this affected pulmonary administration of siRNA as well as their interactions with mucus. The study underlined that the presence of lipid with different net indeed affect cellular behavior of the formulations and should thus be carefully balanced. Furthermore, the study underlined how the use of different models for studying LNPs behavior in mucus led to different results, underlying the importance of using different and complementary investigation tools to get a better understanding of the delivery system under investigation.

Chapter 3 and chapter 4 describe the development of formulations for the treatment of viral and bacterial infections. In chapter 3, an siRNA-based therapy using VIPER block copolymer as delivery system was developed to treat SARS-CoV-2 infections. The formulation was optime to enable target downregulation in lung epithelial cells and was

tested both in 2D and 3D culture models. The inhibitory activity against SARS-CoV-2 was tested in a prophylactic set up *in vitro* in an air-liquid interface culture using lung epithelial cells as well as *ex vivo* in human PCLSs. Finally, polyplexes distribution in the lung as well as pro-inflammatory effects were tested *in vivo* following pulmonary administration. This study confirmed the potential of local siRNA delivery as a promising antiviral therapy in the lungs. Further studies should be addressed to evaluate the activity of siRNA/VIPER polyplexes against SARS-CoV-2 *in vivo*. Chapter 4 focuses on the development of formulation to deliver a novel antibiotic, SV7, to the lungs for the treatment of MRSA infections. SV7 is a benzophenone antibiotic that shows activity against MRSA at low concentrations that, however, shows low aqueous solubility. To improve the solubility profile and to ensure a sustained release, SV7 was encapsulated in PLGA nanoparticles. SV7-loaded NPs were optimized for pulmonary administration in terms of physico-chemical parameters and their activity against MRSA was confirmed both *in vitro* and *in vivo* in a *G. mellonella* infection model. Additionally, the activity on SV7-loaded NPs was confirmed also against intracellular infections. Further *in vivo* mouse experiments should be performed to confirm the activity and safety of the formulation.

Chapter 5, chapter 6 and chapter 7 focus on the development of siRNA therapies against inflammation in asthma and cystic fibrosis. Chapter 6 reviews the development of an siRNA therapy to target the transcription factor GATA-3 in activated Th2 cells as a strategy to treat asthma. Chapter 7 describes the *ex vivo* testing of siRNA/Tf-Mel-PEI polyplexes in a PCLS models of asthma. Here, the safety, cellular uptake as well as downregulation activity against GATA-3 were investigated. The findings support the suitability and translatability of siRNA/Tf-Mel-PEI polyplexes as delivery systems to target T cells in the lung and GATA-3 silencing as a potential novel treatment for allergic asthma.

Chapter 7 describes the *in vitro* testing of siRNA-loaded hybrid lipid/polymer NPs to treat inflammation in cystic fibrosis patients. PLGA NPs were coated with a phospholipid layer of DPPC or DPSE-PEG to overcome the mucus barrier of the lungs typical of cystic fibrosis. Additionally, PEI was included in the formulation to improve loading of siRNA in NPs. Here, hNPs were tested *in vitro* in terms of physicochemical parameters, cellular behavior and mucus permeation. The results suggested that coating of NPs with a phospholipid layer could indeed represent a promising strategy for local delivery to the lungs for the treatment of inflammation in cystic fibrosis.

Chapter 8 reviews potential and challenges of air-liquid interface culture models as strategy to recreate typical features of the respiratory tract *in vitro*. ALI cultures represent a valid tool to recreate the complexity of the lungs, particularly in terms of cellular composition and mucus secretion. ALI models can indeed contribute towards the development of more physiologically relevant models for drug discovery and disease modeling, while reducing the number of experimental animals required for drug development.

Taken together, in this work different strategies to deliver siRNA to the lungs were developed. Care should be taken in optimizing formulations to overcome several barriers that hamper siRNA activity in the lungs, both intracellular and extracellular, such as endosomal escape, mucus and anatomical barriers. The formulation should in fact ensure stability and protection to the therapeutic cargo throughout the respiratory route, from inhalation up to cellular uptake in target cells. Importantly, the formulation should be optimized for the production of an inhalable dosage form, and it should protect the therapeutic cargo also during this process. Within this work we also understood the importance of using different *in vitro*, *ex vivo* and *in vivo* models throughout the process of drug development. Using different model gives indeed a better overview of the potential and limitations of the formulation under investigation, thus leading to more accurate and translatable results. Taken together, the findings presented in this work contribute towards the development of an siRNA therapy for the treatment of lung diseases following direct pulmonary administration.

References

1. Celedón JC, Lam D, Roche N. Forum of International Respiratory Societies. The global impact of respiratory disease. Third Edition. European Respiratory Society, 2021. Accessed 22 September, 2021. firsnet.org/images/publications/FIRS_Master_09202021.pdf. 2021;

2. Boucher RC. An overview of the pathogenesis of cystic fibrosis lung disease. Adv Drug Deliv Rev. 2002;54(11):1359–71.

3. Ratjen F, Bell SC, Rowe SM, Goss CH, Quittner AL, Bush A. Cystic fibrosis. Nat Rev Dis Prim. 2015 Dec;1(1):15010.

4. Network GA. The Global Asthma Report 2022. 2022.

5. Kudo M, Ishigatsubo Y, Aoki I. Pathology of asthma. Front Microbiol. 2013;4(SEP):1–16.

6. Wegmann M. Th2 cells as targets for therapeutic intervention in allergic bronchial asthma. Expert Rev Mol Diagn. 2009;9(1):85–100.

7. Brandsma CA, Van den Berge M, Hackett TL, Brusselle G, Timens W. Recent advances in chronic obstructive pulmonary disease pathogenesis: from disease mechanisms to precision medicine. J Pathol. 2019;250(5):624–35.

8. Marin L, Colombo P, Bebawy M, Young PM, Traini D. Chronic obstructive pulmonary disease: Patho-physiology, current methods of treatment and the potential for simvastatin in disease management. Expert Opin Drug Deliv. 2011;8(9):1205–20.

9. Calderaro A, Buttrini M, Farina B, Montecchini S, De Conto F, Chezzi C. Respiratory Tract Infections and Laboratory Diagnostic Methods: A Review with A Focus on Syndromic Panel-Based Assays. Microorganisms. 2022;10(9).

10. Michalski JE, Kurche JS, Schwartz DA. From ARDS to pulmonary fibrosis: the next phase of the COVID-19 pandemic? Transl Res [Internet]. 2022;241:13–24. Available from: https://doi.org/10.1016/j.trsl.2021.09.001

11. Leslie KO, Wick MR. Lung Anatomy. Pract Pulm Pathol A Diagnostic Approach A Vol Pattern Recognit Ser. Third Edit. 2017;1–13.

12. Person A, Mintz ML. Anatomy and Physiology of the Respiratory Tract. Mintz ML, editor. Disord Respir Tract Common Challenges Prim Care. 2006;11–5.

13. Kandil R, Merkel OM. Pulmonary delivery of siRNA as a novel treatment for lung diseases. Ther Deliv. 2019;10(4):203–6.

14. Kim N, Duncan GA, Hanes J, Suk JS. Barriers to inhaled gene therapy of obstructive lung diseases: A review. J Control Release [Internet]. 2016;240:465–88. Available from: http://dx.doi.org/10.1016/j.jconrel.2016.05.031

15. Merkel OM, Rubinstein I, Kissel T. SiRNA Delivery to the lung: What's new? Adv Drug Deliv Rev [Internet]. 2014;75:112–28. Available from: http://dx.doi.org/10.1016/j.addr.2014.05.018

16. Ruigrok MJR, Frijlink HW, Hinrichs WLJ. Pulmonary administration of small interfering RNA: The route to go? J Control Release [Internet]. 2016;235:14–23. Available from: http://dx.doi.org/10.1016/j.jconrel.2016.05.054

17. Bettini E, Locci M. SARS-CoV-2 mRNA Vaccines: Immunological mechanism and beyond. Vaccines. 2021;9(2):1–20.

18. Friedrich M, Aigner A. Therapeutic siRNA: State-of-the-Art and Future Perspectives. BioDrugs [Internet]. 2022;36(5):549–71. Available from: https://doi.org/10.1007/s40259-022-00549-3

19. Fire A, Xu S, Montgomery MK, Kostas SA, Driver SE, Mello CC. Potent and specific genetic interference by double-stranded RNA in caenorhabditis elegans. Nature. 1998;391(6669):806–11.

20. Mehta A, Michler T, Merkel OM. siRNA Therapeutics against Respiratory Viral Infections—What Have We Learned for Potential COVID-19 Therapies? Adv Healthc Mater. 2021;10(7).

21. Chen J, Tang Y, Liu Y, Dou Y. Nucleic Acid-Based Therapeutics for Pulmonary Diseases. AAPS PharmSciTech. 2018;19(8):3670–80.

22. Merkel OM, Kissel T. Nonviral pulmonary delivery of siRNA. Acc Chem Res. 2012;45(7):961–70.

23. Akinc A, Maier MA, Manoharan M, Fitzgerald K, Jayaraman M, Barros S, et al. The Onpattro story and the clinical translation of nanomedicines containing nucleic acid-based drugs. Nat Nanotechnol [Internet]. 2019;14(12):1084–7. Available from: http://dx.doi.org/10.1038/s41565-019-0591-y

24. Schlich M, Palomba R, Costabile G, Mizrahy S, Pannuzzo M, Peer D, et al. Cytosolic delivery of nucleic acids: The case of ionizable lipid nanoparticles. Bioeng Transl Med. 2021;6(2):1–16.

25. Lam JKW, Liang W, Chan HK. Pulmonary delivery of therapeutic siRNA. Adv Drug Deliv Rev [Internet]. 2012;64(1):1–15. Available from: http://dx.doi.org/10.1016/j.addr.2011.02.006

26. Dong Y, Siegwart DJ, Anderson DG. Strategies, design, and chemistry in siRNA delivery systems. Adv Drug Deliv Rev [Internet]. 2019;144:133–47. Available from: https://doi.org/10.1016/j.addr.2019.05.004

27. Kandil R, Baldassi D, Böhlen S, Müller JT, Jürgens DC, Bargmann T, et al. Targeted GATA3 knockdown in activated T cells via pulmonary siRNA delivery as novel therapy for allergic asthma. J Control Release. 2023;354(January):305–15.

28. Merkel OM, Beyerle A, Librizzi D, Pfestroff A, Behr TM, Sproat B, et al. Nonviral siRNA delivery to the lung: Investigation of PEG-PEI polyplexes and their in vivo performance. Mol Pharm. 2009;6(4):1246–60.

29. Ungaro F, D'Angelo I, Miro A, La Rotonda MI, Quaglia F. Engineered PLGA nano- and micro-carriers for pulmonary delivery: Challenges and promises. J Pharm Pharmacol. 2012;64(9):1217–35.

30. Ding L, Tang S, Wyatt TA, Knoell DL, Oupický D. Pulmonary siRNA delivery for lung disease: Review of recent progress and challenges. J Control Release. 2021;330(November 2019):977–91.

31. Keil TWM, Merkel OM. Dry powder inhalation of siRNA. Ther Deliv. 2019;10(5):265–7.

32. Zimmermann CM, Baldassi D, Chan K, Adams NBP, Neumann A, Porras-Gonzalez DL, et al. Spray drying siRNA-lipid nanoparticles for dry powder pulmonary delivery. J Control Release [Internet]. 2022;351(September):137–50. Available from: https://doi.org/10.1016/j.jconrel.2022.09.021

33. Raemdonck K, Braeckmans K, Demeester J, De Smedt SC. Merging the best of both worlds: Hybrid lipid-enveloped matrix nanocomposites in drug delivery. Chem Soc Rev. 2014;43(1):444–72.

34. Conte G, Costabile G, Baldassi D, Rondelli V, Bassi R, Colombo D, et al. Hybrid Lipid/Polymer Nanoparticles to Tackle the Cystic Fibrosis Mucus Barrier in siRNA Delivery to the Lungs: Does PEGylation Make the Difference? ACS Appl Mater Interfaces. 2022;14(6):7565–78.

35. Baldassi D, Ngo TMH, Merkel OM. Optimization of Lung Surfactant Coating of siRNA Polyplexes for Pulmonary Delivery. Pharm Res [Internet]. 2022;(0123456789). Available from: https://doi.org/10.1007/s11095-022-03443-3

36. Kuzmov A, Minko T. Nanotechnology approaches for inhalation treatment of lung diseases. J Control Release [Internet]. 2015;219:500–18. Available from: https://doi.org/10.1016/j.jconrel.2015.07.024

37. Huang Z, Kłodzińska SN, Wan F, Nielsen HM. Nanoparticle-mediated pulmonary drug delivery: state of the art towards efficient treatment of recalcitrant respiratory tract bacterial infections. Drug Deliv Transl Res [Internet]. 2021;11(4):1634–54. Available from: https://doi.org/10.1007/s13346-021-00954-1

38. Moreno-Sastre M, Pastor M, Salomon CJ, Esquisabel A, Pedraz JL. Pulmonary drug delivery: A review on nanocarriers for antibacterial chemotherapy. J Antimicrob Chemother. 2015;70(11):2945–55.

39. Ungaro F, D'Angelo I, Coletta C, D'Emmanuele Di Villa Bianca R, Sorrentino R, Perfetto B, et al. Dry powders based on PLGA nanoparticles for pulmonary delivery of antibiotics: Modulation of encapsulation efficiency, release rate and lung deposition pattern by hydrophilic polymers. J Control Release [Internet]. 2012;157(1):149–59. Available from: http://dx.doi.org/10.1016/j.jconrel.2011.08.010

40. Mangal S, Gao W, Li T, Zhou QT. Pulmonary delivery of nanoparticle chemotherapy for the treatment of lung cancers: Challenges and opportunities. Acta Pharmacol Sin [Internet]. 2017;38(6):782–97. Available from: http://dx.doi.org/10.1038/aps.2017.34

41. Ware LB. Modeling human lung disease in animals. Am J Physiol Cell Mol Physiol. 2008 Feb;294(2):L149–50.

42. Primavessy D, Metz J, Schnur S, Schneider M, Lehr CM, Hittinger M. Pulmonary in vitro instruments for the replacement of animal experiments. Eur J Pharm Biopharm [Internet]. 2021;168(August):62–75. Available from: https://doi.org/10.1016/j.ejpb.2021.08.005

43. Zscheppang K, Berg J, Hedtrich S, Verheyen L, Wagner DE, Suttorp N, et al. Human Pulmonary 3D Models For Translational Research. Biotechnol J. 2018;13(1):1–12.

44. Silva S, Bicker J, Falcão A, Fortuna A. Air-liquid interface (ALI) impact on different respiratory cell cultures. Eur J Pharm Biopharm. 2023;184(January):62–82.

45. Baldassi D, Gabold B, Merkel OM. Air−Liquid Interface Cultures of the Healthy and Diseased Human Respiratory Tract: Promises, Challenges, and Future Directions. Adv NanoBiomed Res. 2021;1(6):2000111.

46. Francis I, Shrestha J, Paudel KR, Hansbro PM, Warkiani ME, Saha SC. Recent advances in lung-on-a-chip models. Drug Discov Today [Internet]. 2022;27(9):2593–602. Available from: https://doi.org/10.1016/j.drudis.2022.06.004

47. Liu G, Betts C, Cunoosamy DM, Åberg PM, Hornberg JJ, Sivars KB, et al. Use of precision cut lung slices as a translational model for the study of lung biology. Respir Res. 2019;20(1):1–14.

48. Zhang MM, Bahal R, Rasmussen TP, Manautou JE, Zhong X bo. The growth of siRNA-based therapeutics: Updated clinical studies. Biochem Pharmacol. 2021;189:114432.

49. Lamb YN. Inclisiran: First Approval. Drugs [Internet]. 2021;81(3):389–95. Available from: https://doi.org/10.1007/s40265-021-01473-6

50. Tieu T, Wei Y, Cifuentes-Rius A, Voelcker NH. Overcoming Barriers: Clinical Translation of siRNA Nanomedicines. Adv Ther. 2021;4(9):1–24.

51. Vicentini FTMDC, Borgheti-Cardoso LN, Depieri LV, De MacEdo Mano D, Abelha TF, Petrilli R, et al. Delivery systems and local administration routes for therapeutic siRNA. Pharm Res. 2013;30(4):915–31.

52. Mendes BB, Conniot J, Avital A, Yao D, Jiang X, Zhou X, et al. Nanodelivery of nucleic acids. Nat Rev Methods Prim. 2022;2(1).

53. Keil TWM, Baldassi D, Merkel OM. T-cell targeted pulmonary siRNA delivery for the treatment of asthma. Wiley Interdiscip Rev Nanomedicine Nanobiotechnology. 2020;12(5):1–11.

54. Bohr A, Tsapis N, Foged C, Andreana I, Yang M, Fattal E. Treatment of acute lung inflammation by pulmonary delivery of anti-TNF-α siRNA with PAMAM dendrimers in a murine model. Eur J Pharm Biopharm [Internet]. 2020;156(April):114–20. Available from: https://doi.org/10.1016/j.ejpb.2020.08.009

55. Baldassi D, Ambike S, Feuerherd M, Cheng C-C, Peeler DJ, Feldmann DP, et al. Inhibition of SARS-CoV-2 replication in the lung with siRNA/VIPER polyplexes. J Control Release [Internet]. 2022;345(March):661–74. Available from: https://doi.org/10.1016/j.jconrel.2022.03.051

56. Kumar V, Yadavilli S, Kannan R. A review on RNAi therapy for NSCLC: Opportunities and challenges. Wiley Interdiscip Rev Nanomedicine Nanobiotechnology. 2021;13(2):1–26.

57. Saw PE, Song EW. siRNA therapeutics: a clinical reality. Sci China Life Sci. 2020;63(4):485–500.

58. Duncan GA, Jung J, Hanes J, Suk JS. The mucus barrier to inhaled gene therapy. Mol Ther. 2016;24(12):2043–53.

59. Goerke J. Pulmonary surfactant: Functions and molecular composition. Biochim Biophys Acta - Mol Basis Dis. 1998;1408(2–3):79–89.

60. Hu Q, Bai X, Hu G, Zuo YY. Unveiling the Molecular Structure of Pulmonary Surfactant Corona on Nanoparticles. ACS Nano. 2017;11(7):6832–42.

61. De Backer L, Cerrada A, Pérez-Gil J, De Smedt SC, Raemdonck K. Bio-inspired materials in drug delivery: Exploring the role of pulmonary surfactant in siRNA inhalation therapy. J Control Release [Internet]. 2015;220:642–50. Available from: http://dx.doi.org/10.1016/j.jconrel.2015.09.004

62. Benfer M, Kissel T. Cellular uptake mechanism and knockdown activity of siRNA-loaded biodegradable DEAPA-PVA-g-PLGA nanoparticles. Eur J Pharm Biopharm [Internet]. 2012;80(2):247–56. Available from: http://dx.doi.org/10.1016/j.ejpb.2011.10.021

63. De Backer L, Braeckmans K, Stuart MCA, Demeester J, De Smedt SC, Raemdonck K. Bio-inspired pulmonary surfactant-modified nanogels: A promising siRNA delivery system. J Control Release [Internet]. 2015;206:177–86. Available from: http://dx.doi.org/10.1016/j.jconrel.2015.03.015

64. Ernst N, Ulrichskötter S, Schmalix WA, Rädler J, Galneder R, Mayer E, et al. Interaction of Liposomal and Polycationic Transfection Complexes with Pulmonary Surfactant. J Gene Med. 1999;1(5):331–40.

65. Kandil R, Xie Y, Heermann R, Isert L, Jung K, Mehta A, et al. Coming in and Finding Out: Blending Receptor-Targeted Delivery and Efficient Endosomal Escape in a Novel Bio-Responsive siRNA Delivery System for Gene Knockdown in Pulmonary T Cells. Adv Ther. 2019;2(7):1–14.

66. Taranejoo S, Liu J, Verma P, Hourigan K. A review of the developments of characteristics of PEI derivatives for gene delivery applications. J Appl Polym Sci. 2015;132:42096.

67. Garcia-Mouton C, Hidalgo A, Cruz A, Pérez-Gil J. The Lord of the Lungs: The essential role of pulmonary surfactant upon inhalation of nanoparticles. Eur J Pharm Biopharm [Internet]. 2019;144(September):230–43. Available from: https://doi.org/10.1016/j.ejpb.2019.09.020

68. Herman L, De Smedt SC, Raemdonck K. Pulmonary surfactant as a versatile biomaterial to fight COVID-19. J Control Release [Internet]. 2022;342(July 2021):170–88. Available from: https://doi.org/10.1016/j.jconrel.2021.11.023

69. Merkel OM, Librizzi D, Pfestroff A, Schurrat T, Béhé M, Kissel T. In Vivo SPECT and real-time gamma camera imaging of biodistribution and pharmacokinetics of siRNA delivery using an optimized radiolabeling and purification procedure. Bioconjug Chem. 2009;20(1):174–82.

70. Schmiedl A, Krug N, Hohlfeld JM. Influence of plasma and inflammatory proteins on the ultrastructure of exogenous surfactant. J Electron Microsc (Tokyo). 2004;53(4):407–16.

71. García-Mouton C, Hidalgo A, Arroyo R, Echaide M, Cruz A, Pérez-Gil J. Pulmonary Surfactant and Drug Delivery: An Interface-Assisted Carrier to Deliver Surfactant Protein SP-D Into the Airways. Front Bioeng Biotechnol. 2021;8(January):1–12.

72. Tomeh MA, Zhao X. Recent Advances in Microfluidics for the Preparation of Drug and Gene Delivery Systems. Mol Pharm. 2020;17(12):4421–34.

73. Mousseau F, Puisney C, Mornet S, Le Borgne R, Vacher A, Airiau M, et al. Supported pulmonary surfactant bilayers on silica nanoparticles: Formulation, stability and impact on lung epithelial cells. Nanoscale. 2017;9(39):14967–78.

74. Murgia X, Loretz B, Hartwig O, Hittinger M, Lehr CM. The role of mucus on drug transport and its potential to affect therapeutic outcomes. Adv Drug Deliv Rev [Internet]. 2018;124:82–97. Available from: https://doi.org/10.1016/j.addr.2017.10.009

75. Keil TWM, Zimmermann C, Baldassi D, Adams F, Friess W, Mehta A, et al. Impact of Crystalline and Amorphous Matrices on Successful Spray Drying of siRNA Polyplexes for Inhalation of Nano-in-Microparticles. Adv Ther. 2021;4(6):1–15.

76. Wan H, Winton HL, Soeller C, Stewart GA, Thompson PJ, Gruenert DC, et al. Tight junction properties of the immortalized human bronchial epithelial cell lines Calu-3 anmd 16HBE14o-. Eur Respir J. 2000;15(6):1058–68.

77. Itoh M, Nagafuchi A, Moroi S, Tsukita S. Involvement of ZO-1 in cadherin-based cell adhesion through its direct binding to α catenin and actin filaments. J Cell Biol. 1997;138(1):181–92.

78. Traweger A, Fang D, Liu YC, Stelzhammer W, Krizbai IA, Fresser F, et al. The tight junction-specific protein occludin is a functional target of the E3 ubiquitin-protein ligase itch. J Biol Chem. 2002;277(12):10201–8.

79. Han X, Zhang E, Shi Y, Song B, Du H, Cao Z. Biomaterial-tight junction interaction and potential. J Mater Chem B. 2019;7(41):6310–6320.

80. Merckx P, De Backer L, Van Hoecke L, Guagliardo R, Echaide M, Baatsen P, et al. Surfactant protein B (SP-B) enhances the cellular siRNA delivery of proteolipid coated nanogels for inhalation therapy. Acta Biomater [Internet]. 2018;78:236–46. Available from: https://doi.org/10.1016/j.actbio.2018.08.012

81. van Meerloo J, Kaspers GJL, Cloos J. Cell sensitivity assays: the MTT assay. Cancer cell Cult Methods Mol Biol. 2011;731:237–45.

82. Souza C De, Daum N, Lehr C. Carrier interactions with the biological barriers of the lung : Advanced in vitro models and challenges for pulmonary drug delivery ☆. Adv Drug Deliv Rev [Internet]. 2014;75:129–40. Available from: http://dx.doi.org/10.1016/j.addr.2014.05.014

83. Forbes B, Shah A, Martin GP, Lansley AB. The human bronchial epithelial cell line 16HBE14o- as a model system of the airways for studying drug transport. Int J Pharm. 2003;257(1–2):161–7.

84. Callaghan PJ, Ferrick B, Rybakovsky E, Thomas S, Mullin JM. Epithelial barrier function properties of the 16HBE14o- human bronchial epithelial cell culture model. Biosci Rep. 2020;40(10):1–16.

85. Nahar K, Gupta N, Gauvin R, Absar S, Patel B, Gupta V, et al. In vitro , in vivo and ex vivo models for studying particle deposition and drug absorption of inhaled pharmaceuticals. Eur J Pharm Sci [Internet]. 2013;49(5):805–18. Available from: http://dx.doi.org/10.1016/j.ejps.2013.06.004

86. Hu B, Zhong L, Weng Y, Peng L, Huang Y, Zhao Y, et al. Therapeutic siRNA: state of the art. Signal Transduct Target Ther. 2020;5(1).

87. Lam JKW, Liang W, Chan HK. Pulmonary delivery of therapeutic siRNA. Adv Drug Deliv Rev [Internet]. 2012;64(1):1–15. Available from: http://dx.doi.org/10.1016/j.addr.2011.02.006

88. Ridley C, Thornton DJ. Mucins: The frontline defence of the lung. Biochem Soc Trans. 2018;46(5):1099–106.

89. Kubczak M, Michlewska S, Bryszewska M, Aigner A, Ionov M. Nanoparticles for local delivery of siRNA in lung therapy. Adv Drug Deliv Rev. 2021;179.

90. Chow M, Lam J. Dry Powder Formulation of Plasmid DNA and siRNA for Inhalation. Curr Pharm Des [Internet]. 2015;21(27):3854–66. Available from: http://www.eurekaselect.com/openurl/content.php?genre=article&issn=1381-6128&volume=21&issue=27&spage=3854

91. D'Angelo I, Conte C, Miro A, Quaglia F, Ungaro F. Pulmonary drug delivery: a role for polymeric nanoparticles? Curr Top Med Chem. 2015;15(4):386–400.

92. Kulkarni JA, Witzigmann D, Chen S, Cullis PR, Van Der Meel R. Lipid Nanoparticle Technology for Clinical Translation of siRNA Therapeutics. Acc Chem Res. 2019;52(9):2435–44.

93. Hou X, Zaks T, Langer R, Dong Y. Lipid nanoparticles for mRNA delivery. Nat Rev Mater. 2021;6(12):1078–94.

94. Nakamura T, Sato Y, Yamada Y, Abd MM, Kimura S, Younis MA, et al. Extrahepatic targeting of lipid nanoparticles in vivo with intracellular targeting for future nanomedicines. Adv Drug Deliv Rev [Internet]. 2022;188:114417. Available from: https://doi.org/10.1016/j.addr.2022.114417

95. Hald C, Kulkarni JA, Witzigmann D, Lind M, Petersson K, Simonsen JB. The role of lipid components in lipid nanoparticles for vaccines and gene therapy. Adv Drug Deliv Rev [Internet]. 2022;188:114416. Available from: https://doi.org/10.1016/j.addr.2022.114416

96. LoPresti ST, Arral ML, Chaudhary N, Whitehead KA. The replacement of helper lipids with charged alternatives in lipid nanoparticles facilitates targeted mRNA delivery to the spleen and lungs. J Control Release [Internet]. 2022;345(November 2021):819–31. Available from: https://doi.org/10.1016/j.jconrel.2022.03.046

97. Kulkarni JA, Witzigmann D, Chen S, Cullis PR, Van Der Meel R. Lipid Nanoparticle Technology for Clinical Translation of siRNA Therapeutics. Acc Chem Res. 2019;52(9):2435–44.

98. Moss OR. Simulants of lung interstitial fluid. Heal Phys. 1979;36(3):447–8.

99. Rehman ZU, Zuhorn IS, Hoekstra D. How cationic lipids transfer nucleic acids into cells and across cellular membranes: Recent advances. J Control Release [Internet]. 2013;166(1):46–56. Available from: http://dx.doi.org/10.1016/j.jconrel.2012.12.014

100. Cheng X, Lee RJ. The role of helper lipids in lipid nanoparticles (LNPs) designed for oligonucleotide delivery. Adv Drug Deliv Rev [Internet]. 2016;99:129–37. Available from: http://dx.doi.org/10.1016/j.addr.2016.01.022

101. Schroeder A, Levins CG, Cortez C, Langer R, Anderson DG. Lipid-based nanotherapeutics for siRNA delivery. J Intern Med. 2010;267(1):9–21.

102. Fröhlich E. The role of surface charge in cellular uptake and cytotoxicity of medical nanoparticles. Int J Nanomedicine. 2012;7:5577–91.

103. Moss KH, Popova P, Hadrup SR, Astakhova K, Taskova M. Lipid Nanoparticles for Delivery of Therapeutic RNA Oligonucleotides. Mol Pharm. 2019;16(6):2265–77.

104. Cui S, Wang Y, Gong Y, Lin X, Zhao Y, Zhi D, et al. Correlation of the cytotoxic effects of cationic lipids with their headgroups. Toxicol Res (Camb). 2018;7(3):473–9.

105. Grainger CI, Greenwell LL, Lockley DJ, Martin GP, Forbes B. Culture of Calu-3 Cells at the Air Interface Provides a Representative Model of the Airway Epithelial Barrier. Pharm Res. 2006;23(7):1482–90.

106. Leal J, Smyth HDC, Ghosh D. Physicochemical properties of mucus and their impact on transmucosal drug delivery. Int J Pharm. 2017;532(1):555–72.

107. Lai SK, Wang YY, Hanes J. Mucus-penetrating nanoparticles for drug and gene delivery to mucosal tissues. Adv Drug Deliv Rev. 2009;61(2):158–71.

108. Francia V, Schiffelers RM, Cullis PR, Witzigmann D. The Biomolecular Corona of Lipid Nanoparticles for Gene Therapy. Bioconjug Chem. 2020;31(9):2046–59.

109. World Health Organization. https://covid19.who.int/ [Internet]. 2021. Available from: https://covid19.who.int/

110. Leung NHL. Transmissibility and transmission of respiratory viruses. Nat Rev Microbiol [Internet]. 2021;19(8):528–45. Available from: http://dx.doi.org/10.1038/s41579-021-00535-6

111. Bridges JP, Vladar EK, Huang H, Mason RJ. Respiratory epithelial cell responses to SARS-CoV-2 in COVID-19. Thorax. 2021;thoraxjnl-2021-217561.

112. Guan W, Ni Z, Hu Y, Liang W, Ou C, He J, et al. Clinical Characteristics of Coronavirus Disease 2019 in China. N Engl J Med. 2020;382(18):1708–20.

113. FDA. https://www.fda.gov/emergency-preparedness-and-response/coronavirus-disease-2019-covid-19/covid-19-vaccines. 2021.

114. EMA. https://www.ema.europa.eu/en/human-regulatory/overview/public-health-threats/coronavirus-disease-covid-19/treatments-vaccines/covid-19-vaccines. 2021.

115. Wang Y, Zhang D, Du G, Du R, Zhao J, Jin Y, et al. Remdesivir in adults with severe COVID-19: a randomised, double-blind, placebo-controlled, multicentre trial. Lancet [Internet]. 2020;395(10236):1569–78. Available from: http://dx.doi.org/10.1016/S0140-6736(20)31022-9

116. Pfizer press release. https://www.pfizer.com/news/press-release/press-release-detail/pfizer-announces-additional-phase-23-study-results. 2021.

117. Jayk Bernal A, Gomes da Silva MM, Musungaie DB, Kovalchuk E, Gonzalez A, Delos Reyes V, et al. Molnupiravir for Oral Treatment of Covid-19 in Nonhospitalized Patients. N Engl J Med [Internet]. 2021;1–12. Available from: http://www.ncbi.nlm.nih.gov/pubmed/34914868

118. V'kovski P, Kratzel A, Steiner S, Stalder H, Thiel V. Coronavirus biology and replication: implications for SARS-CoV-2. Nat Rev Microbiol [Internet]. 2021;19(3):155–70. Available from: http://dx.doi.org/10.1038/s41579-020-00468-6

119. Levanova A, Poranen MM. RNA interference as a prospective tool for the control of human viral infections. Front Microbiol. 2018;9(SEP).

120. Ambike S, Cheng C, Feuerherd M, Velkov S, Baldassi D, Afridi SQ, et al. Targeting genomic SARS-CoV-2 RNA with siRNAs allows efficient inhibition of viral replication and spread. Nucleic Acids Res. 2021;1–17.

121. Azzi L, Gasperina DD, Veronesi G, Shallak M, Ietto G, Iovino D, et al. Mucosal immune response in BNT162b2 COVID-19 vaccine recipients. EBioMedicine. 2022;75:103788.

122. Cipolla D, Gonda I, Chan HK. Liposomal formulations for inhalation. Ther Deliv. 2013;4(8):1047–72.

123. Cheng Y, Yumul RC, Pun SH. Virus-Inspired Polymer for Efficient In Vitro and In Vivo Gene Delivery. Angew Chemie - Int Ed. 2016;55(39):12013–7.

124. Feldmann DP, Cheng Y, Kandil R, Xie Y, Mohammadi M, Harz H, et al. In vitro and in vivo delivery of siRNA via VIPER polymer system to lung cells. J Control Release [Internet]. 2018;276(February):50–8. Available from:

https://doi.org/10.1016/j.jconrel.2018.02.017

125. Degors IMS, Wang C, Rehman ZU, Zuhorn IS. Carriers break barriers in drug delivery: endocytosis and endosomal escape of gene delivery vectors. Acc Chem Res. 2019;52(7):1750–60.

126. Peeler DJ, Thai SN, Cheng Y, Horner PJ, Sellers DL, Pun SH. pH-sensitive polymer micelles provide selective and potentiated lytic capacity to venom peptides for effective intracellular delivery. Biomaterials [Internet]. 2019;192(November 2018):235–44. Available from: https://doi.org/10.1016/j.biomaterials.2018.11.004

127. Xie Y, Kim NH, Nadithe V, Schalk D, Thakur A, Kılıç A, et al. Targeted delivery of siRNA to activated T cells via transferrin-polyethylenimine (Tf-PEI) as a potential therapy of asthma. J Control Release. 2016;229:120–9.

128. Gerckens M, Alsafadi HN, Wagner DE, Lindner M, Burgstaller G, Königshoff M. Generation of Human 3D Lung Tissue Cultures (3D-LTCs) for Disease Modeling. J Vis Exp. 2019;(144):1–8.

129. Alsafadi HN, Staab-Weijnitz CA, Lehmann M, Lindner M, Peschel B, Königshoff M, et al. An ex vivo model to induce early fibrosis-like changes in human precision-cut lung slices. Am J Physiol - Lung Cell Mol Physiol. 2017;312(6):L896–902.

130. Merkel OM, Marsh LM, Garn H, Kissel T. Flow cytometry-based cell type-specific assessment of target regulation by pulmonary siRNA delivery. Methods Mol Biol. 2013;948(1):1–7.

131. Pramanik S, Mohanto S, Manne R, Rajendran RR, Deepak A, Edapully SJ, et al. Nanoparticle-Based Drug Delivery System: The Magic Bullet for the Treatment of Chronic Pulmonary Diseases. Mol Pharm. 2021;18(10):3671–718.

132. Abstiens K, Goepferich AM. Microfluidic manufacturing improves polydispersity of multicomponent polymeric nanoparticles. J Drug Deliv Sci Technol [Internet]. 2019;49(October 2018):433–9. Available from: https://doi.org/10.1016/j.jddst.2018.12.009

133. Feldmann DP, Merkel OM. The advantages of pulmonary delivery of therapeutic siRNA. Ther Deliv. 2016;7(2):117–38.

134. Wei H, Volpatti LR, Sellers DL, Maris DO, Andrews IW, Hemphill AS, et al. Dual responsive, stabilized nanoparticles for efficient in vivo plasmid delivery. Angew Chemie - Int Ed. 2013;52(20):5377–81.

135. Paray BA, Ahmad A, Khan JM, Taufiq F, Pathan A, Malik A, et al. The role of the multifunctional antimicrobial peptide melittin in gene delivery. Drug Discov Today [Internet]. 2021;26(4):1053–9. Available from: https://doi.org/10.1016/j.drudis.2021.01.004

136. Peeler DJ, Yen A, Luera N, Stayton PS, Pun SH. Lytic Polyplex Vaccines Enhance Antigen-Specific Cytotoxic T Cell Response through Induction of Local Cell Death. Adv Ther. 2021;4(8):1–11.

137. Heinen N, Klöhn M, Steinmann E, Pfaender S. In vitro lung models and their application to study sars-cov-2 pathogenesis and disease. Viruses. 2021;13(5).

138. Braakhuis HM, He R, Vandebriel RJ, Gremmer ER, Zwart E, Vermeulen JP, et al. An air-liquid interface bronchial epithelial model for realistic, repeated inhalation exposure to

airborne particles for toxicity testing. J Vis Exp. 2020;2020(159):1–10.

139. Mura S, Hillaireau H, Nicolas J, Kerdine-Römer S, Le Droumaguet B, Deloménie C, et al. Biodegradable nanoparticles meet the bronchial airway barrier: How surface properties affect their interaction with mucus and epithelial cells. Biomacromolecules. 2011;12(11):4136–43.

140. Merkel OM, Beyerle A, Beckmann BM, Zheng M, Hartmann RK, Stöger T, et al. Polymer-related off-target effects in non-viral siRNA delivery. Biomaterials [Internet]. 2011;32(9):2388–98. Available from: http://dx.doi.org/10.1016/j.biomaterials.2010.11.081

141. Murgia X, Pawelzyk P, Schaefer UF, Wagner C, Willenbacher N, Lehr CM. Size-Limited Penetration of Nanoparticles into Porcine Respiratory Mucus after Aerosol Deposition. Biomacromolecules. 2016;17(4):1536–42.

142. Hoffmann M, Kleine-Weber H, Schroeder S, Krüger N, Herrler T, Erichsen S, et al. SARS-CoV-2 Cell Entry Depends on ACE2 and TMPRSS2 and Is Blocked by a Clinically Proven Protease Inhibitor. Cell. 2020;181(2):271-280.e8.

143. Jia H, Yue X, Lazartigues E. ACE2 mouse models: a toolbox for cardiovascular and pulmonary research. Nat Commun [Internet]. 2020;11(1). Available from: http://dx.doi.org/10.1038/s41467-020-18880-0

144. Puelles VG, Lütgehetmann M, Lindenmeyer MT, Sperhake JP, Wong MN, Allweiss L, Chilla S, Heinemann A, Wanner N, Liu S, Braun F, Lu S, Pfefferle S, Schröder AS, Edler C, Gross O, Glatzel M, Wichmann D, Wiech T, Kluge S, Pueschel K, Aepfelbacher M HT. Multiorgan and Renal Tropism of SARS-CoV-2. N Engl J Med. 2020;383(6):590–2.

145. Viana F, O'Kane CM, Schroeder GN. Precision-cut lung slices: A powerful ex vivo model to investigate respiratory infectious diseases. Mol Microbiol. 2021;(September):1–11.

146. Rosales Gerpe MC, van Vloten JP, Santry LA, de Jong J, Mould RC, Pelin A, et al. Use of Precision-Cut Lung Slices as an Ex Vivo Tool for Evaluating Viruses and Viral Vectors for Gene and Oncolytic Therapy. Mol Ther - Methods Clin Dev [Internet]. 2018;10(September):245–56. Available from: https://doi.org/10.1016/j.omtm.2018.07.010

147. Ruigrok MJR, Xian JL, Frijlink HW, Melgert BN, Hinrichs WLJ, Olinga P. siRNA-mediated protein knockdown in precision-cut lung slices. Eur J Pharm Biopharm [Internet]. 2018;133(October):339–48. Available from: https://doi.org/10.1016/j.ejpb.2018.11.005

148. Foster DJ, Brown CR, Shaikh S, Trapp C, Schlegel MK, Qian K, et al. Advanced siRNA Designs Further Improve In Vivo Performance of GalNAc-siRNA Conjugates. Mol Ther. 2018;26(3):708–17.

149. Ryu G, Shin HW. Sars-cov-2 infection of airway epithelial cells. Immune Netw. 2021;21(1):1–16.

150. Kopf M, Schneider C, Nobs SP. The development and function of lung-resident macrophages and dendritic cells. Nat Immunol. 2015;16(1):36–44.

151. Petithory T, Pieuchot L, Josien L, Ponche A, Anselme K, Vonna L. Size-dependent internalization efficiency of macrophages from adsorbed nanoparticle-based monolayers. Nanomaterials. 2021;11(8).

152. Yin B, Chan CKW, Liu S, Hong H, Wong SHD, Lee LKC, et al. Intrapulmonary Cellular-Level

Distribution of Inhaled Nanoparticles with Defined Functional Groups and Its Correlations with Protein Corona and Inflammatory Response. ACS Nano. 2019;13(12):14048–69.

153. Lukassen S, Chua RL, Trefzer T, Kahn NC, Schneider MA, Muley T, et al. SARS -CoV-2 receptor ACE 2 and TMPRSS 2 are primarily expressed in bronchial transient secretory cells . EMBO J. 2020;39(10):1–15.

154. Liu J, Li Y, Liu Q, Yao Q, Wang X, Zhang H, et al. SARS-CoV-2 cell tropism and multiorgan infection. Cell Discov [Internet]. 2021;7(1):2–5. Available from: http://dx.doi.org/10.1038/s41421-021-00249-2

155. Beyerle A, Braun A, Merkel O, Koch F, Kissel T, Stoeger T. Comparative in vivo study of poly(ethylene imine)/siRNA complexes for pulmonary delivery in mice. J Control Release [Internet]. 2011;151(1):51–6. Available from: http://dx.doi.org/10.1016/j.jconrel.2010.12.017

156. Beyerle A, Braun A, Banerjee A, Ercal N, Eickelberg O, Kissel TH, et al. Inflammatory responses to pulmonary application of PEI-based siRNA nanocarriers in mice. Biomaterials [Internet]. 2011;32(33):8694–701. Available from: http://dx.doi.org/10.1016/j.biomaterials.2011.07.082

157. Lyczak JB, Cannon CL, Pier GB. Lung infections associated with cystic fibrosis. Clin Microbiol Rev. 2002 Apr;15(2):194–222.

158. Vooturi SK, Cheung CM, Rybak MJ, Firestine SM. Design, synthesis, and structure-activity relationships of benzophenone-based tetraamides as novel antibacterial agents. J Med Chem. 2009 Aug;52(16):5020–31.

159. Vooturi SK, Dewal MB, Firestine SM. Examination of a synthetic benzophenone membrane-targeted antibiotic. Org Biomol Chem. 2011 Sep;9(18):6367–72.

160. Wang X, Wang X, Teng D, Mao R, Hao Y, Yang N, et al. Increased intracellular activity of MP1102 and NZ2114 against Staphylococcus aureus in vitro and in vivo. Sci Rep. 2018 Mar;8(1):4204.

161. Garzoni C, Kelley WL. Staphylococcus aureus: new evidence for intracellular persistence. Trends Microbiol. 2009 Feb;17(2):59–65.

162. Kubica M, Guzik K, Koziel J, Zarebski M, Richter W, Gajkowska B, et al. A potential new pathway for Staphylococcus aureus dissemination: the silent survival of S. aureus phagocytosed by human monocyte-derived macrophages. PLoS One. 2008 Jan;3(1):e1409.

163. Abed N, Couvreur P. Nanocarriers for antibiotics: a promising solution to treat intracellular bacterial infections. Int J Antimicrob Agents. 2014 Jun;43(6):485–96.

164. Liang Z, Ni R, Zhou J, Mao S. Recent advances in controlled pulmonary drug delivery. Drug Discov Today. 2015 Mar;20(3):380–9.

165. Cutuli MA, Petronio Petronio G, Vergalito F, Magnifico I, Pietrangelo L, Venditti N, et al. Galleria mellonella as a consolidated in vivo model hosts: New developments in antibacterial strategies and novel drug testing. Virulence. 2019 Dec;10(1):527–41.

166. Deacon J, Abdelghany SM, Quinn DJ, Schmid D, Megaw J, Donnelly RF, et al. Antimicrobial efficacy of tobramycin polymeric nanoparticles for Pseudomonas aeruginosa infections in cystic fibrosis: formulation, characterisation and functionalisation with dornase alfa (DNase). J Control release Off J Control Release Soc. 2015 Jan;198:55–61.

167. Jiang L, Greene MK, Insua JL, Pessoa JS, Small DM, Smyth P, et al. Clearance of intracellular Klebsiella pneumoniae infection using gentamicin-loaded nanoparticles. J Control release Off J Control Release Soc. 2018 Jun;279:316–25.

168. Costabile G, Provenzano R, Azzalin A, Scoffone VC, Chiarelli LR, Rondelli V, et al. PEGylated mucus-penetrating nanocrystals for lung delivery of a new FtsZ inhibitor against Burkholderia cenocepacia infection. Nanomedicine. 2020 Jan;23:102113.

169. Vooturi SK, Firestine SM. Solution-phase parallel synthesis of novel membrane-targeted antibiotics. J Comb Chem. 2010;12(1):151–60.

170. Costabile G, Gasteyer KI, Nadithe V, Van Denburgh K, Lin Q, Sharma S, et al. Physicochemical and In Vitro Evaluation of Drug Delivery of an Antibacterial Synthetic Benzophenone in Biodegradable PLGA Nanoparticles. AAPS PharmSciTech. 2018 Nov;19(8):3561–70.

171. Müller C, Wagner AL, Rockinger U, Winter G, Bracher F. Development of a convenient method for the determination of dimethyl sulfoxide in lyophilised pharmaceuticals by static headspace gas chromatography-mass spectrometry. Anal Methods [Internet]. 2019;11(16):2119–22. Available from: http://dx.doi.org/10.1039/C8AY02574F

172. Günday Türeli N, Torge A, Juntke J, Schwarz BC, Schneider-Daum N, Türeli AE, et al. Ciprofloxacin-loaded PLGA nanoparticles against cystic fibrosis P. aeruginosa lung infections. Eur J Pharm Biopharm Off J Arbeitsgemeinschaft fur Pharm Verfahrenstechnik eV. 2017 Aug;117:363–71.

173. Andima M, Costabile G, Isert L, Ndakala AJ, Derese S, Merkel OM. Evaluation of β-Sitosterol Loaded PLGA and PEG-PLA Nanoparticles for Effective Treatment of Breast Cancer: Preparation, Physicochemical Characterization, and Antitumor Activity. Pharmaceutics. 2018 Nov;10(4).

174. Sanders NN, De Smedt SC, Van Rompaey E, Simoens P, De Baets F, Demeester J. Cystic fibrosis sputum: A barrier to the transport of nanospheres. Am J Respir Crit Care Med. 2000;162(5):1905–11.

175. Lim YH, Tiemann KM, Hunstad DA, Elsabahy M, Wooley KL. Polymeric nanoparticles in development for treatment of pulmonary infectious diseases. Wiley Interdiscip Rev Nanomed Nanobiotechnol. 2016 Nov;8(6):842–71.

176. Kozak D, Anderson W, Vogel R, Chen S, Antaw F, Trau M. Simultaneous size and ζ-potential measurements of individual nanoparticles in dispersion using size-tunable pore sensors. ACS Nano. 2012 Aug;6(8):6990–7.

177. Kozak D, Anderson W, Vogel R, Trau M. Advances in Resistive Pulse Sensors: Devices bridging the void between molecular and microscopic detection. Nano Today. 2011 Oct;6(5):531–45.

178. Hartl N, Adams F, Costabile G, Isert L, Döblinger M, Xiao X, et al. The Impact of Nylon-3 Copolymer Composition on the Efficiency of siRNA Delivery to Glioblastoma Cells. Nanomater (Basel, Switzerland). 2019 Jul;9(7).

179. De Jaeghere F, Allémann E, Leroux JC, Stevels W, Feijen J, Doelker E, et al. Formulation and lyoprotection of poly(lactic acid-co-ethylene oxide) nanoparticles: influence on physical stability and in vitro cell uptake. Pharm Res. 1999 Jun;16(6):859–66.

180. Konan YN, Gurny R, Allémann E. Preparation and characterization of sterile and freeze-dried sub-200 nm nanoparticles. Int J Pharm. 2002 Feb;233(1–2):239–52.

181. Franks F. Freeze-drying of bioproducts: putting principles into practice. Eur J Pharm Biopharm Off J Arbeitsgemeinschaft fur Pharm Verfahrenstechnik eV. 1998 May;45(3):221–9.

182. Pilcer G, Amighi K. Formulation strategy and use of excipients in pulmonary drug delivery. Int J Pharm. 2010 Jun;392(1–2):1–19.

183. Costabile G, d'Angelo I, Rampioni G, Bondì R, Pompili B, Ascenzioni F, et al. Toward Repositioning Niclosamide for Antivirulence Therapy of Pseudomonas aeruginosa Lung Infections: Development of Inhalable Formulations through Nanosuspension Technology. Mol Pharm. 2015 Aug;12(8):2604–17.

184. Shelley H, Babu RJ. Role of Cyclodextrins in Nanoparticle-Based Drug Delivery Systems. J Pharm Sci. 2018 Jul;107(7):1741–53.

185. Loftsson T, Brewster ME. Cyclodextrins as functional excipients: methods to enhance complexation efficiency. J Pharm Sci. 2012 Sep;101(9):3019–32.

186. Breakpoint tables for interpretation of MICs and zone diameters. Version 8.1, 2018. [Internet]. 2018. Available from: http://www.eucast.org

187. Denizot F, Lang R. Rapid colorimetric assay for cell growth and survival. Modifications to the tetrazolium dye procedure giving improved sensitivity and reliability. J Immunol Methods. 1986 May;89(2):271–7.

188. Mosmann T. Rapid colorimetric assay for cellular growth and survival: application to proliferation and cytotoxicity assays. J Immunol Methods. 1983 Dec;65(1–2):55–63.

189. Elmowafy EM, Tiboni M, Soliman ME. Biocompatibility, biodegradation and biomedical applications of poly(lactic acid)/poly(lactic-co-glycolic acid) micro and nanoparticles [Internet]. Vol. 49, Journal of Pharmaceutical Investigation. Springer Singapore; 2019. 347–380 p. Available from: https://doi.org/10.1007/s40005-019-00439-x

190. Kumar P, Nagarajan A, Uchil PD. Analysis of Cell Viability by the Lactate Dehydrogenase Assay. Cold Spring Harb Protoc. 2018 Jun;2018(6).

191. Flannagan RS, Heinrichs DE. Macrophage-driven nutrient delivery to phagosomal Staphylococcus aureus supports bacterial growth. EMBO Rep. 2020 Aug;21(8):e50348.

192. Bege N, Renette T, Jansch M, Reul R, Merkel O, Petersen H, et al. Biodegradable poly(ethylene carbonate) nanoparticles as a promising drug delivery system with "stealth" potential. Macromol Biosci. 2011 Jul;11(7):897–904.

193. Mosaiab T, Farr DC, Kiefel MJ, Houston TA. Carbohydrate-based nanocarriers and their application to target macrophages and deliver antimicrobial agents. Adv Drug Deliv Rev. 2019;151–152:94–129.

194. Imbuluzqueta E, Gamazo C, Ariza J, Blanco-Prieto MJ. Drug delivery systems for potential treatment of intracellular bacterial infections. Front Biosci (Landmark Ed. 2010 Jan;15(2):397–417.

195. Subramaniam S, Joyce P, Thomas N, Prestidge CA. Bioinspired drug delivery strategies for repurposing conventional antibiotics against intracellular infections. Adv Drug Deliv Rev. 2021 Oct;177:113948.

196. Tsai CJ-Y, Loh JMS, Proft T. Galleria mellonella infection models for the study of bacterial diseases and for antimicrobial drug testing. Virulence. 2016 Apr;7(3):214–29.

197. Medveov A, Valk ubomr. Staphylococcus aureus: Characterisation and Quantitative Growth Description in Milk and Artisanal Raw Milk Cheese Production. Struct Funct Food Eng. 2012;(June 2014).

198. Zhou QT, Leung SSY, Tang P, Parumasivam T, Loh ZH, Chan H-K. Inhaled formulations and pulmonary drug delivery systems for respiratory infections. Adv Drug Deliv Rev. 2015 May;85:83–99.

199. Network GA. The Global Asthma Report 2018 [Internet]. 2018. Available from: http://globalasthmareport.org/burden/burden.php

200. Sel S, Wegmann M, Dicke T, Sel S, Henke W, Yildirim AO, et al. Effective prevention and therapy of experimental allergic asthma using a GATA-3-specific DNAzyme. J Allergy Clin Immunol. 2008 Apr;121(4):910-916.e5.

201. Weckmann M, Collison A, Simpson JL, Kopp M V, Wark PAB, Smyth MJ, et al. Critical link between TRAIL and CCL20 for the activation of TH2 cells and the expression of allergic airway disease. Nat Med. 2007 Nov;13(11):1308–15.

202. Wegmann M, Fehrenbach H, Fehrenbach A, Held T, Schramm C, Garn H, et al. Involvement of distal airways in a chronic model of experimental asthma. Clin Exp allergy J Br Soc Allergy Clin Immunol. 2005 Oct;35(10):1263–71.

203. de Groot JC, Ten Brinke A, Bel EH. Management of the patient with eosinophilic asthma: a new era begins. ERJ Open Res. 2015;1(1):00024–2015.

204. Walker JA, Barlow JL, McKenzie ANJ. Innate lymphoid cells--how did we miss them? Nat Rev Immunol. 2013 Feb;13(2):75–87.

205. Ray A, Cohn L. Th2 cells and GATA-3 in asthma: New insights into the regulation of airway inflammation. J Clin Invest. 1999;104(8):985–93.

206. Krug N, Hohlfeld JM, Buhl R, Renz J, Garn H, Renz H. Blood eosinophils predict therapeutic effects of a GATA3-specific DNAzyme in asthma patients. Vol. 140, The Journal of allergy and clinical immunology. United States; 2017. p. 625-628.e5.

207. Lively TN, Kossen K, Balhorn A, Koya T, Zinnen S, Takeda K, et al. Effect of chemically modified IL-13 short interfering RNA on development of airway hyperresponsiveness in mice. J Allergy Clin Immunol. 2008;121(1):88–94.

208. Hannon GJ. RNA interference. Nature. 2002 Jul;418(6894):244–51.

209. Liu Y, Nguyen J, Steele T, Merkel O, Kissel T. A new synthesis method and degradation of hyper-branched polyethylenimine grafted polycaprolactone block mono-methoxyl poly (ethylene glycol) copolymers (hy-PEI-g-PCL-b-mPEG) as potential DNA delivery vectors. Polymer (Guildf). 2009;50(16):3895–904.

210. Olden BR, Cheng Y, Yu JL, Pun SH. Cationic polymers for non-viral gene delivery to human T cells. J Control release Off J Control Release Soc. 2018 Jul;282:140–7.

211. Weber S, Zimmer A, Pardeike J. Solid Lipid Nanoparticles (SLN) and Nanostructured Lipid Carriers (NLC) for pulmonary application: a review of the state of the art. Eur J Pharm Biopharm Off J Arbeitsgemeinschaft fur Pharm Verfahrenstechnik eV. 2014 Jan;86(1):7–22.

212. Okuda T, Morishita M, Mizutani K, Shibayama A, Okazaki M, Okamoto H. Development of spray-freeze-dried siRNA/PEI powder for inhalation with high aerosol performance and strong pulmonary gene silencing activity. J Control release Off J Control Release Soc.

2018 Jun;279:99–113.

213. Schulze J, Kuhn S, Hendrikx S, Schulz-Siegmund M, Polte T, Aigner A. Spray-Dried Nanoparticle-in-Microparticle Delivery Systems (NiMDS) for Gene Delivery, Comprising Polyethylenimine (PEI)-Based Nanoparticles in a Poly(Vinyl Alcohol) Matrix. Small. 2018 Mar;14(12):e1701810.

214. Barnes PJ. Cytokine modulators as novel therapies for asthma. Annu Rev Pharmacol Toxicol. 2002;42(1):81–9.

215. Ishmael FT. The inflammatory response in the pathogenesis of asthma. J Am Osteopath Assoc. 2011 Nov;111(11 Suppl 7):S11-7.

216. Kaletaş BK, van der Wiel IM, Stauber J, Güzel C, Kros JM, Luider TM, et al. Sample preparation issues for tissue imaging by imaging MS. Proteomics. 2009 May;9(10):2622–33.

217. Dicke T, Wegmann M, Sel S, Renz H, Garn H. Gata-3-specific Dnazyme As An Appraoch For Asthma-therapy. J Allergy Clin Immunol. 2007;119(1):S1.

218. Montixi C, Langlet C, Bernard AM, Thimonier J, Dubois C, Wurbel MA, et al. Engagement of T cell receptor triggers its recruitment to low-density detergent-insoluble membrane domains. EMBO J. 1998;17(18):5334–48.

219. Galbraith RM, Werner P, Arnaud P, Galbraith GM. Transferrin binding to peripheral blood lymphocytes activated by phytohemagglutinin involves a specific receptor. Ligand interaction. J Clin Invest. 1980;66(5):1135–43.

220. Kim NH, Nadithe V, Elsayed M, Merkel OM. Tracking and treating activated T cells. J Drug Deliv Sci Technol. 2013;23(1):17–21.

221. Ramishetti S, Kedmi R, Goldsmith M, Leonard F, Sprague AG, Godin B, et al. Systemic Gene Silencing in Primary T Lymphocytes Using Targeted Lipid Nanoparticles. ACS Nano. 2015 Jul;9(7):6706–16.

222. Saraiva M, O'Garra A. The regulation of IL-10 production by immune cells. Nat Rev Immunol. 2010 Mar;10(3):170–81.

223. Chu, I. M., Michalowski AM, Hoenerhoff M, Szauter KM, Luger D, Sato M, et al. GATA3 inhibits lysyl oxidase-mediated metastases of human basal triple-negative breast cancer cells. Oncogene. 2012;31(16):2017–27.

224. Kandil R, Feldmann D, Xie Y, Merkel OM. Evaluating the Regulation of Cytokine Levels After siRNA Treatment in Antigen-Specific Target Cell Populations via Intracellular Staining. Methods Mol Biol. 2019;1943:323–31.

225. Smith SA, Selby LI, Johnston APR, Such GK. The Endosomal Escape of Nanoparticles: Toward More Efficient Cellular Delivery. Bioconjug Chem. 2019 Feb;30(2):263–72.

226. Selby LI, Cortez-Jugo CM, Such GK, Johnston APR. Nanoescapology: progress toward understanding the endosomal escape of polymeric nanoparticles. Wiley Interdiscip Rev Nanomed Nanobiotechnol. 2017 Sep;9(5).

227. Olden BR, Cheng E, Cheng Y, Pun SH. Identifying key barriers in cationic polymer gene delivery to human T cells. Biomater Sci. 2019 Feb;7(3):789–97.

228. Hou KK, Pan H, Lanza GM, Wickline SA. Melittin derived peptides for nanoparticle based siRNA transfection. Biomaterials. 2013 Apr;34(12):3110–9.

229. Elsayed M, Corrand V, Kolhatkar V, Xie Y, Kim NH, Kolhatkar R, et al. Influence of oligospermines architecture on their suitability for siRNA delivery. Biomacromolecules. 2014 Apr;15(4):1299–310.

230. Merkel OM, Zheng M, Debus H, Kissel T. Pulmonary gene delivery using polymeric nonviral vectors. Bioconjug Chem. 2012 Jan;23(1):3–20.

231. Merkel OM, Librizzi D, Pfestroff A, Schurrat T, Buyens K, Sanders NN, et al. Stability of siRNA polyplexes from poly(ethylenimine) and poly(ethylenimine)-g-poly(ethylene glycol) under in vivo conditions: Effects on pharmacokinetics and biodistribution measured by Fluorescence Fluctuation Spectroscopy and Single Photon Emission Com. J Control Release [Internet]. 2009;138(2):148–59. Available from: http://dx.doi.org/10.1016/j.jconrel.2009.05.016

232. Griesenbach U, Geddes DM, Alton EWFW. Gene therapy for cystic fibrosis: an example for lung gene therapy. Gene Ther. 2004 Oct;11 Suppl 1(Suppl 1):S43-50.

233. Caplen NJ, Alton EW, Middleton PG, Dorin JR, Stevenson BJ, Gao X, et al. Liposome-mediated CFTR gene transfer to the nasal epithelium of patients with cystic fibrosis. Nat Med. 1995 Jan;1(1):39–46.

234. Jensen DMK, Cun D, Maltesen MJ, Frokjaer S, Nielsen HM, Foged C. Spray drying of siRNA-containing PLGA nanoparticles intended for inhalation. J Control release Off J Control Release Soc. 2010 Feb;142(1):138–45.

235. Keil TWM, Feldmann DP, Costabile G, Zhong Q, da Rocha S, Merkel OM. Characterization of spray dried powders with nucleic acid-containing PEI nanoparticles. Eur J Pharm Biopharm Off J Arbeitsgemeinschaft fur Pharm Verfahrenstechnik eV. 2019 Oct;143:61–9.

236. Vehring R. Pharmaceutical particle engineering via spray drying. Pharm Res. 2008;25(5):999–1022.

237. Zheng M, Pavan GM, Neeb M, Schaper AK, Danani A, Klebe G, et al. Targeting the blind spot of polycationic nanocarrier-based siRNA delivery. ACS Nano. 2012 Nov;6(11):9447–54.

238. Garn H, Renz H. GATA-3-specific DNAzyme — A novel approach for stratified asthma therapy. Eur J Immunol. 2017;47(1):22–30.

239. Gavitt TD, Hartmann AK, Sawant SS, Mara AB, Szczepanek SM, Rouge JL. A GATA3 Targeting Nucleic Acid Nanocapsule for in Vivo Gene Regulation in Asthma. ACS Nano. 2021;15(7):11192–201.

240. Lungwitz U, Breunig M, Blunk T, Go A. Polyethylenimine-based non-viral gene delivery systems. Eur J Pharm Biopharm 60. 2005;60:247–66.

241. Lamaze C, Dujeancourt A, Baba T, Lo CG, Benmerah A, Dautry-Varsat A. Interleukin 2 receptors and detergent-resistant membrane domains define a clathrin-independent endocytic pathway. Mol Cell. 2001;7(3):661–71.

242. Hou, Kirk K., Pan, Hua, Schlesinger, Paul H., Wickline SA. A Role for Peptides in Overcoming Endosomal Entrapment in siRNA Delivery – A Focus on Melittin. Biotechnol Adv. 2015;1(33):931–40.

243. Snyder, Stephen L., Sobocinski PZ. An improved 2,4,6-trinitrobenzenesulfonic acid method for the determination of amines. Anal Biochem. 1975;64(1):284–8.

244. Neuhaus V, Danov O, Konzok S, Obernolte H, Dehmel S, Braubach P, et al. Assessment of the cytotoxic and immunomodulatory effects of substances in human precision-cut lung slices. J Vis Exp. 2018;2018(135):1–14.

245. Niehof M, Hildebrandt T, Danov O, Arndt K, Koschmann J, Dahlmann F, et al. RNA isolation from precision-cut lung slices (PCLS) from different species. BMC Res Notes. 2017;10(1):1–10.

246. Chen L, Flies DB. Molecular mechanisms of T cell co-stimulation and co-inhibition. Nat Rev Immunol. 2013;13(4):227–42.

247. Kominsky DJ, Campbell EL, Colgan SP. Metabolic Shifts in Immunity and Inflammation. J Immunol. 2010;184(8):4062–8.

248. Ruigrok MJR, Maggan N, Willaert D, Frijlink HW, Melgert BN, Olinga P, et al. siRNA-Mediated RNA Interference in Precision-Cut Tissue Slices Prepared from Mouse Lung and Kidney. AAPS J. 2017;19(6):1855–63.

249. Boucher R. An overview of the pathogenesis of cystic fibrosis lung disease. Adv Drug Deliv Rev. 2002;54(11):1359–71.

250. Stoltz DA, Meyerholz DK, Welsh MJ. Origins of Cystic Fibrosis Lung Disease. N Engl J Med [Internet]. 2015;372(4):351–62. Available from: http://www.nejm.org/doi/10.1056/NEJMra1300109

251. Elizur A, Cannon CL, Ferkol TW. Airway inflammation in cystic fibrosis. Chest [Internet]. 2008;133(2):489–95. Available from: http://dx.doi.org/10.1378/chest.07-1631

252. Setten RL, Rossi JJ, Han S ping. The current state and future directions of RNAi-based therapeutics. Nat Rev Drug Discov [Internet]. 2019;18(6):421–46. Available from: http://dx.doi.org/10.1038/s41573-019-0017-4

253. Thanki K, Blum KG, Thakur A, Rose F, Foged C. Formulation of RNA interference-based drugs for pulmonary delivery: Challenges and opportunities. Ther Deliv. 2018;9(10):731–49.

254. d'Angelo I, Costabile G, Durantie E, Brocca P, Rondelli V, Russo A, et al. Hybrid Lipid/Polymer Nanoparticles for Pulmonary Delivery of siRNA: Development and Fate Upon *In Vitro* Deposition on the Human Epithelial Airway Barrier. J Aerosol Med Pulm Drug Deliv [Internet]. 2017;31(3):jamp.2017.1364. Available from: http://online.liebertpub.com/doi/10.1089/jamp.2017.1364

255. Mehta A, Dalle Vedove E, Isert L, Merkel OM. Targeting KRAS Mutant Lung Cancer Cells with siRNA-Loaded Bovine Serum Albumin Nanoparticles. Pharm Res. 2019;36(9):133.

256. Pantazis P, Dimas K, Wyche JH, Anant S, Houchen CW, Panyam J. Preparation of siRNA-Encapsulated PLGA Nanoparticles. 2012;(May 2015).

257. Schmid SL. Reciprocal regulation of signaling and endocytosis : Implications for the evolving cancer cell. J Cell Biol. 2017;216(9):2623–32.

258. Günther M, Lipka J, Malek A, Gutsch D, Kreyling W, Aigner A. Polyethylenimines for RNAi-mediated gene targeting in vivo and siRNA delivery to the lung. Eur J Pharm Biopharm. 2011;77(3):438–49.

259. Rosen BH, Chanson M, Gawenis LR, Liu J, Sofoluwe A, Zoso A, et al. Animal and model systems for studying cystic fibrosis. J Cyst Fibros. 2018;17(2):S28–34.

260. Ghanem R, Laurent V, Roquefort P, Haute T, Ramel S, Gall T Le, et al. Optimizations of in vitro mucus and cell culture models to better predict in vivo gene transfer in pathological lung respiratory airways: Cystic fibrosis as an example. Pharmaceutics. 2021;13(1):1–25.

261. Pelaz B, Del Pino P, Maffre P, Hartmann R, Gallego M, Rivera-Fernández S, et al. Surface Functionalization of Nanoparticles with Polyethylene Glycol: Effects on Protein Adsorption and Cellular Uptake. ACS Nano. 2015;9(7):6996–7008.

262. Holder AL, Goth-goldstein R, Lucas D, Koshland CP. Particle-Induced Artifacts in the MTT and LDH Viability Assays. Chem Res Toxicol. 2012;25(9):1885–92.

263. Wang H, Naghavi M, Allen C, Barber RM, Bhutta ZA, Carter A, et al. Global, regional, and national life expectancy, all-cause mortality, and cause-specific mortality for 249 causes of death, 1980–2015: a systematic analysis for the Global Burden of Disease Study 2015. Lancet. 2016 Oct;388(10053):1459–544.

264. Bérubé K, Aufderheide M, Breheny D, Clothier R, Combes R, Forbes B, et al. In Vitro Models of Inhalation Toxicity and Disease In Vitro Models of Inhalation Toxicity and Disease The Report of a FRAME Workshop a. Altern Lab Anim. 2009;(January).

265. Spits H, Villaudy J. Modeling human lung infections in mice. Nat Biotechnol. 2019;37(10):1129–30.

266. Shapiro SD. Animal Models of Asthma. Am J Respir Crit Care Med. 2006 Dec;174(11):1171–3.

267. Bal HS, Goshal NG. Morphology of the terminal bronchiolar region of common laboratory mammals. Lab Anim. 1988 Jan;22(1):76–82.

268. Van Patter LE, Blattner C. Advancing Ethical Principles for Non-Invasive, Respectful Research with Nonhuman Animal Participants. Soc Anim. 2020;28(2):171–90.

269. Lacroix G, Koch W, Ritter D, Gutleb AC, Larsen ST, Loret T, et al. Air-Liquid Interface in Vitro Models for Respiratory Toxicology Research: Consensus Workshop and Recommendations. Appl Vitr Toxicol. 2018;4(2):91–106.

270. Dvorak A, Tilley AE, Shaykhiev R, Wang R, Crystal RG. Do airway epithelium air-liquid cultures represent the in vivo airway epithelium transcriptome? Am J Respir Cell Mol Biol. 2011;44(4):465–73.

271. Chary A, Serchi T, Moschini E, Hennen J, Cambier S, Ezendam J, et al. An in vitro coculture system for the detection of sensitization following aerosol exposure. ALTEX. 2019;36(3):403–18.

272. Schürch S, Gehr P, Im Hof V, Geiser M, Green F. Surfactant displaces particles toward the epithelium in airways and alveoli. Respir Physiol. 1990;80(1):17–32.

273. Holt PG, Schon-Hegrad MA, Mcmenamin PG. Dendritic cells in the respiratory tract. Int Rev Immunol. 1990;6(2–3):139–49.

274. Lehnert BE. Pulmonary and thoracic macrophage subpopulations and clearance of particles from the lung. Environ Health Perspect. 1992;97:17–46.

275. BéruBé K, Prytherch Z, Job C, Hughes T. Human primary bronchial lung cell constructs: The new respiratory models. Toxicology. 2010;278(3):311–8.

276. McDowell EM, Barrett LA, Glavin F, Harris CC, Trump BF. The Respiratory Epithelium. I. Human Bronchus. J Natl Cancer Inst. 1978;61(2):539–49.

277. Awatade NT, Wong SL, Hewson CK, Fawcett LK, Kicic A, Jaffe A, et al. Human Primary Epithelial Cell Models: Promising Tools in the Era of Cystic Fibrosis Personalized Medicine. Front Pharmacol. 2018;9(December):1–11.

278. Papazian D, Würtzen PA, Hansen SWK. Polarized Airway Epithelial Models for Immunological Co-Culture Studies. Int Arch Allergy Immunol. 2016;170(1):1–21.

279. Gindele JA, Kiechle T, Benediktus K, Birk G, Brendel M, Heinemann F, et al. Intermittent exposure to whole cigarette smoke alters the differentiation of primary small airway epithelial cells in the air- liquid interface culture. Sci Rep. 2020;10:1–17.

280. Gard AL, Maloney R, Cain BP, Miller CR, Luu RJ, Coppeta JR, et al. High-Throughput Human Primary Cell-Based Airway Model for Evaluating Influenza, Coronavirus, or other Respiratory Viruses in vitro bioRxiv. 2020 Jan;2020.05.23.112797.

281. Pezzulo AA, Starner TD, Scheetz TE, Traver GL, Tilley AE, Harvey BG, et al. The air-liquid interface and use of primary cell cultures are important to recapitulate the transcriptional profile of in vivo airway epithelia. Am J Physiol - Lung Cell Mol Physiol. 2011;300(1):25–31.

282. Rothen-rutishauser B, Blank F, Mühlfeld C, Gehr P. In vitro models of the human epithelial airway barrier to study the toxic potential of particulate matter. Expert Opin Drug Metab Toxicol. 2008;4(8):1075–90.

283. Kreft ME, Lasi E, Kristan K. The Characterization of the Human Nasal Epithelial Cell Line RPMI 2650 Under Different Culture Conditions and Their Optimization for an Appropriate in vitro Nasal Model. Pharm Res. 2014;32(2):665–79.

284. Mercier C, Perek N, Delavenne X. Is RPMI 2650 a Suitable In Vitro Nasal Model for Drug Transport Studies? Vol. 43, European Journal of Drug Metabolism and Pharmacokinetics. 2018. p. 13–24.

285. Sibinovska N, Simon Ž, Kristan K. Suitability of RPMI 2650 cell models for nasal drug permeability prediction. Eur J Pharm Biopharm. 2019;145(October):85–95.

286. Reichl S, Becker K. Cultivation of RPMI 2650 cells as an in-vitro model for human transmucosal nasal drug absorption studies: Optimization of selected culture conditions. J Pharm Pharmacol. 2012;64(11):1621–30.

287. Schlachet I, Sosnik A. Mixed Mucoadhesive Amphiphilic Polymeric Nanoparticles Cross a Model of Nasal Septum Epithelium in Vitro. ACS Appl Mater Interfaces. 2019;11:21360–71.

288. Bequignon E, Dhommée C, Angely C, Thomas L, Bottier M, Escudier E, et al. FcRn-dependent transcytosis of monoclonal antibody in human nasal epithelial cells in vitro: A prerequisite for a new delivery route for therapy? Int J Mol Sci. 2019;20(6):1379.

289. Forbes B. Human airway epithelial cell lines for in vitro drug transport and metabolism. Pharm Sci Technol Today . 2000;3(1):18–27.

290. Ehrhardt C, Kneuer C, Laue M, Schaefer UF, Kim K, Lehr C. 16HBE14o- Human Bronchial Epithelial Cell Layers Express and Caveolin-1. Pharm Res. 2003;20(4):545–51.

291. Ehrhardt C, Kneuer C, Fiegel J, Hanes J, Friedrich U. Influence of apical fluid volume on the development of functional intercellular junctions in the human epithelial cell line 16HBE14o –: implications for the use of this cell line as an in vitro model for bronchial drug absorption studies. Cell Tissue Res . 2002;308(3):391–400.

292. Bleck B, Tse DB, Jaspers I, Curotto MA, Lafaille D, Reibman J, et al. Diesel Exhaust Particle-Exposed Human Bronchial Epithelial Cells Induce Dendritic Cell Maturation. J Immunol. 2006;176(12):7431–7437.

293. Mayer AK, Bartz H, Fey F, Schmidt LM, Dalpke AH. Airway epithelial cells modify immune responses by inducing an anti-inflammatory microenvironment. Eur J Immunol. 2008;38(6):1689–99.

294. Stewart CE, Torr EE, Mohd Jamili NH, Bosquillon C, Sayers I. Evaluation of Differentiated Human Bronchial Epithelial Cell Culture Systems for Asthma Research. J Allergy. 2012;2012(di):1–11.

295. Patel J, Pal D, Vangala V, Gandhi M, Mitra AK. Transport of HIV-Protease Inhibitors across 1 ⎵ , 25di-Hydroxy Vitamin D 3 -Treated Calu-3 Cell Monolayers : Modulation of P-Glycoprotein Activity. Pharm Res. 2002;19(11):1696–703.

296. Fiegel J, Ehrhardt C, Schaefer UF, Lehr C, Hanes J. Large porous particle impingement on lung epithelial cell monolayers--toward improved particle characterization in the lung. Pharm Res. 2003;20(5):788–96.

297. Shen B, Finkbeiner WE. Calu-3 : a human airway epithelial cell line that shows AMP-dependent Cl- secretion. Am J Physiol. 1994;266(5):493–501.

298. AU - Braakhuis HM, AU - He R, AU - Vandebriel RJ, AU - Gremmer ER, AU - Zwart E, AU - Vermeulen JP, et al. An Air-liquid Interface Bronchial Epithelial Model for Realistic, Repeated Inhalation Exposure to Airborne Particles for Toxicity Testing. JoVE. 2020;(159):e61210.

299. Juan C. CARABALLO Cecilia YSHII Whitney WESTPHAL Thomas MONINGER Alejandro P. COMELLAS. Ambient particulate matter affects occludin distribution and increases alveolar transepithelial electrical conductance. Respirology. 2011;16(2):340–9.

300. Lieber M, Smith B, Szakal A, Nelson-rees W, Todaro G. A CONTINUOUS TUMOR-CELL LINE FROM A HUMAN LUNG CARCINOMA WITH PROPERTIES OF TYPE TI ALVEOLAR. Int J Cancer. 1976;70:62–70.

301. Blank F, Rothen-Rutishauser BM, Schurch S, Gehr P. An Optimized In Vitro Model of the Respiratory Tract Wall to Study Particle Cell Interactions. J Aerosol Med. 2006 Sep;19(3):392–405.

302. Öhlinger K, Kolesnik T, Meindl C, Gallé B, Absenger-Novak M, Kolb-Lenz D, et al. Air-liquid interface culture changes surface properties of A549 cells. Toxicol Vitr. 2019 Oct;60:369–82.

303. Wang Y, Adamcakova-dodd A, Steines BR, Jing X, Salem AK, Thorne PS. Comparison of in vitro toxicity of aerosolized engineered nanomaterials using air-liquid interface mono-culture and co-culture models. NanoImpact. 2020;18:100215.

304. Cappellini F, Bucchianico S Di, Karri V, Latvala S, Malmlöf M, Kippler M, et al. Dry Generation of CeO 2 Nanoparticles and Deposition onto a Co-Culture of A549 and THP-1 Cells in Air-Liquid Interface — Dosimetry Considerations and Comparison to Submerged Exposure. Nanomaterials. 2020;10(4):618.

305. Lehmann AD, Daum N, Bur M, Lehr CM, Gehr P, Rothen-Rutishauser BM. An in vitro triple cell co-culture model with primary cells mimicking the human alveolar epithelial barrier. Eur J Pharm Biopharm. 2011;77(3):398–406.

306. Zhang L, Whitsett JA, Stripp BR. Regulation of Clara cell secretory protein gene transcription by thyroid transcription factor- 1. Biochim Biophys Acta. 1997;1350:359–67.

307. Rehan VK, Torday JS, Peleg S, Gennaro L, Vouros P, Padbury J, et al. 1 a , 25-Dihydroxy-3-epi-vitamin D 3 , a natural metabolite of 1 a , 25-dihydroxy vitamin D 3 : production and biological activity studies in pulmonary alveolar type II cells q. Mol Genet Metab. 2002;76:46–56.

308. Woollhead AM, Baines DL. Forskolin-induced Cell Shrinkage and Apical Translocation of Functional Enhanced Green Fluorescent Protein-Human ENaC in H441 Lung Epithelial Cell Monolayers. J Biol Chem. 2006;281(8):5158–68.

309. Papritz M, Pohl C, Wübbeke C, Moisch M, Hofmann H, Iris M, et al. Side-speci fi c effects by cadmium exposure : Apical and basolateral treatment in a coculture model of the blood – air barrier. Toxicol Appl Pharmacol. 2010;245(3):361–9.

310. Sibinovska N, Žakelj S, Roškar R, Kristan K. Suitability and functional characterization of two Calu-3 cell models for prediction of drug permeability across the airway epithelial barrier. Int J Pharm. 2020 Jul;585:119484.

311. Josset L, Menachery VD, Gralinski LE, Agnihothram S, Sova P, Carter VS, et al. Cell host response to infection with novel human coronavirus EMC predicts potential antivirals and important differences with SARS coronavirus. MBio. 2013;4(3):1–11.

312. Qian Z, Travanty EA, Oko L, Edeen K, Berglund A, Wang J, et al. Innate immune response of human alveolar type II cells infected with severe acute respiratory syndrome-coronavirus. Am J Respir Cell Mol Biol. 2013;48(6):742–8.

313. Gray TE, Guzman K, Davis CW, Abdullah LH, Nettesheim P. Mucociliary Differentiation of Serially Passaged Normal Human Tracheobronchial Epithelial Cells. Am J Respir Cell Mol Biol. 1996;14(1):104–12.

314. Sungnak W, Huang N, Bécavin C, Berg M, Queen R, Litvinukova M, et al. SARS-CoV-2 entry factors are highly expressed in nasal epithelial cells together with innate immune genes. Nat Med. 2020;26(5):681–7.

315. Abo KM, Ma L, Matte T, Huang J, Alysandratos KD, Werder RB, et al. Human iPSC-derived alveolar and airway epithelial cells can be cultured at air-liquid interface and express SARS-CoV-2 host factors. bioRxiv. 2020 Jan;2020.06.03.132639.

316. Ashraf S, Brockman-schneider R, Bochkov YA, Pasic TR, Gern JE. Biological characteristics and propagation of human rhinovirus-C in differentiated sinus epithelial cells. Virology. 2013;436(1):143–9.

317. Warner SM, Wiehler S, Michi AN, Proud D. Rhinovirus replication and innate immunity in highly differentiated human airway epithelial cells. Respir Res. 2019;20:1–13.

318. Ziegler P, Bai Y, Tian Y, Abrahamsson S, Green A, Moore J, et al. A three-dimensional Air-Liquid Interface Culture Model for the Study of Epstein-Barr virus Infection in the Nasopharynx. bioRxiv. 2020 Jan;2020.08.31.272096.

319. Jonsdottir HR, Marti S, Geerts D, Rodriguez R, Thiel V, Dijkman R. Establishment of primary transgenic human airway epithelial cell cultures to study respiratory virus–host interactions. Viruses. 2019;11(8):747.

320. Jonsdottir HR, Dijkman R. Coronaviruses and the human airway: A universal system for

virus-host interaction studies Coronaviruses: Emerging and re-emerging pathogens in humans and animals Susanna Lau Emerging viruses. Virol J. 2016;13(1):1–9.

321. De Wit E, Van Doremalen N, Falzarano D, Munster VJ. SARS and MERS: Recent insights into emerging coronaviruses. Nat Rev Microbiol. 2016;14(8):523–34.

322. Wang C, Horby PW, Hayden FG, Gao GF. A novel coronavirus outbreak of global health concern. Lancet. 2020;395(10223):470–3.

323. Zhu N, Zhang D, Wang W, Li X, Yang B, Song J, et al. A novel coronavirus from patients with pneumonia in China, 2019. N Engl J Med. 2020;382(8):727–33.

324. Lu R, Zhao X, Li J, Niu P, Yang B, Wu H, et al. Articles Genomic characterisation and epidemiology of 2019 novel coronavirus : implications for virus origins and receptor binding. Lancet. 2020;395(10224):565–74.

325. Ravindra NG, Alfajaro MM, Gasque V, Wei J, Filler RB, Huston NC, et al. Single-cell longitudinal analysis of SARS-CoV-2 infection in human bronchial epithelial cells. bioRxiv Prepr Serv Biol. 2020 May;2020.05.06.081695.

326. Polack FP, Thomas SJ, Kitchin N, Absalon J, Gurtman A, Lockhart S, et al. Safety and Efficacy of the BNT162b2 mRNA Covid-19 Vaccine. N Engl J Med. 2020 Dec;

327. Jackson LA, Anderson EJ, Rouphael NG, Roberts PC, Makhene M, Coler RN, et al. An mRNA Vaccine against SARS-CoV-2 — Preliminary Report. N Engl J Med. 2020 Jul;383(20):1920–31.

328. Sheahan TP, Sims AC, Graham RL, Menachery VD, Gralinski LE, Case JB, et al. Broad-spectrum antiviral GS-5734 inhibits both epidemic and zoonotic coronaviruses. Sci Transl Med. 2017;9(396).

329. Jiang L, Wang N, Zuo T, Shi X, Poon KMV, Wu Y, et al. Potent neutralization of MERS-CoV by human neutralizing monoclonal antibodies to the viral spike glycoprotein. Sci Transl Med. 2014;6(234):1–10.

330. Lundin A, Dijkman R, Bergström T, Kann N, Adamiak B, Hannoun C, et al. Targeting Membrane-Bound Viral RNA Synthesis Reveals Potent Inhibition of Diverse Coronaviruses Including the Middle East Respiratory Syndrome Virus. PLoS Pathog. 2014;10(5):e1004166.

331. Shalhoub S, Farahat F, Al-Jiffri A, Simhairi R, Shamma O, Siddiqi N, et al. IFN-α2a or IFN-β1a in combination with ribavirin to treat Middle East respiratory syndrome coronavirus pneumonia: A retrospective study. J Antimicrob Chemother. 2015;70(7):2129–32.

332. Liu R, Wang J, Shao Y, Wang X, Zhang H, Shuai L, et al. A recombinant VSV-vectored MERS-CoV vaccine induces neutralizing antibody and T cell responses in rhesus monkeys after single dose immunization. Antiviral Res. 2018;150(December 2017):30–8.

333. de Wilde AH, Wannee KF, Scholte FEM, Goeman JJ, ten Dijke P, Snijder EJ, et al. A Kinome-Wide Small Interfering RNA Screen Identifies Proviral and Antiviral Host Factors in Severe Acute Respiratory Syndrome Coronavirus Replication, Including Double-Stranded RNA-Activated Protein Kinase and Early Secretory Pathway Proteins. J Virol. 2015;89(16):8318–33.

334. Yoshikawa T, Hill T, Li K, Peters CJ, Tseng C-TK. Severe Acute Respiratory Syndrome (SARS) Coronavirus-Induced Lung Epithelial Cytokines Exacerbate SARS Pathogenesis by Modulating Intrinsic Functions of Monocyte-Derived Macrophages and Dendritic Cells. J

Virol. 2009;83(7):3039–48.

335. Blom RAM, Erni ST, Krempaská K, Schaerer O, Van Dijk RM, Amacker M, et al. A triple co-culture model of the human respiratory tract to study immune-modulatory effects of liposomes and virosomes. PLoS One. 2016;11(9):1–25.

336. Riordan JR, Rommens JM, Kerem BS, Alon NOA, Rozmahel R, Grzelczak Z, et al. Identification of the cystic fibrosis gene: Cloning and characterization of complementary DNA. Science (80-). 1989;245(4922):1066–73.

337. Castellani S, Di Gioia S, di Toma L, Conese M. Human cellular models for the investigation of lung inflammation and mucus production in cystic fibrosis. Anal Cell Pathol. 2018;2018(Figure 1).

338. Ehrhardt C, Collnot EM, Baldes C, Becker U, Laue M, Kim KJ, et al. Towards an in vitro model of cystic fibrosis small airway epithelium: Characterisation of the human bronchial epithelial cell line CFBE41o-. Cell Tissue Res. 2006;323(3):405–15.

339. Scott H. Randell, M. Leslie Fulcher WO, Olsen and JC. Primary Epithelial Cell Models for Cystic Fibrosis Research. Methods Mol Biol. 2011;2:285–310.

340. Mou H, Brazauskas K, Rajagopal J. Personalized medicine for cystic fibrosis: Establishing human model systems. Pediatr Pulmonol. 2015;50(May):S14–23.

341. Schögler A, Blank F, Brügger M, Beyeler S, Tschanz SA, Regamey N, et al. Characterization of pediatric cystic fibrosis airway epithelial cell cultures at the air-liquid interface obtained by non-invasive nasal cytology brush sampling. Respir Res. 2017;18(1):1–10.

342. Brewington JJ, Filbrandt ET, LaRosa FJ, Moncivaiz JD, Ostmann AJ, Strecker LM, et al. Brushed nasal epithelial cells are a surrogate for bronchial epithelial CFTR studies. JCI insight. 2018;3(13):1–14.

343. Stacey L. Martiniano, Scott D. Sagel ETZ. Cystic fibrosis: a model system for precision medicine. Curr Opin Pediatr. 2016;28(3):312–7.

344. Lopes-Pacheco M. CFTR modulators: Shedding light on precision medicine for cystic fibrosis. Front Pharmacol. 2016;7(SEP):1–20.

345. Van Goor F, Hadida S, Grootenhuis PDJ, Burton B, Cao D, Neuberger T, et al. Rescue of CF airway epithelial cell function in vitro by a CFTR potentiator, VX-770. Proc Natl Acad Sci U S A. 2009;106(44):18825–30.

346. Van Goor F, Hadida S, Grootenhuis PDJ, Burton B, Stack JH, Straley KS, et al. Correction of the F508del-CFTR protein processing defect in vitro by the investigational drug VX-809. Proc Natl Acad Sci U S A. 2011;108(46):18843–8.

347. Awatade NT, Uliyakina I, Farinha CM, Clarke LA, Mendes K, Solé A, et al. Measurements of Functional Responses in Human Primary Lung Cells as a Basis for Personalized Therapy for Cystic Fibrosis. EBioMedicine. 2015;2(2):147–53.

348. Pranke IM, Hatton A, Simonin J, Jais JP, Le Pimpec-Barthes F, Carsin A, et al. Correction of CFTR function in nasal epithelial cells from cystic fibrosis patients predicts improvement of respiratory function by CFTR modulators. Sci Rep. 2017;7(1):1–11.

349. Manunta MDI, Tagalakis AD, Attwood M, Aldossary AM, Barnes JL, Munye MM, et al. Delivery of ENaC siRNA to epithelial cells mediated by a targeted nanocomplex: A therapeutic strategy for cystic fibrosis. Sci Rep. 2017;7(1):1–12.

350. Tagalakis AD, Munye MM, Ivanova R, Chen H, Smith CM, Aldossary AM, et al. Effective silencing of ENaC by siRNA delivered with epithelial-targeted nanocomplexes in human cystic fibrosis cells and in mouse lung. Thorax. 2018;73(9):847–56.

351. Mitchell G, Grondin G, Bilodeau G, Cantin AM, Malouin F. Infection of polarized airway epithelial cells by normal and small-colony variant strains of Staphylococcus aureus is increased in cells with abnormal cystic fibrosis transmembrane conductance regulator function and is influenced by NF-κB. Infect Immun. 2011;79(9):3541–51.

352. Kiedrowski MR, Gaston JR, Kocak BR, Coburn SL, Lee S, Pilewski JM, et al. Staphylococcus aureus Biofilm Growth on Cystic Fibrosis Airway Epithelial Cells Is Enhanced during Respiratory Syncytial Virus Coinfection . mSphere. 2018;3(4):1–17.

353. Michelle Di Paola, Amber J. Park, Saumel Ahmadi, Elyse J. Roach, Yu-Sheng Wu, Michaela Struder-Kypke, Joseph S. Lam, Christine E. Bear CMK. SLC6A14 Is a Genetic Modifier of Cystic Fibrosis That Regulates Pseudomonas aeruginosa Attachment to Human Bronchial Epithelial Cells. MBio. 2017;8(6):1–14.

354. Hasan S, Sebo P, Osicka R. A guide to polarized airway epithelial models for studies of host–pathogen interactions. FEBS J. 2018;285(23):4343–58.

355. Yonker LM, Mou H, Chu KK, Pazos MA, Leung H, Cui D, et al. Development of a Primary Human Co-Culture Model of Inflamed Airway Mucosa. Sci Rep. 2017;7(1):1–12.

356. Halldorsson S, Gudjonsson T, Gottfredsson M, Singh PK, Gudmundsson GH, Baldursson O. Azithromycin maintains airway epithelial integrity during Pseudomonas aeruginosa infection. Am J Respir Cell Mol Biol. 2010;42(1):62–8.

357. Moreau-Marquis S, O'Toole GA, Stanton BA. Tobramycin and FDA-approved iron chelators eliminate Pseudomonas aeruginosa biofilms on cystic fibrosis cells. Am J Respir Cell Mol Biol. 2009;41(3):305–13.

358. Lashua LP, Melvin JA, Deslouches B, Pilewski JM, Montelaro RC, Bomberger JM. Engineered cationic antimicrobial peptide (eCAP) prevents Pseudomonas aeruginosa biofilm growth on airway epithelial cells. J Antimicrob Chemother. 2016;71(8):2200–7.

359. Barnes PJ. Targeting cytokines to treat asthma and chronic obstructive pulmonary disease. Nat Rev Immunol. 2018;18(7):454–66.

360. Lambrecht BN, Hammad H. The airway epithelium in asthma. Nat Med. 2012;18(5):684–92.

361. Barnes PJ. Immunology of asthma and chronic obstructive pulmonary disease. Nat Rev Immunol. 2008;8(3):183–92.

362. Blume C, Davies DE. In vitro and ex vivo models of human asthma. Eur J Pharm Biopharm. 2013;84(2):394–400.

363. Xiao C, Puddicombe SM, Field S, Haywood J, Broughton-Head V, Puxeddu I, et al. Defective epithelial barrier function in asthma. J Allergy Clin Immunol. 2011;128(3):549–56.

364. Gras D, Bourdin A, Vachier I, De Senneville L, Bonnans C, Chanez P. An ex vivo model of severe asthma using reconstituted human bronchial epithelium. J Allergy Clin Immunol. 2012;129(5):1259-1266.e1.

365. Hackett TL, Warner SM, Stefanowicz D, Shaheen F, Pechkovsky D V., Murray LA, et al. Induction of epithelial-mesenchymal transition in primary airway epithelial cells from

patients with asthma by transforming growth factor-β1. Am J Respir Crit Care Med. 2009;180(2):122–33.

366. Carlini F, Picard C, Garulli C, Piquemal D, Roubertoux P, Chiaroni J, et al. Bronchial epithelial cells from asthmatic patients display less functional HLA-G isoform expression. Front Immunol. 2017;8(JAN):1–11.

367. Jevnikar Z, Östling J, Ax E, Calvén J, Thörn K, Israelsson E, et al. Epithelial IL-6 trans-signaling defines a new asthma phenotype with increased airway inflammation. J Allergy Clin Immunol. 2019;143(2):577–90.

368. Holden NS, Rider CF, Bell MJ, Velayudhan J, King EM, Kaur M, et al. Enhancement of inflammatory mediator release by β 2- adrenoceptor agonists in airway epithelial cells is reversed by glucocorticoid action. Br J Pharmacol. 2010;160(2):410–20.

369. Woodman LB, Wan WYH, Milone R, Grace K, Sousa A, Williamson R, et al. Synthetic response of stimulated respiratory epithelium: Modulation by prednisolone and iKK2 inhibition. Chest. 2013;143(6):1656–66.

370. Hardyman MA, Wilkinson E, Martin E, Jayasekera NP, Blume C, Swindle EJ, et al. TNF-α-mediated bronchial barrier disruption and regulation by src-family kinase activation. J Allergy Clin Immunol. 2013;132(3):665-675.e8.

371. Sexton DJ, Chen T, Martik D, Kuzmic P, Kuang G, Chen J, et al. Specific inhibition of tissue kallikrein 1 with a human monoclonal antibody reveals a potential role in airway diseases. Biochem J. 2009;422(2):383–92.

372. Lopez-Guisa JM, Powers C, File D, Cochrane E, Jimenez N DJ. Airway epithelial cells from asthmatic children differentially express proremodeling factors. J Allergy Clin Immunol. 2012;129(4):990–7.

373. Healey GD, Evans N, Hopkin JM, Davies G, Walker W. Evaluation of nasal epithelium sampling as a tool in the preclinical development of siRNA-based therapeutics for asthma. J Cell Mol Med. 2013;17(3):356–64.

374. Gras D, Martinez-Anton A, Bourdin A, Garulli C, De Senneville L, Vachier I, et al. Human bronchial epithelium orchestrates dendritic cell activation in severe asthma. Eur Respir J. 2017;49(3):1–11.

375. Jiao D, Wong CK, Tsang MSM, Chu IMT, Liu D, Zhu J, et al. Activation of Eosinophils Interacting with Bronchial Epithelial Cells by Antimicrobial Peptide LL-37: Implications in Allergic Asthma. Sci Rep. 2017;7(1):1–13.

376. Wawrzyniak P, Wawrzyniak M, Wanke K, Sokolowska M, Bendelja K, Rückert B, et al. Regulation of bronchial epithelial barrier integrity by type 2 cytokines and histone deacetylases in asthmatic patients. J Allergy Clin Immunol. 2017;139(1):93–103.

377. Haghi M, Hittinger M, Zeng Q, Oliver B, Traini D, Young PM, et al. Mono- and Cocultures of Bronchial and Alveolar Epithelial Cells Respond Differently to Proinflammatory Stimuli and Their Modulation by Salbutamol and Budesonide. Mol Pharm. 2015;12(8):2625–32.

378. Reeves SR, Kolstad T, Lien TY, Herrington-Shaner S, Debley JS. Fibroblast-myofibroblast transition is differentially regulated by bronchial epithelial cells from asthmatic children. Respir Res. 2015;16(1):1–12.

379. Paplinksa-Goryca M, Misiukiewicz-Stepien P, Nejman-Gryz P, Proboszcz M, Mlacki M, Gorska K, et al. Epithelial-macrophage-dendritic cell interactions impact alarmins

expression in asthma and COPD. Clin Immunol. 2019;108421.

380. Siegel RL, Miller KD, Jemal A. Cancer statistics, 2020. CA Cancer J Clin. 2020;70(1):7–30.

381. Stevens JL, Baker TK. The future of drug safety testing: expanding the view and narrowing the focus. Drug Discov Today. 2009;14(3–4):162–7.

382. Weigelt B, Ghajar CM, Bissell MJ. The need for complex 3D culture models to unravel novel pathways and identify accurate biomarkers in breast cancer. Adv Drug Deliv Rev. 2014;69–70:42–51.

383. Jakiela B, Gielicz A, Plutecka H, Hubalewska M, Mastalerz L, Bochenek G, et al. Eicosanoid biosynthesis during mucociliary and mucous metaplastic differentiation of bronchial epithelial cells. Prostaglandins Other Lipid Mediat. 2013;106:116–23.

384. Shaykhiev R, Zuo WL, Chao IW, Fukui T, Witover B, Brekman A, et al. EGF shifts human airway basal cell fate towarda smoking-Associated airway epithelial phenotype. Proc Natl Acad Sci U S A. 2013;110(29):12102–7.

385. Lee J, Ryu SH, Kang SM, Chung WC, Gold KA, Kim ES, et al. Prevention of bronchial hyperplasia by EGFR pathway inhibitors in an organotypic culture model. Cancer Prev Res. 2011;4(8):1306–15.

386. Horie M, Saito A, Mikami Y, Ohshima M, Morishita Y, Nakajima J, et al. Characterization of human lung cancer-associated fibroblasts in three-dimensional in vitro co-culture model. Biochem Biophys Res Commun. 2012;423(1):158–63.

387. Correia LL, Johnson JA, McErlean P, Bauer J, Farah H, Rassl DM, et al. SOX2 drives bronchial dysplasia in a novel organotypic model of early human squamous lung cancer. Am J Respir Crit Care Med. 2017;195(11):1494–508.

388. Zanoni M, Piccinini F, Arienti C, Zamagni A, Santi S, Polico R, et al. 3D tumor spheroid models for in vitro therapeutic screening: A systematic approach to enhance the biological relevance of data obtained. Sci Rep. 2016;6(August 2015):1–11.

389. Kim M, Mun H, Sung CO, Cho EJ, Jeon HJ, Chun SM, et al. Patient-derived lung cancer organoids as in vitro cancer models for therapeutic screening. Nat Commun. 2019;10(1).

390. Han K, Pierce SE, Li A, Spees K, Anderson GR, Seoane JA, et al. CRISPR screens in cancer spheroids identify 3D growth-specific vulnerabilities. Nature. 2020;580(April 2019):136–141.

391. Di Liello R, Ciaramella V, Barra G, Venditti M, Della Corte CM, Papaccio F, et al. Ex vivo lung cancer spheroids resemble treatment response of a patient with NSCLC to chemotherapy and immunotherapy: Case report and translational study. ESMO Open. 2019;4(4):1–6.

392. Meenach SA, Tsoras AN, McGarry RC, Mansour HM, Hilt JZ, Anderson KW. Development of three-dimensional lung multicellular spheroids in air- and liquid-interface culture for the evaluation of anticancer therapeutics. Int J Oncol. 2016;48(4):1701–9.

393. Gupta SK, Torrico Guzmán EA, Meenach SA. Coadministration of a tumor-penetrating peptide improves the therapeutic efficacy of paclitaxel in a novel air-grown lung cancer 3D spheroid model. Int J Cancer. 2017;141(10):2143–53.

394. Movia D, Bazou D, Volkov Y, Prina-mello A. Multilayered Cultures of NSCLC cells grown at the Air-Liquid Interface allow the efficacy testing of inhaled anti-cancer drugs. Sci Rep. 2018;8(August):1–19.

395. Movia D, Bazou D, Prina-mello A. ALI multilayered co-cultures mimic biochemical mechanisms of the cancer cell- fibroblast cross-talk involved in NSCLC MultiDrug Resistance. BMC Cancer. 2019;19:1–21.

396. Zhang YM, Zhang ZM, Guan QL, Liu YQ, Wu ZW, Li JT, et al. Co-culture with lung cancer A549 cells promotes the proliferation and migration of mesenchymal stem cells derived from bone marrow. Exp Ther Med. 2017;14(4):2983–91.

397. Gagnadoux F, Hureaux J, Vecellio L, Urban T, Le Pape A, Valo I, et al. Aerosolized chemotherapy. J Aerosol Med Pulm Drug Deliv. 2008;21(1):61–70.

398. Lee WH, Loo CY, Traini D, Young PM. Inhalation of nanoparticle-based drug for lung cancer treatment: Advantages and challenges. Asian J Pharm Sci. 2015;10(6):481–9.

399. Joshi N, Shirsath N, Singh A, Joshi KS, Banerjee R. Endogenous lung surfactant inspired pH responsive nanovesicle aerosols: Pulmonary compatible and site-specific drug delivery in lung metastases. Sci Rep. 2014;4:7085.

400. Rosière R, Van Woensel M, Gelbcke M, Mathieu V, Hecq J, Mathivet T, et al. New Folate-Grafted Chitosan Derivative to Improve Delivery of Paclitaxel-Loaded Solid Lipid Nanoparticles for Lung Tumor Therapy by Inhalation. Mol Pharm. 2018;15(3):899–910.

401. Almuqbil RM, Heyder RS, Bielski ER, Durymanov M, Reineke JJ, da Rocha SRP. Dendrimer Conjugation Enhances Tumor Penetration and Efficacy of Doxorubicin in Extracellular Matrix-Expressing 3D Lung Cancer Models. Mol Pharm. 2020;17(5):1648–62.

402. Zhang C, Zhang S, Zhi D, Zhao Y, Cui S, Cui J. Co-delivery of paclitaxel and survivin siRNA with cationic liposome for lung cancer therapy. Colloids Surfaces A Physicochem Eng Asp. 2020;585:124054.

403. Tuder RM, Petrache I. Pathogenesis of chronic obstructive pulmonary disease. J Clin Invest. 2012;122(8):2749–55.

404. MacNee W. Pathogenesis of chronic obstructive pulmonary disease. Proc Am Thorac Soc. 2005;2(4):258–66.

405. Gao W, Li L, Wang Y, Zhang S, Adcock IM, Barnes PJ, et al. Bronchial epithelial cells: The key effector cells in the pathogenesis of chronic obstructive pulmonary disease? Respirology. 2015;20(5):722–9.

406. Schamberger AC, Staab-weijnitz CA, Mise-racek N, Eickelberg O. Cigarette smoke alters primary human bronchial epithelial cell differentiation at the air-liquid interface. Sci Rep. 2015;5:1–9.

407. Haswell LE, Hewitt K, Thorne D, Richter A, Gaça MD. Cigarette smoke total particulate matter increases mucous secreting cell numbers in vitro : A potential model of goblet cell hyperplasia. Toxicol Vitr. 2010;24(3):981–7.

408. Gohy S, Carlier FM, Fregimilicka C, Detry B, Lecocq M, Ladjemi MZ, et al. Altered generation of ciliated cells in chronic obstructive pulmonary disease. Sci Rep. 2019;9:1–12.

409. Meiners S, Eickelberg O, Schamberger AC, Mise N, Jia J, Genoyer E, et al. Cigarette Smoke – Induced Disruption of Bronchial Epithelial Tight Junctions Is Prevented by Transforming Growth Factor- b. Am J Respir Cell Mol Biol. 2014;50(6):1040–52.

410. Heijink IH, Bruin HG De, Dennebos R, Jonker MR, Noordhoek JA, Brandsma C, et al. Cigarette smoke-induced epithelial expression of WNT-5B : implications for COPD. Eur

Respir J. 2016;48:504–15.

411. Comer DM, Kidney JC, Ennis M, Elborn JS. Airway epithelial cell apoptosis and inflammation in COPD, smokers and nonsmokers David. Eur Respir J. 2013;41(5):1058–67.

412. Amatngalim GD, Schrumpf A, Henic A. Antibacterial Defense of Human Airway Epithelial Cells from Chronic Obstructive Pulmonary Disease Patients Induced by Acute Exposure to Nontypeable Haemophilus influenzae : Modulation by Cigarette Smoke. J Innate Immun. 2017;(9):359–74.

413. Azzopardi D, Haswell LE, Foss-smith G, Hewitt K, Asquith N, Corke S, et al. Evaluation of an air – liquid interface cell culture model for studies on the inflammatory and cytotoxic responses to tobacco smoke aerosols. Toxicol Vitr. 2015;29:1720–8.

414. Zarcone MC, Schadewijk A Van, Duistermaat E, Hiemstra PS, Kooter IM. Diesel exhaust alters the response of cultured primary bronchial epithelial cells from patients with chronic obstructive pulmonary disease (COPD) to non-typeable Haemophilus influenzae. Respir Res. 2017;18(1):27.

415. Ladjemi MZ, Lecocq M, Weynand B, Bowen H, Gould HJ, Snick J Van, et al. Increased IgA production by B-cells in COPD via lung epithelial interleukin-6 and TACI pathways. Eur Respir J. (45):980–93.

416. Osei ET, Noordhoek JA, Hackett TL, Spanjer AIR, Postma DS, Timens W, et al. Interleukin-1 α drives the dysfunctional cross-talk of the airway epithelium and lung fibroblasts in COPD. Eur Respir J. (48):359–69.

417. Gindele JA, Mang S, Pairet N, Christ I, Gantner F, Lamb DJ. Opposing effects of in vitro differentiated macrophages sub-type on epithelial wound healing. PLoS One. 2017;12(9):1–15.

418. Marin L, Traini D, Bebawy M, Colombo P, Buttini F, Haghi M, et al. Multiple dosing of simvastatin inhibits airway mucus production of epithelial cells : Implications in the treatment of chronic obstructive airway pathologies. Eur J Pharm Biopharm. 2013;84(3):566–72.

419. Tatsuta M, Kan-o K, Ishii Y, Yamamoto N, Ogawa T, Fukuyama S, et al. Effects of cigarette smoke on barrier function and tight junction proteins in the bronchial epithelium : protective role of cathelicidin LL-37. Respir Res. 2019;20(251):1–14.

420. Schmid A, Baumlin N, Ivonnet P, Dennis JS, Campos M, Krick S. Roflumilast partially reverses smoke-induced mucociliary dysfunction. Respir Res. 2015;1–11.

421. Gohy ST, Hupin C, Fregimilicka C, Detry BR, Bouzin C, Chevronay HG, et al. Imprinting of the COPD airway epithelium for dedifferentiation and mesenchymal transition. Eur Respir J. (45):1258–72.

422. Lamb DJ, Bucher H, Mang S, Keck M, Schiele F, Wittenbrink M, et al. Neutralization of both IL-1 a / IL-1 b plays a major role in suppressing combined cigarette smoke / virus-induced pulmonary in fl ammation in mice. Pulm Pharmacol Ther. 2017;44:96–105.

423. Reus AA, Maas WJM, Jansen HT, Constant S, Staal YCM, Triel JJ Van, et al. Toxicology in Vitro Feasibility of a 3D human airway epithelial model to study respiratory absorption. Toxicol Vitr. 2014;28(2):258–64.

424. Huang S, Wiszniewski L, Constant S, Roggen E. Toxicology in Vitro Potential of in vitro

reconstituted 3D human airway epithelia (MucilAir ™) to assess respiratory sensitizers. Toxicol Vitr. 2013;27(3):1151–6.

425. Mercier C, Jacqueroux E, He Z, Hodin S, Perek N, Boudard D, et al. Pharmacological characterization of the 3D MucilAir ™ nasal model. Eur J Pharm Biopharm. 2019;139(April):186–96.

426. Rotoli BM, Barilli A, Visigalli R, Ferrari F, Frati C, Lagrasta CA, et al. Characterization of ABC Transporters in EpiAirway ™ , a Cellular Model of Normal Human Bronchial Epithelium. Int J Mol Sci. 2020;21(9):3190.

427. Hoffmann W, Gradinaru J, Farcal L, Caul-Futy M, Huang S, Wiszniewski L, et al. Establishment of a Human 3D Tissue-Based Assay for Upper Respiratory Tract Absorption. Appl Vitr Toxicol. 2018;4(2):139–48.

428. Furubayashi T, Inoue D, Nishiyama N, Tanaka A. Comparison of Various Cell Lines and Three-Dimensional Mucociliary Tissue Model Systems to Estimate Drug Permeability Using an In Vitro Transport Study to Predict Nasal Drug Absorption in Rats. Pharmaceutics. 2020;12(1):79.

429. Iskandar AR, Xiang Y, Frentzel S, Talikka M, Leroy P, Kuehn D, et al. Impact assessment of cigarette smoke exposure on organotypic bronchial epithelial tissue cultures: A comparison of mono-culture and coculture model containing fibroblasts. Toxicol Sci. 2015;147(1):207–21.

430. Kooter IM, Gröllers-Mulderij M, Duistermaat E, Kuper F, Schoen ED. Factors of concern in a human 3D cellular airway model exposed to aerosols of nanoparticles. Toxicol Vitr. 2017;44(December 2016):339–48.

431. Sancey L, Sabido O, He Z, Rossetti F, Guignandon A, Bin V, et al. Multiparametric investigation of non functionalized - AGuIX nanoparticles in 3D human airway epithelium models demonstrates preferential targeting of tumor cells. J Nanobiotechnology. 2020;1–18.

432. Mistry A, Bowen LE, Dzierlenga MW, Hartman JK, Slattery SD. Toxicology in Vitro Development of an in vitro approach to point-of-contact inhalation toxicity testing of volatile compounds , using organotypic culture and air-liquid interface exposure. Toxicol Vitr. 2020;69(August):104968.

433. Outlaw, Victor K.; Bovier, Francesca T.; Mears, Megan C.; Cajmat, Maria N.; Zhu, Yun; Lin, Michelle J.; Addetia, Amin; Lieberman, Nicole A. P.; Peddu, Vikas; Xie, Xuping; Shi, Pei-Yong; Greninger, Alexander L.; Gellman, Samuel H.; Bente, Dennis A.; Moscon M. Inhibition of Coronavirus Entry In Vitro and Ex Vivo by a Lipid-Conjugated Peptide Derived from the SARS-CoV-2 Spike Glycoprotein HRC Domain. 2020;11(5):1–14.

434. Huang S, Boda B, Vernaz J, Ferreira E, Wiszniewski L, Constant S. Establishment and characterization of an in vitro human small airway. Eur J Pharm Biopharm. 2017;118:68–72.

435. Barosova H, Maione AG, Septiadi D, Sharma M, Haeni L, Balog S, et al. Use of EpiAlveolar Lung Model to Predict Fibrotic Potential of Multiwalled Carbon Nanotubes. ACS Nano. 2020;14(4):3941–56.

436. Bolmarcich J, Jackson GR, Oldach J, Bachelor M, Wilbert S, Kenney T, et al. In Vitro Human Airway Models for Study of Goblet Cell Hyperplasia and Mucus Production : Effects of Th2 Cytokines, Double-Stranded RNA, and Tobacco Smoke. Appl Vitr Toxicol.

2017;4(4):1–15.

437. De Matos, Raphael; Vuilleumier, Jeremy; Mas, Christophe; Constant, Samuel; Staedler, Davide; Gerber-Lemaire S. Inhibitor-conjugated harmonic nanoparticles targeting fibroblast activation protein. RSC Adv. 2019;9:31659–69.

438. Signer J, Jonsdottir HR, Albrich WC, Strasser M, Züst R, Ryter S, et al. In vitro virucidal activity of Echinaforce®, an Echinacea purpurea preparation, against coronaviruses, including common cold coronavirus 229E and SARS-CoV-2. Virol J. 2020;17(1):136.

439. Mas C, Boda B, CaulFuty M, Huang S, Wiszniewski L, Constant S. Antitumour efficacy of the selumetinib and trametinib MEK inhibitors in a combined human airway-tumour-stroma lung cancer model. J Biotechnol. 2015;205:111–9.

440. Kilin V, Mas C, Constant S, Wolf JP, Bonacina L. Health state dependent multiphoton induced autofluorescence in human 3D in vitro lung cancer model. Sci Rep. 2017;7(1):1–10.

441. Schimek K, Frentzel S, Luettich K, Bovard D, Rütschle I, Boden L, et al. Human multi-organ chip co-culture of bronchial lung culture and liver spheroids for substance exposure studies. Sci Rep. 2020;10:1–13.

442. Dellaquila A, Thomée EK, McMillan AH, Lesher-Pérez SC. Lung-on-a-chip platforms for modeling disease pathogenesis. Organ-on-a-chip Eng Microenviron Saf Effic Test. 2019;133–80.

443. Shrestha J, Razavi Bazaz S, Aboulkheyr Es H, Yaghobian Azari D, Thierry B, Ebrahimi Warkiani M, et al. Lung-on-a-chip: the future of respiratory disease models and pharmacological studies. Crit Rev Biotechnol. 2020 Feb;40(2):213–30.

444. Zamprogno P, Wüthrich S, Achenbach S, Thoma G, Stucki JD, Hobi N, et al. Second-generation lung-on-a-chip with an array of stretchable alveoli made with a biological membrane. Commun Biol. 2021;4(1):168.

445. Huh D, Matthews BD, Mammoto A, Montoya-Zavala M, Hsin HY, Ingber DE. Reconstituting Organ-Level Lung Functions on a Chip. Science (80-). 2010 Jun;328(5986):1662 LP – 1668.

446. Liu Z, Mackay S, Gordon DM, Anderson JD, Haithcock DW, Garson CJ, et al. Co-cultured microfluidic model of the airway optimized for microscopy and micro-optical coherence tomography imaging. Biomed Opt Express. 2019;10(10):5414–30.

447. Kızılkurtlu AA, Polat T, Akpek* GBA and A. Lung on a Chip for Drug Screening and Design. Vol. 24, Current Pharmaceutical Design. 2018. p. 5386–96.

448. Lenz A, Stoeger T, Cei D, Schmidmeir M, Semren N. Efficient Bioactive Delivery of Aerosolized Drugs to Human Pulmonary Epithelial Cells Cultured in Air – Liquid Interface Conditions. 2014;51(4):526–35.

449. Schmid O, Jud C, Umehara Y, Mueller D, Bucholski A, Gruber F, et al. Biokinetics of Aerosolized Liposomal Ciclosporin A in Human Lung Cells in Vitro Using an Air-Liquid Cell Interface Exposure System. J Aerosol Med Pulm Drug Deliv. 2017;30(6):411–24.

450. Klein SG, Serchi T, Hoffmann L, Blömeke B, Gutleb AC. An improved 3D tetraculture system mimicking the cellular organisation at the alveolar barrier to study the potential toxic effects of particles on the lung. Part Fibre Toxicol. 2013;10(1).

451. Tsoutsoulopoulos A, Gohlsch K, Möhle N, Breit A, Hoffmann S, Krischenowski O, et al.

Validation of the CULTEX® Radial Flow System for the assessment of the acute inhalation toxicity of airborne particles. Toxicol Vitr. 2019;58:245–55.

452. Aufderheide M, Förster C, Beshay M, Branscheid D, Emura M. A new computer-controlled air–liquid interface cultivation system for the generation of differentiated cell cultures of the airway epithelium. Exp Toxicol Pathol. 2016;68(1):77–87.

453. Polk WW, Sharma M, Sayes CM, Hotchkiss JA, Clippinger AJ. Aerosol generation and characterization of multi-walled carbon nanotubes exposed to cells cultured at the air-liquid interface. Part Fibre Toxicol. 2016;13(1):20.

454. Ji J, Hedelin A, Malmlöf M, Kessler V, Seisenbaeva G, Gerde P, et al. Development of Combining of Human Bronchial Mucosa Models with XposeALI® for Exposure of Air Pollution Nanoparticles. PLoS One. 2017 Jan;12(1):e0170428.

455. Upadhyay S, Palmberg L. Air-Liquid Interface: Relevant In Vitro Models for Investigating Air Pollutant-Induced Pulmonary Toxicity. Toxicol Sci. 2018 Jul;164(1):21–30.

456. Jeannet N, Fierz M, Kalberer M, Burtscher H, Geiser M. Nano Aerosol Chamber for In-Vitro Toxicity (NACIVT) studies. Nanotoxicology. 2015 Jan;9(1):34–42.

457. Ihalainen M, Jalava P, Ihantola T, Kasurinen S, Uski O, Sippula O, et al. Design and validation of an air-liquid interface (ALI) exposure device based on thermophoresis. Aerosol Sci Technol. 2019 Feb;53(2):133–45.

458. Ding Y, Weindl P, Lenz AG, Mayer P, Krebs T, Schmid O. Quartz crystal microbalances (QCM) are suitable for real-time dosimetry in nanotoxicological studies using VITROCELL®Cloud cell exposure systems. Part Fibre Toxicol. 2020;17(1):1–20.

List of abbreviations

ALI	Air-liquid Interface
AF488	Alexa Fluor 488
AF647	Alexa Fluor 647
ARDS	Acute Respiratory Distress Syndrome
BALF	Bronchoalveolar Lavage Fluid
CARDS	COVID-19 Associated Acute Respiratory Distress Syndrome
CF	Cystic Fibrosis
CFTR	Cystic Fibrosis Transmembrane conductance Regulator
CLSM	Confocal Laser Scanning Microscopy
COPD	Chronic Obstructive Pulmonary Disease
DAPI	4′,6–diamidino–2-phenylindole dihydrochloride
DCM	Dichloromethane
DLS	Dynamic light scattering
DMSO	Dimethyl Sulfoxide
DOTAP	1,2-dioleoyl-3-trimethylammonium-propane
DPPC	1,2-dipalmitoyl-sn-glycero-3- phosphocholine
dsRNA	Double strand RNA
DSPC	1,2-distearoyl-sn-glycero-3-phosphocholine
DSPE-PEG	N-(carbonyl-methoxypolyethyleneglycol-2000)-1,2-distearoyl-sn-glycero-3-phosphoethanolamine
DSPG	1,2-distearoyl-sn-glycero-3-phospho-(1'-rac-glycerol)
ELISA	Enzyme-linked Immunosorbent Assay
EMA	European Medicine Agency
EMEM	Egle’s Minimum Essential Medium
ET	Extrathoracic Region
FBS	Fetal Bovine Serum
FDA	Food and Drug Administration
GAPDH	Glyceraldehyde-3-phosphate dehydrogenase
GFP	Green Fluorescence Protein
HEPES	(4-(2-hydroxylethyl)-1-piperazineethanesulfonic acid)
LDH	Lactate Dehydrogenase
LNPs	Lipid Nanoparticles
LPS	Lipopolysaccharides
MFI	Median Fluorescence Intensity

MIC	Minimum Inhibitory Concentration
mRNA	Messenger RNA
MRSA	Methicillin-Resistant *S. aureus*
MSSA	Methicillin-Sensitive *S. aureus*
MTT	3-(4,5-dimethylthiazol-2-yl)-2,5-diphenyltetrazolium bromide
NPs	Nanoparticles
NTA	Nanoparticle Tracking Analysis
ORF1	Open Reading Frame 1
PBS	Dulbecco's Phosphate Buffered Saline
PCLS	Precision-Cut Lung Slices
PCR	Polymerase Chain Reaction
PDI	Polydispersity Index
pDNA	Plasmid DNA
PEG	Polyethylene Glycol
PEI	Polyethylenimine
PLGA	Poly(lactic-co-glycolic acid)
Pp1ab	Polyprotein 1ab
PVA	Polyvinyl Alcohol
RISC	RNA-Induced Silencing Complex
RNAi	RNA Interference
SDS-PAGE	Sodium Dodecyl-Sulfate Polyacrylamide Gel Electrophoresis
shRNA	Short Hairpin RNA
siRNA	Small Interfering RNA
SP-A	Surfactant Protein A
SP-B	Surfactant Protein B
SP-C	Surfactant Protein C
TB	Tracheobronchial Region
TEER	Transepithelial Electrical Resistance
Th1	T helper 1 Cells
Th2	T helper 2 Cells
TNBS	2,4,6-Trinitrobenzene Sulfonic Acid
VIPER	Virus-Inspired Polymer for Endosomal Release

List of publications and conference contributions

List of Publications

Keil TWM†, **Baldassi D**†, Merkel OM. T-cell targeted pulmonary siRNA delivery for the treatment of asthma. Wiley Interdiscip Rev Nanomed Nanobiotechnol. 2020 Sep;12(5):e1634. doi: 10.1002/wnan.1634. Epub 2020 Apr 8. PMID: 32267622; PMCID: PMC7116616.

† These authors contributed equally.

Baldassi D†, Gabold B†, Merkel O. Air-liquid interface cultures of the healthy and diseased human respiratory tract: promises, challenges and future directions. Adv Nanobiomed Res. 2021 May 6;1(6):2000111. doi: 10.1002/anbr.202000111. PMID: 34345878; PMCID: PMC7611446.

† These authors contributed equally.

Keil TW, Zimmermann C, **Baldassi D**, Adams F, Friess W, Mehta A, Merkel OM. Impact of crystalline and amorphous matrices on successful spray drying of siRNA polyplexes for inhalation of nano-in-microparticles. Adv Ther (Weinh). 2021 May 7;4(6):2100073. doi: 10.1002/adtp.202100073. PMID: 34337144; PMCID: PMC7611418.

Ambike S, Cheng CC, Feuerherd M, Velkov S, **Baldassi D**, Afridi SQ, Porras-Gonzalez D, Wei X, Hagen P, Kneidinger N, Stoleriu MG, Grass V, Burgstaller G, Pichlmair A, Merkel OM, Ko C, Michler T. Targeting genomic SARS-CoV-2 RNA with siRNAs allows efficient inhibition of viral replication and spread. Nucleic Acids Res. 2022 Jan 11;50(1):333-349. doi: 10.1093/nar/gkab1248. PMID: 34928377; PMCID: PMC8754636.

Baldassi D, Ambike S, Feuerherd M, Cheng CC, Peeler DJ, Feldmann DP, Porras-Gonzalez DL, Wei X, Keller LA, Kneidinger N, Stoleriu MG, Popp A, Burgstaller G, Pun SH, Michler T, Merkel OM. Inhibition of SARS-CoV-2 replication in the lung with siRNA/VIPER polyplexes. J Control Release. 2022 May;345:661-674. doi: 10.1016/j.jconrel.2022.03.051. Epub 2022 Mar 29. PMID: 35364120; PMCID: PMC8963978.

Conte G, Costabile G, **Baldassi D**, Rondelli V, Bassi R, Colombo D, Linardos G, Fiscarelli EV, Sorrentino R, Miro A, Quaglia F, Brocca P, d'Angelo I, Merkel OM, Ungaro F. Hybrid Lipid/Polymer Nanoparticles to Tackle the Cystic Fibrosis Mucus Barrier in

siRNA Delivery to the Lungs: Does PEGylation Make the Difference? ACS Appl Mater Interfaces. 2022 Feb 16;14(6):7565-7578. doi: 10.1021/acsami.1c14975. Epub 2022 Feb 2. PMID: 35107987; PMCID: PMC8855343.

Baldassi D, Ngo TMH, Merkel OM. Optimization of Lung Surfactant Coating of siRNA Polyplexes for Pulmonary Delivery. Pharm Res. 2022 Nov 29:1–15. doi: 10.1007/s11095-022-03443-3. Epub ahead of print. PMID: 36447020; PMCID: PMC9708138.

Zimmermann CM, **Baldassi D**, Chan K, Adams NBP, Neumann A, Porras-Gonzalez DL, Wei X, Kneidinger N, Stoleriu MG, Burgstaller G, Witzigmann D, Luciani P, Merkel OM. Spray drying siRNA-lipid nanoparticles for dry powder pulmonary delivery. J Control Release. 2022 Nov;351:137-150. doi: 10.1016/j.jconrel.2022.09.021. Epub 2022 Sep 22. PMID: 36126785; PMCID: PMC7613708.

Kandil R, **Baldassi D**†, Böhlen S, Müller JT, Jürgens DC, Bargmann T, Dehmel S, Xie Y, Mehta A, Sewald K, Merkel OM. Targeted GATA3 knockdown in activated T cells via pulmonary siRNA delivery as novel therapy for allergic asthma. J Control Release. 2023 Feb;354:305-315. doi: 10.1016/j.jconrel.2023.01.014. Epub 2023 Jan 13. PMID: 36634709.

† These authors contributed equally.

Jin Y, Adams F, Isert L, **Baldassi D**, Merkel OM. Spermine-Based Poly(β-amino ester)s for siRNA Delivery against Mutated KRAS in Lung Cancer. Mol Pharm. 2023 Aug 14. doi: 10.1021/acs.molpharmaceut.3c00206. Epub ahead of print. PMID: 37578116.

Conference contributions

- 13th World Meeting on Pharmaceutics, Biopharmaceutics and Pharmaceutical Technology (Rotterdam, The Netherelands, 2022)
  Oral presentation "*In vitro* and *ex vivo* delivery of siRNA via VIPER polymer system as a potential treatment for COVID-19"
- Gattefossé Student Academy on Pharmaceutical Sciences (Lyon, France, 2021)
  Oral presentation "Non-viral delivery systems for pulmonary administration of siRNA and small molecules"
- Controlled Release Society World Meeting (virtual, 2021)

Presentation "*In vitro* and *ex vivo* delivery of siRNA via VIPER polymer system as a potential treatment for COVID-19"

- International Society for Aereosols in Medicine congress (virtual, 2021)
  Poster presentation "Targeted GATA3 knockdown in activated T cells via pulmonary siRNA delivery as a novel therapy for allergic asthma"
- Controlled Release Society - German Chapter (virtual, 2021)
  Short oral presentation " PLGA nanoparticles for sustained release of a novel antibiotic against MRSA"
- Controlled Release Society - German Chapter (Munich, Germany, 2020)
  Poster presentation "Antimicrobial efficacy of a synthetic benzophenone antibiotic loaded in PLGA nanoparticles for the treatment of *S. aureus* lung infections"
- International Conference on Nanomedicines and Nanotechnology (Munich, Germany, 2019)
  Poster presentation "*In vitro* evaluation of siRNA-loaded hybrid NPs for the treatment of cystic fibrosis"

Acknowledgments

The present thesis was prepared under the supervision of Prof. Dr. Olivia Monika Merkel at the department of Pharmacy, Pharmaceutical Technology and Biopharmaceutics at the Ludwig-Maximilian University of Munich, Germany.

This work could not have been possible without the support and guidance of my supervisors, colleagues, collaboration partners, friends and family.

My first and deepest thank you goes to Prof. Merkel. Thank you for giving me the chance to join your lab first as a master intern and then as a PhD student. In your lab and with your scientific and personal guidance, I could grow as a researcher and as a person. I will always be thankful for the trust you have placed in me, joining your group and working on such innovative and interesting projects has been more than I could ever ask for. Thank you for all the possibilities you offered me during these four years.

I would also like to thank Prof. Dr. Winter and Prof. Dr. Friess for the great working atmosphere in the Department and for keeping the three groups together, particularly during the challenging times of the COVID-19 pandemic.

Thank you also to the examination board members for kindly taking the time to review my work.

I would like to express sincere gratitude to the Researchers with whom I had the opportunity to collaborate during my PhD. Thank you Prof. Francesca Ungaro and Prof. Ivana D'Angelo from Università degli Studi Federico II of Naples (Italy), Dr. Thomas Michler and Shubhankar Ambike from the Technical University of Munich, Dr. Dominik Witzigmann from the University of British Columbia, Prof. Sören Schubert and Birgit Gross from the Max von Pettenkofer-Institut Munich für Hygiene und Medizinische Mikrobiologie, Dr. Gerald Burgstaller from the Helmholtz Center Munich and Katherina Sewald from the Fraunhofer Institute of Toxicology and Experimental Medicine Hannover. Thank you for sharing your knowledge and deep expertise with me as well as for the many precious tips and scientific discussions.

I would like to extend my sincere thanks to Gabriella, Aditi and Rike, three incredible women and former post-docs of AK Merkel. I have learnt a lot from each of you and you have always been there to help and support at any time, thank you!

Many thanks and gratitude go also to all the present and former members of Ak Merkel: thank you, Simone, Ben, Valentin, Natascha, Siyu, David, Gabriele, Fabian, Cynthia,

Joschka, Adrian, Nora and Xiao. It was a pleasure to work and have fun with you. Special thanks go to Gabi for being always so kind and helpful and to Lorenz, for always bringing good mood and for support with microscopy experiments.

Special thanks go to my lab mates Bettina, Christoph and Tobi. You have been my second family in Munich, and these 3 and a half years wouldn't have been the same without you. Thank you for all the laughs, jokes and songs we have played together, I have enjoyed every single moment. Bettina, you have always been there for me, even in the most difficult times, I don't know how I could have made it without you. I am thankful I can now call you my Friend. Gemma, thank you for the many laughs and adventures we had together.

A big thank you goes to my former students for giving me the chance to guide and teach them, particularly to Hanh, Evin, Ghizal and Federica. You did an incredible work and I wish you all the best for your future careers.

Heartfelt thanks also to my friends back in Italy, who have always been there, no matter how distant or old we get. Thank you, Vale and Marco for - who knows how many - years of friendship, thank you Matteo, Alessia, Gradino, Cristi, Panda, Chiaro, Sam, Jacky, Dana, Pilli, Willy, Gabro, Jack, Michele, Francesca, Eleonora e Davide for all the laughs and great time we always have together.

Warm thanks go also to Noelia and Aurora for their kindness and sweetness, and to all my extended family, aunts, uncles and cousins, for always being a supportive and caring family. Heartfelt thank you goes to my grandparents, for their example and love.

All of this wouldn't have been possible without the love and care of my Family. Mamma e Papà, thank you with all my heart for your unconditional love and support no matter what. Jacopo, thank you for being the best brother I could ever ask for.

And finally, thank you, Francisco, for showing me that real love knows no boundaries and that, no matter how far apart we are and how many difficulties there may be, you will always be by my side.